Building White Matter: The Role of PI(3,5)P$_2$ Biosynthesis in Myelin Formation, Stability, and Repair

by

Yevgeniya A. Mironova

A dissertation submitted in partial fulfillment
of the requirements for the degree of
Doctor of Philosophy
(Cellular and Molecular Biology)
in the University of Michigan
2016

Doctoral Committee:

       Professor Roman J. Giger, Chair
       Associate Professor Anthony Antonellis
       Assistant Professor Asim Beg
       Research Investigator Guy M. Lenk
       Professor Miriam H. Meisler
       Assistant Professor Brian A. Pierchala

DEDICATION

In loving memory of my Grandmother Natella

ACKNOWLEDGMENTS

I am truly grateful to everyone who helped me make this dissertation possible. I feel very privileged for the opportunity to work with animal models in my research, and I am thankful to the University of Michigan Unit of Laboratory Animals and Medicine for providing animals with excellent care.

I would like to thank my thesis committee - Drs. Roman Giger, Anthony Antonellis, Asim Beg, Guy Lenk, Miriam Meisler, and Brian Pierchala. Thank you for your feedback and helpful advice over the years. I would also like to thank Brian Pierchala and Anthony Antonellis for serving on my preliminary exam committee and giving me the opportunity to rotate in your labs. Thank you, Brian, for generously letting me use your confocal microscope. I would also like to thank Asim for your extremely helpful feedback during my committee meetings, advice on choosing a postdoc mentor, and our small collaboration. I have to give special thanks to Miriam Meisler and Guy Lenk – our collaboration was very productive, and I am tremendously grateful for all the research feedback, reagents, mice, and letters of recommendation I received from both of you. Without you my thesis would not be possible. Thank you very much and I am hopeful that the work we've done together will serve as a stepping stone for future discoveries, papers, and successful grant applications!

I am very grateful to the Hovda lab at UCLA for taking a chance on me when I was an undergraduate seeking exposure to neuroscience research. I would especially like to thank my undergraduate mentor and supervisor Dr. Neil Harris for his support and all the opportunities

iii

My very first graduate school interview was at the University of Michigan, and my very first faculty interview was with Roman Giger. Even then I realized that Roman was a fantastic mentor and I could only hope he would give me a chance to join his lab. I am not the first person to say this, but Roman truly puts people in his lab above all else, and no matter how busy he is, he always finds time to get back to us with comments, discuss the experiments, or provide letters of recommendation. Thank you, Roman, joining your lab was one of the most important decisions in my academic career, and I am very happy for doing so.

Perhaps the most true testament to Roman's excellence as a mentor is the quality of people that join his lab. Not only is everyone extremely smart and hardworking, but they are also wonderful people. I would like to thank former lab members Yuntao Duan, Jesse Winters, and Steve Raiker. Yuntao - thank you for teaching me the basics of cloning and being a good collaborator. Jesse – your Journal of Neuroscience paper provided me with a beautiful framework for my thesis. Steve – thank you for being the ephys pioneer in the lab. I am extremely lucky to not only have wonderful colleagues in my labmates, but also consider them my friends. Choya and Xiaofeng – thank you for providing a warm, yet sufficiently mature presence in the lab. Choya – your lab party organizing skills rival your science, which is beyond reproach. Xiaofeng – your sweet and friendly demeanor make the lab a better place every day, and I am really excited about the developments in your story! Rafi and Ryan – ice and fire, you are a fantastic addition to the lab, however different you may be. Ryan – I will miss your quiet tenacity and killer unexpected jokes, it was a great pleasure to be your desk neighbor. Rafi – you are definitely one memorable Turkish delight, and I enjoyed our verbal sparring and shared passion for high quality coffee. Ashley – you've been in the lab for only a little bit, but you fit so perfectly it seems like you've been around for a while. Thank you for your humor, delightful lab

treats, and fantastic scientific insights. Lucas – welcome to the lab, I am excited to see where science will lead you. Jing-Ping – you are one of the most gifted and creative people I've ever met, and I can't really think of anything you can't do AND do it better than anyone else. Your fantastic outside-the-box (or in your case, "turn a box into a 2-photon") thinking inspired me to take a more creative approach to science, with unexpected and delightful results. I will miss working with you but I hold on to a hope that we will work again together some day. Big thanks to all our undergraduate students, past and present, for making sure the lab runs smoothly. I feel truly fortunate to remain friends with former lab members. Katie Baldwin - thank you for being a fantastic graduate student to follow in the lab, your phenomenal sense of humor and our fun "mental health breaks", including pop culture discussions and building strange sculptures out of vendor toys. Of course I'd like to thank Travis Dickendesher – right when we met I realized we would definitely get along! You are truly a one of a kind, and I am grateful that I can call such a hilarious, outrageous, hardworking, and brilliant person my best friend.

Thank you all my friends back in California, elsewhere in the US, and here in Michigan, your support is incredibly important to me. I would like to thank Emily, David, Gabriel, Elyse, Alex, Yu-Yu, Gustavo, Karthik, Erin, Justine, Blu for being wonderful people in my life here in Ann Arbor, and I hope we will keep in touch. I want to thank my friends back in Russia where I began my path towards becoming a scientist. All the people I met during at the Moscow State University are an inspiration and I and miss you dearly. Importantly, I would like to thank my friend Sergei Shpiz – he was a brilliant researcher and became faculty at the age of 30, but his life was tragically cut short last year.

Of course I have to thank my family back in Russia and here in the US. I am truly fortunate to have a family who never considered my passion for science a frivolous pursuit, and

always respected my research aspirations. My Grandpa, aunt, and cousins back in Russia - I miss you and I wish you were here. My late Grandma Natella – as a fellow scientist, I hope you would be proud of me. My Grandma Lida – thank you for being a great example of someone for whom the age is just a number! My Dad – you always had this borderline delusional faith in my abilities, which is simultaneously humbling and inspiring. Thank you for being a driving force behind many pivotal events in my life that ultimately led to this moment. My Mom – together, we've been through some truly tough times, and the way you handled the worst that life has given you is nothing short of awe-inspiring. You are my toughest critic and my biggest champion.

And finally, I would like to thank Conor Doss. You've sat through my countless presentation rehearsals, proofread hundreds of pages, bore witness to an occasional meltdown and you've weathered them all with kindness, patience, and love. You are one of the kindest and smartest people I've ever met, and every day you inspire me to be a better person. Thank you.

TABLE OF CONTENTS

Chapter

-Inducible *Fig4* ablation in adult mice causes rapid health

LIST OF FIGURES

LIST OF TABLES

LIST OF ABBREVIATIONS

AMPA   α-amino-3-hydroxy-5-methyl-4-isoxazolepropionic acid
                    receptor

CAP   Compound action potential

CMT   Charcot Marie Tooth

CNPase   2'3'-cyclic nucleotide 3'-phosphodiesterase

CNS   Central nervous system

Cre   Cre recombinase

CV   Conduction velocity

Dpi   Days post injection

DRG   Dorsal root ganglia

DWMI   Diffuse white matter injury

FDR   False discovery rate

FIG4   Factor induced gene 4

GABA   Gamma-Aminobutyric acid

ISH   *In situ* hybridization

KO   Knockout

LAMP   Lysosome associated membrane protein

LE/Lys   Late endosome/lysosome

LOF   Loss of function

LPC   Lysophosphatidylcholine

LTD   Long-term depression

LTP   Long-term potentiation

MAG   Myelin associated glycoprotein

MBP   Myelin basic protein

MCLN   Mucolipin 1

MOG	Myelin oligodendrocyte protein
MRF	Myelin regulatory factor
MS	Multiple sclerosis
mTORC	Mechanistic (mammalian) target of rapamycin complex
Myrf	Myelin regulatory factor
NBQX	2,3-dihydroxy-6-nitro-7-sulfamoyl-benzo[f]quinoxaline-2,3-dione
NFO	Newly formed oligodendrocytes
NMDA	N-methyl-D-aspartate receptor
NPC1	Niemann-Pick disease, type C1
NRG	Neuregulin
OL	Oligodendrocyte
OLIG2	Oligodendrocyte transcription factor
OPC	Oligodendrocyte precursor
P0	Myelin protein zero
PDGFRα	Platelet-derived growth factor receptor/receptor alpha
PFA	Paraformaldehyde
PI(3,5)P$_2$	Phosphatidylinositol-3,5-bisphosphate
PLP	Proteolipid protein
PMD	Pelizaeus-Merzbacher disease
PNS	Peripheral nervous system
PVL	Periventricular leukomacia
RGC	Retinal ganglion cells
Rheb	Ras homolog enriched in brain
SAC3	Suppressor of actin
SC	Schwann cell
SCP	Schwann cell precursor
SNARE	N-ethylmaleimide-sensitive factor attachment protein receptor complex
SynCre	Synapsin Cre
TEM	Transmission electron microscope

TFEB	Transcription factor EB
TPC	Two-pore channel
TRPML	Transient receptor potential cation channel
TTX	Tetrodotoxin
VAMP	Vesicle-associated membrane protein
WT	Wildtype
YVS	Yunis-Varon Syndrome

ABSTRACT

Neuron-glia interactions are the cornerstone of a functional nervous system. Formation of white matter (myelin) is mediated by neurons and myelinating glia and is essential for the rapid propagation of action potentials. Increased white matter volume is evolutionarily correlated with cognitive superiority of higher vertebrates. Impaired myelin formation or damage to the existing myelin sheath have devastating functional consequences, such as paralysis, intellectual disability, and blindness. In the central nervous system (CNS), myelin formation and maintenance are highly orchestrated multi-step processes that require proper migration, neuronal contact, and differentiation of oligodendrocyte precursors (OPCs), mediated by both intrinsic and extrinsic mechanisms. Here we demonstrate that one of the most fundamental eukaryotic cell processes – intracellular trafficking – plays a crucial role in CNS myelination. In particular, we show that the signaling lipid phosphatidylinositol-3,5-bisphosphate [$PI(3,5)P_2$] is required in neurons and in oligodendrocytes (OLs) for normal CNS myelination. In mice, mutations of *Fig4, Pikfyve* or *Vac14,* encoding key components of the $PI(3,5)P_2$ biosynthetic complex, each lead to impaired OL maturation, severe CNS hypomyelination, and delayed propagation of compound action potentials. Primary OLs deficient in *Fig4* or *Pikfyve* accumulate large vesicular structures and exhibit impaired terminal differentiation. Live-cell imaging of OLs after genetic or pharmacological inhibition of $PI(3,5)P_2$ synthesis reveals impaired trafficking of myelin building blocks through the endolysosomal system in primary cells and brain tissue. To test whether $PI(3,5)P_2$ biosynthesis is required for adult myelin maintenance and repair, we generated tamoxifen-inducible global *Fig4* knockout mice, *Fig4$^{-/flox}$,CAGCreER*. Strikingly, adult *Fig4*

deletion leads to rapid deterioration in mice with severe motor impairment, tremor, weight loss, and death within two months of *Cre* induction. The peripheral nervous system (PNS) shows severe defects, suggestive of damaged neurons and Schwann cells, the PNS myelinating glia. In the same animals, CNS myelin remains relatively intact, demonstrating differential vulnerability of myelinated CNS vs. PNS fibers to impaired $PI(3,5)P_2$ biosynthesis. Our preliminary data suggest that inducible *Fig4* loss in adult mice prevents CNS myelin repair. Collectively, my thesis work extends understanding of the $PI(3,5)P_2$ biosynthetic complex as a key regulator of CNS and PNS myelin formation and dynamics.

CHAPTER I:

Introduction

Building White Matter: Myelin Formation, Maintenance, and Repair

1.1 Abstract

Neuron-glia interactions are the cornerstone of a functioning nervous system. In particular, formation of white matter (myelin) is mediated by neurons and myelinating glia and is essential for rapid propagation of action potentials. Increased white matter volume is evolutionarily correlated with cognitive superiority of higher vertebrates. Impaired communication between neurons and myelinating glia results in faulty white matter formation and has devastating functional consequences, such as paralysis, intellectual disability, and blindness. In the central nervous system, myelin formation and maintenance are highly orchestrated multi-step processes that require proper migration, neuronal contact, and differentiation of oligodendrocyte precursors mediated by both intrinsic and extrinsic mechanisms. One of the most fundamental eukaryotic cell processes – intracellular trafficking – plays a crucial role in myelin formation in both CNS and PNS. A deeper understanding of the molecular mechanisms underlying the role of trafficking in myelin formation, stability, and repair is of great interest, as it will allow insights into neuropathology of white matter diseases.

1.2 Myelin and vertebrate evolution

Neuron-neuron communication in the nervous system is essential for its proper function. Invertebrate species, such as cephalopods, evolved to develop large caliber axons that allow rapid propagation of action potential (Hartline and Colman, 2007). In contrast, evolutionary pressures in vertebrate species to adapt to various environments required advanced cognitive abilities and thus resulted in efficient and compact nervous systems. To maintain rapid communication between neurons at reduced axonal size in a closed skull, additional insulation to decrease neuronal capacitance and increase saltatory conduction emerged as a key evolutionary advantage of vertebrate species. Myelin, or "white matter", was first described almost two centuries ago by the German physician-scientist Rudolf Virchow (Virchow, 1854), and has been a subject of active research ever since. Myelin constitutes approximately 50% of the adult human brain (Baraban et al., 2015). For a long time myelin was considered to be a largely static structure serving as insulation for action potential propagation, however, increasing evidence suggests that it possesses many other functions, such as providing axons with metabolic support and maintaining their integrity (Nave, 2010). Furthermore, recent studies indicate that ensheathment of previously unmyelinated axons or changes in existing myelin thickness can serve as an additional way of modifying neuronal plasticity in learning and memory, thus presenting with a whole new avenue for research and therapeutic approaches (Fields, 2008, Gibson et al., 2014, McKenzie et al., 2014).

The earliest phylogenetic evidence of compact myelin was observed in sharks and its first appearance is dated to 400 million years ago (Hartline and Colman, 2007). Some invertebrate species have structures resembling myelin wraps, but true compact myelin is thought to be a jawed vertebrate invention. Peripheral nervous system (PNS) myelin is made by Schwann cells

at a 1:1 ratio (axon: Schwann cell) with axons, whereas the CNS myelinating glia – oligodendrcoytes (OL) – are capable of ensheathing up to 50 axons at a time. PNS myelin phylogenetically preceded CNS (Mc et al., 1958). PNS myelin development begins embryonically and is largely complete by 14 days in postnatal mice (Woodhoo and Sommer, 2008). In contrast, the bulk of CNS myelin in mice is formed in the first postnatal month but cortical myelination continues well into the following several months of the mouse's life. In humans, the majority of CNS myelination happens in the first two years after birth, but cortical myelination is an ongoing process in the second and third decades of life (Lebel et al., 2012, Yeung et al., 2014).

1.3 Myelin structure and composition

Structurally, both CNS and PNS myelin is a lipid-rich extension of myelinating glia. Compact myelin is wrapped around the axon 5-20 times with very little space between the loops and minimum intracellular material. Compact myelin can be easily observed by transmission electron microscopy due to its dense and ordered structure. Structurally and functionally, myelin is divided into several regions: internodes, juxtaparanodes, paranodes, and nodes of Ranvier (Figure 1.1B). Internodes are regions of compact myelin and are typically the longest segments. Juxtaparanodes are characterized by clustering of potassium channels on the axonal membrane that regulate electrical properties of the insulated axon. Paranodes are a non-compact myelin (paranodal loops) that serve as anchor points of myelin to the axonal membrane (Poliak and Peles, 2003). Nodes of Ranvier are unmyelinated segments containing clusters of specialized sodium channels on axonal membrane that regenerate action potential. Decreased axonal capacitance and regeneration of action potential at the nodes of Ranvier increases action

potential speed up to a factor of 10 in myelinated vs. nonmyelinated axons. Compact myelin thickness is measured as diameter of axon/diameter of myelinated axon (the g-ratio) and the optimal g-ratio is calculated as 0.77 for the CNS and 0.6 for PNS, with some spatial variations thereof (de Hoz and Simons, 2015). Increased (hypomyeliation) or decreased (hypermyelination) g-ratios result in altered speed of action potential. One of the key features of PNS myelin is the continuous presence of Schwann cell processes and basal lamina over nodes, whereas in the CNS the nodes are bare and are usually a contact site with astrocytes (Hildebrand, 1971, Raine, 1984). A more detailed anatomical organization of myelin is provided elsewhere (Poliak and Peles, 2003).

Myelin consists of approximately 70% lipid in dry weight. Proteins constitute the remaining 30% of myelin and their expression is almost exclusively restricted to the white matter (O'Brien and Sampson, 1965). The high lipid: protein ratio is a unique feature of myelin compared to plasma membranes. Of the lipid content, cholesterol is the most abundant, with other noted lipid components including galactolipids cereboside and sulfatide. The cholesterol used in myelin sheath generation is synthesized *de novo* in the CNS and is supplied from multiple sources, including the cell-autonomous OL lineage production and external delivery from neurons and astrocytes (Zhang and Liu, 2015). Cholesterol provides myelin sheath with rigidity that allows for optimal axonal insulation and decreased capacitance. In addition, cholesterol constitutes lipid raft domains that associate with key myelin-associated proteins. Mice with reduced capability for CNS cholesterol synthesis demonstrate severely impaired myelination (Saher et al., 2005). Galactolipids provide myelin structure with fluidity for optimal packing and are localized on the outer leaflets. When the function of galactocereboside enzyme is impaired thus reducing lipid synthesis, compact myelin is still formed, however, there are

numerous abnormalities in perinodal structures and the nodes of Ranvier architecture. These defects lead to impaired electrical properties in the CNS and manifest as tremor in mice (Coetzee et al., 1996, Dupree et al., 1998).

Myelin protein components serve specific roles in generating and maintaining myelin structure. The relative abundance of myelin-associated proteins does not correlate directly with their requirement for myelin formation and compaction. Interestingly, differential splice isoforms of myelin-associated proteins are specific to various vertebrate taxa, suggesting they may serve as potential evolutionary adaptations (Hartline and Coleman 2007). Some of the *bona fide* CNS and PNS myelin proteins are described below.

PLP

Proteolipid protein (PLP) is the most abundant CNS myelin protein, constituting approximately 50%of total myelin protein content (Dubois-Dalcq et al., 1986). PLP is a marker of mature OLs *in vitro* and of myelinated CNS *in vivo*. PLP is localized to the myelin membrane (intraperiod line, Figure 1.1C-D), where it interacts homophilically and stabilizes extracellular loops (Barkovich, 2000, Baumann and Pham-Dinh, 2001). PLP interacts with cholesterol and is transported to the plasma membrane in specialized lipid rafts (Simons et al., 2000). Multiple mouse lines in which PLP and its isoform DM20 are misexpressed or improperly trafficked demonstrate a wide range of neurological abnormalities, from extensive OL death and dysmyelination to very mild pathology (Yool et al., 2000). *PLP1* is a human disease gene, and *PLP1* gene duplication causes Pelizaeus-Merzbacher Disease (PMD), a congenital abnormality associated with motor defects, seizures, and intellectual disability. Surprisingly, germline *Plp1* deletion does not result in severe myelination defects in mice, however, myelin eventually loses

integrity, most likely due to decreased lamina stability (Klugmann et al., 1997). PLP synthesis and trafficking in myelinating OLs are described in greater detail below.

MBP

Myelin basic protein is the principal component of compact myelin in both PNS and CNS, and is one of its few "obligatory" protein components. *Shiverer* mice and *long evans shaker* rats deficient for *Mbp* have little to no compact myelin and die prematurely (Roach et al., 1983, Roach et al., 1985, Kwiecien et al., 1998). MBP is a small highly basic protein that is expressed as multiple isoforms and is necessary for myelin compaction, as it resides in the cytosolic parts of the myelin at the major dense line (Figure 1.1C-D, named so for its dark appearance on the electron micrographs) and interacts with negatively charged lipids (Barkovich, 2000). MBP has a unique synthesis fate - it is transported to the myelin sheath as mRNA and is translated locally (Colman et al., 1982). *Mbp* mRNA transport potentially prevents premature membrane compaction (Muller et al., 2013). Intriguingly, initiation of *Mbp* mRNA transport and local translation has been linked to electrical activity in neurons (Wake et al., 2011).

MAG

Myelin-associated glycoprotein (MAG) is the principal component of the non-compact myelin in the CNS and PNS. MAG is well characterized as a potent inhibitor of axonal growth after injury (Mironova and Giger, 2013, Baldwin and Giger, 2015). MAG is enriched in paranodal loops and adaxonal (axon-adjacent) OL membranes (Figure 1.1D), and is important for establishing the initial axon-glia interaction during initiation of myelin formation. MAG is expressed in early immature oligodendrocytes and is a part of myelin-associated machinery in

the adulthood. A more detailed discussion of MAG trafficking is outlined below. Despite its importance in axon-glia contact, $Mag^{-/-}$ knockout mice have a mild hypomeylination phenotype, indicating that MAG is dispensable for compact myelin formation. Nonetheless, $Mag^{-/-}$ animals show structural abnormalities in the periaxonal myelin compartment and demonstrate subtle defects in fine motor tasks (Li et al., 1994, Pan et al., 2005), suggesting sub-optimal physiological conditions for nerve impulse propagation.

CNPase

Glial 2'3'-cyclic nucleotide 3'-phosphodiesterase (CNPase) is an abundant myelin protein in the CNS and PNS that resides in paranodal loops and is not a part of compact myelin. *In vitro* and *in vivo*, CNPase is expressed in premyelinating oligodendrocytes and remains present in the mature axoglial unit. The role of CNPase in myelin stability is not completely understood - however, it's been shown as necessary in maintaining paranodal structures (Rasband et al., 2005). *Cnp* genetic deletion in mice does not result in hypomyelination, but it causes eventual loss of axonal integrity, neurodegeneration, and early death (Lappe-Siefke et al., 2003). Overall, CNPase is considered an important mediator of axoglial communication necessary for myelin stability.

MOG

Myelin oligodendrocyte glycoprotein (MOG) is another non-compact myelin glycoprotein, and until recently its function remained unknown. MOG is expressed late in myelin development and serves as one of the late stage markers for OL maturation *in vitro* (Emery et al., 2009). MOG is expressed mostly in the CNS, with some weak PNS presence (Pagany et al.,

2003). MOG is dispensable for myelin formation, and *Mog*^{-/-} mutants present with no notable defects in compact myelin structure (Delarasse et al., 2003). Von Büdingen et al. recently identified MOG as a novel binding partner of nerve growth factor (NGF) (von Budingen et al., 2015). MOG sequesters free NGF and thus prevents it from binding and activating tropomyosin receptor kinase A (TrkA) on nociceptive unmyelinated axons in the spinal cord. This interaction is thought to be important for preventing abnormal sprouting of small nociceptive fibers and can thus potentially indirectly regulate neuropathic pain. Therefore, these data suggest a novel possibility of myelin-associated proteins regulating the circuitry of unmyelinated axons.

MOG has been extensively studied as a potential autoimmune target in demyelinating encephalopathies. MOG immunization is a classical mouse model of experimental encephalomyelitis (EAE), however, physiological relevance of that model to human disease is rather controversial (Reindl et al., 2013).

P0

Myelin protein zero (P0) is a major structural glycoprotein of the PNS myelin. *P0* global mutants have severely compromised compact myelin formation and functional deficits (Giese et al., 1992, Zielasek et al., 1996). Impaired P0 function in human patients underlies several neuropathies, such as Dejerine-Sottas disease (Martini, 1999). P0 is often considered as a structural equivalent of PLP in the PNS, as it functions to ensure structural integrity of the myelin coil. Nonetheless, these two proteins are not interchangeable, and substituting P0 for PLP in the PNS is devastating to internode formation and leads to early lethality in mice (Yin et al., 2015). P0 interacts with another PNS protein peripheral myelin protein 22 (PMP22), and this interaction is important for formation and maintenance of myelin sheath (D'Urso et al., 1999).
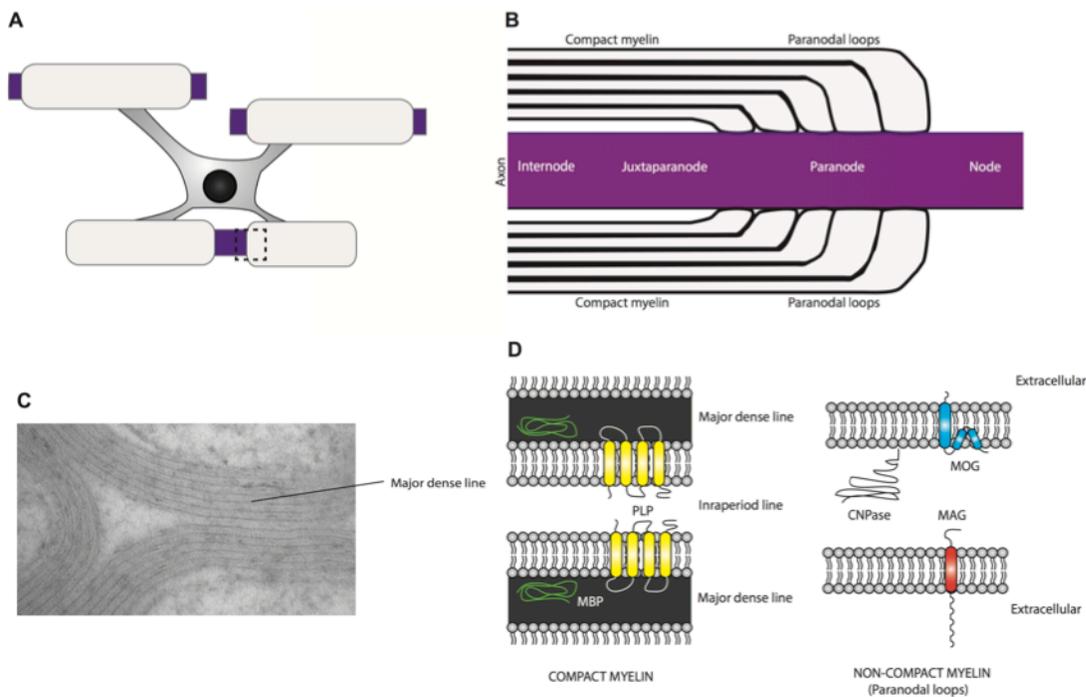
Figure 1.1 CNS myelin: anatomy and ultrastructure (A) Myelinating oligodendrocyte is capable of ensheathing multiple axons at a time. (**B**) A heminode longitudinal section demonstrating anatomical subsets of myelin organization. (**C**) A high magnification transmission electron micrograph of a myelinated fiber in the mature mouse optic nerve (250,000x). Distinct lamination of compact myelin can be easily identified, with major dense line as the darkest part of the structure. (**D**) Molecular organization of compact and non-compact myelin. PLP localizes to the membrane of compact myelin loops where it interacts homophilically to stabilize the loop lamination. MBP is localized in the cytosol of compact myelin loops, where it interacts with negatively charged phospholipids and serves as a sieve maintaining myelin compaction. Principal components of the non-compact myelin are CNPase, MAG on the adaxonal membrane, and MOG on the outer leaflets. Adapted with permission from (Barkovich, 2000) and (Baumann and Pham-Dinh, 2001).

1.4 Myelinating glia of the PNS – Schwann cells

Schwann cells were discovered by Theodor Schwann in 1839 and are thus among the earliest characterized glial cells. Schwann cells arise early during embryogenesis as neural crest derived cells and their development has been extensively characterized (Le Douarin and Smith, 1988). Schwann cell precursors (SCPs) oversee some aspects of axon guidance in the developing PNS. SCPs lack basal lamina and are critically dependent on axonal contact and Neuregulin 1

9

(NRG1) supply (Armati and Mathey, 2010). In contrast, immature Schwann cells are capable of autocrine self-sustenance. Immature Schwann cells are responsible for radial sorting of axons, which eventually leads to the 1:1 relationship between axons and myelinating Schwann cells. NRG1-ErbB signaling is essential for myelination in the PNS.

1.5 Myelinating glia of the CNS – oligodendrocytes

The OL lineage is among the most morphologically and dynamically diverse cellular populations in the brain. It was originally described by a Spanish neuroscientist Pio del Rio Hortega (Perez-Cerda et al., 2015) in the early 20th century. Oligodendrocyte progenitors (OPCs) are simple bipolar glial cells that arise in the spinal cord and forebrain during embryonic development as spatially and temporally distinct waves of precursors (Kessaris et al., 2006). Specifically, OPCs originate in ventral ventricular zone of the dorsal spinal cord at E12.5 and at E15.5. In the forebrain, three waves of OPC generation can be distinguished: early ventral wave from the medial ganglionic eminence and ventral telencephalon at E12.5, second wave from lateral and caudal eminences at E15.5, and the last wave at P0 from the cortical ventricular zone (Kessaris et al., 2006, Crawford et al., 2016b). In the adult brain, dorsally derived OPC populations are dominant (Kessaris et al., 2006, Crawford et al., 2016b). What dictates the distinct population specification of migrating OLs is not very well understood, however, differentially derived OPCs show preference in myelinating particular tracts (Tripathi et al., 2011). Recent evidence suggests OPCs employ blood vessels for navigation from the ventral spinal cord and subventricular zone to dorsal spinal cord and outer layers of the cerebral cortex (Tsai et al., 2016). OPCs are a highly migratory population that remains in the CNS at all ages, albeit at diminished density, and it demonstrates distinct spatial tiling and self-repulsion (Hughes

et al., 2013). OPCs divide asymmetrically and immature oligodendrocytes are rarely "unemployed" – they either die or become myelinating OLs (Hughes et al., 2013, Hill et al., 2014b). OPC lineage is staged by easily identifiable morphological changes and the presence of distinct molecular markers, including transcription factors and cell-surface proteins (classical markers attributed to each stage are listed in the Figure 1.2).
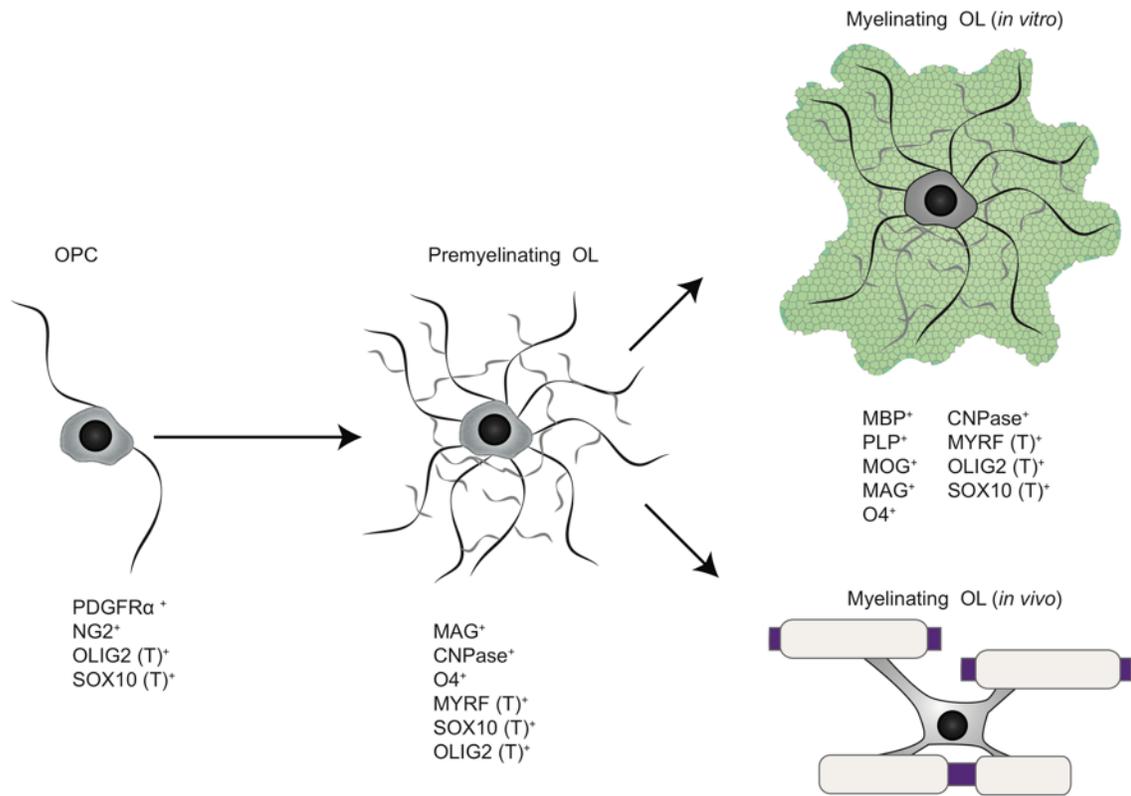
Figure 1.2. Morphological and molecular stages of the OL lineage. Oligodendrdocyte precursors (OPCs) are simple bipolar cells expressing, among other molecules, transcription factors Olig2 and Sox10, and cell-surface markers PDGFRα and NG2. NG2 cells in the adult CNS retain proliferative capabilities, but have a more elaborate morphology (not shown). Premyelinating OLs are postmitotic cells with a complex ramified structure that allows them to make contacts with multiple axons. Immature OL is a transient stage *in vivo*, characterized by expression of O4, CNPase, MAG, and Myelin regulatory factor (Myrf), with downregulation of NG2 and PDGFRα. *In vitro*, mature OLs appear as an "unrolled" membrane sheet robustly expressing myelin markers MBP, MOG, MAG, and PLP in distinct membrane compartments. Myelinating OLs *in vivo* are only found in association with axons. T = transcription factor.

11

In order to generate myelin sheaths, OPCs have to exit proliferation cycle, make nascent axoglial contact and proceed through terminal differentiation (Pfeiffer et al., 1993). Upon differentiation, a large proportion of OLs die at the immature stage, but some make it to myelinating state (Ethan Hughes, personal communications). A myelinating OL undergoes one of the most remarkable transformations of all cell types, generating approximately 5000 μm^2 of myelin membrane every day (Pfeiffer et al., 1993). The biophysics of CNS myelin formation is subject of extensive research (Snaidero et al., 2014). The most recent evidence suggests that initiation of myelination and axon wrapping are mediated by actin dynamics and disassembly at the leading edge of the myelinating OL (Nawaz et al., 2015, Zuchero et al., 2015). Interestingly, MBP and actin have non-overlapping domains in the membrane expansion of myelinating OLs, and *in vitro* evidence suggests an indirect competitive interaction between MBP and actin disassembly (Zuchero et al., 2015). Zebrafish studies demonstrated that once an OL is committed to myelinating a particular axon, the process of ensheathing happens during a short period of time (Czopka et al., 2013, Nawaz et al., 2015) and afterwards is subject to limited modification. Myelinating OLs greatly contribute to the metabolic support and stability of neurons, notably by supplying axons with lactate for ATP regeneration (Lee et al., 2012, Saab et al., 2013).

The mechanisms controlling the OL lineage at all stages are of great interest as they must dictate homeostatic maintenance of the precursor pool, it's adequate migration, differentiation, and myelination, both *de novo* and for replacement of damaged or dying oligodendrocytes (Bergles and Richardson, 2015). Multiple mechanisms have been suggested to regulate these processes. The OL lineage is highly responsive to the mitogen platelet-derived growth factor (PDGF) and its availability is considered as one of the limiting steps in the OPC pool maintenance (Durand and Raff, 2000). OPCs are highly self-repulsive (Hughes et al., 2013),

indicating a strong cell-autonomous regulation of their spatial distribution throughout the brain. Astrocytes and the OL lineage cells are gap-junction coupled, and astrocytic regulation, whether direct or indirect (via neurons) greatly affects myelin dynamics (Ishibashi et al., 2006, Orthmann-Murphy et al., 2007, Hill and Grutzendler, 2014). For example, combined genetic deletion of astrocyte-specific gap junction proteins connexin *Cx30* and OL-specific *Cx47* results in premature lethality and myelination defects in mouse models (Tress et al., 2012). In addition, astrocytes are a major source of mitogenic factors such as PDGF and neurotrophin-3 (NT3) necessary for OPC proliferation, thus exuding a non-cell-autonomous control over the OL lineage (Barres and Raff, 1993).

Neuron-OL interaction is one of the most studied intercellular couplings in the nervous system. In particular, neuronal signals that contribute to either myelination-permissive or prohibitive environments for the immature OL (Fields, 2015) are a subject of extensive research. One of the most intriguing aspects of oligodendrocyte biology is their unique propensity for myelinating only axons and not any other neuronal structures (soma and dendrites) or any other cells (other OLs, astrocytes, microglia) *in vivo*. Furthermore, only a subset of axons is myelinated in the CNS, and myelinated and non-myelinated axons are readily found in the same anatomical structure. For example, in the corpus callosum only 30% axons are myelinated (Sturrock, 1980). This suggests the presence of either anti- or pro-myelinating cues expressed by respective axonal populations. Interestingly, *in vitro* OLs are highly promiscuous in their ensheathing activity, and can make myelin wraps on polysterene fibers of a diameter above 0.4 μm, and even on fixed axons and dendrites (Lee et al., 2013, Mei et al., 2014). While such myelin wraps never achieve the true compact myelin structure, their very presence strongly indicates the existence of inhibitory cues *in vivo* that dictate the OL preference for one

population of axons over the other. Multiple cell-adhesion molecules have been identified as negative regulators of CNS myelination (Sharma et al., 2015). A recent RNA sequencing screen identified junction adhesion molecule 2 (JAM2) as a novel soma- and dendrite-specific protein that is inhibitory to myelination. *In vitro*, OLs fail to make myelin wraps on micropillars coated with JAM2-Fc, suggesting its inhibitory activity *in trans*. In *Jam2* knockout mice, there is a significantly increased number of myelinated cell bodies in the spinal cord compared to wild-type, suggesting dis-inhibition of myelination occurring in the absence of JAM2 (Redmond et al., 2015, personal communications). JAM2 is certainly not the only inhibitor of myelination, other notable cell-autonomous and non-cell-autonomous myelination "breaks" include leucine-rich repeat and immunoglobulin-like domain contain protein (LINGO1), polysialylated-neural cell adhesion molecules (PSA-NCAMs), Jagged1 and its ligand Notch, and limbic system-associated membrane protein (LSAMP) (Wang et al., 1998, Mi et al., 2005, Sharma et al., 2015). Of signaling pathways, β-catenin-Wnt and Notch have been shown to inhibit transition from OPC to myelinating OL (Park and Appel, 2003, Fancy et al., 2009, Langseth et al., 2010). Recent evidence suggests that Wnt signaling regulates OPC interaction with endothelial cells, detachment from blood vessels, and subsequent maturation (Tsai et al., 2016). Interestingly, there is a large body of evidence indicating that disruption of such fundamental cellular process as trafficking in both neurons and oligodendrocytes can lead to profound defects in myelination (Mironova et al., 2016), chapter II). A more detailed discussion of that pathway is provided below.

There is increasing evidence suggesting that neuronal electrical activity can contribute to OL differentiation and myelination. The current consensus in the field is that myelination is shaped by activity-dependent and activity-independent mechanisms (Zuchero and Barres, 2013).

The absolute necessity of neuronal activity for white matter formation, however, is a subject of an ongoing debate. Current evidence suggests that electrical activity exudes distinct effects on OL proliferation, differentiation, and axon wrapping. For example, classic studies by Barres and Raff revealed that after blocking electrical activity in the optic nerve with tetrodotoxin (TTX), OPC proliferation decreases dramatically (Barres and Raff, 1993). However, a recent elegant live imaging study in zebrafish spinal cord revealed that TTX silencing of action potentials in axons does not affect the OL proliferation and differentiation *per se*, but rather influences their choice of which axons to myelinate (more on this study below, (Mensch et al., 2015). These discrepancies may be attributed to inherent differences in model systems and their respective limitations.

OPCs are the only non-neuronal cell type that expresses both N-methyl-d-aspartate (NMDA) and alpha-amino-3-hydroxyl-5-methyl-4-isoxazole-propionate (AMPA) receptors and harbor functional post-synaptic sites (Bergles et al., 2000, Karadottir et al., 2005). Unmyelinated axons and OPCs form transient synaptic structures, which can be detrimental under pathological conditions associated with excessive glutamate release (Lin et al., 2005, Ziskin et al., 2007). Establishing the true physiological importance of glutamatergic signaling between neurons and OPCs has been rather challenging. For example, genetic deletion of the obligatory NMDAR subunit NR1 specifically in the OL lineage does not have significant effects on OPC/OL proliferation, differentiation, and myelination (De Biase et al., 2011). An intriguing new study suggests that a well-established PNS myelination regulator NRG1 enhances CNS myelination by initiating a switch from activity-independent to NMDA- (i.e. activity)-dependent mode *in vitro* (Lundgaard et al., 2013). Another recent *in vitro* study, however, demonstrated that DRGs and OPCs communicate via nonsynaptic vesicular release along the axonal length (Wake et al.,

2015), and OLs preferentially myelinate electrically active axons. Intriguingly, recent evidence suggests that PLP participates in relaying glutamatergic signal in the migratory OPCs, which is an unexpected function for a primarily structural myelin protein (Harlow et al., 2015). OPCs also express gamma-aminobytric acid (GABAR) receptors and receive inhibitory inputs. Inhibitory neuron- OPC interaction is well characterized in the cerebellum, where NG2^{+} glia receive GABAergic inputs from Purkinje cells (Lin et al., 2005, Etxeberria et al., 2010). Fyn kinase signaling has been extensively studied as a potential molecular conduit unifying neuronal electrical activity and myelination. Fyn kinase plays an important role in multiple pathways involved in myelination, such as pro-differentiation/survival OL signaling, transport, and local translational control (Kramer-Albers and White, 2011). Importantly, Fyn kinase signaling is linked to *Mbp* mRNA synthesis and transport that is activated by neuronal electrical signal (Wake et al., 2011).

1.6 Disorders of myelin

In the absence of myelin axonal conduction velocity precipitously drops in both CNS and PNS. Furthermore, sub-optimal myelin thickness or aberrant myelin formation can also have a profound effect on neuronal communication (Fields, 2015). Given the metabolically beneficial relationship between myelinating glia and axons, there is an increased risk of neurodegeneration associated with faulty myelin (Nave and Trapp, 2008), thus resulting in further neurological damage. Myelin formation is incredibly complex, and there are multiple congenital disorders associated with improper myelin development and function. Noted developmental disorders associated with impaired CNS myelination are leukodystrophies, which include, among many others, Pelizaeus-Merchbacher disease, spastic paraplegia type S, and Niemann-Pick disease.

These conditions are characterized by intellectual disability, seizures, and reduced lifespan. There is increasing evidence that myelin defects are associated with schizophrenia (Nave and Ehrenreich, 2014). In addition to congenital abnormalities, OPCs are highly vulnerable to environmental factors during embryonic development and early infancy. In particular, white matter lesions are frequently observed in premature infants under 1500 g in weight at the time of birth (Khwaja and Volpe, 2008). Hypoxia-ischemia (HI) and inflammation are the most common causes of white matter injury associated with prematurity. Noted clinical conditions associated with HI white matter damage are pervintricular leukomacia (PVL) and diffuse white matter injury (DWMI). Interestingly, in the neonatal rat model of PVL infusion of AMPAR antagonist NBQX alleviates some of the PVL symptoms, suggesting the role of glutamatergic toxicity in disease development (Follett et al., 2000). DWMI is associated with chronic hypoxia in preterm babies, and is characterized by impaired myelinating properties of the OL lineage. Zonouzi and colleagues recently identified that hypoxia results in decreased GABAergic input onto $NG2^+$ glia in the cerebellum, thus leading to their impaired proliferation and differentiation. Systemic administration of the GABAergic drugs tiagabine and vigabatrin ameliorates the negative effects of hypoxia on the OPC proliferation and terminal differentiation (Zonouzi et al., 2015).

PNS myelin disorders are associated with multiple neurological conditions, most notably peripheral neuropathies, such as Guillain-Barre syndrome and Charcot Marie Tooth (CMT) disease. Traditionally, neuropathies are classified as 1) demyelinating, characterized by histological evidence of degenerating myelin (onion bulbs, myelin outfoldings, etc.) and reduced conduction velocity of peripheral nerves, and 2) axonal, with amplitude decrease and distal weakness (Dyck and Lambert, 1968). There are also neuropathies that bear manifestations of

both axonal damage and demyelination - for example, CMT4J (Chow et al., 2007). A more detailed discussion of CMT4J pathophysiology and molecular mechanism is below.

1.7 Myelination and white matter repair in the adult CNS

In the CNS, developmentally formed myelin is a fairly stable structure, however, it does undergo remodeling in adulthood. In mature mice, myelination in the cerebral cortex is an ongoing process (Hughes et al., 2013, Hill et al., 2014b, Schain et al., 2014). Adult OPCs (or NG2+ glia) originate at least in part from subventricular zone (SVZ, (Menn et al., 2006) and are found in the brain at all life stages. Interestingly, white matter OPCs divide more actively than their grey matter counterparts and the OPC proliferation rate is brain region-dependent. For example, OPCs divide more actively in the corpus callosum than in the optic nerve (Young et al., 2013). Intriguingly, a new report suggests that *de novo* myelination in the adult CNS can happen in response to persistent neuronal activity and thus may serve as an additional regulator of plasticity in learning and memory (de Hoz and Simons, 2015). Depriving mice of social interaction in the third and fourth postnatal weeks results in significantly decreased cortical myelination (Makinodan et al., 2012). Of note, this type of activity-dependent myelination is mediated by NRG1-erBB3 signaling. Repeated optogenetic stimulation of cortical projection neurons leads to increased myelin thickness and OPC proliferation, although a direct causal relationship has not been established (Gibson et al., 2014). Interfering with OPC differentiation in the adult mouse CNS impedes on the animal's ability to learn new motor tasks (McKenzie et al., 2014). These data corroborate imaging data indicating increased region-specific white matter volume in humans gaining proficiency in complex games and motor tasks such as juggling and playing piano (Bengtsson et al., 2005, Scholz et al., 2009, Lee et al., 2010). Intriguingly, a new

study examining incorporation of ^{14}C in oligodendrocytes suggests a very limited OL turnover in the human corpus callosum that cannot account for the turnover of myelin itself (Yeung et al., 2014). Furthermore, Yeung et al. established that in postmortem brain samples from individuals aged 0.2-92 years, the number of oligodendrocytes peaked at 5 years of age and then remained stable since. These data suggest a fascinating possibility that human and rodent adult myelination dynamics may be fundamentally different (Yeung et al., 2014). Given the drastic differences in human vs. rodent astrocytes (Oberheim et al., 2009), it is feasible that human myelinating OLs are more potent in their myelinating ability compared to murine and rat counterparts.

In the event of a myelinating OL death or damage to the existing myelin sheath, OPCs generate new immature OLs to restore myelin. In the rodent CNS, existing myelinating OLs are incapable of "taking over" or repairing the lesion (Crawford et al., 2016a). Myelin formed in the adult CNS is thinner with shorter internodes, however, differential sodium channel clustering and expression presumably allows compensation for sub-optimal myelination and action potential propagates normally (Brill et al., 1977). Intriguingly, after demyelinating lesion in the cerebellar peduncle, "naked" axons make *de novo* synaptic contacts onto OPCs, and pharmacologic inhibition of OPC AMPAR and NMDAR impairs remyelination (Gautier et al., 2015).

There is a substantial mechanistic overlap between myelination in the developing and adult CNS, however, there are some distinctions – notably, the OPC origin and their ability to proliferate and differentiate (Crawford et al., 2016b). In the adult brain, the majority of OPCs are dorsally derived, and in aged mice they display limited ability to differentiate and form mature myelin sheaths (Crawford et al., 2016b). In contrast, ventrally derived OPCs, despite their reduced presence in the aged brain, display a constant rate of differentiation. These data suggest

an interesting possibility of targeting differentially derived OPCs for potential therapeutic endeavors.

Like most post-mitotic neural cell types, OLs are fragile and highly vulnerable to stroke, trauma, or inflammation. The most notorious human condition associated with damage to the myelin sheath is multiple sclerosis (MS), an autoimmune condition in which inflammatory response is directed towards the white matter. MS attacks vary in their severity and functional consequences, but can lead to devastating pathologies, such as impaired cognition, compromised motor and sensory functions, and blindness (Hauser et al., 2013). While some progress has been made in stalling MS episodes by pharmacological targeting of immune cells, very little can be currently done to restore myelin damage. The key strategy in repairing MS lesions is to enhance the ability of adult OPCs to differentiate and myelinate. Remarkable advances have been made in differentiating human OPCs either from pluripotent stem cells or differentiated cells such as fibroblasts by genetic reprogramming (Goldman, 2016). A combination of only 3 transcription factors (Sox10, Olig2, and Zfp536) as reported by (Yang et al., 2013) is sufficient to reprogram rat fibroblasts into OPCs that are myelination-competent. Amazingly, human OPCs derived from reprogrammed cells are capable of successfully restoring myelin in *shiverer* hypomyelinated mutant mice (Wang et al., 2013). The most exciting application of this approach is high-throughput drug screening of human OPC populations in search for small molecules capable of augmenting OL differentiation and myelination *ex vivo*. Najim et al. recently identified small molecules miconazole and clobetasol as potent enhancers of myelination in the CNS and remyelination after injury (Najm et al., 2015). While still a distant future, there is hope that otherwise incurable conditions such as congenital leukodystrophies may be corrected by an OPC transplant and/or pharmacological treatment (Osorio and Goldman, 2016).

In contrast to the CNS, peripheral nervous system is capable of efficient and successful regeneration after injury. Schwann cells themselves contribute extensively to PNS myelin and axonal repair. Schwann cells are capable of assuming an immature state with a dramatic change in their protein expression, and this de-differentiation greatly contributes to the efficiency of PNS lesion repair. Schwann cells actively participate in axonal regeneration and clearance of myelin debris via phagocytosis and autophagy (Woodhoo and Sommer, 2008).

1.8 Intracellular trafficking and myelination

Myelinating glia are highly polarized cells with distinct membrane compartments that resemble apical and basolateral organization of epithelial cells (Masaki, 2012). Different components of myelin sheath are trafficked via distinct routes depending on their final destination. Given the massive and rapid membrane expansion that myelinating cells must undergo in order to generate compact myelin, intracellular transport is critical for their proper function. In addition, bidirectional axo-glial interaction in myelination requires neurons to communicate in a timely manner whether or not their axons are to be myelinated. Given the tremendous distance between distal axonal compartments and neuronal soma, properly functioning neuronal intracellular transport plays an important role in myelin formation. Here we review some of the core concepts of endolysosomal trafficking and what is currently known about its role in myelin formation and maintenance.

Endolysosomal axis of the intracellular trafficking pathway

Intracellular trafficking is a conserved process that operates in all eukaryotic cells. In highly simplified terms, trafficking encompasses the secretory pathway, wherein cargo is

synthesized in the endoplasmic reticulum (ER) and is subsequently released at the plasma membrane, and endocytic pathway, where the material is endocytosed at the plasma membrane and either transported for degradation or recycled back (with or without additional modifications, Figure 1.3). Each trafficking organelle is characterized by its own set of functional markers, notably N-ethylmaleimide-sensitive factor attachment protein receptor complex (SNARE), Ras-associated binding proteins (Rab GTPases), ADP ribosylation factor (Arf) GTPases, and phosphoinositides (PIPs). These dynamic markers define the identity of the organelle at a given time and mediate cargo progression. PIP function and synthesis are described in greater detail below. Early endosomes (EE) are the principal sorting stations of the endocytic pathway, as they receive cargo endocytosed from the plasma membrane. EEs have distinct tubo-vesicular subdomains that harbor sites of efficient cargo sorting to either late endosome/lysosome, retrograde Golgi transport, or recycling endosome. Hallmark EE proteins are Rab5 GTPase and Rab5 effector early endosome antigen 1 (EEA1). Cargo destined for recycling is transferred to recycling endosomes where it is transported back to the plasma membrane. As the EE differentiates into late endosome or multivesicular body (LE, MVB), it undergoes a switch from Rab5 to Rab7 GTPases and lumenal acidification. LE is responsible for hydrolysis of cargo and its delivery to lysosome, as well as transfer of materials necessary for lysosomal maintenance. Hybrid endosome-lysosome structures are referred to as endolysosomes (Huotari and Helenius, 2011). Lysosomal hallmark proteins are lysosomal associated membrane proteins (LAMPs) and various hydrolases. Lysosomes also fuse with autophagosomes which are responsible for delivering organelle content (Lodish, 2008). Interestingly, emerging evidence suggests that late endosome-lysosomal (LE/Lys) stage of membrane transport has a much more complicated role in cellular homeostasis than simply cargo recycling and disposal. The discovery of a lysosomal

22

gene network (Coordinated Lysosomal Expression and Regulation or CLEAR) and its master regulator transcription factor EB (TFEB) identified the late endosome/lysosome (LE/Lys) compartment of the endolysosomal axis as a crucial hub of cellular nutrient sensing and transcriptional feedback regulation (Sardiello et al., 2009, Settembre et al., 2011). Furthermore, materials trafficked to the lysosome were previously considered destined exclusively for disposal, however, there is evidence suggesting that multiple proteins can be stored and released from lysosomes in a regulated fashion (Blott and Griffiths, 2002) (Figure 1.3).
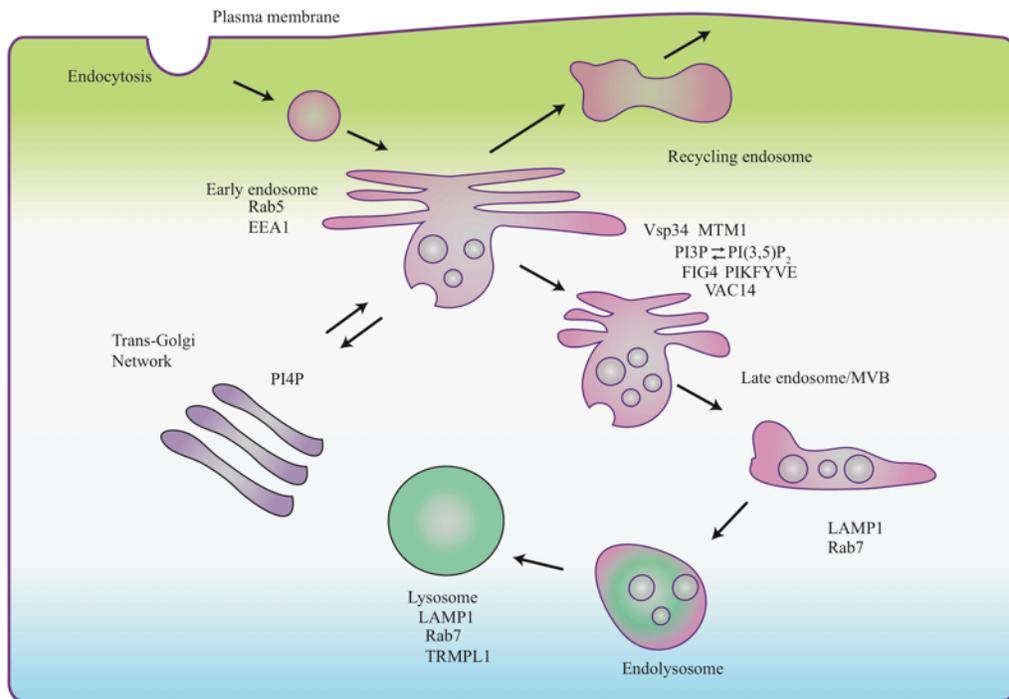
Figure 1.3 Endolysosomal trafficking. An overview of the endolysosomal trafficking pathway and some of its hallmark regulators. Modified with permission from (Huotari and Helenius, 2011) and (McCartney et al., 2014a).

Phosphoinositides in intracellular transport

Given the continuous nature of intracellular trafficking and the necessity for accurate transition of cargo to and from the appropriate organelles, a rapidly adaptive signaling system regulating the effector protein network is essential. Several species of signaling phosphoinositides (PIPs) are well-defined regulators of intracellular transport. PIPs are phosphorylated forms of phosphatidylinositol (PI), and there are seven known PIP species in mammalian cells. In particular, PI3P and $PI(3,5)P_2$ regulate distinct stages of endolysosomal trafficking. PI3P an abundant PIP involved in a multitude of intracellular processes. It is generated from PI by a 3-Kinase Vsp34 and is localized to early endosomes and MVB vesicles (Gillooly et al., 2000, Gillooly et al., 2001). PI3P is dephosphorylated by several 3-phosphatases of myotubularin family (MTM1). PI3P interacts with multiple EE proteins, in particular indirectly with EE proteins Rab5 and EEA1. PI3P regulates nutrient sensing and autophagy, among other processes (Bridges et al., 2012).

$PI(3,5)P_2$ was discovered relatively recently due to its extremely low abundance in cells under basal conditions (Dove et al., 1997). Nonetheless, it is a critically important PIP for a multitude of cellular processes. Recent freeze-fracture analysis confirmed alleged $PI(3,5)P_2$ localization to early endosome vesicular compartment (Takatori and Fujimoto, 2016). $PI(3,5)P_2$ is actively involved in nutrient sensing and osmotic shock regulation in yeast, regulates fission in the LE/Lys compartment, autophagy, MVB formation, and transport to the trans-Golgi network (Zolov et al., 2012, McCartney et al., 2014a, Jin et al., 2016). $PI(3,5)P_2$ binds to and activates multiple proteins, including Raptor, S6K, Ca^{2+} channel TRMPL1 (Mucolipin 1), and two-pore TPC channels (Dong et al., 2010, Bridges et al., 2012, Shen et al., 2012, Wang et al., 2012, Jin et al., 2014). $PI(3,5)P_2$ is generated continuously from its much more abundant precursor PI3P by a

unique macromolecular complex consisting of the 5-kinase PIKFYVE, 5-phosphatase factor induced gene 4 (FIG4), and a scaffold VAC14 (Figure 1.4). PIKFYVE (or FAB1) is a large protein bearing a FYVE domain that is involved in endolysosomal dynamics. PIKFYVE is responsible for generation of all $PI(3,5)P_2$, although confirming so is problematic due to low $PI(3,5)P_2$ abundance (Zolov et al., 2012). PIKFYVE is absolutely essential for normal cell functions, and *Pikfyve* germline mouse mutants die at the pre-implantation stage at E3.5 due to impaired DNA synthesis (Ikonomov et al., 2011). PIKFFYVE activity can be modulated pharmacologically with small molecule inhibitors YM201636 and apilimod (Zhang et al., 2012, McCartney et al., 2014b). Bath application of either inhibitor in nanomolar - low micromolar range results in rapid decrease of $PI(3,5)P_2$ levels and subsequent accumulation of enlarged LE/Lys organelles in cells (Jefferies et al., 2008, Ikonomov et al., 2009, Cai et al., 2013), Chapter II). VAC14 is a scaffold protein consisting mostly of HEAT repeats and it interacts with and stabilizes PIKFYVE and FIG4. Loss of *Vac14* results in perinatal lethality of mouse mutants (Jin et al., 2008, Zhang et al., 2007). The missense *Vac14* mutation L156G (infantile gliosis or *ingls*) destabilizes the VAC14-PIKFYVE interaction and, depending on genetic background, results in either perinatal lethality of mutant mice, or limited lifespan associated with severe multi-organ defects (Jin et al., 2008). On a cellular level, loss of *Vac14* also results in accumulation of enlarged vesicles positive for LE/Lys markers LAMP1 and Rab7. VAC14 interacts with Rab5 and Rab7 suggesting its other functions besides the $PI(3,5)P_2$ biosynthetic complex (Jin et al., 2008). A new study identified human Vac14 mutation, ….FIG4/SAC3 is a 5-phosophatase that removes the 5-phosphate on $PI(3,5)P_2$, thus regulating the turnover of PI3P and $PI(3,5)P_2$. Paradoxically, genetic *Fig4* inactivation results in decreased levels of $PI(3,5)P_2$, due to the role of FIG4 in stabilizing and activating PIKFYVE (Botelho et al., 2008).
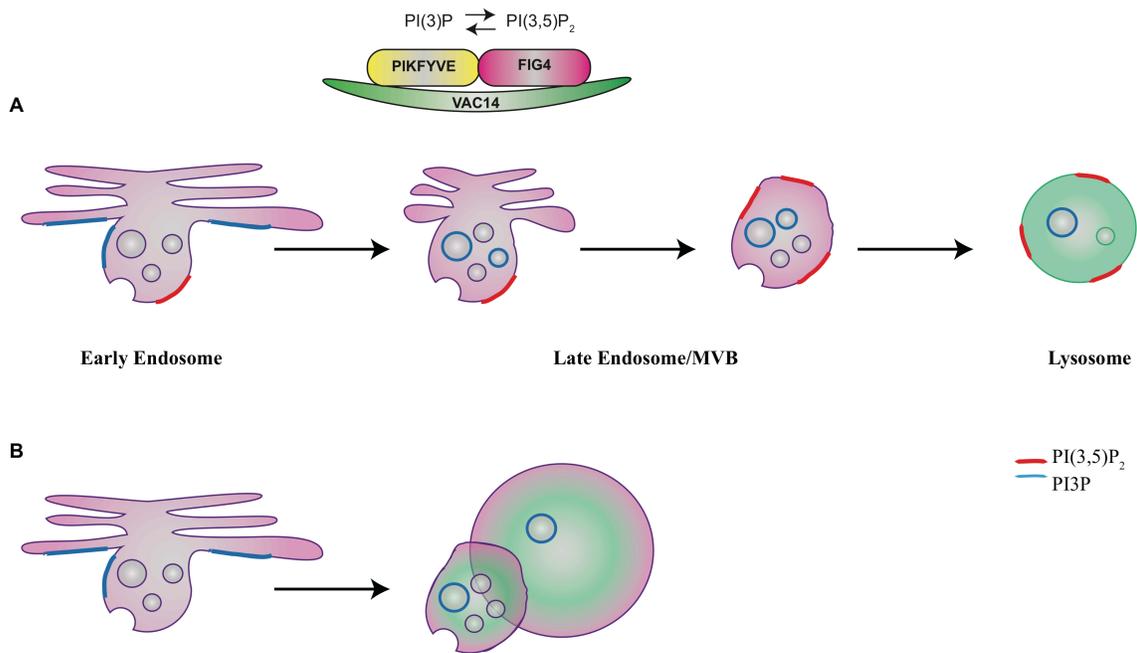
Figure 1.4 The PI(3,5)P$_2$ biosynthetic complex in health and disease. (A) Rapid and persistent interconversion of PI3P and PI(3,5)P$_2$ signaling PIPs is executed by a macromolecular complex including 5-kinase PIKFYVE, 5-phosphatase FIG4, and a scaffold VAC14. The complex is putatively localized to the early endosome membranes, however, there is evidence of its association with late endosomes and lysosomes (Zhang et al., 2012). **(B)** Reduced PI(3,5)P$_2$ levels due to impaired function of its biosynthetic complex leads to accumulation of LE/Lys material in the cell, which is deleterious to its health. Modified with permission from (Huotari and Helenius, 2011) and (McCartney et al., 2014a).

In culture, *Fig4$^{-/-}$* cells, including neural cell types, accumulate enlarged LAMP1 vesicles, and this defect can be rescued by overexpression of *WT-Fig4*. *Fig4* germline mutant mice present with a complex pathological phenotype, including impaired gait, fur discoloration, skeletal, spleen, heart, and neurological abnormalities. Notably, *Fig4*-deficient CNS and PNS show a striking region-specific spongiform-like neurodegeneration. Lifespan of *Fig4$^{-/-}$* mice is greatly reduced, and depending on genetic background they survive up to 6 weeks postnatally

(Chow et al., 2007). *Fig4* loss of function in *Drosophila* similarly leads to neurological defects (Kyotani et al., 2016). Intriguingly, transgenically overexpressing *Fig4* in neurons using neuron-specific enolase promoter (*NSE-Fig4*) on otherwise null *Fig4* background in mice rescues the majority of pathological manifestations associated with *Fig4* loss of function *in vivo* (Winters et al., 2011, Ferguson et al., 2012b). These data suggest the critical importance of properly functioning FIG4 in neurons. When FIG4 is rendered catalytically dead and expressed under the same *NSE* promoter, some, but not all *Fig4*$^{-/-}$-associated defects are rescued, suggesting the importance of both catalytic and non-catalytic FIG4 functions in neurons (Lenk et al., 2016a). Similar observations were made in a *Drosophila* model of FIG4 catalytic inactivity, indicating its highly conserved function (Bharadwaj et al., 2016).

FIG4 is a human disease gene that is associated with several autosomal-recessive disorders. Most notably, mutations in FIG4 cause Charcot Marie-Tooth Disease Type 4J (CMT4J) – a devastating variant of CMT peripheral neuropathy that leads to wheelchair dependence in human patients (Chow et al., 2007, Zhang et al., 2008, Nicholson et al., 2011, Menezes et al., 2014). CMT4J patients are compound heterozygotes, with one null allele and another carrying a missense I41T mutation that destabilizes FIG4 but does not disrupt its catalytic activity (Lenk et al., 2011). Interestingly, human CMT4J patients are cognitively neurotypical and present with no CNS abnormalities. In mouse models, I41T overexpression on a null *Fig4* background rescues pathological phenotypes in a dose-dependent manner, indicating that the I41T mutation does not disrupt FIG4 function entirely. I41T is not the only FIG4 mutation associated with CMT-like neuropathy (Nicholson et al., 2011), as other *Fig4* mutations have been reported in CMT patients, with a highly variable age of onset and severity of disease. A D783V mutation in the *FIG4* C-terminal domain results in polymycrogyria with epilepsy, with

limited PNS pathology (Baulac et al., 2014). A characterized family had 6 affected siblings, with severe anatomical defects of the cerebral cortex and epileptic and neuropsychiatric disorder manifestations. Interestingly, unlike *I41T-Fig4*, *D783V-Fig4* is not able to substantially rescue the vacuolation phenotype in cultured *Fig4*$^{-/-}$ fibroblasts, suggesting it as a more deleterious mutation. A complete loss of *FIG4* function due to two loss-of-function mutations is the genetic cause of Yunis-Varon (YVS) syndrome, an extremely severe congenital disorder. YVS patients present with gross skeletal abnormalities, profound neurodegeneration, and early death (Campeau et al., 2013). To this date, YVS is the most severe disorder associated with impaired phosphoinositide biosynthesis, underscoring the crucial importance of PIP homeostasis for normal physiology. Furthermore, a new study identified *VAC14* as another human disease gene, providing further evidence for the necessity of PI(3,5)P$_2$ for normal health (Lenk et al., 2016b).

Building white matter: trafficking of myelin blocks in myelinating oligodendrcoytes

Myelin-associated proteins are generated and distributed via distinct routes of the endolysosomal axis (Winterstein et al., 2008) (Figure 1.5). PLP, MAG, and MOG are transported to the plasma membrane where they are subsequently endocytosed via the clathrin-dependent (MAG and MOG) and independent (PLP) pathways. While MAG and PLP are transiently accumulated in the LE/Lys compartment of the OL cell body and processes, MOG is trafficked to the plasma membrane via a recycling endosome. It is possible that these distinct trafficking routes permit a more efficient deposit of myelin proteins to their final destinations – PLP in compact myelin, MAG in paranodal loops and MOG at the outer myelin leaflets. PLP transport has been characterized extensively due to the abundance of this protein in compact myelin and pathological conditions associated with mislocalized PLP in developing OLs.

Intriguingly, PLP can be stored in the LE/Lys compartment of cultured primary OLs and Oli-neu cell line under standard OL culture conditions (Trajkovic et al., 2006). However, in the OL-neuron co-cultures or in the presence of neuronal medium, PLP is released from LE/Lys storage is transported to the apical membrane (more on that in Chapters II and IV).
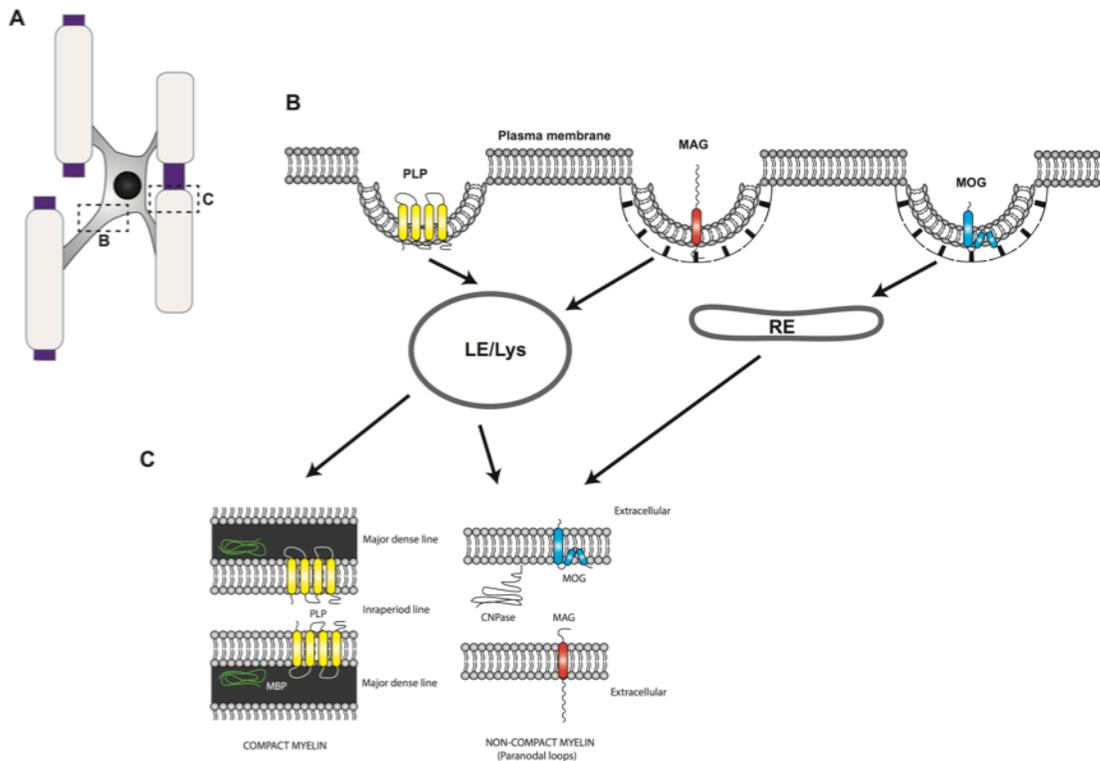
Figure 1.5 Distinct trafficking fates of myelin building blocks. **(A)** Myelinating oligodendrocyte. **(B)** Distinct trafficking fates of myelin-associated proteins at the plasma membrane and their ultimate destination at the myelin sheath **(C)**. Modified with permission from (White and Kramer-Albers, 2014).

Neuronal intracellular transport and myelin regulation

Intracellular trafficking is heavily utilized in neurons due to their polarized organization and considerable distance between neuronal compartments. Several recent studies indicate a potential functional relationship between neuronal vesicular release and OL myelination. Mentsch et al. demonstrated that selectively silencing axons by blocking VAMP2 vesicular release results in shortened internode and preferential selection by OLs for axons with normal vesicular function (Mensch et al., 2015). These data indicate the necessity of synaptic exocytosis for stabilization of nascent myelination. In contrast, Wake et al. demonstrated in mammalian DRG/OL co-culture that myelination is influenced by vesicular release from axons that is not synaptic but takes place along the length of the axon. The actual cargo content of vesicular exchange between neurons and OPCs/OLs remains to be established. However, all studies underscore the importance of vesicular transport in neurons for myelin formation. There is a great spike of interest in exosomal mediated cell-cell interaction (Chivet et al., 2012). Exosomes are small secretory vesicles that originate in multivesicular bodies and can deliver various forms of cargo from one cell to another, including RNA, proteins, and lipids. In neurons, exosomal release is involved in synaptic plasticity (Lachenal et al., 2011, Chivet et al., 2012). De-differentiated Schwann cells secrete exosomes that enhance PNS axonal regeneration after injury (Lopez-Verrilli et al., 2013). Oligodendrocytes release PLP and CNPase via exosomes (Kramer-Albers et al., 2007) and can cell-autonomously inhibit myelination via exosomal communication (Bakhti et al., 2011). A recent study showed that neuronal activity leads to Ca^{2+} entry through AMPA and NMDA receptors on OPCs that triggers exosomal release. (Fruhbeis et al., 2012, Fruhbeis et al., 2013). Exosomes are then taken up by neurons, and that uptake exudes beneficial effect on neuronal health under stress conditions, indicating this pathway as a regulator of

axoglial support. It would be of great interest to examine whether impaired exosomal release in neurons influences myelination in the CNS.

Disorders of trafficking and myelination

Impaired endolysosomal trafficking is an underlying cause of multiple conditions associated with CNS and PNS hypomyelination in human patients and animal models. As mentioned above, mistrafficking of PLP results in hypomyelination disorders in human patients and mouse models. *PLP1* gene duplication in PMD causes accumulation of PLP in the LE/Lys compartment, which leads to abnormal cholesterol aggregation and misrouting of cerebosides (Simons et al., 2002). Such fundamental impairment of lipid raft assembly and lipid-protein targeting to myelination sites downregulates cholesterol synthesis, causes severe defects in white matter formation, and can lead to oligodendrocyte death. Intriguingly, dietary supply of cholesterol to PMD mice promotes myelin synthesis and alleviates axonal damage and motor defects (Saher et al., 2012).

Impaired cholesterol trafficking underlies Niemann Pick Disease (NPC), a devastating leukodystrophy with intracellular lipid accumulation and severely impaired myelin. NPC1 is a LE/Lys membrane protein that serves as a critical regulator of cholesterol efflux in the LE/Lys compartment. Intriguingly, *Npc1* conditional deletion in both neurons and oligodendrocytes in mice results in a CNS hypomyelination phenotype (Yu and Lieberman, 2013). Yu et al. suggested that absence of NPC1 results in impaired Fyn kinase activity as evidenced by its reduced phosphorylation in the brain tissue of conditional mutants. Fyn kinase localizes to cholesterol-rich lipid rafts, providing a potential functional link between NPC1 LOF and Fyn kinase perturbed activity, however a direct mechanistic relationship is yet to be established. Tet-

inducible transgenic *WT-Npc1* overexpression under *Eno2* (*NSE*) promoter rescues hypomyelination in $Npc1^{-/-}$ mice (Lopez et al., 2011), suggesting a non-cell autonomous regulation of NPC1-dependent myelination, most likely due to the regulation of cholesterol supply and demand. However, a complementary experiment of overexpressing *Npc1* in the OLs is yet to be performed, and overexpressing *Npc1* in GFAP$^+$ astrocytes does not correct any pathology in *Npc1* germline knockouts.

Interestingly, *Fig4* mutant mice, along with the previously described neurological phenotypes, present with severe CNS and PNS hypomyelination (Winters et al., 2011). Strikingly, transgenically overexpressing *Fig4* in neurons rescues hypomyelination phenotype observed in the global knockout, suggesting a non-cell-autonomous contribution of neuronal FIG4 to myelination. However, catalytically dead *Fig4* overexpression does not rescue hypomyelination to the extent of the *WT-Fig4* (Lenk et al., 2016a) suggesting that dynamic PI(3,5)P$_2$ biosynthesis is necessary for myelination. MRI in infants with Yunis-Varon syndrome revealed corpus callosum thinning, indicating impaired CNS myelination as a consequence of FIG4 loss of function in humans (Campeau et al., 2013). The role of PI(3,5)P$_2$ in CNS myelination is the central focus Chapters II and III. Human patients for CMT4J do not present with CNS hypomyelination, however, their PNS shows myelin defects. PNS conditional *Fig4* deletion demonstrates that deleting *Fig4* specifically in motor neurons (F*ig4$^{-/flox}$,HB9Cre* mice) results in neurodegeneration and mild hypomyelination. Condtional *Fig4* ablation in Schwann cells also leads to hypomyelination that worsens with age (*Fig4$^{-/flox}$,P0Cre* mice, (Vaccari et al., 2015).

Mutations in human *TRPML1* (*MCOLN1*) cause mucolipidosis IV, a lysosomal storage disorder with severe white matter pathology (Grishchuk et al., 2014). As TRPML is a cation

channel localized to the LE/Lys and activated by PI(3,5)P$_2$ (Dong et al., 2010), there may be an intriguing mechanistic link between impaired PI(3,5)P$_2$ biosynthesis, faulty intracellular transport, and myelination defects.

1.9 Outstanding questions on myelination

Substantial advances in imaging and biotechnology resulted in great progress towards understanding myelin function in health and disease. Isolating and culturing primary oligodendrocytes provided critical insights into the OL lineage dynamics. Recent advances in mouse genetics and live imaging permit myelin observation in the intact brain over extended periods of time (Hughes et al., 2013, Schain et al., 2014). For example, Spectral Confocal Reflectance microscopy (SCoRe) takes advantage of reflective properties of compact myelin and allows imaging white matter *in vivo* and fixed human brain specimen with no additional manipulation (Schain et al., 2014). Increasing sophistication in three-dimensional rendering of TEM data permits examining myelin sheaths in much greater detail and has already resulted in unexpected discoveries. For example, recent evidence demonstrated that in the cerebral cortex, myelination does not abide by a standard pattern of evenly spaced internodes. Instead, there are fairly long stretches of unmyelinated axons that presumably permit a more efficient lateral axon-axon communication (Tomassy et al., 2014). It is completely unknown what mechanisms can be dictating such myelin distribution. Along with techniques that allow monitoring myelin and the OL lineage in a living brain, multiple advances have been made in establishing methods towards dissecting mechanistic aspects of neuron-glia interaction. It is now possible to genetically manipulate electrophysiological aspects of OPCs/neuron interaction (De Biase and Bergles,

2011), interrupt myelin protein synthesis in the adult CNS (Koenning et al., 2012), monitor *de novo* MBP production *in vitro*, and measure calcium signaling in OPCs/OLs (Wake et al., 2015).

Multiple exciting questions remain. The dynamics of the OL lineage in developing and adult brain are still very poorly understood. Experiments targeting exosomal neuron-OL interaction bear enormous potential for gaining insights into molecular mechanisms of myelination. Activity-dependent aspects of myelination are just starting to get elucidated. The contribution of myelin dynamics to synaptic integration and neuronal plasticity is an exciting novel topic. Establishing critical differences between human and rodent OL lineage will bear profound consequences for treatment of myelin disorders. Myelin does constitute half of the human brain, and therefore our deeper understanding of its function in health and disease is the key to the most important question of them all - how does brain really work?

1.10 References

Armati PJ, Mathey EK (2010) The biology of oligodendrocytes. Cambridge ; New York: Cambridge University Press.

Arroyo EJ, Scherer SS (2000) On the molecular architecture of myelinated fibers. Histochemistry and cell biology 113:1-18.

Bakhti M, Winter C, Simons M (2011) Inhibition of myelin membrane sheath formation by oligodendrocyte-derived exosome-like vesicles. J Biol Chem 286:787-796.

Baldwin KT, Giger RJ (2015) Insights into the physiological role of CNS regeneration inhibitors. Front Mol Neurosci 8:23.

Baraban M, Mensch S, Lyons DA (2015) Adaptive myelination from fish to man. Brain Res.

Barkovich AJ (2000) Concepts of myelin and myelination in neuroradiology. AJNR Am J Neuroradiol 21:1099-1109.

Barres BA, Raff MC (1993) Proliferation of oligodendrocyte precursor cells depends on electrical activity in axons. Nature 361:258-260.

Baulac S, Lenk GM, Dufresnois B, Ouled Amar Bencheikh B, Couarch P, Renard J, Larson PA, Ferguson CJ, Noe E, Poirier K, Hubans C, Ferreira S, Guerrini R, Ouazzani R, El Hachimi KH, Meisler MH, Leguern E (2014) Role of the phosphoinositide phosphatase FIG4 gene in familial epilepsy with polymicrogyria. Neurology 82:1068-1075.

Baumann N, Pham-Dinh D (2001) Biology of oligodendrocyte and myelin in the mammalian central nervous system. Physiological reviews 81:871-927.

Behnia R, Munro S (2005) Organelle identity and the signposts for membrane traffic. Nature 438:597-604.

Bengtsson SL, Nagy Z, Skare S, Forsman L, Forssberg H, Ullen F (2005) Extensive piano practicing has regionally specific effects on white matter development. Nat Neurosci 8:1148-1150.

Bercury KK, Macklin WB (2015) Dynamics and mechanisms of CNS myelination. Developmental cell 32:447-458.

Bergles DE, Richardson WD (2015) Oligodendrocyte Development and Plasticity. Cold Spring Harb Perspect Biol 8.

Bergles DE, Roberts JD, Somogyi P, Jahr CE (2000) Glutamatergic synapses on oligodendrocyte precursor cells in the hippocampus. Nature 405:187-191.

Bharadwaj R, Cunningham KM, Zhang K, Lloyd TE (2016) FIG4 regulates lysosome membrane homeostasis independent of phosphatase function. Hum Mol Genet 25:681-692.

Blott EJ, Griffiths GM (2002) Secretory lysosomes. Nature reviews Molecular cell biology 3:122-131.

Botelho RJ, Efe JA, Teis D, Emr SD (2008) Assembly of a Fab1 phosphoinositide kinase signaling complex requires the Fig4 phosphoinositide phosphatase. Molecular biology of the cell 19:4273-4286.

Bridges D, Ma JT, Park S, Inoki K, Weisman LS, Saltiel AR (2012) Phosphatidylinositol 3,5-bisphosphate plays a role in the activation and subcellular localization of mechanistic target of rapamycin 1. Molecular biology of the cell 23:2955-2962.

Brill MH, Waxman SG, Moore JW, Joyner RW (1977) Conduction velocity and spike configuration in myelinated fibres: computed dependence on internode distance. J Neurol Neurosurg Psychiatry 40:769-774.

Bucci C, Thomsen P, Nicoziani P, McCarthy J, van Deurs B (2000) Rab7: a key to lysosome biogenesis. Molecular biology of the cell 11:467-480.

Cai X, Xu Y, Cheung AK, Tomlinson RC, Alcazar-Roman A, Murphy L, Billich A, Zhang B, Feng Y, Klumpp M, Rondeau JM, Fazal AN, Wilson CJ, Myer V, Joberty G, Bouwmeester T, Labow MA, Finan PM, Porter JA, Ploegh HL, Baird D, De Camilli P, Tallarico JA, Huang Q (2013) PIKfyve, a class III PI kinase, is the target of the small molecular IL-12/IL-23 inhibitor apilimod and a player in Toll-like receptor signaling. Chemistry & biology 20:912-921.

Campeau PM, Lenk GM, Lu JT, Bae Y, Burrage L, Turnpenny P, Roman Corona-Rivera J, Morandi L, Mora M, Reutter H, Vulto-van Silfhout AT, Faivre L, Haan E, Gibbs RA, Meisler MH, Lee BH (2013) Yunis-Varon syndrome is caused by mutations in FIG4, encoding a phosphoinositide phosphatase. American journal of human genetics 92:781-791.

Carbajal KS, Mironova Y, Ulrich-Lewis JT, Kulkarni D, Grifka-Walk HM, Huber AK, Shrager P, Giger RJ, Segal BM (2015) Th Cell Diversity in Experimental Autoimmune Encephalomyelitis and Multiple Sclerosis. Journal of immunology 195:2552-2559.

Chen C, Westenbroek RE, Xu X, Edwards CA, Sorenson DR, Chen Y, McEwen DP, O'Malley HA, Bharucha V, Meadows LS, Knudsen GA, Vilaythong A, Noebels JL, Saunders TL, Scheuer T, Shrager P, Catterall WA, Isom LL (2004) Mice lacking sodium channel beta1 subunits display defects in neuronal excitability, sodium channel expression, and nodal architecture. J Neurosci 24:4030-4042.

Chivet M, Hemming F, Pernet-Gallay K, Fraboulet S, Sadoul R (2012) Emerging role of neuronal exosomes in the central nervous system. Frontiers in physiology 3:145.

Chow CY, Zhang Y, Dowling JJ, Jin N, Adamska M, Shiga K, Szigeti K, Shy ME, Li J, Zhang X, Lupski JR, Weisman LS, Meisler MH (2007) Mutation of FIG4 causes neurodegeneration in the pale tremor mouse and patients with CMT4J. Nature 448:68-72.

Christian KM, Song H, Ming GL (2014) Functions and dysfunctions of adult hippocampal neurogenesis. Annual review of neuroscience 37:243-262.

Coetzee T, Fujita N, Dupree J, Shi R, Blight A, Suzuki K, Suzuki K, Popko B (1996) Myelination in the absence of galactocerebroside and sulfatide: normal structure with abnormal function and regional instability. Cell 86:209-219.

Colman DR, Kreibich G, Frey AB, Sabatini DD (1982) Synthesis and incorporation of myelin polypeptides into CNS myelin. The Journal of cell biology 95:598-608.

Coman I, Barbin G, Charles P, Zalc B, Lubetzki C (2005) Axonal signals in central nervous system myelination, demyelination and remyelination. Journal of the neurological sciences 233:67-71.

Crawford AH, Tripathi RB, Foerster S, McKenzie I, Kougioumtzidou E, Grist M, Richardson WD, Franklin RJ (2016a) Pre-Existing Mature Oligodendrocytes Do Not Contribute to Remyelination following Toxin-Induced Spinal Cord Demyelination. Am J Pathol 186:511-516.

Crawford Abbe H, Tripathi Richa B, Richardson William D, Franklin Robin JM (2016b) Developmental Origin of Oligodendrocyte Lineage Cells Determines Response to Demyelination and Susceptibility to Age-Associated Functional Decline. Cell Reports 15:761-773.

Czopka T, Ffrench-Constant C, Lyons DA (2013) Individual oligodendrocytes have only a few hours in which to generate new myelin sheaths in vivo. Developmental cell 25:599-609.

D'Urso D, Ehrhardt P, Muller HW (1999) Peripheral myelin protein 22 and protein zero: a novel association in peripheral nervous system myelin. J Neurosci 19:3396-3403.

De Biase LM, Bergles DE (2011) Same players, different game: AMPA receptor regulation in oligodendrocyte progenitors. Nat Neurosci 14:1358-1360.

De Biase LM, Kang SH, Baxi EG, Fukaya M, Pucak ML, Mishina M, Calabresi PA, Bergles DE (2011) NMDA receptor signaling in oligodendrocyte progenitors is not required for oligodendrogenesis and myelination. J Neurosci 31:12650-12662.

de Hoz L, Simons M (2015) The emerging functions of oligodendrocytes in regulating neuronal network behaviour. BioEssays : news and reviews in molecular, cellular and developmental biology 37:60-69.

Delarasse C, Daubas P, Mars LT, Vizler C, Litzenburger T, Iglesias A, Bauer J, Della Gaspera B, Schubart A, Decker L, Dimitri D, Roussel G, Dierich A, Amor S, Dautigny A, Liblau R, Pham-Dinh D (2003) Myelin/oligodendrocyte glycoprotein-deficient (MOG-deficient) mice reveal lack of immune tolerance to MOG in wild-type mice. J Clin Invest 112:544-553.

Dessaud E, Yang LL, Hill K, Cox B, Ulloa F, Ribeiro A, Mynett A, Novitch BG, Briscoe J (2007) Interpretation of the sonic hedgehog morphogen gradient by a temporal adaptation mechanism. Nature 450:717-720.

Dong XP, Shen D, Wang X, Dawson T, Li X, Zhang Q, Cheng X, Zhang Y, Weisman LS, Delling M, Xu H (2010) PI(3,5)P(2) controls membrane trafficking by direct activation of mucolipin Ca(2+) release channels in the endolysosome. Nature communications 1:38.

Dove SK, Cooke FT, Douglas MR, Sayers LG, Parker PJ, Michell RH (1997) Osmotic stress activates phosphatidylinositol-3,5-bisphosphate synthesis. Nature 390:187-192.

Duan Y, Wang SH, Song J, Mironova Y, Ming GL, Kolodkin AL, Giger RJ (2014) Semaphorin 5A inhibits synaptogenesis in early postnatal- and adult-born hippocampal dentate granule cells. eLife 3.

Dubois-Dalcq M, Behar T, Hudson L, Lazzarini RA (1986) Emergence of three myelin proteins in oligodendrocytes cultured without neurons. The Journal of cell biology 102:384-392.

Dugas JC, Emery B (2013) Purification and culture of oligodendrocyte lineage cells. Cold Spring Harbor protocols 2013:810-814.

Dupree JL, Coetzee T, Suzuki K, Popko B (1998) Myelin abnormalities in mice deficient in galactocerebroside and sulfatide. J Neurocytol 27:649-659.

Durand B, Raff M (2000) A cell-intrinsic timer that operates during oligodendrocyte development. BioEssays : news and reviews in molecular, cellular and developmental biology 22:64-71.

Dyck PJ, Lambert EH (1968) Lower motor and primary sensory neuron diseases with peroneal muscular atrophy. I. Neurologic, genetic, and electrophysiologic findings in hereditary polyneuropathies. Arch Neurol 18:603-618.

Egami Y, Taguchi T, Maekawa M, Arai H, Araki N (2014) Small GTPases and phosphoinositides in the regulatory mechanisms of macropinosome formation and maturation. Frontiers in physiology 5:374.

Emery B, Agalliu D, Cahoy JD, Watkins TA, Dugas JC, Mulinyawe SB, Ibrahim A, Ligon KL, Rowitch DH, Barres BA (2009) Myelin gene regulatory factor is a critical transcriptional regulator required for CNS myelination. Cell 138:172-185.

Emery B, Dugas JC (2013) Purification of oligodendrocyte lineage cells from mouse cortices by immunopanning. Cold Spring Harbor protocols 2013:854-868.

Etxeberria A, Mangin JM, Aguirre A, Gallo V (2010) Adult-born SVZ progenitors receive transient synapses during remyelination in corpus callosum. Nat Neurosci 13:287-289.

Fancy SP, Baranzini SE, Zhao C, Yuk DI, Irvine KA, Kaing S, Sanai N, Franklin RJ, Rowitch DH (2009) Dysregulation of the Wnt pathway inhibits timely myelination and remyelination in the mammalian CNS. Genes Dev 23:1571-1585.

Faust PL, Kaye EM, Powers JM (2010) Myelin lesions associated with lysosomal and peroxisomal disorders. Expert review of neurotherapeutics 10:1449-1466.

Ferguson CJ, Lenk GM, Jones JM, Grant AE, Winters JJ, Dowling JJ, Giger RJ, Meisler MH (2012a) Neuronal expression of Fig4 is both necessary and sufficient to prevent spongiform neurodegeneration. Hum Mol Genet 21:3525-3534.

Ferguson CJ, Lenk GM, Jones JM, Grant AE, Winters JJ, Dowling JJ, Giger RJ, Meisler MH (2012b) Neuronal expression of Fig4 is necessary and sufficient to prevent spongiform neurodegeneration. Hum Mol Genet.

Ferguson CJ, Lenk GM, Meisler MH (2009) Defective autophagy in neurons and astrocytes from mice deficient in PI(3,5)P2. Hum Mol Genet 18:4868-4878.

Fields RD (2008) White matter in learning, cognition and psychiatric disorders. Trends Neurosci 31:361-370.

Fields RD (2015) A new mechanism of nervous system plasticity: activity-dependent myelination. Nat Rev Neurosci 16:756-767.

Folkerth RD (1999) Abnormalities of developing white matter in lysosomal storage diseases. J Neuropathol Exp Neurol 58:887-902.

Follett PL, Rosenberg PA, Volpe JJ, Jensen FE (2000) NBQX attenuates excitotoxic injury in developing white matter. J Neurosci 20:9235-9241.

Fruhbeis C, Frohlich D, Kramer-Albers EM (2012) Emerging roles of exosomes in neuron-glia communication. Frontiers in physiology 3:119.

Fruhbeis C, Frohlich D, Kuo WP, Amphornrat J, Thilemann S, Saab AS, Kirchhoff F, Mobius W, Goebbels S, Nave KA, Schneider A, Simons M, Klugmann M, Trotter J, Kramer-Albers EM (2013) Neurotransmitter-triggered transfer of exosomes mediates oligodendrocyte-neuron communication. PLoS Biol 11:e1001604.

Gautier HO, Evans KA, Volbracht K, James R, Sitnikov S, Lundgaard I, James F, Lao-Peregrin C, Reynolds R, Franklin RJ, Karadottir RT (2015) Neuronal activity regulates remyelination via glutamate signalling to oligodendrocyte progenitors. Nat Commun 6:8518.

Gibson EM, Purger D, Mount CW, Goldstein AK, Lin GL, Wood LS, Inema I, Miller SE, Bieri G, Zuchero JB, Barres BA, Woo PJ, Vogel H, Monje M (2014) Neuronal activity promotes oligodendrogenesis and adaptive myelination in the mammalian brain. Science 344:1252304.

Giese KP, Martini R, Lemke G, Soriano P, Schachner M (1992) Mouse P0 gene disruption leads to hypomyelination, abnormal expression of recognition molecules, and degeneration of myelin and axons. Cell 71:565-576.

Gillooly DJ, Morrow IC, Lindsay M, Gould R, Bryant NJ, Gaullier JM, Parton RG, Stenmark H (2000) Localization of phosphatidylinositol 3-phosphate in yeast and mammalian cells. EMBO J 19:4577-4588.

Gillooly DJ, Simonsen A, Stenmark H (2001) Cellular functions of phosphatidylinositol 3-phosphate and FYVE domain proteins. Biochem J 355:249-258.

Goldman SA (2016) Stem and Progenitor Cell-Based Therapy of the Central Nervous System: Hopes, Hype, and Wishful Thinking. Cell Stem Cell 18:174-188.

Grishchuk Y, Sri S, Rudinskiy N, Ma W, Stember KG, Cottle MW, Sapp E, Difiglia M, Muzikansky A, Betensky RA, Wong AM, Bacskai BJ, Hyman BT, Kelleher RJ, 3rd, Cooper JD, Slaugenhaupt SA (2014) Behavioral deficits, early gliosis, dysmyelination and synaptic dysfunction in a mouse model of mucolipidosis IV. Acta neuropathologica communications 2:133.

Harlow DE, Saul KE, Komuro H, Macklin WB (2015) Myelin Proteolipid Protein Complexes with alphav Integrin and AMPA Receptors In Vivo and Regulates AMPA-Dependent Oligodendrocyte Progenitor Cell Migration through the Modulation of Cell-Surface GluR2 Expression. J Neurosci 35:12018-12032.

Hartline DK, Colman DR (2007) Rapid conduction and the evolution of giant axons and myelinated fibers. Curr Biol 17:R29-35.

Hauser SL, Chan JR, Oksenberg JR (2013) Multiple sclerosis: Prospects and promise. Ann Neurol 74:317-327.

Hildebrand C (1971) Ultrastructural and light-microscopic studies of the nodal region in large myelinated fibres of the adult feline spinal cord white matter. Acta Physiol Scand Suppl 364:43-79.

Hill RA, Grutzendler J (2014) In vivo imaging of oligodendrocytes with sulforhodamine 101. Nat Methods 11:1081-1082.

Hill RA, Patel KD, Goncalves CM, Grutzendler J, Nishiyama A (2014) Modulation of oligodendrocyte generation during a critical temporal window after NG2 cell division. Nat Neurosci 17:1518-1527.

Hofmann I, Munro S (2006) An N-terminally acetylated Arf-like GTPase is localised to lysosomes and affects their motility. Journal of cell science 119:1494-1503.

Hughes EG, Kang SH, Fukaya M, Bergles DE (2013) Oligodendrocyte progenitors balance growth with self-repulsion to achieve homeostasis in the adult brain. Nat Neurosci 16:668-676.

Huotari J, Helenius A (2011) Endosome maturation. EMBO J 30:3481-3500.

Hutagalung AH, Novick PJ (2011) Role of Rab GTPases in membrane traffic and cell physiology. Physiological reviews 91:119-149.

Ikonomov OC, Sbrissa D, Delvecchio K, Xie Y, Jin JP, Rappolee D, Shisheva A (2011) The phosphoinositide kinase PIKfyve is vital in early embryonic development: preimplantation lethality of PIKfyve-/- embryos but normality of PIKfyve+/- mice. J Biol Chem 286:13404-13413.

Ikonomov OC, Sbrissa D, Shisheva A (2009) YM201636, an inhibitor of retroviral budding and PIKfyve-catalyzed PtdIns(3,5)P2 synthesis, halts glucose entry by insulin in adipocytes. Biochem Biophys Res Commun 382:566-570.

Inoue K (2005) PLP1-related inherited dysmyelinating disorders: Pelizaeus-Merzbacher disease and spastic paraplegia type 2. Neurogenetics 6:1-16.

Ishibashi T, Dakin KA, Stevens B, Lee PR, Kozlov SV, Stewart CL, Fields RD (2006) Astrocytes promote myelination in response to electrical impulses. Neuron 49:823-832.

Jean S, Cox S, Nassari S, Kiger AA (2015) Starvation-induced MTMR13 and RAB21 activity regulates VAMP8 to promote autophagosome-lysosome fusion. EMBO reports 16:297-311.

Jean S, Kiger AA (2012) Coordination between RAB GTPase and phosphoinositide regulation and functions. Nature reviews Molecular cell biology 13:463-470.

Jefferies HB, Cooke FT, Jat P, Boucheron C, Koizumi T, Hayakawa M, Kaizawa H, Ohishi T, Workman P, Waterfield MD, Parker PJ (2008) A selective PIKfyve inhibitor blocks PtdIns(3,5)P(2) production and disrupts endomembrane transport and retroviral budding. EMBO reports 9:164-170.

Jin N, Chow CY, Liu L, Zolov SN, Bronson R, Davisson M, Petersen JL, Zhang Y, Park S, Duex JE, Goldowitz D, Meisler MH, Weisman LS (2008) VAC14 nucleates a protein complex essential for the acute interconversion of PI3P and PI(3,5)P(2) in yeast and mouse. EMBO J 27:3221-3234.

Jin N, Lang MJ, Weisman LS (2016) Phosphatidylinositol 3,5-bisphosphate: regulation of cellular events in space and time. Biochem Soc Trans 44:177-184.

Jin N, Mao K, Jin Y, Tevzadze G, Kauffman EJ, Park S, Bridges D, Loewith R, Saltiel AR, Klionsky DJ, Weisman LS (2014) Roles for PI(3,5)P2 in nutrient sensing through TORC1. Molecular biology of the cell 25:1171-1185.

Kang SH, Fukaya M, Yang JK, Rothstein JD, Bergles DE (2010) NG2+ CNS glial progenitors remain committed to the oligodendrocyte lineage in postnatal life and following neurodegeneration. Neuron 68:668-681.

Karadottir R, Cavelier P, Bergersen LH, Attwell D (2005) NMDA receptors are expressed in oligodendrocytes and activated in ischaemia. Nature 438:1162-1166.

Karim SA, Barrie JA, McCulloch MC, Montague P, Edgar JM, Kirkham D, Anderson TJ, Nave KA, Griffiths IR, McLaughlin M (2007) PLP overexpression perturbs myelin protein composition and myelination in a mouse model of Pelizaeus-Merzbacher disease. Glia 55:341-351.

Kessaris N, Fogarty M, Iannarelli P, Grist M, Wegner M, Richardson WD (2006) Competing waves of oligodendrocytes in the forebrain and postnatal elimination of an embryonic lineage. Nat Neurosci 9:173-179.

Khwaja O, Volpe JJ (2008) Pathogenesis of cerebral white matter injury of prematurity. Arch Dis Child Fetal Neonatal Ed 93:F153-161.

Klugmann M, Schwab MH, Puhlhofer A, Schneider A, Zimmermann F, Griffiths IR, Nave KA (1997) Assembly of CNS myelin in the absence of proteolipid protein. Neuron 18:59-70.

Koenning M, Jackson S, Hay CM, Faux C, Kilpatrick TJ, Willingham M, Emery B (2012) Myelin gene regulatory factor is required for maintenance of myelin and mature oligodendrocyte identity in the adult CNS. J Neurosci 32:12528-12542.

Kramer-Albers EM, Bretz N, Tenzer S, Winterstein C, Mobius W, Berger H, Nave KA, Schild H, Trotter J (2007) Oligodendrocytes secrete exosomes containing major myelin and stress-protective proteins: Trophic support for axons? Proteomics Clin Appl 1:1446-1461.

Kramer-Albers EM, White R (2011) From axon-glial signalling to myelination: the integrating role of oligodendroglial Fyn kinase. Cell Mol Life Sci 68:2003-2012.

Kwiecien JM, O'Connor LT, Goetz BD, Delaney KH, Fletch AL, Duncan ID (1998) Morphological and morphometric studies of the dysmyelinating mutant, the Long Evans shaker rat. J Neurocytol 27:581-591.

Kyotani A, Azuma Y, Yamamoto I, Yoshida H, Mizuta I, Mizuno T, Nakagawa M, Tokuda T, Yamaguchi M (2016) Knockdown of the Drosophila FIG4 induces deficient locomotive behavior, shortening of motor neuron, axonal targeting aberration, reduction of life span and defects in eye development. Exp Neurol 277:86-95.

Lachenal G, Pernet-Gallay K, Chivet M, Hemming FJ, Belly A, Bodon G, Blot B, Haase G, Goldberg Y, Sadoul R (2011) Release of exosomes from differentiated neurons and its regulation by synaptic glutamatergic activity. Mol Cell Neurosci 46:409-418.

Langseth AJ, Munji RN, Choe Y, Huynh T, Pozniak CD, Pleasure SJ (2010) Wnts influence the timing and efficiency of oligodendrocyte precursor cell generation in the telencephalon. J Neurosci 30:13367-13372.

Lappe-Siefke C, Goebbels S, Gravel M, Nicksch E, Lee J, Braun PE, Griffiths IR, Nave KA (2003) Disruption of Cnp1 uncouples oligodendroglial functions in axonal support and myelination. Nat Genet 33:366-374.

Le Douarin NM, Smith J (1988) Development of the peripheral nervous system from the neural crest. Annu Rev Cell Biol 4:375-404.

Lebel C, Gee M, Camicioli R, Wieler M, Martin W, Beaulieu C (2012) Diffusion tensor imaging of white matter tract evolution over the lifespan. Neuroimage 60:340-352.

Lee B, Park JY, Jung WH, Kim HS, Oh JS, Choi CH, Jang JH, Kang DH, Kwon JS (2010) White matter neuroplastic changes in long-term trained players of the game of "Baduk" (GO): a voxel-based diffusion-tensor imaging study. Neuroimage 52:9-19.

Lee H, Raiker SJ, Venkatesh K, Geary R, Robak LA, Zhang Y, Yeh HH, Shrager P, Giger RJ (2008) Synaptic function for the Nogo-66 receptor NgR1: regulation of dendritic spine morphology and activity-dependent synaptic strength. J Neurosci 28:2753-2765.

Lee S, Chong SY, Tuck SJ, Corey JM, Chan JR (2013) A rapid and reproducible assay for modeling myelination by oligodendrocytes using engineered nanofibers. Nat Protoc 8:771-782.

Lee Y, Morrison BM, Li Y, Lengacher S, Farah MH, Hoffman PN, Liu Y, Tsingalia A, Jin L, Zhang PW, Pellerin L, Magistretti PJ, Rothstein JD (2012) Oligodendroglia metabolically support axons and contribute to neurodegeneration. Nature 487:443-448.

Lenk GM, Ferguson CJ, Chow CY, Jin N, Jones JM, Grant AE, Zolov SN, Winters JJ, Giger RJ, Dowling JJ, Weisman LS, Meisler MH (2011) Pathogenic mechanism of the FIG4 mutation responsible for Charcot-Marie-Tooth disease CMT4J. PLoS genetics 7:e1002104.

Lenk GM, Frei CM, Miller AC, Wallen RC, Mironova YA, Giger RJ, Meisler MH (2016) Rescue of neurodegeneration in the Fig4 null mouse by a catalytically inactive FIG4 transgene. Hum Mol Genet 25:340-347.

Lenk GM, Meisler MH (2014) Mouse models of PI(3,5)P2 deficiency with impaired lysosome function. Methods in enzymology 534:245-260.

Lenk GM, Szymanska K, Debska-Vielhaber G, Rydzanicz M, Walczak A, Bekiesinska-Figatowska M, Vielhaber S, Hallmann K, Stawinski P, Buehring S, Hsu DA, Kunz WS, Meisler MH, Ploski R (2016b) Biallelic Mutations of VAC14 in Pediatric-Onset Neurological Disease. American journal of human genetics 99:188-194.

Li C, Tropak MB, Gerlai R, Clapoff S, Abramow-Newerly W, Trapp B, Peterson A, Roder J (1994) Myelination in the absence of myelin-associated glycoprotein. Nature 369:747-750.

Lin SC, Huck JH, Roberts JD, Macklin WB, Somogyi P, Bergles DE (2005) Climbing fiber innervation of NG2-expressing glia in the mammalian cerebellum. Neuron 46:773-785.

Lodish HF (2008) Molecular cell biology. New York: W.H. Freeman.

Lopez ME, Klein AD, Dimbil UJ, Scott MP (2011) Anatomically defined neuron-based rescue of neurodegenerative Niemann-Pick type C disorder. J Neurosci 31:4367-4378.

Lopez-Verrilli MA, Picou F, Court FA (2013) Schwann cell-derived exosomes enhance axonal regeneration in the peripheral nervous system. Glia 61:1795-1806.

Lundgaard I, Luzhynskaya A, Stockley JH, Wang Z, Evans KA, Swire M, Volbracht K, Gautier HO, Franklin RJ, Charles F-C, Attwell D, Karadottir RT (2013) Neuregulin and BDNF induce a switch to NMDA receptor-dependent myelination by oligodendrocytes. PLoS Biol 11:e1001743.

Maier O, Hoekstra D, Baron W (2008) Polarity development in oligodendrocytes: sorting and trafficking of myelin components. Journal of molecular neuroscience : MN 35:35-53.

Makinodan M, Rosen KM, Ito S, Corfas G (2012) A critical period for social experience-dependent oligodendrocyte maturation and myelination. Science 337:1357-1360.

Marinelli C, Bertalot T, Zusso M, Skaper SD, Giusti P (2016) Systematic Review of Pharmacological Properties of the Oligodendrocyte Lineage. Frontiers in cellular neuroscience 10:27.

Martini R (1999) P0-deficient knockout mice as tools to understand pathomechanisms in Charcot-Marie-Tooth 1B and P0-related Dejerine-Sottas syndrome. Ann N Y Acad Sci 883:273-280.

Masaki T (2012) Polarization and myelination in myelinating glia. ISRN neurology 2012:769412.

Mayinger P (2012) Phosphoinositides and vesicular membrane traffic. Biochimica et biophysica acta 1821:1104-1113.

Mc AJ, Milburn NS, Chapman GB (1958) The fine structure of Schwann cells, nodes of Ranvier and Schmidt-Lanterman incisures in the central nervous system of the crab, Cancer irroratus. J Ultrastruct Res 2:171-176.

McCartney AJ, Zhang Y, Weisman LS (2014a) Phosphatidylinositol 3,5-bisphosphate: low abundance, high significance. BioEssays : news and reviews in molecular, cellular and developmental biology 36:52-64.

McCartney AJ, Zolov SN, Kauffman EJ, Zhang Y, Strunk BS, Weisman LS, Sutton MA (2014b) Activity-dependent PI(3,5)P2 synthesis controls AMPA receptor trafficking during synaptic depression. Proc Natl Acad Sci U S A 111:E4896-4905.

McKenzie IA, Ohayon D, Li H, de Faria JP, Emery B, Tohyama K, Richardson WD (2014) Motor skill learning requires active central myelination. Science 346:318-322.

Mei F, Fancy SP, Shen YA, Niu J, Zhao C, Presley B, Miao E, Lee S, Mayoral SR, Redmond SA, Etxeberria A, Xiao L, Franklin RJ, Green A, Hauser SL, Chan JR (2014) Micropillar arrays as a high-throughput screening platform for therapeutics in multiple sclerosis. Nat Med 20:954-960.

Menezes MP, Waddell L, Lenk GM, Kaur S, MacArthur DG, Meisler MH, Clarke NF (2014) Whole exome sequencing identifies three recessive FIG4 mutations in an apparently dominant pedigree with Charcot-Marie-Tooth disease. Neuromuscul Disord 24:666-670.

Menn B, Garcia-Verdugo JM, Yaschine C, Gonzalez-Perez O, Rowitch D, Alvarez-Buylla A (2006) Origin of oligodendrocytes in the subventricular zone of the adult brain. J Neurosci 26:7907-7918.

Mensch S, Baraban M, Almeida R, Czopka T, Ausborn J, El Manira A, Lyons DA (2015) Synaptic vesicle release regulates myelin sheath number of individual oligodendrocytes in vivo. Nat Neurosci 18:628-630.

Mi S, Miller RH, Lee X, Scott ML, Shulag-Morskaya S, Shao Z, Chang J, Thill G, Levesque M, Zhang M, Hession C, Sah D, Trapp B, He Z, Jung V, McCoy JM, Pepinsky RB (2005) LINGO-1 negatively regulates myelination by oligodendrocytes. Nat Neurosci 8:745-751.

Mironova YA, Giger RJ (2013) Where no synapses go: gatekeepers of circuit remodeling and synaptic strength. Trends Neurosci 36:363-373.

Mironova YA, Lenk GM, Lin JP, Lee SJ, Twiss JL, Vaccari I, Bolino A, Havton LA, Min SH, Abrams CS, Shrager P, Meisler MH, Giger RJ (2016) PI(3,5)P biosynthesis regulates oligodendrocyte differentiation by intrinsic and extrinsic mechanisms. eLife 5.

Mizuguchi R, Sugimori M, Takebayashi H, Kosako H, Nagao M, Yoshida S, Nabeshima Y, Shimamura K, Nakafuku M (2001) Combinatorial roles of olig2 and neurogenin2 in the coordinated induction of pan-neuronal and subtype-specific properties of motoneurons. Neuron 31:757-771.

Muller C, Bauer NM, Schafer I, White R (2013) Making myelin basic protein -from mRNA transport to localized translation. Frontiers in cellular neuroscience 7:169.

Najm FJ, Madhavan M, Zaremba A, Shick E, Karl RT, Factor DC, Miller TE, Nevin ZS, Kantor C, Sargent A, Quick KL, Schlatzer DM, Tang H, Papoian R, Brimacombe KR, Shen M, Boxer MB, Jadhav A, Robinson AP, Podojil JR, Miller SD, Miller RH, Tesar PJ (2015) Drug-based modulation of endogenous stem cells promotes functional remyelination in vivo. Nature 522:216-220.

Nave KA (2010) Myelination and support of axonal integrity by glia. Nature 468:244-252.

Nave KA, Ehrenreich H (2014) Myelination and oligodendrocyte functions in psychiatric diseases. JAMA Psychiatry 71:582-584.

Nave KA, Trapp BD (2008) Axon-glial signaling and the glial support of axon function. Annual review of neuroscience 31:535-561.

Nawaz S, Sanchez P, Schmitt S, Snaidero N, Mitkovski M, Velte C, Bruckner BR, Alexopoulos I, Czopka T, Jung SY, Rhee JS, Janshoff A, Witke W, Schaap IA, Lyons DA, Simons M (2015) Actin filament turnover drives leading edge growth during myelin sheath formation in the central nervous system. Developmental cell 34:139-151.

Nicholson G, Lenk GM, Reddel SW, Grant AE, Towne CF, Ferguson CJ, Simpson E, Scheuerle A, Yasick M, Hoffman S, Blouin R, Brandt C, Coppola G, Biesecker LG, Batish SD, Meisler MH (2011) Distinctive genetic and clinical features of CMT4J: a severe neuropathy caused by mutations in the PI(3,5)P(2) phosphatase FIG4. Brain : a journal of neurology 134:1959-1971.

O'Brien JS, Sampson EL (1965) Lipid composition of the normal human brain: gray matter, white matter, and myelin. J Lipid Res 6:537-544.

Oberheim NA, Takano T, Han X, He W, Lin JH, Wang F, Xu Q, Wyatt JD, Pilcher W, Ojemann JG, Ransom BR, Goldman SA, Nedergaard M (2009) Uniquely hominid features of adult human astrocytes. J Neurosci 29:3276-3287.

Ohno M, Hiraoka Y, Matsuoka T, Tomimoto H, Takao K, Miyakawa T, Oshima N, Kiyonari H, Kimura T, Kita T, Nishi E (2009) Nardilysin regulates axonal maturation and myelination in the central and peripheral nervous system. Nat Neurosci 12:1506-1513.

Orthmann-Murphy JL, Freidin M, Fischer E, Scherer SS, Abrams CK (2007) Two distinct heterotypic channels mediate gap junction coupling between astrocyte and oligodendrocyte connexins. J Neurosci 27:13949-13957.

Osorio MJ, Goldman SA (2016) Glial progenitor cell-based treatment of the childhood leukodystrophies. Exp Neurol.

Pagany M, Jagodic M, Schubart A, Pham-Dinh D, Bachelin C, Baron van Evercooren A, Lachapelle F, Olsson T, Linington C (2003) Myelin oligodendrocyte glycoprotein is expressed in the peripheral nervous system of rodents and primates. Neurosci Lett 350:165-168.

Pan B, Fromholt SE, Hess EJ, Crawford TO, Griffin JW, Sheikh KA, Schnaar RL (2005) Myelin-associated glycoprotein and complementary axonal ligands, gangliosides, mediate axon stability in the CNS and PNS: neuropathology and behavioral deficits in single- and double-null mice. Exp Neurol 195:208-217.

Park HC, Appel B (2003) Delta-Notch signaling regulates oligodendrocyte specification. Development 130:3747-3755.

Perez-Cerda F, Sanchez-Gomez MV, Matute C (2015) Pio del Rio Hortega and the discovery of the oligodendrocytes. Front Neuroanat 9:92.

Perlman SJ, Mar S (2012) Leukodystrophies. Advances in experimental medicine and biology 724:154-171.

Pfeiffer SE, Warrington AE, Bansal R (1993) The oligodendrocyte and its many cellular processes. Trends Cell Biol 3:191-197.

Poliak S, Peles E (2003) The local differentiation of myelinated axons at nodes of Ranvier. Nat Rev Neurosci 4:968-980.

Prolo LM, Vogel H, Reimer RJ (2009) The lysosomal sialic acid transporter sialin is required for normal CNS myelination. J Neurosci 29:15355-15365.

Pusic AD, Kraig RP (2014) Youth and environmental enrichment generate serum exosomes containing miR-219 that promote CNS myelination. Glia 62:284-299.

Raiker SJ, Lee H, Baldwin KT, Duan Y, Shrager P, Giger RJ (2010) Oligodendrocyte-myelin glycoprotein and Nogo negatively regulate activity-dependent synaptic plasticity. J Neurosci 30:12432-12445.

Raine CS (1984) On the association between perinodal astrocytic processes and the node of Ranvier in the C.N.S. J Neurocytol 13:21-27.

Rasband MN, Tayler J, Kaga Y, Yang Y, Lappe-Siefke C, Nave KA, Bansal R (2005) CNP is required for maintenance of axon-glia interactions at nodes of Ranvier in the CNS. Glia 50:86-90.

Reindl M, Di Pauli F, Rostasy K, Berger T (2013) The spectrum of MOG autoantibody-associated demyelinating diseases. Nat Rev Neurol 9:455-461.

Rempe D, Vangeison G, Hamilton J, Li Y, Jepson M, Federoff HJ (2006) Synapsin I Cre transgene expression in male mice produces germline recombination in progeny. Genesis 44:44-49.

Roach A, Boylan K, Horvath S, Prusiner SB, Hood LE (1983) Characterization of cloned cDNA representing rat myelin basic protein: absence of expression in brain of shiverer mutant mice. Cell 34:799-806.

Roach A, Takahashi N, Pravtcheva D, Ruddle F, Hood L (1985) Chromosomal mapping of mouse myelin basic protein gene and structure and transcription of the partially deleted gene in shiverer mutant mice. Cell 42:149-155.

Saab AS, Tzvetanova ID, Nave KA (2013) The role of myelin and oligodendrocytes in axonal energy metabolism. Current opinion in neurobiology 23:1065-1072.

Saher G, Brugger B, Lappe-Siefke C, Mobius W, Tozawa R, Wehr MC, Wieland F, Ishibashi S, Nave KA (2005) High cholesterol level is essential for myelin membrane growth. Nat Neurosci 8:468-475.

Saher G, Rudolphi F, Corthals K, Ruhwedel T, Schmidt KF, Lowel S, Dibaj P, Barrette B, Mobius W, Nave KA (2012) Therapy of Pelizaeus-Merzbacher disease in mice by feeding a cholesterol-enriched diet. Nat Med 18:1130-1135.

Salzer JL (2003) Polarized domains of myelinated axons. Neuron 40:297-318.

Sardiello M, Palmieri M, di Ronza A, Medina DL, Valenza M, Gennarino VA, Di Malta C, Donaudy F, Embrione V, Polishchuk RS, Banfi S, Parenti G, Cattaneo E, Ballabio A (2009) A gene network regulating lysosomal biogenesis and function. Science 325:473-477.

Schain AJ, Hill RA, Grutzendler J (2014) Label-free in vivo imaging of myelinated axons in health and disease with spectral confocal reflectance microscopy. Nat Med 20:443-449.

Schardt A, Brinkmann BG, Mitkovski M, Sereda MW, Werner HB, Nave KA (2009) The SNARE protein SNAP-29 interacts with the GTPase Rab3A: Implications for membrane trafficking in myelinating glia. Journal of neuroscience research 87:3465-3479.

Scholz J, Klein MC, Behrens TE, Johansen-Berg H (2009) Training induces changes in white-matter architecture. Nat Neurosci 12:1370-1371.

Schuller U, Heine VM, Mao J, Kho AT, Dillon AK, Han YG, Huillard E, Sun T, Ligon AH, Qian Y, Ma Q, Alvarez-Buylla A, McMahon AP, Rowitch DH, Ligon KL (2008)

Acquisition of granule neuron precursor identity is a critical determinant of progenitor cell competence to form Shh-induced medulloblastoma. Cancer cell 14:123-134.

Schulze U, Vollenbroker B, Braun DA, Van Le T, Granado D, Kremerskothen J, Franzel B, Klosowski R, Barth J, Fufezan C, Wolters DA, Pavenstadt H, Weide T (2014) The Vac14-interaction network is linked to regulators of the endolysosomal and autophagic pathway. Molecular & cellular proteomics : MCP 13:1397-1411.

Schweitzer JK, Krivda JP, D'Souza-Schorey C (2009) Neurodegeneration in Niemann-Pick Type C disease and Huntington's disease: impact of defects in membrane trafficking. Curr Drug Targets 10:653-665.

Settembre C, Di Malta C, Polito VA, Garcia Arencibia M, Vetrini F, Erdin S, Erdin SU, Huynh T, Medina D, Colella P, Sardiello M, Rubinsztein DC, Ballabio A (2011) TFEB links autophagy to lysosomal biogenesis. Science 332:1429-1433.

Sharma K, Schmitt S, Bergner CG, Tyanova S, Kannaiyan N, Manrique-Hoyos N, Kongi K, Cantuti L, Hanisch UK, Philips MA, Rossner MJ, Mann M, Simons M (2015) Cell type- and brain region-resolved mouse brain proteome. Nat Neurosci 18:1819-1831.

Shen D, Wang X, Li X, Zhang X, Yao Z, Dibble S, Dong XP, Yu T, Lieberman AP, Showalter HD, Xu H (2012) Lipid storage disorders block lysosomal trafficking by inhibiting a TRP channel and lysosomal calcium release. Nat Commun 3:731.

Simons M, Kramer EM, Macchi P, Rathke-Hartlieb S, Trotter J, Nave KA, Schulz JB (2002) Overexpression of the myelin proteolipid protein leads to accumulation of cholesterol and proteolipid protein in endosomes/lysosomes: implications for Pelizaeus-Merzbacher disease. The Journal of cell biology 157:327-336.

Simons M, Kramer EM, Thiele C, Stoffel W, Trotter J (2000) Assembly of myelin by association of proteolipid protein with cholesterol- and galactosylceramide-rich membrane domains. The Journal of cell biology 151:143-154.

Simons M, Lyons DA (2013) Axonal selection and myelin sheath generation in the central nervous system. Current opinion in cell biology 25:512-519.

Simons M, Trajkovic K (2006) Neuron-glia communication in the control of oligodendrocyte function and myelin biogenesis. Journal of cell science 119:4381-4389.

Snaidero N, Mobius W, Czopka T, Hekking LH, Mathisen C, Verkleij D, Goebbels S, Edgar J, Merkler D, Lyons DA, Nave KA, Simons M (2014) Myelin membrane wrapping of CNS axons by PI(3,4,5)P3-dependent polarized growth at the inner tongue. Cell 156:277-290.

Stenmark H (2009) Rab GTPases as coordinators of vesicle traffic. Nature reviews Molecular cell biology 10:513-525.

Sturrock RR (1980) Myelination of the mouse corpus callosum. Neuropathol Appl Neurobiol 6:415-420.

Takatori S, Fujimoto T (2016) A novel imaging method revealed phosphatidylinositol 3,5-bisphosphate-rich domains in the endosome/lysosome membrane. Communicative & Integrative Biology 9:e1145319.

Tomassy GS, Berger DR, Chen HH, Kasthuri N, Hayworth KJ, Vercelli A, Seung HS, Lichtman JW, Arlotta P (2014) Distinct profiles of myelin distribution along single axons of pyramidal neurons in the neocortex. Science 344:319-324.

Toth AB, Terauchi A, Zhang LY, Johnson-Venkatesh EM, Larsen DJ, Sutton MA, Umemori H (2013) Synapse maturation by activity-dependent ectodomain shedding of SIRPalpha. Nat Neurosci 16:1417-1425.

Trajkovic K, Dhaunchak AS, Goncalves JT, Wenzel D, Schneider A, Bunt G, Nave KA, Simons M (2006) Neuron to glia signaling triggers myelin membrane exocytosis from endosomal storage sites. The Journal of cell biology 172:937-948.

Tress O, Maglione M, May D, Pivneva T, Richter N, Seyfarth J, Binder S, Zlomuzica A, Seifert G, Theis M, Dere E, Kettenmann H, Willecke K (2012) Panglial gap junctional communication is essential for maintenance of myelin in the CNS. J Neurosci 32:7499-7518.

Tripathi RB, Clarke LE, Burzomato V, Kessaris N, Anderson PN, Attwell D, Richardson WD (2011) Dorsally and ventrally derived oligodendrocytes have similar electrical properties but myelinate preferred tracts. J Neurosci 31:6809-6819.

Tsai HH, Niu J, Munji R, Davalos D, Chang J, Zhang H, Tien AC, Kuo CJ, Chan JR, Daneman R, Fancy SP (2016) Oligodendrocyte precursors migrate along vasculature in the developing nervous system. Science 351:379-384.

Vaccari I, Carbone A, Previtali SC, Mironova YA, Alberizzi V, Noseda R, Rivellini C, Bianchi F, Del Carro U, D'Antonio M, Lenk GM, Wrabetz L, Giger RJ, Meisler MH, Bolino A (2015) Loss of Fig4 in both Schwann cells and motor neurons contributes to CMT4J neuropathy. Hum Mol Genet 24:383-396.

Virchow R (1854) Ueber das ausgebreitete Vorkommen einer dem Nervenmark analogen Substanz in den thierischen Geweben. Archiv für pathologische Anatomie und Physiologie und für klinische Medicin 6:562-572.

von Budingen HC, Mei F, Greenfield A, Jahn S, Shen YA, Reid HH, McKemy DD, Chan JR (2015) The myelin oligodendrocyte glycoprotein directly binds nerve growth factor to modulate central axon circuitry. The Journal of cell biology 210:891-898.

Wake H, Lee PR, Fields RD (2011) Control of local protein synthesis and initial events in myelination by action potentials. Science 333:1647-1651.

Wake H, Ortiz FC, Woo DH, Lee PR, Angulo MC, Fields RD (2015) Nonsynaptic junctions on myelinating glia promote preferential myelination of electrically active axons. Nat Commun 6:7844.

Wang S, Bates J, Li X, Schanz S, Chandler-Militello D, Levine C, Maherali N, Studer L, Hochedlinger K, Windrem M, Goldman SA (2013) Human iPSC-derived oligodendrocyte progenitor cells can myelinate and rescue a mouse model of congenital hypomyelination. Cell Stem Cell 12:252-264.

Wang S, Sdrulla AD, diSibio G, Bush G, Nofziger D, Hicks C, Weinmaster G, Barres BA (1998) Notch receptor activation inhibits oligodendrocyte differentiation. Neuron 21:63-75.

Wang W, Zhang X, Gao Q, Xu H (2014) TRPML1: an ion channel in the lysosome. Handb Exp Pharmacol 222:631-645.

Wang X, Zhang X, Dong XP, Samie M, Li X, Cheng X, Goschka A, Shen D, Zhou Y, Harlow J, Zhu MX, Clapham DE, Ren D, Xu H (2012) TPC proteins are phosphoinositide-activated sodium-selective ion channels in endosomes and lysosomes. Cell 151:372-383.

White R, Kramer-Albers EM (2014) Axon-glia interaction and membrane traffic in myelin formation. Frontiers in cellular neuroscience 7:284.

Winters JJ, Ferguson CJ, Lenk GM, Giger-Mateeva VI, Shrager P, Meisler MH, Giger RJ (2011) Congenital CNS hypomyelination in the Fig4 null mouse is rescued by neuronal expression of the PI(3,5)P(2) phosphatase Fig4. J Neurosci 31:17736-17751.

Winterstein C, Trotter J, Kramer-Albers EM (2008) Distinct endocytic recycling of myelin proteins promotes oligodendroglial membrane remodeling. Journal of cell science 121:834-842.

Woodhoo A, Sommer L (2008) Development of the Schwann cell lineage: from the neural crest to the myelinated nerve. Glia 56:1481-1490.

Yaghootfam A, Gieselmann V, Eckhardt M (2005) Delay of myelin formation in arylsulphatase A-deficient mice. Eur J Neurosci 21:711-720.

Yang N, Zuchero JB, Ahlenius H, Marro S, Ng YH, Vierbuchen T, Hawkins JS, Geissler R, Barres BA, Wernig M (2013) Generation of oligodendroglial cells by direct lineage conversion. Nat Biotechnol 31:434-439.

Yao D, McGonigal R, Barrie JA, Cappell J, Cunningham ME, Meehan GR, Fewou SN, Edgar JM, Rowan E, Ohmi Y, Furukawa K, Furukawa K, Brophy PJ, Willison HJ (2014) Neuronal expression of GalNAc transferase is sufficient to prevent the age-related neurodegenerative phenotype of complex ganglioside-deficient mice. J Neurosci 34:880-891.

Ye F, Chen Y, Hoang T, Montgomery RL, Zhao XH, Bu H, Hu T, Taketo MM, van Es JH, Clevers H, Hsieh J, Bassel-Duby R, Olson EN, Lu QR (2009) HDAC1 and HDAC2 regulate oligodendrocyte differentiation by disrupting the beta-catenin-TCF interaction. Nat Neurosci 12:829-838.

Yeung MS, Zdunek S, Bergmann O, Bernard S, Salehpour M, Alkass K, Perl S, Tisdale J, Possnert G, Brundin L, Druid H, Frisen J (2014) Dynamics of oligodendrocyte generation and myelination in the human brain. Cell 159:766-774.

Yin X, Kiryu-Seo S, Kidd GJ, Feltri ML, Wrabetz L, Trapp BD (2015) Proteolipid protein cannot replace P0 protein as the major structural protein of peripheral nervous system myelin. Glia 63:66-77.

Yool DA, Edgar JM, Montague P, Malcolm S (2000) The proteolipid protein gene and myelin disorders in man and animal models. Hum Mol Genet 9:987-992.

Young KM, Psachoulia K, Tripathi RB, Dunn SJ, Cossell L, Attwell D, Tohyama K, Richardson WD (2013) Oligodendrocyte dynamics in the healthy adult CNS: evidence for myelin remodeling. Neuron 77:873-885.

Yu T, Lieberman AP (2013) Npc1 acting in neurons and glia is essential for the formation and maintenance of CNS myelin. PLoS genetics 9:e1003462.

Zhang J, Liu Q (2015) Cholesterol metabolism and homeostasis in the brain. Protein Cell 6:254-264.

Zhang X, Chow CY, Sahenk Z, Shy ME, Meisler MH, Li J (2008) Mutation of FIG4 causes a rapidly progressive, asymmetric neuronal degeneration. Brain : a journal of neurology 131:1990-2001.

Zhang Y, Chen K, Sloan SA, Bennett ML, Scholze AR, O'Keeffe S, Phatnani HP, Guarnieri P, Caneda C, Ruderisch N, Deng S, Liddelow SA, Zhang C, Daneman R, Maniatis T, Barres BA, Wu JQ (2014) An RNA-sequencing transcriptome and splicing database of glia, neurons, and vascular cells of the cerebral cortex. J Neurosci 34:11929-11947.

Zhang Y, McCartney AJ, Zolov SN, Ferguson CJ, Meisler MH, Sutton MA, Weisman LS (2012) Modulation of synaptic function by VAC14, a protein that regulates the phosphoinositides PI(3,5)P(2) and PI(5)P. EMBO J 31:3442-3456.

Zhang Y, Zolov SN, Chow CY, Slutsky SG, Richardson SC, Piper RC, Yang B, Nau JJ, Westrick RJ, Morrison SJ, Meisler MH, Weisman LS (2007) Loss of Vac14, a regulator

of the signaling lipid phosphatidylinositol 3,5-bisphosphate, results in neurodegeneration in mice. Proc Natl Acad Sci U S A 104:17518-17523.

Zielasek J, Martini R, Toyka KV (1996) Functional abnormalities in P0-deficient mice resemble human hereditary neuropathies linked to P0 gene mutations. Muscle Nerve 19:946-952.

Ziskin JL, Nishiyama A, Rubio M, Fukaya M, Bergles DE (2007) Vesicular release of glutamate from unmyelinated axons in white matter. Nat Neurosci 10:321-330.

Zolov SN, Bridges D, Zhang Y, Lee WW, Riehle E, Verma R, Lenk GM, Converso-Baran K, Weide T, Albin RL, Saltiel AR, Meisler MH, Russell MW, Weisman LS (2012) In vivo, Pikfyve generates PI(3,5)P2, which serves as both a signaling lipid and the major precursor for PI5P. Proc Natl Acad Sci U S A 109:17472-17477.

Zonouzi M, Scafidi J, Li P, McEllin B, Edwards J, Dupree JL, Harvey L, Sun D, Hubner CA, Cull-Candy SG, Farrant M, Gallo V (2015) GABAergic regulation of cerebellar NG2 cell development is altered in perinatal white matter injury. Nat Neurosci 18:674-682.

Zou J, Hu B, Arpag S, Yan Q, Hamilton A, Zeng YS, Vanoye CG, Li J (2015) Reactivation of Lysosomal Ca2+ Efflux Rescues Abnormal Lysosomal Storage in FIG4-Deficient Cells. J Neurosci 35:6801-6812.

Zuchero JB, Barres BA (2013) Intrinsic and extrinsic control of oligodendrocyte development. Current opinion in neurobiology 23:914-920.

Zuchero JB, Fu MM, Sloan SA, Ibrahim A, Olson A, Zaremba A, Dugas JC, Wienbar S, Caprariello AV, Kantor C, Leonoudakis D, Lariosa-Willingham K, Kronenberg G, Gertz K, Soderling SH, Miller RH, Barres BA (2015) CNS myelin wrapping is driven by actin disassembly. Developmental cell 34:152-167.

CHAPTER II:

PI(3,5)P$_2$ Biosynthesis Regulates Oligodendrocyte Differentiation

by Intrinsic and Extrinsic Mechanisms

2.1 Abstract

Proper development of the CNS axon-glia unit requires bi-directional communication between axons and oligodendrocytes (OLs). We show that the signaling lipid phosphatidylinositol-3,5-bisphosphate [PI(3,5)P$_2$] is required in neurons and in OLs for normal CNS myelination. In mice, mutations of *Fig4, Pikfyve* or *Vac14,* encoding key components of the PI(3,5)P$_2$ biosynthetic complex, each lead to impaired OL maturation, severe CNS hypomyelination and delayed propagation of compound action potentials.   Primary OLs deficient in *Fig4* accumulate large LAMP1$^+$ and Rab7$^+$ vesicular structures and exhibit reduced membrane sheet expansion.   PI(3,5)P$_2$ deficiency leads to accumulation of myelin-associated glycoprotein (MAG) in LAMP1$^+$ perinuclear vesicles that fail to migrate to the nascent myelin sheet. Live-cell imaging of OLs after genetic or pharmacological inhibition of PI(3,5)P$_2$ synthesis revealed impaired trafficking of plasma membrane-derived MAG through the endolysosomal system in primary cells and brain tissue. Collectively, our studies identify PI(3,5)P$_2$ as a key regulator of myelin membrane trafficking and myelinogenesis.

2.2 Introduction

In the vertebrate CNS, the majority of long axons is myelinated. Myelin greatly increases the conduction velocity of action potentials and provides metabolic support for axons. Bidirectional axo-glial signaling is critical for nervous system myelination and fiber stability (Nave and Trapp, 2008, Simons and Lyons, 2013). Myelin development is regulated by oligodendrocyte (OL) intrinsic mechanisms (Zuchero and Barres, 2013), astrocyte secreted factors (Ishibashi et al., 2006), neuronal electrical activity (Barres and Raff, 1993, Ishibashi et al., 2006) and axon derived chemical signals (Coman et al., 2005, Ohno et al., 2009, Winters et al., 2011, Yao et al., 2014). Disorders associated with defective CNS white matter range from multiple sclerosis and inherited leukodystrophies to psychiatric disorders (Fields, 2008, Makinodan et al., 2012, Perlman and Mar, 2012).

FIG4 is an evolutionarily conserved lipid phosphatase that removes the 5' phosphate group from phosphatidylinositol(3,5)bisphosphate [$PI(3,5)P_2$] to produce PI(3)P. Together with its antagonistic kinase PIKFYVE and the scaffold protein VAC14, FIG4 forms an enzyme complex that regulates the interconversion of PI(3)P and $PI(3,5)P_2$ on membranes of the late endosomal/ lysosomal (LE/Lys) compartment (Jin et al., 2008, McCartney et al., 2014a). In addition to its 5'-phosphatase activity, FIG4 function is required to stabilize the enzyme complex. $PI(3,5)P_2$ directly regulates the lysosomal cation channels TRPML1, TPC1 and TPC2 (Dong et al., 2010, Wang et al., 2012, Wang et al., 2014). Reduced activity of these lysosomal channels and the resulting osmotic enlargement of the LE/Lys may underlie vacuolization in *Fig4* null cells (Lenk and Meisler, 2014). Consistent with this model, overexpression of TRPML1 in *Vac14* and *Fig4* mutant cells appears to rescues vacuolization (Dong et al., 2010, Zou et al., 2015). In *Drosophila,* loss of TRPML1 generates a muscle vacuolization phenotype reminiscent of FIG4 deficiency (Bharadwaj et al., 2016).

FIG4 deficiency is particularly harmful for neural cells with elaborate morphologies, including projection neurons and myelinating glia. Mutations of human *FIG4* result in neurological disorders including Charcot-Marie-Tooth type 4J, a severe form of peripheral neuropathy (Chow et al., 2007, Nicholson et al., 2011), polymicrogyria with epilepsy (Baulac et al., 2014), and Yunis-Varon syndrome (Campeau et al., 2013). Mice null for *Fig4* exhibit severe tremor, brain region-specific spongiform degeneration, hypomyelination, and juvenile lethality (Chow et al., 2007, Ferguson et al., 2009, Winters et al., 2011). We previously demonstrated that a *Fig4* transgene driven by the neuron-specific enolase (*NSE*) promoter rescued juvenile lethality and neurodegeneration in global *Fig4* null mice, and that these phenotypes were not rescued by an astrocyte-specific *Fig4* transgene (Ferguson et al., 2012b). The neuron-specific transgene also rescued conduction in peripheral nerves (Ferguson et al., 2012b) and structural defects in CNS myelination (Winters et al., 2011). Conversely, inactivation of *Fig4* specifically in neurons resulted in region-specific neurodegeneration (Ferguson et al., 2012b).

The cellular and molecular mechanisms relating loss of *Fig4* to hypomyelination are poorly understood. To further characterize the requirement of PI(3,5)P$_2$ for CNS myelination, we manipulated individual components of the PI(3,5)P$_2$ biosynthetic complex. *Pikfyve* and *Vac14* global null mice die prematurely, before the onset of CNS myelination (Zhang et al., 2007, Ikonomov et al., 2011). To circumvent this limitation, we employed a combination of conditional null alleles and hypomorphic alleles in the mouse. Our study shows that multiple strategies to perturb the FIG4/PIKFYVE/VAC14 enzyme complex, and by extension the lipid product PI(3,5)P$_2$, result in the common endpoints of arrested OL differentiation, impaired myelin protein trafficking through the LE/Lys compartment, and severe CNS hypomyelination. We demonstrate that these defects in myelin biogenesis are functionally relevant and result in faulty conduction of electrical impulses.

2.3 Results

Conditional ablation of *Fig4* in neurons or the OL lineage results in CNS hypomyelination

In the early postnatal brain, *Fig4* is broadly expressed and enriched in oligodendrocyte progenitor cells (OPCs) and newly formed OLs (NFOs) (Zhang et al., 2014). Mice in which exon 4 of the *Fig4* gene is flanked by *loxP* sites (Ferguson et al., 2012b) were used to generate *Fig4$^{-/flox}$,SynCre* and *Fig4$^{-/flox}$,Olig2Cre* mice deficient for *Fig4* in neurons or OLs, respectively. Myelin development in these conditional mutants, as well as the *Fig4* global mutant (*Fig4$^{-/-}$*) and control mice (*Fig4$^{+/+}$* and *Fig4$^{flox/+}$*), was analyzed by Fluoromyelin Green labeling (Figure 2.1). In control brains, the corpus callosum and internal capsule were prominently labeled (Figure 2.1A and 1A'). Staining of these structures was weaker in *Fig4$^{-/flox}$,SynCre* brains and further reduced in *Fig4$^{-/flox}$,Olig2Cre* and *Fig4$^{-/-}$* brains (Figure 2.1B-1D'). For a quantitative comparison of the myelination defects, whole brain membranes were prepared from P21 pups and analyzed by immunoblotting with antibodies specific for the myelin markers myelin-associated glycoprotein (MAG), 2',3'-cyclic-nucleotide 3'-phosphodiesterase (CNPase), proteolipid protein (PLP), and myelin basic protein (MBP) (Figure 2.1E). Compared to *Fig4$^{+/+}$* membranes, a significant reduction in myelin proteins was evident in *Fig4$^{-/-}$* mice, *Fig4$^{-/flox}$,SynCre* mice and *Fig4$^{-/flox}$,Olig2Cre* mice (Figure 2.1F -1I). The finding that the neuronal marker classIII *β*-tubulin is not significantly decreased in any of these mice indicates that the decrease in CNS myelin is not secondary to neuronal loss. While the *Olig2* promoter is highly active in the OL lineage, activity has also been reported in astrocytes and a subset of neurons (Dessaud et al., 2007, Zhang et al., 2014). To independently assess the role of *Fig4* in the OL lineage, we generated *Fig4$^{-/flox}$,PdgfraCreER* mice that permit tamoxifen inducible gene ablation. At postnatal-days (P)5 and 6, before the onset of CNS myelination, *Fig4$^{-/flox}$,PdgfraCreER* pups

were injected with 4-hydroxytamoxifen and brains were analyzed at P20-P21. Inducible ablation of *Fig4* in the OL-linage resulted in reduced expression of the myelin proteins CNPase, MAG, and MBP, as assessed by Western blot analysis (Figure 2.2A-2B') as well as myelin loss in forebrain structures and cerebellar white matter (Figure 2.2C-2D'). Fewer *Plp1*^{+} OLs were present in optic nerve sections of *Fig4*[-/flox]*,PdgfraCreER* mice (Figure 2.2E and 2E'). Together, these studies indicate that proper CNS myelination is dependent upon OL cell-autonomous (intrinsic) functions of *Fig4,* in addition to non-OL-autonomous (extrinsic) functions of *Fig4* provided by neurons.

As previously described, *Fig4*[-/flox]*,SynCre* mice exhibit impaired movement and region-specific vacuolization and neurodegeneration (Figure 2.3A", 2.3B", 2.3C", 2.3D") (Ferguson et al., 2012b). In contrast, *Fig4*[-/flox]*,Olig2Cre* mice exhibit very mild vacuolization in brain (Figure 2.3A''', 2.3B''', 2.3C''', 2.3D'''). Consistent with the known expression of the *Olig2* promoter in motor neurons (Mizuguchi et al., 2001) ventral spinal cord of *Fig4*[-/flox]*,Olig2Cre* mice shows extensive vacuolization (Figure 2.3D'''), similar to *Fig4*[-/flox]*, Mnx1Cre* (otherwise referred to as *Fig4*[-/flox]*,Hb9Cre)* mice (Figure 2.3E) (Vaccari et al., 2015). Analysis of *Fig4*[-/flox]*,Hb9Cre* spinal cord identified enlarged vacuoles within motoneuron axons, greatly extending their diameter and pushing the axoplasm into a thin peripheral rim near the plasma membrane (Figure 2.3F). In contrast to the movement disability and reduced survival of *Fig4*[-/flox]*,SynCre* mice (Ferguson et al., 2012b), the movement of *Fig4*[-/flox]*,Olig2Cre* mice is normal and no premature death was observed, with the oldest now surviving beyond 14 months of age (Figure 2.3G).   There are no obvious defects in mobility of littermate controls and *Fig4*[-/flox]*,Olig2Cre* conditional mutant mice at P23, as demonstrated in the Videos 1 and 2.

Fig4 deficiency in neurons or OLs leads to developmental dysmyelination of the optic nerve

Analysis of P21 retina revealed the presence of numerous vacuoles in the inner retina of _Fig4$^{-/flox}$,SynCre_ mice but no defects in overall morphology or stratification (Figure 2.4A'). No vacuoles were detected in the _Fig4$^{-/flox}$,Olig2Cre_ retina (Figure 2.4A''). For ultrastructural analysis, optic nerves of _Fig4_ conditional knock-out mice were processed for transmission electron microscopy (TEM). In P21 _Fig4_ control mice (retaining at least one intact allele of _Fig4_), the fraction of myelinated axons in the optic nerve is 79± 2%. In optic nerves of _Fig4$^{-/flox}$,SynCre_ mice, only 9± 3% of axons are myelinated and in _Fig4$^{-/flox}$,Olig2Cre_ mice only 12± 1% of axons are myelinated (Figure 2.4B-B'' and 2.4D). To assess myelin health, we determined the g-ratio (the ratio of the inner axonal diameter to the total fiber diameter) of myelinated axons in the optic nerve of _Fig4_ control and conditional mutants. Compared to control mice, a small but significant increase in g-ratio was observed in _Fig4$^{-/flox}$,SynCre_ and _Fig4$^{-/flox}$,Olig2Cre_ mice, an indication of myelin thinning (Figure 2.4E). To determine whether the optic nerve hypomyelination at P21 reflects a transient delay in myelin development, rather than a lasting defect, we repeated the analysis with adult mice. Similar to P21 optic nerves, ultrastructural analysis of both types of adult optic nerves revealed profound hypomyelination (Figure 2.4C-C''). At P60-75, 92± 2% of axons are myelinated in _Fig4_ control nerves. This is reduced to 16± 4% in _Fig4$^{-/flox}$,SynCre_ mice and 12± 2% in _Fig4$^{-/flox}$,Olig2Cre_ mice (Figure 2.4F). It is noteworthy that conditional ablation of _Fig4_ either in neurons or OLs leads to preferential absence of myelin sheaths on small and intermediate caliber axons, while many large caliber axons undergo myelination (Figure 2.4B', 2.4B'', 2.4C' and 2.4C'').

Few axons in the optic nerve of adult _Fig4$^{-/flox}$,SynCre_ mice showed signs of degeneration (Figure 2.4C'). No evidence for axonal degeneration was observed in _Fig4$^{-/flox}$,Olig2Cre_ optic

nerves. CNS hypomyelination in *Fig4$^{-/flox}$,Olig2Cre* mice was still present at P150, the oldest time point examined by TEM (data not shown). Thus, the optic nerve hypomyelination observed at P21 is not transient in nature but persists into adulthood. We conclude that selective ablation of *Fig4* either in neurons or in the OL lineage leads to profound CNS dysmyelination.

Conditional ablation of *Fig4* in neurons or the OL lineage impairs nerve conduction

To determine whether the morphological defects in CNS myelin of *Fig4* conditional mutants result in functional deficits, we performed electrophysiological recordings. We measured the conduction velocity and amplitude of compound action potentials (CAPs) in optic nerves acutely isolated from P21 mice. Global deletion of *Fig4* (*Fig4$^{-/-}$*) results in a dramatic reduction in a population of fast conducting fibers and a corresponding increase in the proportion of slowly conducting fibers (Figure 2.5A, 2.5B, 2.5E) (Winters et al., 2011). The average velocity of the largest peak in *Fig4* control nerves carrying at least one intact allele of *Fig4* is 1.9± 0.1 m/s but in *Fig4$^{-/-}$* nerves this is reduced to 0.7± 0.2 m/s. A similar CAP redistribution was observed in optic nerves prepared from *Fig4$^{-/flox}$,SynCre* mice (0.7± 0.1 m/s) and *Fig4$^{-/flox}$,Olig2Cre* mice (0.6± 0.03 m/s) (Figure 2.5C, 2.5D, 2.5E). Thus, consistent with biochemical and morphological analyses (Figure 2.1 and 2.4), loss of *Fig4* in neurons or in the OL-lineage results in slowed nerve conduction.

Reduced number of mature OLs in *Fig4$^{-/flox}$,Olig2Cre* and *Fig4$^{-/flox}$,SynCre* optic nerves

To assess the cellular basis of the CNS hypomyelination phenotype, we stained optic nerve cross sections from *Fig4* conditional mutants for markers in the OL lineage. Compared to *Fig4* control optic nerves, the diameter of nerves from P21 *Fig4$^{-/flox}$,SynCre* and *Fig4^{-}*

/flox,Olig2Cre mice were each reduced by 20%. The density of NG2$^+$ progenitor cells in optic nerve tissue sections is comparable among the three genotypes (Figure 2.6A-2.6A'' and 2.6D). The density of Olig2$^+$ cells, a marker that labels immature and mature OLs, is reduced, as is labeling of *Plp1*, a mature OL marker (Figure 2.6B-2.6B'', 2.6C-2.6C'', 2.6E and 2.6F). These studies indicate that OPCs are present at normal density and tissue distribution in the *Fig4* conditional null optic nerves, but they fail to generate the normal population of mature myelin-forming OLs.

Loss of *Fig4* attenuates OL differentiation *in vitro*

For a more detailed analysis of the OL lineage, we isolated primary OPCs from P6-P14 *Fig4* pups by anti-PDGFRα immunopanning (Emery and Dugas, 2013). Yields of OPCs per brain did not differ between control and *Fig4*-deficient mice (data not shown). OPCs were cultured for two days *in vitro* (DIV2) under proliferating conditions, fixed and analyzed by double-immunofluorescence staining of Ki67 and PDGFRα. The density of Ki67$^+$/PDGFRα$^+$ cells in *Fig4$^{+/+}$* and *Fig4$^{-/-}$* cultures is very similar (Figure 2.8A-B). After culture under standard differentiation conditions for 4 days, absence of PDGF and presence of triiodothyronine (T3), OPCs isolated from *Fig4$^{+/+}$* (control) or *Fig4$^{-/-}$* pups both acquire a highly arborized morphology and positive staining for OL markers. The density of NG2$^+$ cells and CNPase$^+$ cells, normalized to Hoechst 33342 dye$^+$ nuclei, is comparable among wildtype and *Fig4*-deficient cultures (Figure 2.7A-2.7B', and 2.7C). However, the fraction of cells expressing the more mature OL markers MAG and MBP was significantly reduced in *Fig4$^{-/-}$* cultures (Figure 2.7A-2.7B', and 2.7C). A more detailed categorization of post-mitotic OLs, based on actin and MBP double-labeling, revealed a significantly decreased number of *Fig4*-deficient OLs that matured to a stage with

lamellar MBP$^+$ membrane sheets (Zuchero et al., 2015) (Figure 2.7D-E).   The reduced number

of mature OLs in *Fig4$^{-/-}$* cultures was not caused by increased cell death (Figure 2.8C-E). For a

quantitative assessment of protein expression in primary OLs from *Fig4$^{+/+}$* and *Fig4$^{-/-}$* brains,

DIV 3 cultures were lysed and analyzed by capillary Western blotting   (Figure 2.9A-C). FIG4 is

clearly detected in *Fig4$^{+/+}$* OL lysates but not in *Fig4$^{-/-}$* OL lysates.   In *Fig4$^{-/-}$* lysates MAG is

significantly reduced. Collectively, these data suggest that the initial programs of OL maturation

progress normally in the absence of *Fig4* while later stages of OL-differentiation, including

lamellar membrane expansion, are *Fig4*-dependent.

**Independent perturbation of three components of the PI(3,5)P$_2$ biosynthetic complex all
result in severe CNS hypomyelination**

Together with the kinase PIKFYVE and the scaffolding protein VAC14, FIG4 forms a

biosynthetic complex necessary for acute interconversion of PI(3) and PI(3,5)P$_2$. The complex is

located on the cytosolic surface of vesicles trafficking through the LE/Lys compartment

(McCartney et al., 2014a).   As an independent test of the effect of perturbation of the

FIG4/PIKFYVE/VAC14   enzyme   complex   on   CNS   myelination,   we   generated

Pikfyve$^{flox/flox}$,Olig2cre mice predicted to be more severely deficient in PI(3,5)P$_2$ than the FIG4

and VAC14 mutants. Consistent with this expectation, the phenotype of the *Pikfyve* mutant mice

is much more severe, with a significant tremor (Videos 3 and 4) and death at 2 weeks of age (n=

16 pups). FluoroMyelin Green staining of P13 brain tissue revealed profound hypomyelination

of the corpus callosum, internal capsule and cerebellar white matter of *Pikfyve$^{flox/flox}$,Olig2cre*

pups (Figure 2.10A-A'). *In situ* hybridization of *Plp1* revealed a virtual absence of mature OLs

in the *Pikfyve$^{flox/flox}$,Olig2cre* brain, including structures in the forebrain and cerebellar white

matter (Figure 2.10B-2.10D').   Toluidine blue staining of P13 optic nerve sections revealed

many fibers with clearly visible myelin profiles in *Pikfyve* positive control mice and a striking

absence of myelin profiles in *Pikfyve$^{flox/flox}$;Olig2cre* conditional mutants (Figure 2.11B-D).

Moreover, deficiency of *Pikfyve* in OLs results in a pronounced accumulation of large

perinuclear vesicles in the optic nerve (Figure 2.11B, D). Defects in differentiation of *Pikfyve$^{-/-}$*

OL cultures are more pronounced than in *Fig4$^{-/-}$* OL cultures. Deficiency of *Pikfyve* reduces

OPC proliferation (Figure 2.10E-E', and 2.10G) and results in a 95± 1% reduction in cells that

progress to the MBP^{+} stage, compared with wildtype cells (Figure 2.10F-F', and 2.10H).   In

addition to *Fig4* and *Pikfyve* mutants, we also examined myelinogenesis in the well-

characterized recessive *Vac14* mouse mutant L156R (*Vac14^{L156R}*) (Jin et al., 2008). The L156R

missense mutation impairs the interaction of VAC14 with PIKFYVE, but not with FIG4 (Figure

2.12A).   Similar to *Fig4$^{-/-}$* mice, *Vac14$^{L156R/L156R}$* mice exhibit ~50% reduction in PI(3,5)P$_2$.

Immunoblots of brain membranes prepared from *Vac14$^{L156R/L156R}$* mice showed significantly

reduced levels of the myelin markers MAG, CNPase, and MBP (Figure 2.12B-E). The electrical

properties of optic nerve from *Vac14^{L156R}* homozygous mice were also impaired, with a

significant increase in the population of slowly conducting fibers (Figure 2.12F-H). Consistent

with this observation, toluidine blue staining of optic nerve sections of adult wild-type mice

revealed many myelinated fibers but optic nerves of adult *Vac14$^{L156R/L156R}$* mice showed few

myelinated fibers (Figure 2.13A-D). Thus, independent genetic disruptions of the

FIG4/PIKFYVE/VAC14 enzyme complex all result in severe hypomyelination and a PI(3,5)P$_2$

dosage-dependent decline in CNS white matter development.

Myelin proteins are present within enlarged LAMP1$^+$ perinuclear vacuoles in primary OLs from *Fig4$^{-/-}$* mice

The FIG4/PIKFYVE/VAC14 biosynthetic complex regulates intracellular PI(3,5)P$_2$ and thereby influences membrane trafficking through the endo-lysosomal system. DIV2 primary OPC cultures established from *Fig4* control (*Fig4$^{+/+}$* or *Fig4$^{-/+}$*) and *Fig4$^{-/-}$* mice were fixed and subjected to anti-LAMP1 and anti-PDGFRα double-immunofluorescence labeling. The majority of *Fig4$^{-/-}$* OPCs showed normal-sized lysosomes with a diameter of < 1μm, while a few cells (< 20 %) exhibited enlarged LAMP1$^+$ vesicles (Figure 2.15A-B). Upon OL differentiation, an increase in size and number of perinuclear LAMP1$^+$ vesicles is observed in *Fig4$^{-/-}$* cultures. The enlarged perinuclear LAMP1$^+$ structures are prominently labeled with anti-MAG (Figure 2.15C-D''). In a parallel approach, *Fig4$^{-/-}$* OLs were transfected with *Rab7-YFP*, a reporter for LE. Enlarged perinuclear vacuoles in Fi*g4$^{-/-}$* OLs are positive for Rab7-YFP (Figure 2.16A-A'). Live imaging of primary OLs revealed that the majority of enlarged perinuclear vacuoles in *Fig4$^{-/-}$* OLs are stable for several days. However, vacuole size varies and live imaging revealed that some vacuoles appear and disappear over a period of 12 hours (Video 5). Collectively, these studies demonstrate that in *Fig4$^{-/-}$* OLs, myelin building blocks that are normally trafficked through the LE/Lys are present in abnormal, enlarged vesicles the majority of which is stable for several days.

Cell surface derived MAG is trapped in large vacuoles in the LE/Lys compartment of *Fig4$^{-/-}$* OLs

In developing OLs, myelin proteins such as MAG and PLP transiently accumulate on the plasma membrane (PM) at the cell soma, prior to undergoing endocytosis and LE/Lys dependent

transport to the myelin sheet (Winterstein et al., 2008). To monitor trafficking of MAG, we used antibody tagging in live OL cultures.   In wildtype OLs, anti-MAG-Alexa488 binds to MAG on the PM surface, undergoes endocytosis and is targeted to LAMP1^{+} vesicles in the LE/Lys compartment (Figure 2.16B-B''). In these wildtype cultures, anti-MAG^{+} vesicles are small, with a median volume of 0.3± 0.06 μm^{3}, and partially overlap with LysoTracker^{+} vesicles (Figure 2.14A-A"). In contrast, in *Fig4$^{-/-}$* OLs, anti-MAG-Alexa488 is endocytosed and accumulates in LAMP1^{+} perinuclear vacuoles with greatly enlarged size (≥5 μm^{3}, mean volume 94± 41 μm^{3}) and also in smaller MAG^{+}/LAMP1^{+} vesicles with a median volume of 0.7± 0.25 μm^{3}. The average size of all vesicles in *Fig4$^{-/-}$* OLs is 1.65 ± 0.32 μm^{3} (Figure 2.14B-B" and C, Figure 2.16C-C"). This suggests that independent of *Fig4* genotype, MAG is transported to the PM and is rapidly endocytosed.   In *Fig4$^{-/-}$* OLs, large MAG^{+}/LAMP1^{+} vesicles rarely overlap with LysoTracker staining (Figure 2.14B-B"), suggesting that large vesicles may exhibit reduced acidification. As an independent approach to assess whether perturbation of PI(3,5)P$_2$ synthesis causes accumulation of MAG in large perinuclear vacuoles, wildtype OL cultures were treated with 1 μM apilimod, a potent inhibitor of PIKfyve (Cai et al., 2013).   Treatment with apilimod for 90-120 min leads to the formation of large perinuclear vacuoles laden with MAG (Figure 2.14D-D"), similar to those in *Fig4$^{-/-}$* OLs.   To evaluate the specificity of the anti-MAG-Alexa488 antibody, experiments were repeated with primary OLs isolated from *Mag$^{-/-}$* pups (Pan et al., 2005).   Bath application of anti-MAG-Alexa488 to *Mag$^{-/-}$* OLs treated with vehicle or apilimod did not result in immunostaining, demonstrating that the antibody is specific for MAG (Figure 2.17A-D''). The myelin protein MOG has a different endocytotic fate from MAG, trafficking through recycling endosomes (RE) but not the lysosomal compartment (Winterstein et al., 2008). Simultaneous antibody labeling of cell surface MAG and MOG in live OLs

confirmed distinct endocytotic trafficking routes in both *Fig4* control and *Fig4*[^-/-] cultures. Importantly, in *Fig4*[^-/-] OLs, MOG was not present in the enlarged vacuoles that are typically laden with MAG (Figure 2.18A-B''). This suggests that the defect in *Fig4*[^-/-] OLs in trafficking of myelin building blocks from the PM is specific for trafficking through the LE/Lys compartment and does not affect trafficking through the RE.

Fig4[^-/-] OLs display impaired MAG trafficking through the LE/Lys compartment

The perinuclear location and large size of MAG$^+$ vacuoles suggests that their mobility may be compromised, potentially leading to impaired trafficking of MAG and other myelin building blocks transported via the LE/Lys route. To explore this possibility, we assessed movement of MAG$^+$ vesicles in live OLs using time-lapse imaging (Figure 2.19A-B'). Small vesicles labeled with anti-MAG-Alexa488 are observed in *Fig4*$^{+/+}$ and *Fig4*$^{-/-}$ primary OLs, with average volumes of 0.3 μm^3 and 0.7 μm^3, respectively. The average velocity of these "normal-sized" vesicles is comparable in *Fig4*$^{+/+}$ and *Fig4*$^{-/-}$ cells: 0.09± 0.01 $\mu m/s$ and 0.07± 0.01 $\mu m/s$, respectively (Figure 2.19C). The large MAG$^+$ vesicles in the *Fig4*$^{-/-}$ OLs with an average volume of 94± 41 μm^3 are more stationery, with an average velocity of 0.033± 0.005 $\mu m/s$ (Figure 2.19C), and they fail to reach the nascent myelin sheet. These data suggest that trafficking of MAG and other LE/Lys dependent myelin building blocks is impaired in the *Fig4*$^{-/-}$ OLs. Collectively, these studies indicate that PI(3,5)P$_2$ is critical for myelin protein trafficking through the LE/Lys compartment in developing OLs.

PI(3,5)P$_2$ is important for myelin membrane trafficking in live brain slices

Inter-cellular communication is critical for proper development of the axo-glial unit. To extend the studies of myelin protein trafficking to a system that contains intact axo-glial units, we prepared acute forebrain slices from P10-P14 mice and kept them in oxygenated artificial cerebrospinal fluid. Trafficking of MAG was monitored by bath application of mouse anti-MAG-Alexa555 for 2 hours at 32°C. To distinguish between endocytosed MAG and PM localized MAG, brain slices were fixed and incubated with a secondary anti-mouse-Alexa488 conjugated antibody under non-permeabilizing conditions. Endocytosed MAG containing vesicles were prominently found in OL perinuclear regions and along cellular processes that form the myelin internode (Figure 2.20A-A"). Only a small fraction of MAG is labeled with both antibodies, and thus localized to the PM on the cell surface (Figure 2.20A-A"). To visualize cells in the OL lineage, we repeated MAG trafficking studies with brain slices from the *ROSA-LacZ/EGFP*,*Olig2Cre* reporter mouse. Vesicular MAG labeling was abundant in EGFP$^+$ cells, indicating that endocytosis of PM localized MAG does occur in cells of the OL-lineage and vesicular labeling is not the result of nonspecific antibody uptake by microglia or other cell types (Figure 2.21A-C). To control for antibody specificity, brain slices from *Mag$^{-/-}$* mice were processed in parallel and revealed no significant labeling (Figure 2.21D-F). Thus, acute brain slices provide an opportunity to study myelin protein trafficking in live tissue. To assess whether PI(3,5)P$_2$ is required for endocytosis and trafficking of PM derived MAG in live brain tissue, the experiment was repeated with forebrain slices prepared from *Pikfyve$^{flox/flox}$*,*Olig2Cre* pups. Strikingly, in the absence of PI(3,5)P$_2$, MAG$^+$ labeling was restricted to abnormal perinuclear accumulations, and trafficking to cell processes was virtually absent (Figure 2.20B'-10B"). The

data demonstrate that in brain slices, as well as cultured cells, $PI(3,5)P_2$ is required for proper membrane trafficking from the PM through the LE/Lys compartment.

2.4 Discussion

Multiple independent means of perturbing the FIG4/VAC14/PIKFVYE enzyme complex all lead to profound CNS hypomyelination. Remarkably, conditional ablation of *Fig4* either in neurons or OLs is sufficient to disrupt normal CNS myelination, indicating that both OL-intrinsic and OL-extrinsic mechanisms of OL maturation function in a *Fig4*-dependent manner. The hypomyelination phenotype in *Fig4* conditional mutants and $VAC14^{L156R}$ mice is physiologically relevant since it is associated with substantially reduced amplitude and conduction velocity of compound action potentials. Primary OPCs deficient in *Fig4* progress normally to the stage of NFOs but their differentiation into mature OLs is impaired. In $Fig4^{-/-}$ OLs, MAG is trafficked to the PM, undergoes endocytosis and is localized to enlarged $LAMP1^+$ perinuclear vacuoles. The reduced motility of the enlarged $MAG/LAMP1^+$ vacuoles and their perinuclear position suggests that myelin building blocks are trapped in the LE/Lys compartment and cannot be delivered to the developing myelin sheath. Conditional deletion of *Pikfyve* in the OL lineage leads to more pronounced defects characterized by impaired OL differentiation, greatly reduced myelin membrane trafficking and profound CNS dysmyelination. Together, these studies firmly establish a critical role for the FIG4/PIKFYVE/VAC14 enzyme complex, and by extension its lipid product $PI(3,5)P_2$, in myelin protein trafficking through the LE/Lys system in developing OLs and proper assembly of the axo-glial unit.

Impaired PI(3,5)P$_2$ metabolism attenuates OL differentiation

Immunohistological studies of *Fig4$^{-/flox}$,Olig2Cre* optic nerves and experiments with *Fig4$^{-/-}$* primary OLs did not detect a significant change in OPC density or reduction in viability. OPCs deficient for *Fig4* progress and differentiate normally to the stage of newly formed OLs (NFOs), a postmitotic cell type characterized as PDGFRα$^-$, GalC$^+$, MOG$^-$ (Zhang et al., 2014). However, differentiation of NFOs into mature OLs is PI(3,5)P$_2$-dosage dependent. The arrest of OL differentiation becomes more severe as PI(3,5)P$_2$ levels are reduced to ~ 50% of wildtype levels, in *Fig4* and *VAC14* mice, or completely depleted in *Pikfyve* mutant mice. OL maturation is highly regulated, and can be attenuated or blocked by perturbation of numerous signaling pathways and transcriptional programs (Emery et al., 2009, Bercury and Macklin, 2015, Marinelli et al., 2016). The fate of immature OLs that fail to progress to the mature stage remains unclear. However, these cells are likely to be short-lived and destined to die. The number of activated caspase-3$^+$ cells in the OL lineage of *Fig4$^{-/-}$* mice is not significantly increased (Winters et al., 2011), suggesting that immature OLs either do not die in large numbers or die in a caspase-independent manner. Additional studies are needed to determine exactly at which stage of OL lineage progression PI(3,5)P$_2$ deficiency impairs differentiation and how PI(3,5)P$_2$ regulates progression to a mature myelin producing cell.

Fig4-dependent trafficking of myelin building blocks through the LE/Lys

Like epithelial cells, OLs are polarized, with the myelin sheath resembling the apical membrane domain and the membrane near the OL cell body the basolateral membrane domain (Salzer, 2003, Maier et al., 2008, Masaki, 2012). Myelin-producing OLs synthesize and transport large quantities of myelin building blocks (lipids and proteins) in order to segmentally

ensheath multiple axons. Myelinogenesis also requires membrane sorting and trafficking to specific subdomains of the nascent myelin membrane sheath. Indeed, the final destination of myelin proteins may vary between compact myelin (e.g. PLP), peri-axonal loops (MAG) or abaxonal loops (MOG) of non-compact myelin (Arroyo and Scherer, 2000, Salzer, 2003, White and Kramer-Albers, 2014). As in other polarized cells, OL proteins may be targeted through direct transport pathways from the Golgi to their final destination (Salzer, 2003). Alternative strategies are also employed to target key myelin constituents to their final destination. The mRNA for MBP, encoding a protein important for axon wrapping and myelin compaction, is packaged into RNA-granules and transported to distal sites within OL processes for regulated translation (Muller et al., 2013). MAG, PLP, and MOG are synthesized in the endoplasmatic reticulum and transported through the Golgi network to the PM near the OL cell body (analogous to the basolateral domain) as an intermediate target. From there MOG is targeted to the recycling endosome (RE) while MAG and PLP are targeted to the LE/Lys for delivery to the myelin sheath (analogous to the apical membrane domain) (Simons and Trajkovic, 2006, Maier et al., 2008, Winterstein et al., 2008). LAMP1 is a marker for LE/Lys and we show that MAG is targeted to LAMP1$^+$ vesicles in both *Fig4$^{+/+}$* and *Fig4$^{-/-}$* OLs. A key feature of the MAG/LAMP1 double-labeled vesicles in *Fig4$^{-/-}$* mutant OLs is their greatly enlarged size and perinuclear position. The average velocity of these vesicles is significantly reduced, suggesting impaired membrane trafficking through the LE/Lys compartment. Trafficking defects in *Fig4$^{-/-}$* OLs are confined to the LE/Lys compartment as trafficking of MOG through RE occurs apparently normal, independent of *Fig4* genotype. The severe CNS hypomyelination phenotype in *Fig4$^{-/flox}$,Olig2Cre* mice is likely not the result of impaired MAG trafficking alone, but rather the result of mistrafficking of numerous myelin building blocks normally migrating through the

LE/Lys compartment. For example, cholesterol (in part bound to PLP) and glycosphingolipids are endocytosed from the PM and stored in LE/Lys vesicles (Trajkovic et al., 2006, Winterstein et al., 2008). During OL maturation, neuronal signals trigger a profound redistribution of PLP-containing membrane domains; endocytosis is reduced and PLP together with cholesterol and glycosphingolipids is moved from the LE/Lys to the PM (Trajkovic et al., 2006). In humans, impaired trafficking of PLP due to mutation or altered dosage of the *Plp1* gene, causes Pelizaeus-Merzbacher disease (PMD) and Spastic Paraplegia Type 2 (SPG2), developmental disorders with severe neurological impairment (Inoue, 2005). Overexpression of PLP in mice leads to accumulation of the protein in autophagic vesicles and LE/Lys, leading to reduction of other myelin proteins such MBP, MAG, and MOG (Karim et al., 2007). As in *Fig4*^{-/-} mice, PMD results in reduced number of OLs and CNS dysmyelination. Failure of lysosomal trafficking or function is thus a common underlying mechanism for a growing number of hereditary disorders that cause CNS dysmyelination, including PMD, Niemann-Pick type C disease, and several lysosomal storage diseases (Folkerth, 1999, Yaghootfam et al., 2005, Prolo et al., 2009, Schweitzer et al., 2009, Faust et al., 2010, Grishchuk et al., 2014).

PI(3,5)P$_2$-dependent trafficking of myelin membrane components in developing OLs

Different phosphoinositides exhibit unique distribution to intracellular membrane compartments and have been implicated as key regulators of membrane sorting and targeted vesicular trafficking (Mayinger, 2012). PI(3,5)P$_2$, for example, decorates vesicles in the LE/Lys compartment and serves as a docking site for cytosolic proteins (Mayinger, 2012). PIP binding proteins frequently interact with small GTPases belonging to the Rab or Arf families, establishing a combinatorial code that defines membrane identity (Behnia and Munro, 2005,

Stenmark, 2009, Jean and Kiger, 2012, Mayinger, 2012, Egami et al., 2014). The phosphorylation status of PIPs and the activation state of small GTPases can be rapidly modified, providing an identification code that is both unique and dynamic, two prerequisites for targeted membrane transport. In HeLa cells, for example, the lysosomal membrane is characterized by the presence of PI(3,5)P_2 and the small GTPases Rab7 and Arf-like (Bucci et al., 2000, Hofmann and Munro, 2006). In fibroblasts cultured from $Fig4^{-/-}$ or $VAC14^{L156R/L156R}$ mice, PI(3,5)P_2 levels are reduced by ~50% leading to formation of greatly enlarged LAMP1$^+$ vacuoles (Chow et al., 2007, Jin et al., 2008, Zou et al., 2015). In $Fig4^{-/-}$ OLs, Rab7-YFP localizes to large perinuclear vacuoles (Figure 2.16). In HeLa cells, overexpression of constitutively active Rab7 leads to formation of large LAMP1$^+$ and LAMP2$^+$ vacuoles (Bucci et al., 2000). A direct interaction of VAC14 with the Rab7 GTPase activating protein (GAP) TBC1D15 has recently been described in HeLa cells (Schulze et al., 2014). This suggests the existence of a large protein complex that controls the interconversion of PI(3)P and PI(3,5)P_2 and the activity of select Rab GTPases, an emerging theme for directed membrane trafficking (Jean et al., 2015). Rab GTPases constitute a large protein family whose members are localized to distinct intracellular membrane microdomains to coordinate vesicle trafficking (Stenmark, 2009, Hutagalung and Novick, 2011). The GTPase Rab3A is expressed in OLs and has been shown to participate in membrane trafficking and myelination (Schardt et al., 2009). As discussed above, transport of myelin membrane components, including PLP, cholesterol and MAG, involves membrane sorting and trafficking through the LE/Lys compartment prior to insertion into the nascent myelin sheath (White and Kramer-Albers, 2014). Thus, interference with PI(3,5)P_2 synthesis, turnover, or binding partners that define LE/Lys membrane identity results in impaired cargo delivery of key myelin membrane components required for membrane expansion and sheath formation.

Neuronal *Fig4* participates in CNS myelination

The severe hypomyelination phenotype in *Fig4$^{-/flox}$, SynCre* mice suggests that *Fig4*-dependent neuronal signals are necessary for proper CNS myelination. When coupled with our previous finding that transgenic *Fig4* directed by the NSE promoter on a *Fig4$^{-/-}$* background (*Fig4$^{-/-}$,NSE-Fig4*) rescues the myelination defect (Winters et al., 2011, Ferguson et al., 2012b), this suggests that normal levels of *Fig4* in neurons is necessary for CNS myelination and that neuronal overexpression of recombinant *Fig4* on a global *Fig4$^{-/-}$* background is sufficient to drive CNS myelination. Multiple lines of evidence have demonstrated that neuron-derived signals regulate OL maturation and axon myelination (Coman et al., 2005, Trajkovic et al., 2006, Ohno et al., 2009, Winters et al., 2011, Yu and Lieberman, 2013, Yao et al., 2014). We speculate that neuronal *Fig4* regulates LE/Lys-dependent transport and axonal presentation of a "pro-myelination" signal(s) necessary for OL differentiation and CNS axon myelination and that transgenic overexpression of *Fig4* in neurons (NSE-Fig4) leads to an elevated production of "pro-myelination" signals(s) sufficient to rescue the deficiency of *Fig4* in the OL lineage of the *Fig4$^{-/-}$,NSE-Fig4* transgenic mice. Alternatively, neuronal *Fig4* may accelerate the loss of "anti-myelination" signal(s) on the axonal surface, e.g., through endocytosis. Inter-cellular communication may occur through paracrine action of secreted molecules or shedding vesicles. Exosomes are extracellular vesicles produced by many cells that facilitate transport and exchange of proteins, mRNAs and regulatory RNAs with important functions in cellular processes including myelination (Fruhbeis et al., 2012, Pusic and Kraig, 2014). Because *Fig4* plays an important role in membrane trafficking through the LE/Lys system, it is possible that protein secretion or the content and abundance of exosomes may be altered in the mutant mice. Two independent approaches to delete *Fig4* in the OL lineage (*Olig2Cre* and *PdgfraCreER*)

revealed that *Fig4* is required in the OL lineage for proper CNS myelination. These data were corroborated by *in vitro* studies with primary OLs. Taken together, our observations suggest that endogenous levels of *Fig4* gene expression in both neurons and OLs are necessary for normal CNS myelination.

Technical limitations in the specificity of transgene promoters may affect the interpretation of these experiments. For neuron-specific loss-of-function we employed female *SynapsinCre/+* mice driven by a synapsin-1 gene (SYN1) promoter fragment (Rempe et al., 2006), and for neuron-specific gain-of-function studies we used a 4.6 kb *NSE* promoter fragment (Winters et al., 2011, Ferguson et al., 2012a). While these are commonly used strategies, it is recognized that in the developing mouse the *NSE* (ENO2) and *SYN1* promoters may have some leakiness that results in transient expression in non-neuronal cells including glia. A low level of expression of the endogenous *SYN1* and *ENO2* genes in OPCs/OLs has been reported (Zhang et al., 2014), but it is not clear whether this expression is retained by the promoter fragments that were used to drive transgene expression. Independent of these technical limitations, we provide multiple lines of evidence that genetic manipulations that compromise PI(3,5)P$_2$ synthesis profoundly impact OL differentiation and CNS myelination.

Novel assay to monitor myelin protein trafficking in brain tissue

Acutely prepared brain slices are viable for several hours when maintained in oxygenated ACSF, a method commonly used for electrophysiological recordings (Lee et al., 2008). Studies with primary OLs suggest that newly synthesized myelin proteins are initially transported to the PM near the cell soma where they interact with lipids and other myelin proteins (Winterstein et al., 2008). These myelin-like structures are then thought to be endocytosed and trafficked to

specific subdomains of the nascent myelin membrane sheath. Using acute brain slices combined with genetic labeling of cell in the OL lineage and confocal microscopy, we show that antibody-labeled MAG on the PM becomes rapidly endocytosed and is found in small vesicles in the OL cell soma and long processes that form internodes. Since sorting and trafficking of myelin building blocks are key components of myelinogenesis, future studies using acute brain slices may be productively combined with pharmacological and genetic manipulations to obtain detailed understanding of membrane trafficking in developing OLs.

2.5 Methods

Transgenic mice – All mice were housed and cared for in accordance with NIH guidelines, and all research conducted was done with the approval of the University of Michigan Committee on Use and Care of Animals. The spontaneous $Fig4^{-/-}$ null mutation plt (Chow et al., 2007) is maintained as two congenic lines, C57BL/6J.plt/+ and C3HeB/FeJ.plt/+. F1 plt/plt homozygotes obtained from crosses between these lines survive to 30-45 days, permitting analysis of myelination, and these were used for most experiments. A subset of *in vitro* experiments was carried out on cells from the C3HeB/FeJ.plt congenic mice. The conditional $Fig4^{flox}$ allele was described elsewhere (Ferguson et al., 2012b) and is maintained on strain C3HeB/FeJ from which the retinal degeneration locus *rd* was removed by repeated backcrossing and selection. Neuron-specific conditional knockout mice ($Fig4^{-/flox}$,*SynCre*) were generated and maintained as previously described (Ferguson et al., 2012b). The *Olig2Cre/+* line (Schuller et al., 2008) and the *PdgfraCre-ER/+* (Kang et al., 2010) (Jackson Laboratory stock # 018280) were used to delete *Fig4* in the OL lineage. For inducible gene ablation in $Fig4^{-/flox}$,*PdfraCreER* mice, 4-hydroxytamoxifen (4OH-tamoxifen) (Sigma-Aldrich, MO) was injected directly into the

70

stomach of P5 pups, which is easily identified by its milky-white color. 4OH-tamoxifen was dissolved in 100% ethanol at 10 mg/ml and 5 μl/day were administered for 2 days. *Fig4$^{-/flox}$,Hb9Cre* (*Fig4$^{-/flox}$,Mnx1Cre*) mice have been described previously (Vaccari et al., 2015). The spontaneous point mutant *VAC14^{L156R}* is deficient in PIKfyve binding (Jin et al., 2008) and was maintained on a C3HeB/FeJ strain background from which the retinal degeneration locus *rd* was removed by repeated backcrossing. *Pikfyve$^{flox/flox}$* mice were generated on the C57BL/6J strain background (Christian et al., 2014) and were crossed with *Olig2Cre/+* mice. *Mag$^{-/-}$* mice on a C57BL/6J background have been described elsewhere (Pan et al., 2005). LacZ/ EGFP reporter mice (Jackson laboratory stock #003920) were crossed with *Olig2Cre/+* mice.

Transmission electron microscopy (TEM) – Postnatal day (P)21 and P60-P75 mice were deeply anesthetized with ketamine (200 mg/kg)/xylazine (20 mg/kg body weight) and perfused transcardially with ice-cold phosphate buffer saline (PBS) for 2 min, followed by 4% paraformaldehyde (PFA) and 2.5% glutaraldehyde in Sorensen's buffer and embedded in epoxy resin as described (Winters et al., 2011). Semi-thin sections were stained with toluidine blue for light microscopy. TEM micrographs were taken at 10,500-13,500x magnification with a Philips CM-100 or a JEOL 100CX microscope and analyzed using FIJI software. *Fig4$^{-/flox}$,Hb9Cre* (Vaccari et al., 2015), *Fig4$^{-/flox}$,Olig2Cre* and *Fig4$^{-/flox}$,SynCre* conditional mutants were analyzed and compared to littermate controls. Throughout the study, control mice are defined as mice that have at least one intact copy of the *Fig4* allele and include the following genotypes (i) *Fig4$^{+/-}$*, (ii) *Fig4$^{-/flox}$*, (iii) *Fig4$^{+/flox}$,Olig2Cre* and (iv) *Fig4$^{+/flox}$,SynCre*.

Immunohistochemistry - Mice between P10 and adulthood were perfused transcardially with ice-cold 4% PFA in PBS. Brains were post-fixed in perfusion solution for 2 hours at 4°C for *in situ* hybridization. For immunofluorescence labeling, brains were postfixed overnight and

cryoprotected in 30% sucrose in PBS. For FluoroMyelin staining, brains were cryosectioned at

25-40 µm. Free-floating sections were rinsed 3x 5min in PBS and then stained with

FluoroMyelin Green (Millipore, MA, 1:200) in PBS for 20min. Sections were washed with PBS,

mounted onto microscope slides, coverslipped with Prolong Gold antifade supplemented with

DAPI (Life Technologies, CA) and imaged with an Olympus IX71 microscope attached to a

DP72 camera. For immunofluorescence labeling of optic nerves, nerves were rapidly dissected,

kept in perfusion solution for 30 min and cryoprotected in 30% sucrose in PBS. Cross sections

(12-20 µm) were mounted onto microscope slides, rinsed 3x for 5min in PBS and incubated for

1h in blocking solution: 1% horse serum and 0.1% Triton-X100 in PBS (anti-Olig2) or 4%

normal goat serum and 0.3% Triton-X100 in PBS (anti-NG2). Primary antibody incubation was

done overnight at 4°C in blocking solution with rabbit anti-Olig2 (1:1000 Millipore) or rabbit

anti-NG2 (1:800, Abcam, UK). The next day, sections were rinsed 3x 5min with PBS, incubated

with appropriate secondary antibodies for 1 h at room temperature (1:1000, Alexa-conjugated,

Life technologies), rinsed in PBS and mounted in Prolong Gold supplemented with DAPI.

RNA in situ hybridization - cDNA fragments of *Mbp and Plp1* (Ye et al., 2009) were used to

produce digoxigenin-labeled cRNA probe by run-off *in vitro* transcription. Brains were

cryosectioned at 25 µm and mounted directly onto Superfrost[+] microscope slides (Fisher

Scientific, MA). Optic nerve sections were prepared as described above and postfixed in 4%

PFA/PBS overnight at 4°C. The following day, sections were rinsed with 1x PBS and

dehydrated with series of ethanol dilutions (50%, 70%, 95%, and 100%). Sections were then

treated with 50µg/ml proteinase K in PBS/5mM EDTA for 15 min (optic nerves) and 30 min for

brain sections. All subsequent steps were performed as described previously (Winters et al.,

2011).

Isolation of brain membranes – P21 mouse brains were homogenized in a Wheaton Dounce tissue homogenizer cooled on ice. Brain membranes were isolated by centrifugation in a discontinuous sucrose gradient as described previously (Winters et al., 2011).

Isolation of brain tissue - P21 control littermate and *Fig4$^{-/flox}$,PdfrαCreER* brains were isolated and rapidly dissected on ice. Tissue was separated into two groups: 1) cerebellum + brainstem and 2) neocortex + hippocampus + thalamus ("forebrain"). Tissue was lysed in a radio-immunoprecipitation assay buffer (RIPA) using a tissue homogenizer and triturated with a 16G needle. Lysates were spun at 14,000 rpm for 15min at 4°C and supernatants were analyzed by Western blotting as described below.

Western blot analysis - Equal amounts of protein (7.5-15 μg) from brain membranes were separated by SDS-PAGE and transferred onto PVDF membranes (Millipore). Membranes were blocked in 3% dry milk dissolved in Tris-HCl pH 7.4 buffered saline containing 0.3% Triton X-100 for at least 1 h and incubated with primary antibody overnight at 4°C. Primary antibodies included mouse anti-βIII tubulin (1:20,000; Promega, WI), rabbit anti-MAG (1:1000; Winters et al., 2011), rat anti-MBP (1:1000; Millipore), mouse anti-CNPase (1:1000, Abcam), anti-PLP (1:1000, Abcam), and mouse anti-Fig4 (1:200, NeuroMab, CA). Primary antibodies were detected using either horseradish peroxidase (HRP)-conjugated secondary antibodies (1:2000-15000; Millipore Bioscience Research Reagents) or Alexa-conjugated secondary antibodies (1:20,000, Molecular Probes). The Licor C-DiGit and Odyssey imaging systems and software were used for visualization and quantification of protein bands (Licor, NE).

Electrophysiology: Recordings were carried out as described elsewhere (Carbajal et al., 2015). Briefly, juvenile (P21-P23) and adult (3-4 months) mice were sacrificed by CO_2 inhalation. Optic nerves were rapidly dissected, incubated at room temperature in oxygenated artificial

cerebrospinal fluid (ACSF) for 45 minutes and then transferred to a temperature-controlled recording chamber (held at 37± 0.4°C) with oxygenated ACSF. Each end of the nerve was drawn into the tip of a suction pipette electrode. The stimulating electrode was connected to a constant-current stimulus isolation unit (WPI, FL) driven by Axon pClamp 10.3 software and a 50 μs pulse was applied to the retinal end of the nerve. The recording electrode was applied to the chiasmatic end of the nerve and connected to the input of a differential AC amplifier (custom-made). A second pipette, placed near the recording pipette but not in contact with the nerve, served to subtract most of the stimulus artifact from the recordings. Signals were digitized at 100 kHz through a data acquisition system (Axon Digidata 1440A, Axon pClamp 10.3, Molecular Devices, CA).

Primary OL cultures and immunocytochemistry – OPCs were isolated from P6-14 mouse pups with the following genotypes (i) *Fig4$^{+/+}$*, (ii) *Fig4$^{+/-}$*, (iii) *Fig4$^{-/-}$*, (iv) *Fig4$^{-/flox}$,Olig2Cre* or (v) *Pikfyve$^{flox/flox}$,Olig2Cre*. For immunopanning, anti-PDGFRα (BD Biosciences, CA) or O4 antibody (hybridoma cells kindly provided by Dr Jonah Chan) coated plates were used, as described (Dugas and Emery, 2013). For the first two days *in vitro*, OPCs were cultured on poly-D-lysine (Sigma-Aldrich) coated glass coverslips in DMEM-SATO medium supplemented with forskolin (Sigma, 10ng/ml), PDGF (20ng/ml, Peprotech, NJ), CNTF (10ng/ml, Peprotech), and NT3 (1ng/ml, Peprotech). For differentiation studies, OPCs were switched to medium supplemented with T3 (40ng/ml, Sigma-Aldrich) without growth factors. Cells were allowed to differentiate for 4-6 days prior to fixation in 4% PFA/PBS at RT for 15min. For immunofluorescence labeling, cells were rinsed 3x 5min each in PBS, permeabilized with 0.1% Triton-X100 in PBS for 30 min and blocked for 60 min in 3% BSA in PBS. The following primary antibodies were used: rabbit anti-NG2 (1:500, Millipore), rat anti-PDGFRα (1:1000, BD

Biosciences, CA), rabbit anti-PDGFRα (1:500, Cell Signaling, MA), rat anti-MBP (1:300, Millipore), rabbit anti-CNPase (1:1000, Assay Biotech, CA), rabbit anti-Ki67 (1:1000, Abcam), mouse anti-MAG (1:300, Millipore), rat anti-Lamp1 (1:1000, Abcam), mouse anti-GFAP (1:2000, Sigma-Aldrich). Cells were incubated with primary antibodies overnight at 4°C. The following day, cells were rinsed 3x 5min each with PBS, and incubated with secondary antibodies for 1hr in blocking solution. Following several rinses in PBS, cells were incubated with the nuclear markers Hoechst 33342 or ToPro3 dye (Life Technologies) and imaged with an Olympus IX71 inverted microscope (Olympus, JP) with a DP72 camera or a Leica SP5 confocal microscope (Leica, DE). Representative confocal images were taken at 63x magnification as z-stacks with 1 μm intervals. Maximum intensity z projections were generated using Fiji. For cell viability experiments, the Live/Dead kit (Life Technologies) was used following the manufacturer's instructions. For actin staining, Actin Red 555 (Life Technologies) was used following the manufacturer's instructions.

For live cell imaging, OPCs were switched to T3 supplemented differentiation medium and kept at 37°C in a 5% CO_2 incubator equipped with an IncuCyte Zoom imaging system (Essen Bioscience, MI). Images were taken with a 20x objective every 2 hours for 3 days. Data were analyzed using the IncuCyte Zoom software and Fiji.

Live cell imaging - O4[+] primary OLs were isolated by immunopanning as described above and cultured in 35 mm glass bottom dishes (Mattek, MA). After 2-3 days under differentiation conditions, anti-MAG-Alexa488 conjugated antibody (1:500, Millipore, MAB1567A4) was added to the culture medium for 12-14 hours. The following day, LysoTracker Deep Red (1:2000, Life Technologies) was added to the culture medium for 30-45 min. Fifteen minutes before imaging, the culture medium was replaced by 1x HBSS (Life Technologies) containing

Prolong Live Antifade reagent (Life Technologies, 1:100) and Hoechst dye 33342 (1:50,000) or NucRed Live 647 (Life Technologies). Cells were imaged at 37°C and ambient CO_2 for 15-20 min/dish using a Leica SP5 confocal microscope. Confocal Z-stacks, xyt, and xyzt videos were acquired. As a specificity control for the anti-MAG-Alexa488 antibody, OLs were prepared from $Mag^{-/-}$ and age-matched $Mag^{+/+}$ pups and imaged under identical conditions. Mouse monoclonal anti-MOG antibody (Millipore) was conjugated with Alex555 using the Antibody Labeling Kit (Life Technologies). Some OL cultures were incubated with anti-MOG-Alexa555 (1:250) and anti-MAG-Alexa488 as described above. To some cultures 1 μM apilimod (Axon 1369; Axon Medchem BV) in DMSO was added 90-120 minutes prior to imaging. Images and videos were processed using Leica AS LF and Fiji. Tracking and movement analysis of anti-MAG-Alexa488$^+$ particles in live cells was performed using Imaris (Bitplane, UK).

Ex vivo MAG labeling – To monitor MAG trafficking in acute brain tissue, sagittal slices were prepared from P13-P14 pups with the following genotypes, (i) *Pikfyve* control mice, (ii) littermates *Pikfyve* $^{flox/flox}$,*Olig2Cre* mice, (iii) *Mag$^{-/-}$,* mice and (iv) P18 *LacZ/EGFP, Olig2Cre* (Toth et al., 2013). Briefly, mice were decapitated, brains rapidly dissected and submerged in ice-cold ACSF (Toth et al., 2013). From forebrain tissue, hippocampi were removed and discarded. Cortex and striatum were sectioned at 300 μm using a tissue slicer (WPI, FL). Brain slices were kept in oxygenated (95% O_2, 5% CO_2) ACSF at RT for 40-60 min prior to incubation with anti-MAG-Alexa -555 (1:500) in oxygenated ACSF at 32°C for 2 hours. Brain slices were then fixed in 4% PFA for 25 min, rinsed 3 times for 10 min each in PBS and incubated overnight with a goat anti-mouse Alexa 488 secondary antibody (1:1000) in 3% BSA at 4°C. The following day, slices were rinsed 3 times for 10min each in PBS, incubated with LiveRed 647 for 25 min at RT, rinsed 3 times for 10min each in PBS, and mounted in Prolong antifade with

DAPI. Individual MAG^{+} cells in deep cortical layers and striatum were imaged using a Leica SP5 confocal microscope.

Primary OL transfection – For transfection of primary OPC/OLs, Lipofectamine2000 (Life Technologies) was used, following a protocol previously established for transfection of primary neurons (Duan et al., 2014). Briefly, 250 ng of *LAMP1-mCherry* or *Rab7-YFP* plasmid DNA were combined with 1 µl of Lipofectamine2000 (Invitrogen, CA) in optiMEM and mixed thoroughly. Transfection solution was added to OL culture medium and cells were incubated for 2.5 hours. Afterwards, the medium was completely replaced with fresh T3 supplemented medium. To visualize MAG trafficking, anti-MAG-Alexa488 antibody was added to the culture medium as described above. The following day, live imaging of LAMP1-mCherry[+]/anti-MAG-Alexa488^{+} OLs was carried out as described above.

Western blot analysis of OPC cultures - OPCs were allowed to expand in PDGF supplemented culture medium for 7-8 days, passaged and plated in 6-well culture dishes at a density of 200,000-300,000 cells/well and kept for 3 days in T3 supplemented medium. Cells were then processed for Western blotting as previously described (Raiker et al., 2010). Capillary immunoassays were performed using the automated Wes system (ProteinSimple, San Jose CA). All procedures were performed according to manufacturer's protocol. In brief, 0.8 µg of lysate (4 µl) were mixed with 2 µl of 5x fluorescent master mix and boiled for 5 min. These samples were dispensed into microplates along with blocking solution, primary and secondary antibodies and chemiluminescent substrate. After centrifugation, microplate was loaded into the Wes instrument for subsequent protein separation on capillaries and immuno-detection using the standard electrophores, immunolabeling, detection scheme of Wes. Data were analyzed by using Compass

software (ProteinSimple) and peak areas were used for quantification. Erk1 peak area was used for normalization between samples. Three independent preparations were processed.

*Statistical analysi*s - To assess myelination in the optic nerve, ten non-overlapping TEM images were randomly selected and the fraction of myelinated axons quantified as described (Winters et al., 2011). At least 600 axons were quantified per nerve. G-ratio analysis was performed as described previously (Winters et al., 2011). At least 100 axons per optic nerve were analyzed. For Western blot analysis, Western band intensity was measured using LI-COR Studio Image Software. All band intensities were normalized either to βIII-tubulin (brain lysates and membranes) or actin (OPC cultures). Normalized Western blot band intensity for control samples was set as 1 for each experiment. For optic nerve electrophysiology, data analysis was performed offline using Clampfit software. In order to analyze individual peaks, each trace was fitted as a sum of three or four Gaussians using Origin Pro software (Chen et al., 2004). A peak with the largest amplitude in each trace was used for conduction velocity analysis.

For quantification of *Plp1*, Olig2, and NG2 labeled cells, the number of respective positive cells was quantified per optic nerve cross section and normalized to the section area (arbitrary units in FIJI). At least four sections per nerve were analyzed.

For quantification of OL markers *in vitro*, ten non-overlapping images were taken at random positions for each coverslip/well and cells positive for a marker of interest counted and normalized to the number of Hoechst 33342 dye positive cells in the same image. A minimum of 900 cells was quantified for each individual experiment with *Fig4* cultures and a minimum of 120 cells was quantified for each individual experiment with *Pikfyve* cultures. GFAP$^+$ astrocytes were excluded from quantification. The analysis of actin/MBP postmitotic OL morphology was performed as characterized previously (Zuchero et al., 2015).

For cell viability experiments, the Live/Dead kit was used the number of live (green) and dead (red) cells was quantified and the live/total cell ratio was calculated. For all experiments, Hoechst 33342 normalized cell density in control groups was set as 1. At least three independent experiments with duplicate coverslips were used for the analysis. For live imaging of MAG$^+$ vesicles in primary OLs, Imaris software (Bitplane) was used to calculate individual particle speed and size. Four independent experiments were analyzed for $Fig4^{+/+}$ and $Fig4^{-/-}$ cultures. MAG$^+$ particles of at least $0.01\mu m^3$ in volume were included in data analysis.

One-way ANOVA followed by Tukey posthoc was used for TEM optic nerve analysis. One-way ANOVA followed by Dunnett's posthoc was used for Western blot analysis and electrophysiology with more than two groups. The unpaired Student t-test was used for analysis in all experiments with two groups.

2.6 Author Contributions.

Y.A.M, M.H.M., and R.J.G. designed the study. Y.A.M., G.M.L., J.P.L., S.J.L., I.V., S.H.M., performed the experiments. The rest of the authors contributed reagents, assisted with manuscript preparation, and provided experimental feedback. Y.A.M., M.H.M., and R.J.G. wrote the manuscript.

2.7 Acknowledgements
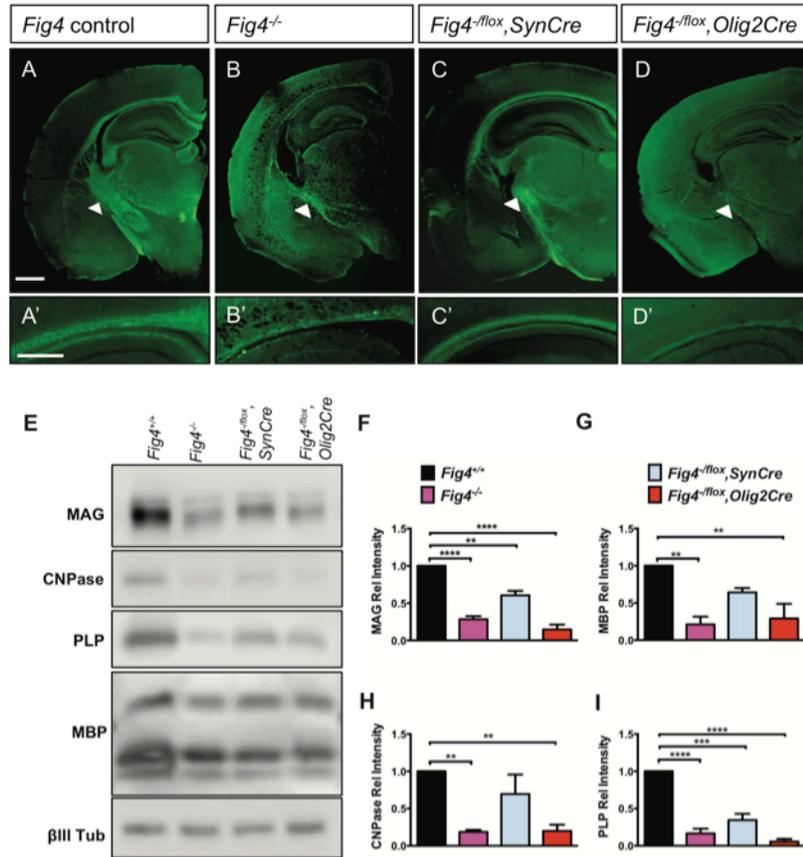
Figure 2.1 Conditional ablation of *Fig4* in neurons or OLs leads to CNS hypomyelination.
(A-D) Coronal sections of juvenile (P21-30) mouse forebrain stained with FluoroMyelin Green.
(A) *Fig4* control mice (harboring at least one *Fig4* WT allele), **(B)** *Fig4* germline null mice
(*Fig4*$^{-/-}$), **(C)** *Fig4*$^{-/flox}$,*SynCre* mice and **(D)** *Fig4*$^{-flox}$,*Olig2Cre* mice.   Thinning of the corpus
callosum and internal capsule (white arrowheads) is observed in *Fig4*$^{-/-}$, *Fig4*$^{-/flox}$,*SynCre,* and
Fig4^{-flox},*Olig2Cre* mice. **(A'-D')** Higher magnification images of the corpus callosum. Scale bar
(A-D), 1 mm and (A'-D'), 400 μm. **(E)** Representative Western blots of P21 brain membranes
prepared from *Fig4*$^{+/+}$ (WT), *Fig4* $^{-/-}$, *Fig4*$^{-/flox}$,*SynCre* and *Fig4*$^{-/flox}$,*Olig2Cre* mice probed with
antibodies specific for the myelin proteins MAG, CNPase, PLP, and MBP. To control for protein
loading, membranes were probed for the neuronal marker class III β-tubulin (βIII Tub). **(F-I)**
Quantification of Western blot signals for MAG, MBP, CNPase, and PLP in *Fig4*$^{+/+}$ (black
bars), *Fig4*$^{-/-}$ (purple bars), *Fig4*$^{-/flox}$,*SynCre* (light blue bars), and *Fig4*$^{-flox}$,*Olig2Cre* (red bars)
brain membranes. Quantification of myelin protein signals is normalized to βIII Tub. Relative
protein intensities compared to WT brain are shown as mean value ± SEM.   For each of the four
genotypes, three independent membrane preparations were carried out. One-way ANOVA with
multiple comparisons, Dunnett posthoc test; ** ($p < 0.01$), *** ($p < 0.001$) and **** ($p < 0.0001$).
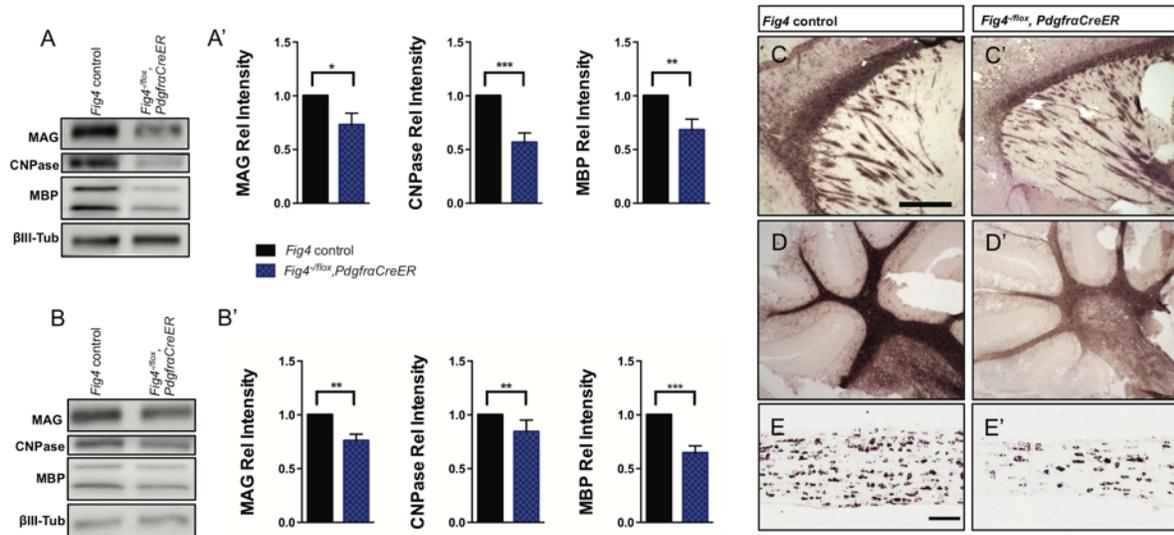
Figure 2.2 CNS hypomyelination in *Fig4$^{-/flox}$,PdgfraCreER* mice. Representative Western blots of (**A**) P21 forebrain and (**B**) P21 hindbrain (cerebellum/brainstem) lysates prepared from *Fig4* control littermate mice (*Fig4$^{+/flox}$,PdgfraCre-ER*) and *Fig4$^{-/flox}$,PdgfraCreER* mutant mice, probed with antibodies specific for the myelin proteins MAG, CNPase and MBP. To control for protein loading, blots were probed for the neuronal marker class III β-tubulin (βIII Tub). (**A'** and **B'**) Quantification of Western blot signals for MAG, CNPase and MBP in (A') forebrain and (B') cerebellum/brainstem lysates. Relative protein intensities compared to control tissue are shown as mean value ± SEM. Six pairs of control littermate and *Fig4$^{-/flox}$,PdgfraCreER* mice were analyzed and quantified. Unpaired Student's *t*-test, *p= 0.0323 (MAG), **p= 0.0096 (A', MBP), **p= 0038 (B' CNPase), 0027 (B', MAG), ***p= 0.0006 (A', CNPase), ***p= 0.0004 (B', MBP). (**C** and **C'**) Sagittal sections of P21 forebrain of control littermate *(Fig4$^{+/flox}$,PdgfraCreER)* and *Fig4$^{-/flox}$,PdgfraCreER* mutant mice probed for *Mbp* mRNA expression. (**D** and **D'**) Sagittal sections of P21 cerebellum of control littermate *(Fig4$^{+/flox}$,PdgfraCreER)* and *Fig4$^{-/flox}$,PdgfraCre-ER* mutant mice probed for *Mbp* mRNA expression. (**E** and **E'**) Longitudinal optic nerve sections probed for *Plp1* mRNA expression. Scale bar (C-D'), 500 μm and (E and E'), 200 μm.

Figure showing histology panels. Column headers: *Fig4^{flox/-}*, *Fig4^{-/-}*, *Fig4^{flox/-},Syn-cre*, *Fig4^{flox/-},Olig2-cre*. Row labels: neocortex (A, A', A'', A'''), cerebellum (B, B', B'', B'''), DRG (C, C', C'', C'''), Spinal Cord Ventral Horn (D, D', D'', D''').

Scale bars: 200 μm (neocortex), 200 μm (cerebellum), 50 μm (DRG), 200 μm (spinal cord).

E — *Fig4^{flox/-},Hb9cre* — 100 μm

F — *Fig4^{flox/-},Hb9cre* — 2 μm

G — Survival curve. % surviving vs Age (months). *Fig4^{flox/-},Olig2-cre* (n=5); *Fig4^{flox/-},Syn-cre* (n=15).

Figure 2.3 Loss of *Fig4* in the OL-lineage or neurons differentially affects spongiform degeneration and lifespan. (**A-D'''**) Hematoxylin/eosin stained tissue sections of P30 mouse neocortex, cerebellum, dorsal root ganglion (DRG) and spinal cord ventral horn. Tissue sections of mice with the following genotypes are shown: (**A, B, C, D**) control mice (*Fig4$^{flox/-}$*), (**A', B', C' D'**) *Fig4* germline null mice (*Fig4$^{-/-}$*), (**A", B", C", D"**) *Fig4$^{-/flox}$,SynCre* conditional mutants and (**A''', B''', C''', D'''**) *Fig4$^{-/flox}$,Olig2Cre* conditional mutants. Most notable are the large vacuolar (sponge-like) structures in different regions of the *Fig4$^{-/-}$* nervous system, including (**A'**) deep layers of the neocortex, (**B'**) deep cerebellar nuclei, (**C'**) DRGs and (**D'**) ventral horn of the spinal cord. (**A"-D"**) A milder but similar phenotype is observed in *Fig4$^{-/flox}$,SynCre* mice. (**A'''**) In the *Fig4$^{-/flox}$,Olig2Cre* neocortex small vacuoles are observed in all layers of the neocortex. (**B'''** and **C'''**) In *Fig4$^{-/flox}$,Olig2Cre* mice deep cerebellar nuclei and DRGs look largely normal. (**D'''**) The large vacuoles in the spinal cord ventral horn of *Fig4$^{-/flox}$,Olig2Cre* mice likely represent motoneurons, as the *Olig2* promoter is known to drive cre expression in motoneurons and the OL-linage. (**E**) The *Hb9-cre* driver line was used for conditional deletion of *Fig4* specifically in motoneurons. Toluidine blue stained section of *Fig4$^{-/flox}$,Hb9Cre* ventral horn shows multiple large vacuolar structures within the gray and white matter of the spinal cord. Examples of vacuolar structures are labeled with asterisks. Apparently normal motoneuron profiles are indicated by arrows. (**F**) Electron micrograph of *Fig4$^{-/flox}$,Hb9Cre* ventral horn with large vacuolar structures labeled by asterisks. Vacuolar structures are mostly devoid of electron-dense material and found in axons surrounded by thin myelin sheaths (arrows). Vacuoles cause peripheral displacement of axoplasm and mitochondria. The arrowhead points to a dystrophic axon with accumulation of numerous smaller vesicles. (**G**) Viability of *Fig4* conditional mutants. Kaplan-Meier plot shows an average life-span of 6 months for *Fig4$^{-/flox}$,SynCre* mice (n= 15), while *Fig4$^{-/flox}$,Olig2Cre* mice (n= 5) are viable for 12-14 months (the oldest mice currently in our colony).
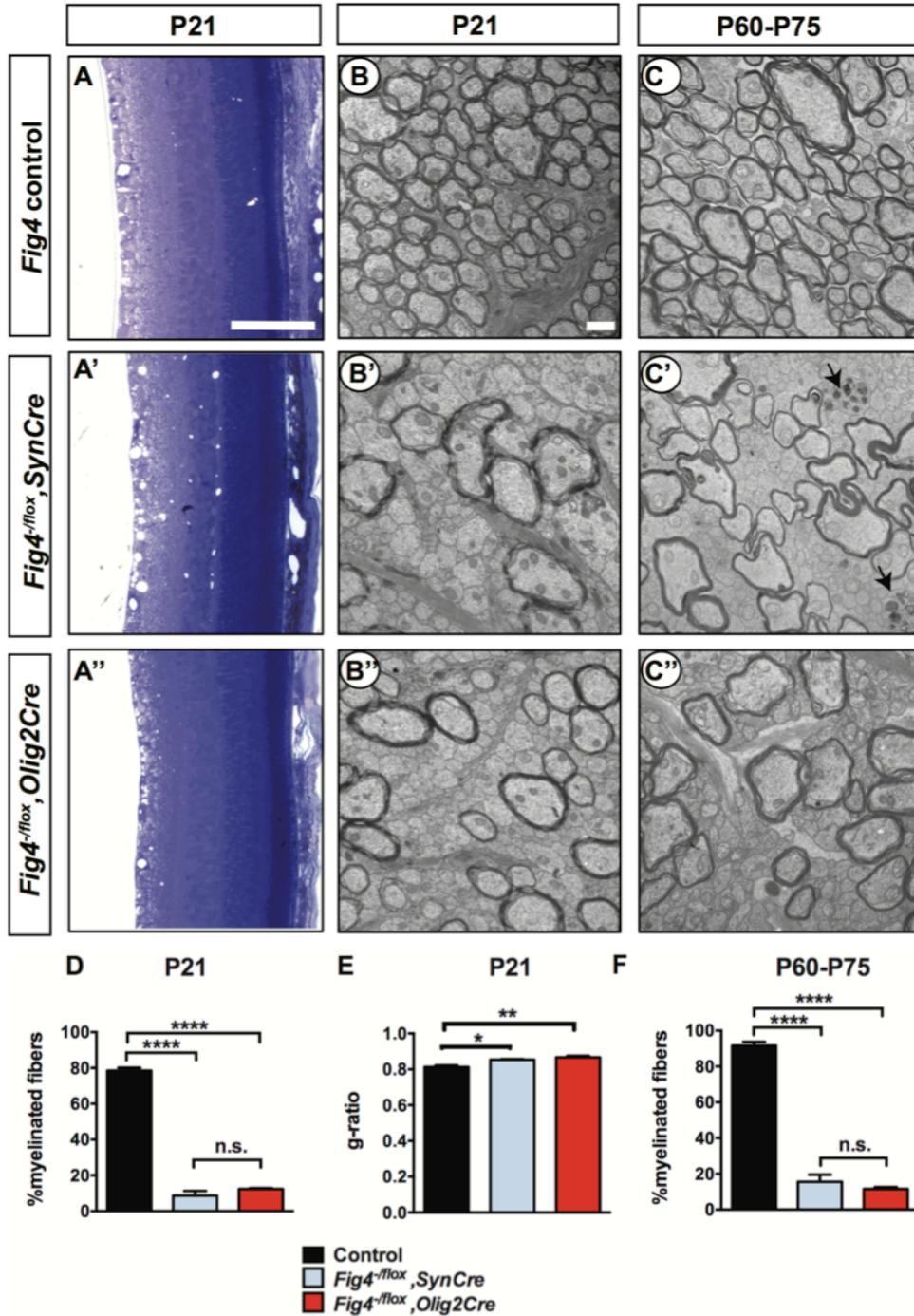
Figure 2.4 Conditional ablation of *Fig4* in neurons or in OLs leads to severe dysmyelination of the optic nerve. (A-A'') Sagittal sections of juvenile (P21) mouse retina embedded in epoxy resin and stained with toluidine blue. (A) *Fig4* control mice, harboring at least one *Fig4* WT allele, (A') *Fig4⁻ᐟflox,SynCre* mice and (A'') *Fig4⁻ᐟflox,Olig2Cre* mice. Scale bar, 100 μm. **(B-B'')** Representative TEM images of optic nerve cross sections of P21 (B) *Fig4* control, (B') *Fig4⁻ᐟflox,SynCre* and (B'') *Fig4⁻ᐟflox,Olig2Cre* mice. **(C-C'')** Representative TEM images of optic

nerve cross sections of adult (P60-75) mice. (C) *Fig4* control, (C') *Fig4$^{-/flox}$,SynCre* and (C'') *Fig4$^{-/flox}$,Olig2Cre* mice. Black arrows in C' indicate the presence of dystrophic axons. Scale bar (B-C'') = 1 μm. **(D)** Quantification of percentage of myelinated fibers in the optic nerve at P21 and P60-75. At P21, *Fig4* controls (n=3 mice, 3 nerves); *Fig4$^{-/flox}$,SynCre* (n= 2 mice, 3 nerves) and *Fig4$^{-/flox}$,Olig2Cre* (n= 3 mice, 3 nerves). **(E)** Quantification of myelinated fiber g-ratios in the optic nerve at P21, n=3 animals, 3 nerves for all groups. **(F)** Quantification of myelinated fibers in the optic nerve at P60-P75. *Fig4* control (n= 4 mice, 4 nerves), *Fig4$^{-/flox}$,SynCre* (n= 4 mice, 4 nerves); *Fig4$^{-/flox}$,Olig2Cr*e (n= 3 mice, 4 nerves). Results are shown as mean value ± SEM, one-way ANOVA with multiple comparisons, Tukey posthoc test; n.s. (p > 0.05), *(p=0.0211), **(p=0.0055), **** (p < 0.0001).
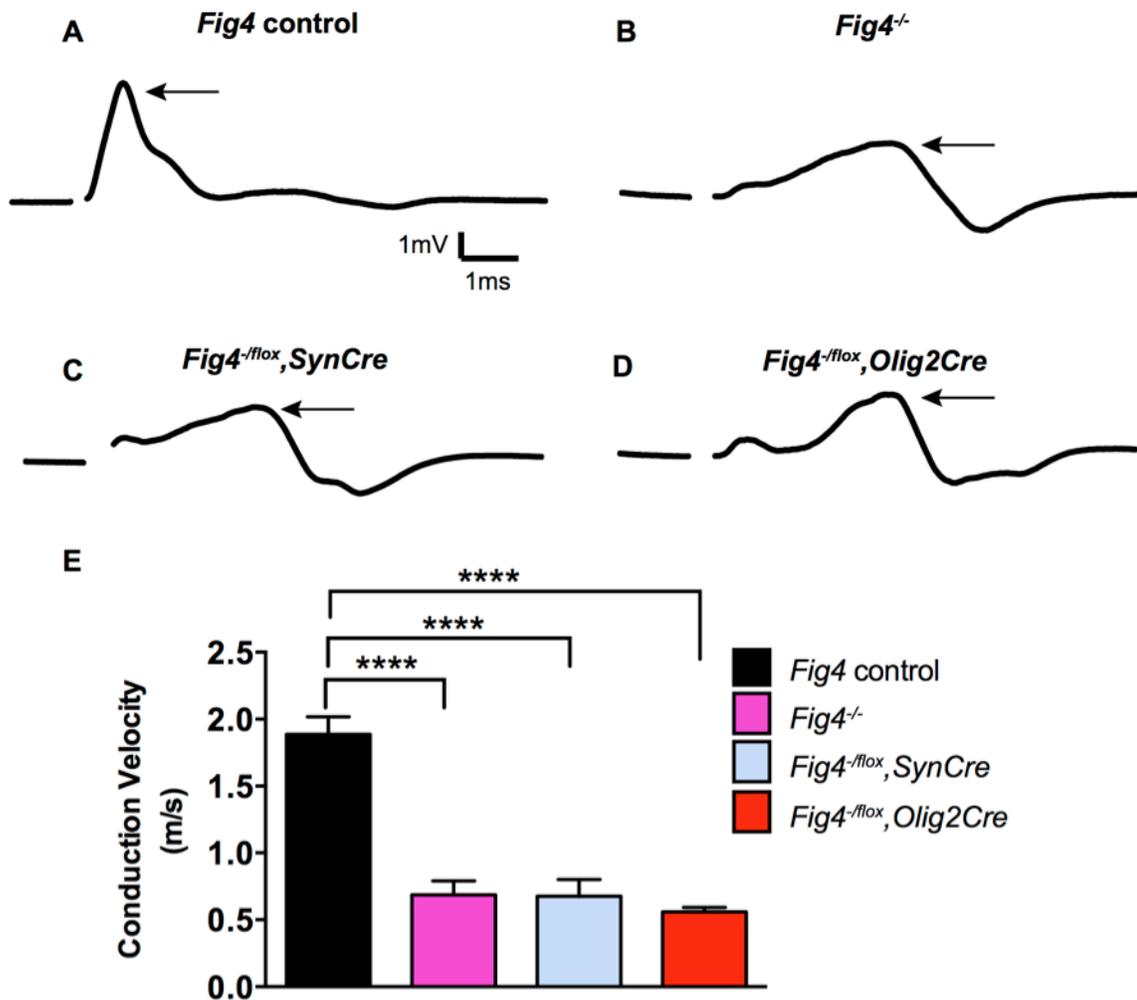
Figure 2.5 Conditional ablation of *Fig4* in neurons or OLs leads to impaired conduction of electrical impulses in the optic nerve. Compound action potential (CAP) recordings from acutely isolated optic nerves of P21 mice. **(A)** Representative CAP traces recorded from *Fig4* control mice, harboring at least one *Fig4* WT allele (n= 14 nerves), **(B)** *Fig4* $^{-/-}$ mice (n= 5 nerves), **(C)** *Fig4*$^{-/flox}$,*SynCre* mice (n= 11 nerves) and **(D)** *Fig4*$^{-/flox}$,*Olig2Cre* mice (n= 9 nerves). For each graph, the arrow indicates the largest amplitude peak, as identified by Gaussian fit. **(E)** Quantification of average conduction velocity of largest amplitude peaks identified in **A-D**. Results are shown as mean value ± SEM, one-way ANOVA with multiple comparisons, Dunnett posthoc, **** ($p < 0.0001$).
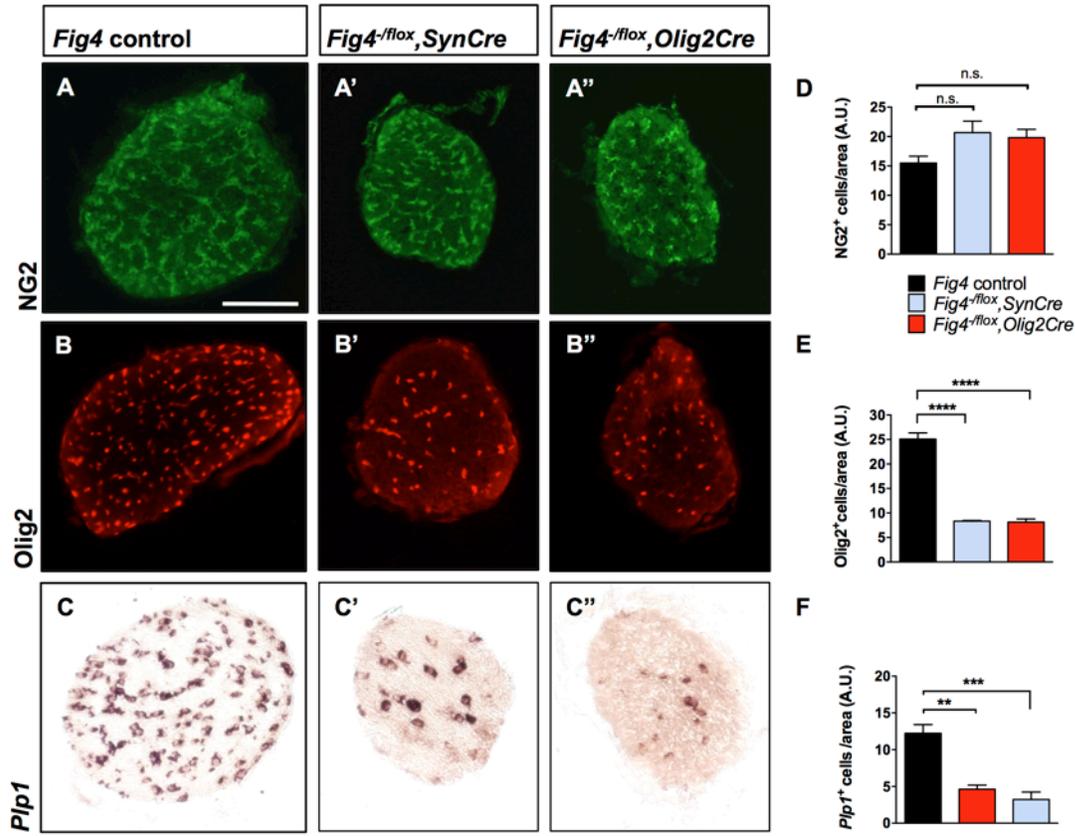
Figure 2.6 Conditional ablation of *Fig4* in neurons or OLs results in a decrease of mature OLs. **(A, B, C)** Optic nerve cross sections from P21 *Fig4* control mice, harboring at least one *Fig4* WT allele, **(A', B', C')** *Fig4$^{-/flox}$,SynCre* mice and **(A'', B'', C'')** *Fig4$^{-/flox}$,Olig2Cre* mice were stained with anti-NG2, anti-Olig2 or probed for *Plp1* mRNA expression. Scale bar = 100 μm. **(D-F)** Quantification of labeled cells in optic nerve cross sections normalized to area in arbitrary units (A.U.). **(D)** The density of NG2$^+$ cells in *Fig4* control (n= 4 mice), *Fig4$^{-/flox}$,SynCre* (n= 3 mice) and *Fig4$^{-/flox}$,Olig2Cre* (n= 3 mice) optic nerves is not significantly (n.s.) different. **(E)** Quantification of the density of Olig2$^+$ cells in *Fig4* control (n= 6 mice), *Fig4$^{-/flox}$,SynCre* (n= 3 mice) and *Fig4$^{-/flox}$,Olig2Cre* (n= 4 mice) optic nerves. **(F)** Quantification of the density of *Plp1$^+$* cells in *Fig4* control (n= 8 mice), *Fig4$^{-/flox}$,SynCre* (n= 4 mice) and *Fig4$^{-/flox}$,Olig2Cre* (n= 4 mice) optic nerves. Results are shown as mean value ± SEM, one-way ANOVA with multiple comparisons, Dunnett's posthoc test. ** ($p = 0.001$), *** ($p = 0.0002$) and **** ($p < 0.0001$).
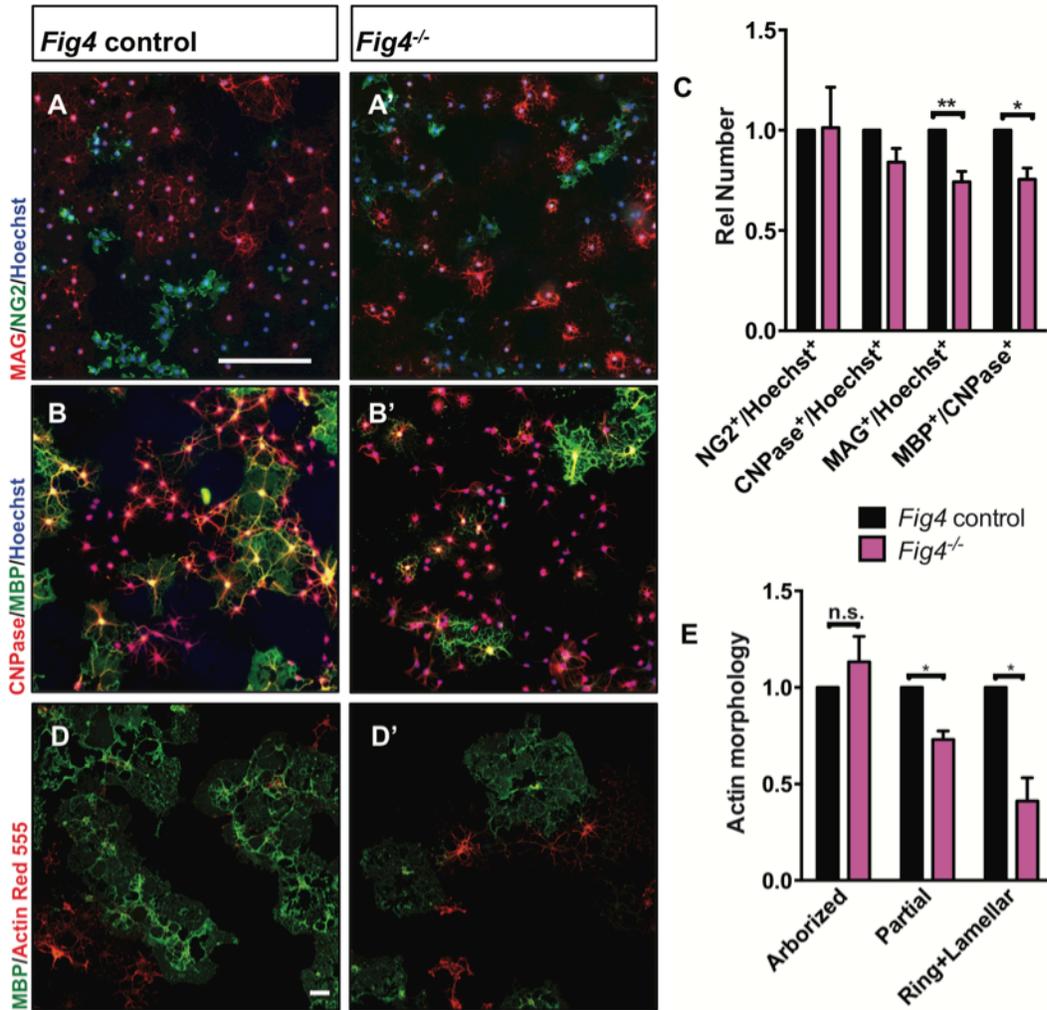
Figure 2.7 *Fig4*-**deficient OLs show impaired differentiation and membrane expansion** *in vitro.* Representative images of *Fig4* control *(Fig4$^{+/+}$ or Fig4$^{+/-}$)* and *Fig4$^{-/-}$* primary OLs after 4 days in differentiation medium, fixed and stained for the OL-lineage markers (**A** and **A'**) NG2 and MAG; (**B** and **B'**) CNPase and MBP. Scale bar in A-B', 200 μm. (**C**) Quantification of NG2, CNPase, MAG, and MBP/CNPase labeled cells in *Fig4* control (n= 3) and *Fig4$^{-/-}$* (n= 3) cultures normalized to Hoechst 33342 dye labeled cells. The ratio of immunolabeled cells over Hoechst^{+} cells in *Fig4* control cultures was set at 1. Results are shown as mean value ± SEM, multiple t-test analysis with Holm-Sidak method. **p= 0.0075 (MAG), *p= 0.012 (MBP). (**D** and **D'**) Confocal images of MBP^{+} and Actin Red 555^{+} OLs in *Fig4* control and *Fig4$^{-/-}$* cultures. Nuclei were labeled with TO-PRO-3, scale bar = 20 μm. (**E**) Quantification of the fraction of "arborized" (actin rich, no MBP), "partial" (partial actin disassembly, onset of MBP expansion), and "ring + lamellar" (full MBP expansion, actin disassembly) in *Fig4* control cultures (n= 4) and *Fig4$^{-/-}$* (n= 4) cultures. Results are shown as mean value ± SEM, multiple t-test analysis with Holm-Sidak method. *p= 0.0008 ("partial"), *p= 0.009 ("ring + lamellar").
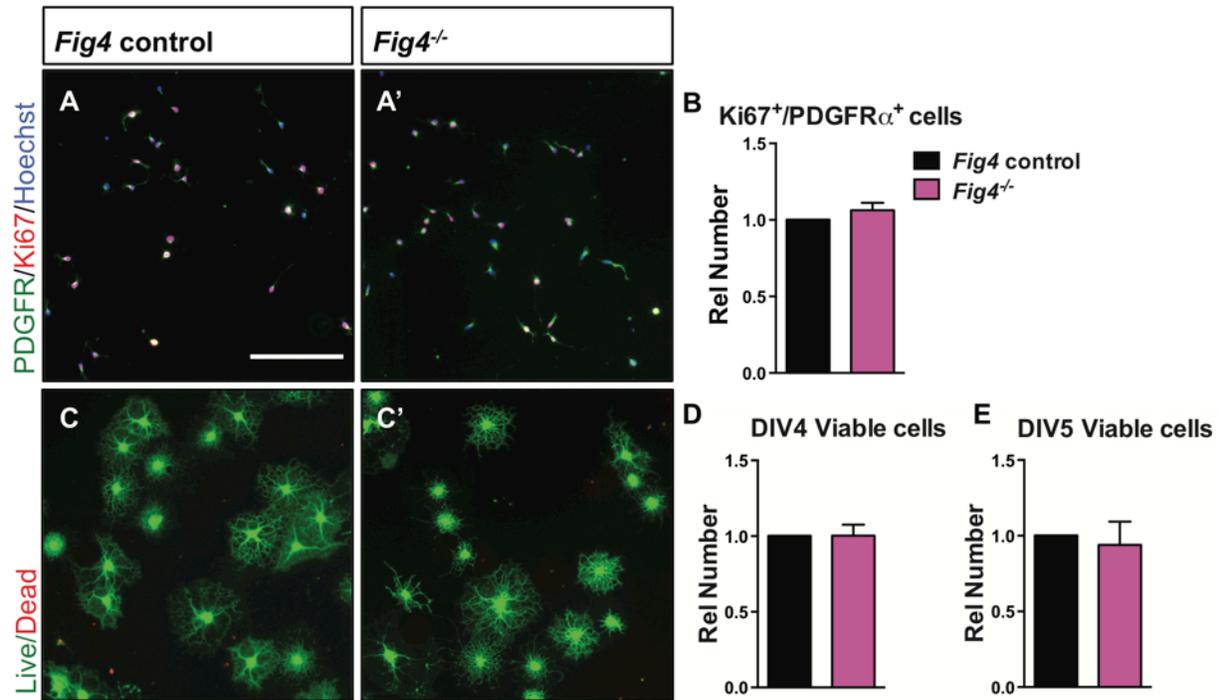
Figure 2.8 Loss of *Fig4$^{-/-}$* in primary OLs does not affect cell proliferation or cell death. (A-A') Representative images of control (*Fig4$^{+/+}$*or *Fig4$^{+/-}$*) and *Fig4$^{-/-}$* OPCs cultured for 2 days under proliferative conditions, fixed and stained with anti-PDGFRα (green) and Ki67 (red). Hoechst 33342 dye was included for nuclear staining of all cells. Scale bar = 200 µm. (**B**) Quantification of PDGFRα and Ki67 double-labeled cells. The number of double stained cells in *Fig4* control cultures was set at 1 and is comparable to *Fig4$^{-/-}$* cultures (n= 4 experiments per genotype). Results are shown as mean value ± SEM, unpaired Student's *t*-test. (**C-C'**) Representative images of OLs after 4 days in T3 containing differentiation medium. Cultures were fixed and stained with calcein-AM (green, living cells) and ethidium homodimer (red, dead cells). Scale bar = 200 µm. Quantification of live cells after 4 days (**D**) and 5 days (**E**) in differentiation medium revealed no differences among the two genotypes. *Fig4* control cultures (n= 4) and *Fig4$^{-/-}$* cultures (n= 4). Results are shown as mean value ± SEM, unpaired Students *t*-test.
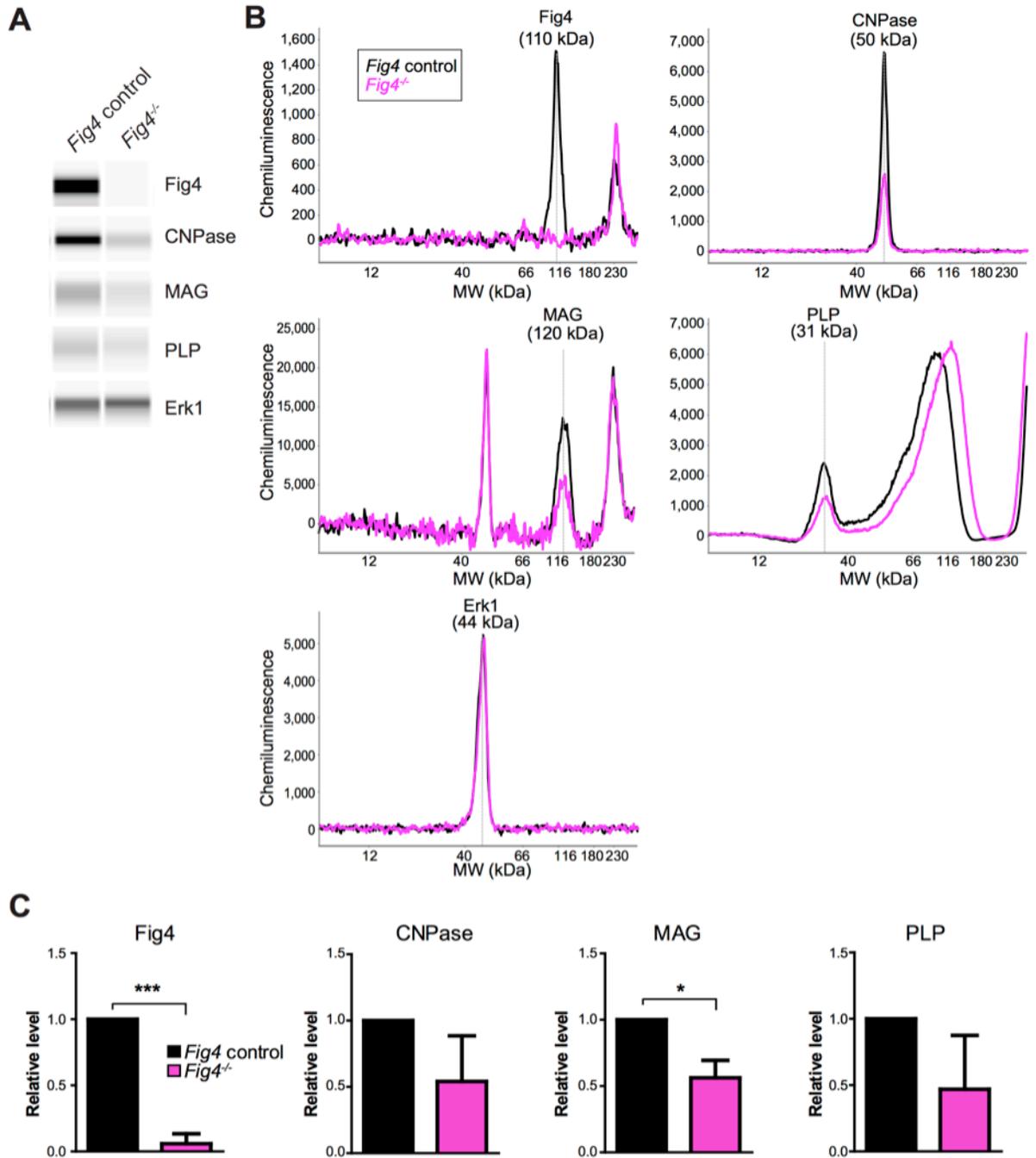
Figure 2.9 Capillary Western analysis of primary OL lysates. (**A**) Representative capillary immunoassay data of *Fig4* control and *Fig4*^{-/-} OPC/OLs are shown in Simple Western lane view. (**B**) Representative chemiluminescence signal intensity graphs and protein molecular weight of individual proteins. *Fig4* control and *Fig4*^{-/-} OPC/OLs lysates are shown as black and pink lines respectively. Specific peaks corresponding to each protein target are marked. (**C**) Quantification of protein of Erk1-normalized peak area of each protein target. Three independent experiments were used for quantification. Results are shown as mean value ± SD. *, $P<0.05$; ***, $P<0.005$
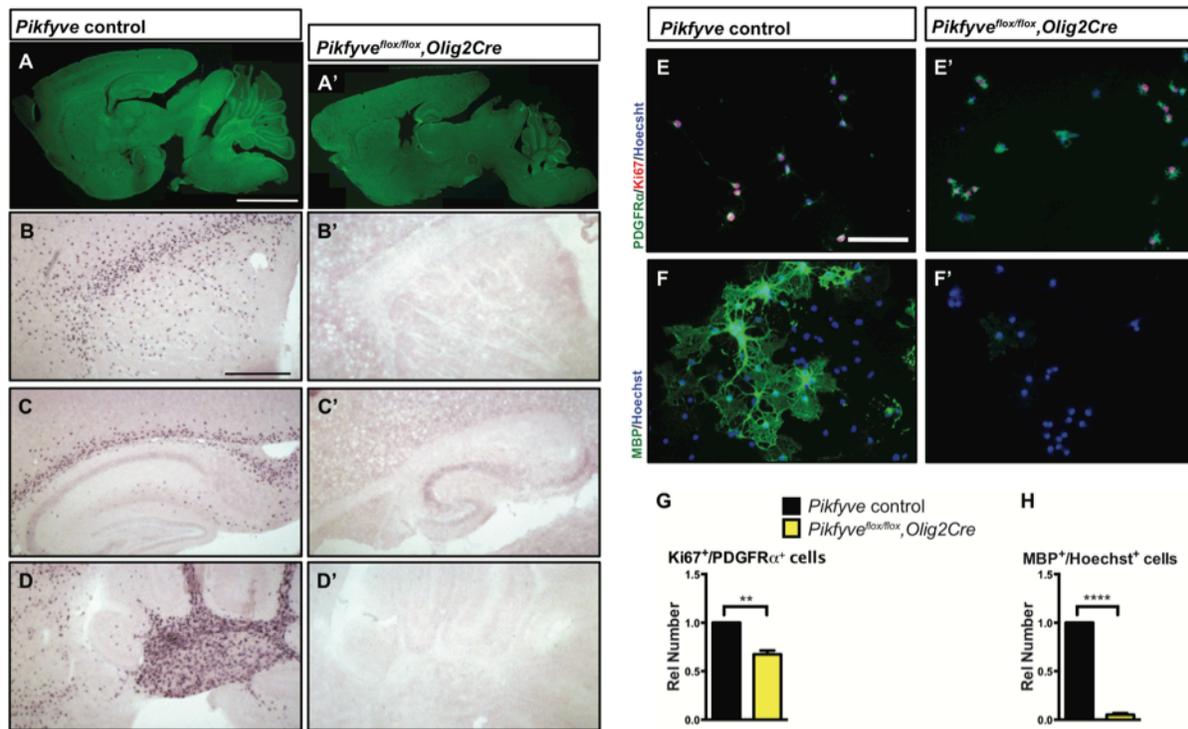
Figure 2.10 Conditional deletion of *Pikfyve* in OLs results in profound CNS hypomyelination. **(A-D')** Sagittal sections of P13 mouse brains. **(A)** *Pikfyve* control (*Pikfyve^{flox/+}* or *Pikfyve^{flox/flox}*; n= 3) mice and **(A')** *Pikfyve* conditional null (*Pikfyve^{flox/flox},Olig2Cre;* n= 3) mice stained with FluoroMyelin Green. In *Pikfyve^{flox/flox},Olig2Cre*, no myelin staining was observed, Scale bar, 1 mm. **(B-D')** *Plp1 in situ* hybridization shows virtual absence of mature OLs in P13 *Pikfyve^{flox/flox},Olig2Cre* brain tissue, including **(B and B')** internal capsule and corpus callosum, **(C' and C')** hippocampus and corpus callosum and **(D and D')** cerebellar white matter. Scale bar **(A, A')** = 1000 μm, (B-D') = 500 μm. **(E-H)** Cultures of primary OPCs/OLs isolated from *Pikfyve* control and *Pikfyve^{flox/flox},Olig2cre* mouse pups. (**E**, **E'**) At DIV2, cells were fixed and stained with anti-PDGFRα, anti-Ki67and Hoechst 33342 dye. **(F, F')** After 3 days in differentiation medium, supplemented with T3, cells were fixed and stained with anti-MBP and Hoechst 33342. **(G)** Quantification of proliferating OPCs revealed a *Pikfyve*-dependent reduction in Ki67^+/PDGFRα^+ double-labeled cells (n= 3 experiments per genotype). **(H)** Quantification of MBP^+ OLs normalized to Hoechst^+ cells shows a highly significant decrease in the number of MBP^+ OLs in *Pikfyve^{flox/flox},Olig2cre* cultures (n= 3 experiments per genotype). Unpaired Student's *t*-test; mean value ± SEM. ** (p = 0.011) and **** (p < 0.0001).
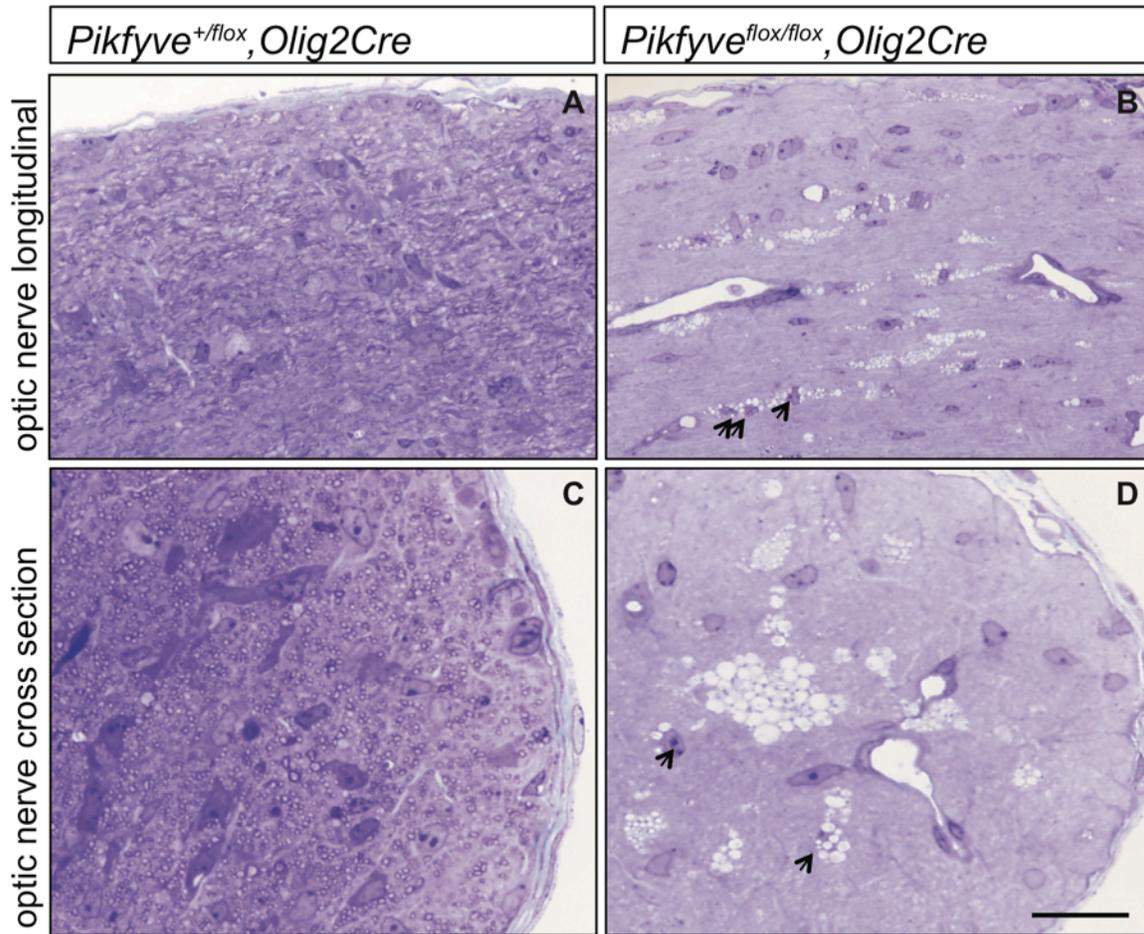
Figure 2.11 Optic nerve axons are not myelinated in *Pikfyve^{flox/flox},Olig2Cre* mice.
Semi-thin sections of P14 optic nerves in (A, B) longitudinal and (C, D) cross sectional view stained with toluidine blue. In control optic nerve (*Pikfyve^{flox/+},Olig2Cre*) many myelinated fibers are observed (n=3 pups). In *Pikfyve^{flox/flox},Olig2Cre* conditional mutants (n= 3 pups), there is a striking absence of myelinated axons in the optic nerve. Arrows in photomicrographs B and D point to presumptive oligodendrocytes laden with large vacuoles. Scale bar =15 μm.
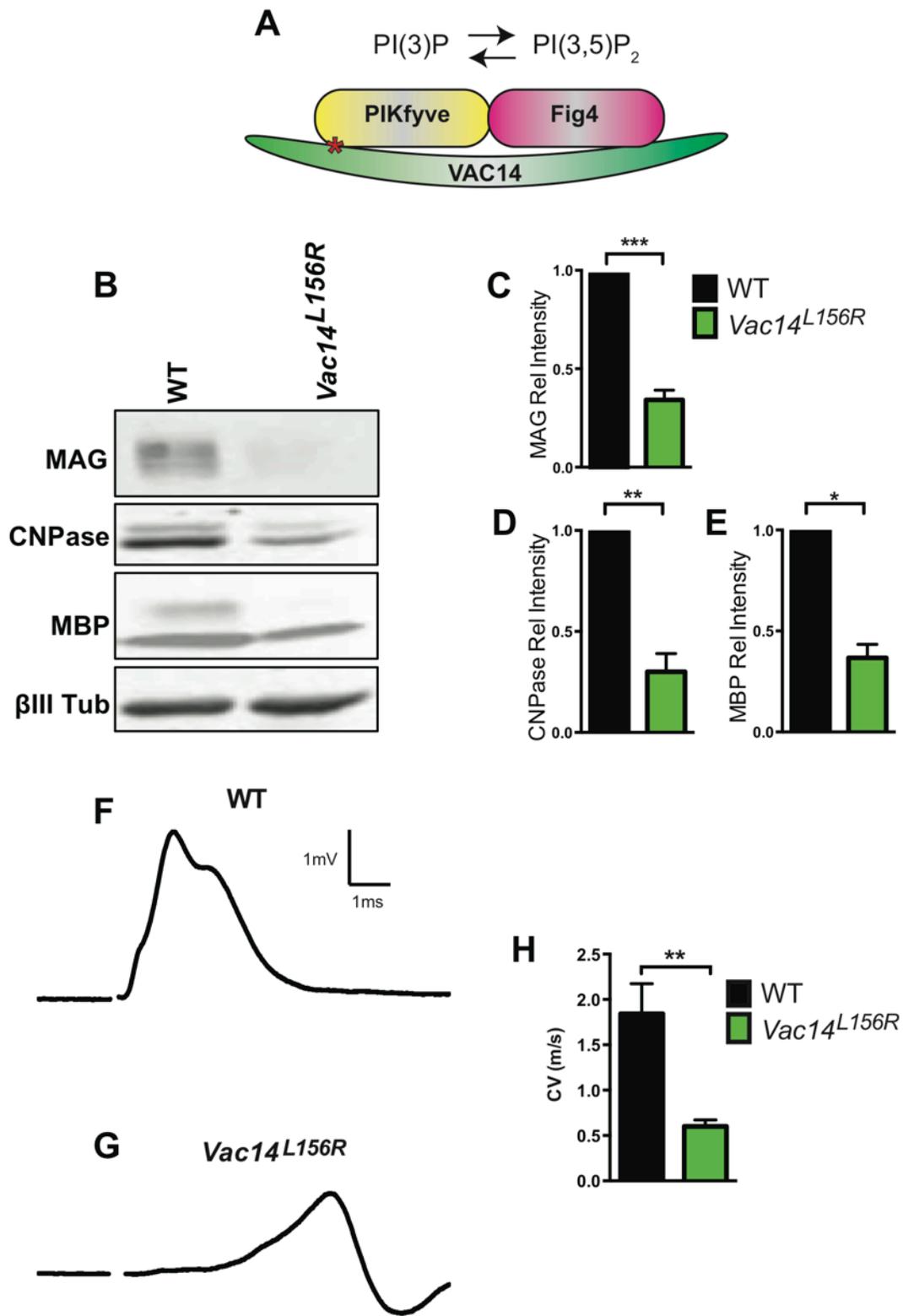
Figure 2.12 Homozygosity for *VAC14*[L156R] leads to CNS hypomyelination and impaired conduction of compound action potentials.

(**A**) Schematic of the PIKfyve/Vac14/Fig4 enzyme complex and its phosphoinositide products PI(3)P and PI(3,5)P$_2$. The red asterisk in VAC14 indicates the L156R point mutation that perturbs the interaction with PIKfyve, but not with Fig4. (**B**) Western blot analysis of brain membranes prepared from adult (P90-120) WT and $VAC14^{L156R}/VAC14^{L156R}$ littermate mice revealed a reduction in the myelin markers MAG, CNPase, and MBP. Anti-class III β-tubulin (βIII-Tub), a neuronal marker, is shown as a loading control. (**C-E**) Quantification of protein bands detected by Western blotting, shows a significant decrease in MAG, CNPase, and MBP in *VAC14* mutant brain tissue (n= 3 independent blots per genotype). Unpaired Student's *t*-test; mean value ± SEM. *** (p < 0.001), **p= 0.0015 and * p=0.0238. (**F** and **G**) Representative CAP traces recorded from acutely isolated optic nerves of WT and $VAC14^{L156T}$ homozygous mice. (**H**) Quantification of average conduction velocity (CV) of largest amplitude peaks identified in F and G. Results are shown as mean value ± SEM, unpaired Student's *t*-test, ** p=0.0063. WT n= 6 nerves, 3 mice and for $Vac14^{L156R}$ mutants n= 6 nerves, 3 mice.
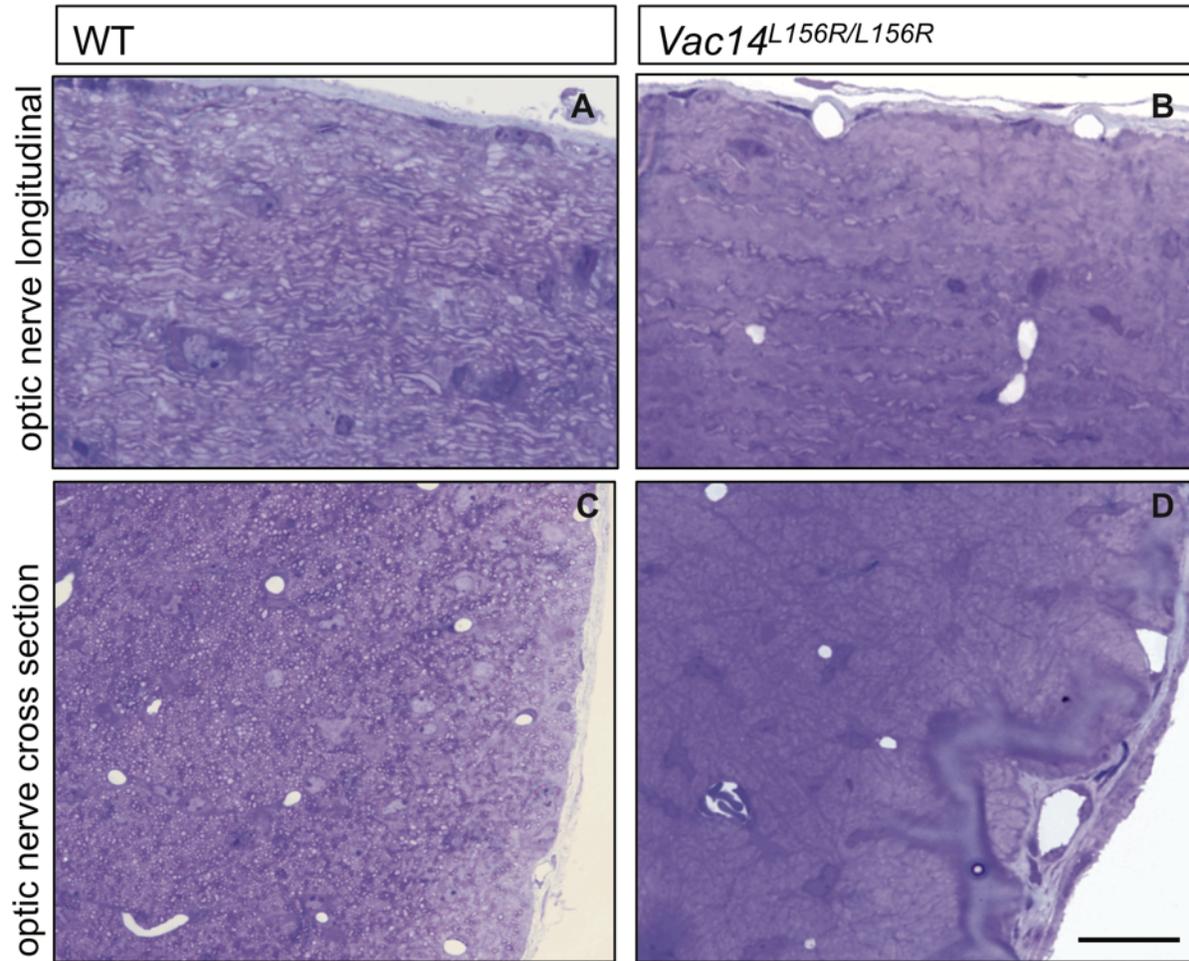
Figure 2.13 Severe optic nerve hypomyelination in *VAC14$^{L156R/L156R}$* mice. Semi-thin sections of P21 optic nerves in (**A, B**) longitudinal and (**C, D**) cross sectional view stained with toluidine blue. In wildtype (WT) optic nerve sections many myelinated fibers are observed (n= 3 pups). In marked contrast very few axons are myelinated in the *VAC14$^{L156R/L156R}$* optic nerves (n = 2). Scale bar =15 μm.
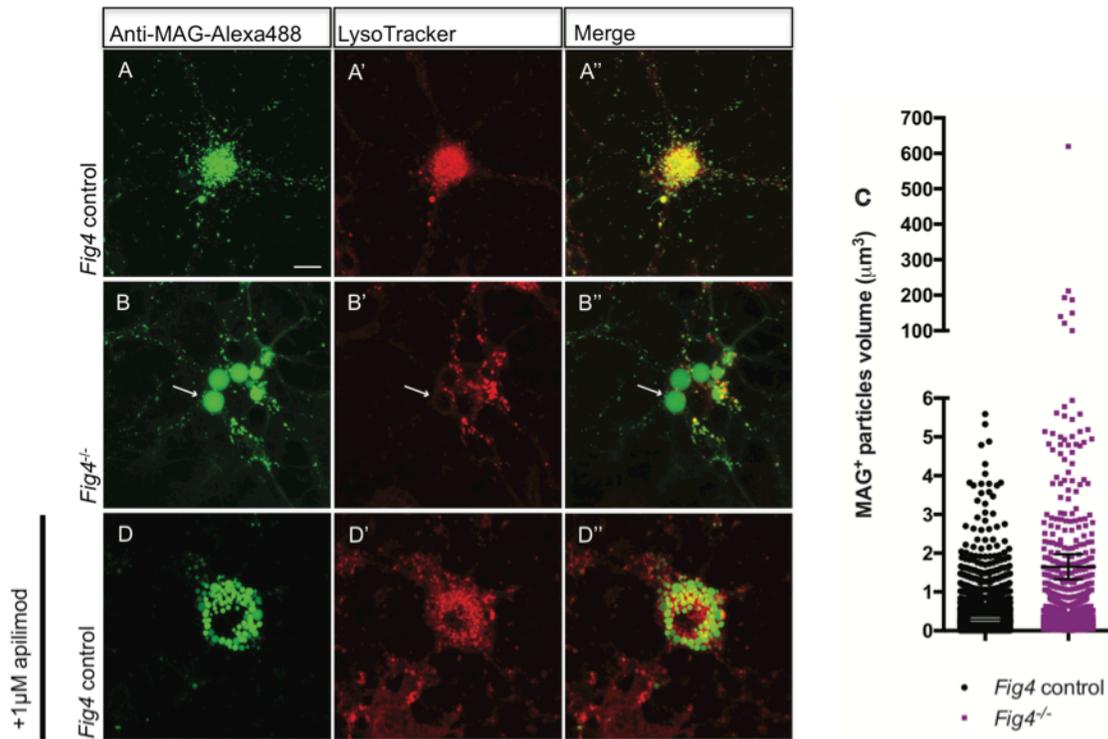
Figure 2.14 In *Fig4^{-/-}* OLs, MAG accumulates in large perinuclear vacuoles. Confocal images of live OLs acutely labeled with bath applied anti-MAG-Alexa488 (green) and LysoTracker Deep Red. **(A-A'')** *Fig4* control (*Fig4^{+/+}* or *Fig4^{+/-}*) OLs incubated with anti-MAG-Alexa488 and LysoTracker, single channel and merged images are shown. **(B-B'')** *Fig4^{-/-}* OLs incubated with anti-MAG-Alexa488 and Lysotracker shows accumulation of MAG in large perinuclear vacuoles (arrows), single channel and merged images are shown. Of note, large perinuclear MAG^+ vacuoles do not stain with LysoTracker. **(C)** Scatter plot depicting the volume of anti-MAG-Alexa488^+ particles in live *Fig4* control and *Fig4^{-/-}* OLs. Each dot represents an individual vesicle (n= 4 experiments, 9 cells per genotype). Mean volume ± SEM are shown. **(D-D'')** Wildtype OLs were incubated with anti-MAG-Alexa488 and LysoTracker and then acutely treated with the PIKfyve inhibitor apilimod. MAG accumulates in large perinuclear vacuoles, the majority of which does not stain with LysoTracker (n= 4 for *Fig4* controls and n= 4 for *Fig4^{-/-}* cultures). For apilimod treatment, n= 3 independent cultures. Maximum projection confocal z-stack images are shown, scale bar = 10 μm.
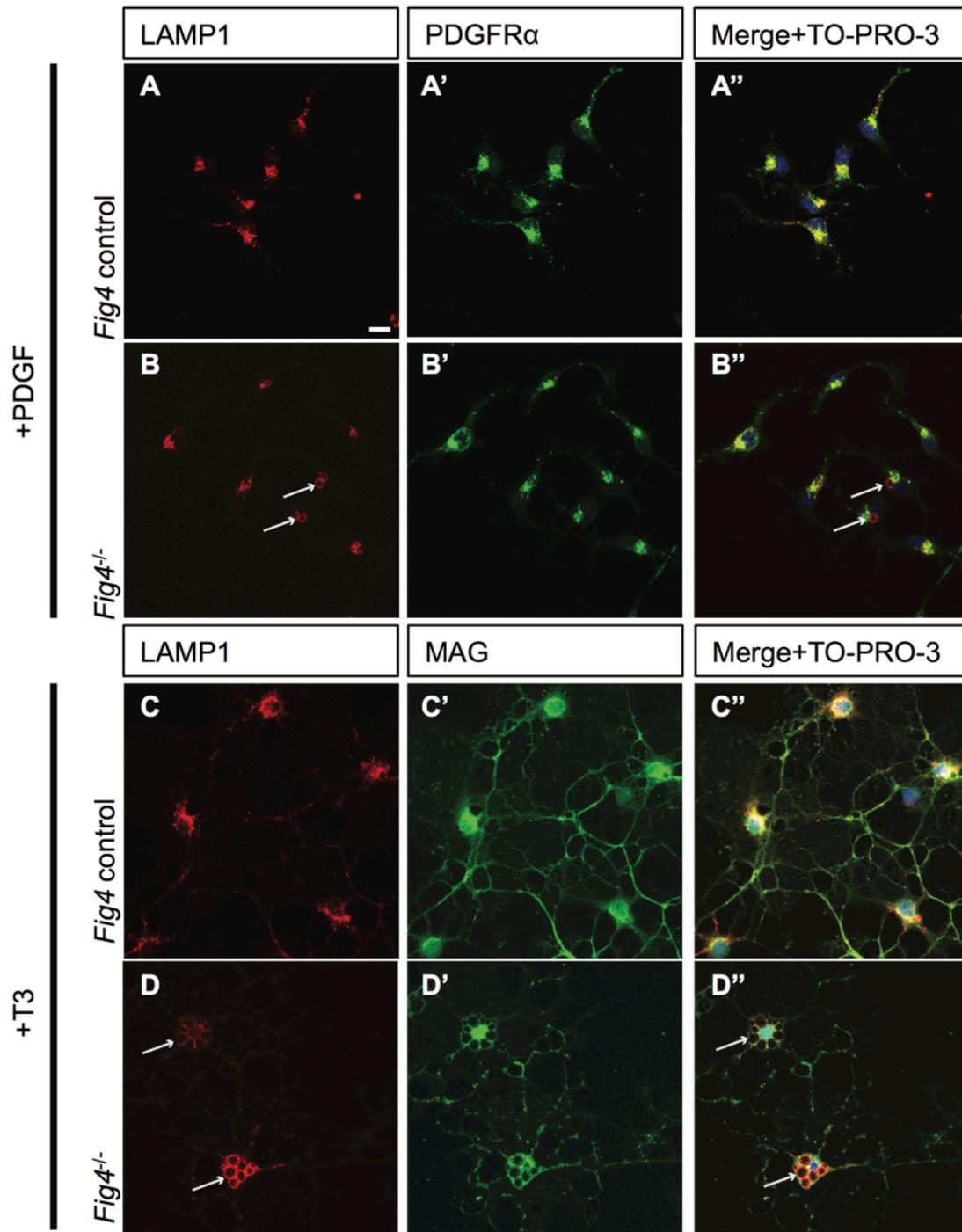
Figure 2.15 *Fig4*^{-/-} OLs show enlarged perinuclear vacuoles that stain positive for LAMP1. Confocal images of (**A-A"**) *Fig4* control (*Fig4*^{+/+} or *Fig4*^{+/-}) and (**B-B"**) *Fig4*^{-/-} OPCs cultured for two days in the presence of PDGF, fixed and double-stained with anti-LAMP1 and anti-PDGFRα antibodies. TO-PRO-3 dye was added to stain nuclei. Few OPCs (<20%) in *Fig4*^{-/-} cultures showed enlarged LAMP1^{+} vesicles (white arrows). (**C-D"**) Confocal images of (**C-C"**) *Fig4* control and (**D-D"**) *Fig4*^{-/-} OLs after 4 days in T3 containing differentiation medium.

Cultures were fixed and double-stained with anti-LAMP1 and anti-MAG antibodies. TO-PRO-3 dye was added to stain nuclei. In *Fig4*$^{-/-}$ cultures, the majority of OLs (>65%) showed multiple large perinuclear vacuoles that were double-positive for LAMP1 and MAG (white arrows). Observations were made in 4 independent experiments per culture condition. Scale bar, A-D" = 10 μm
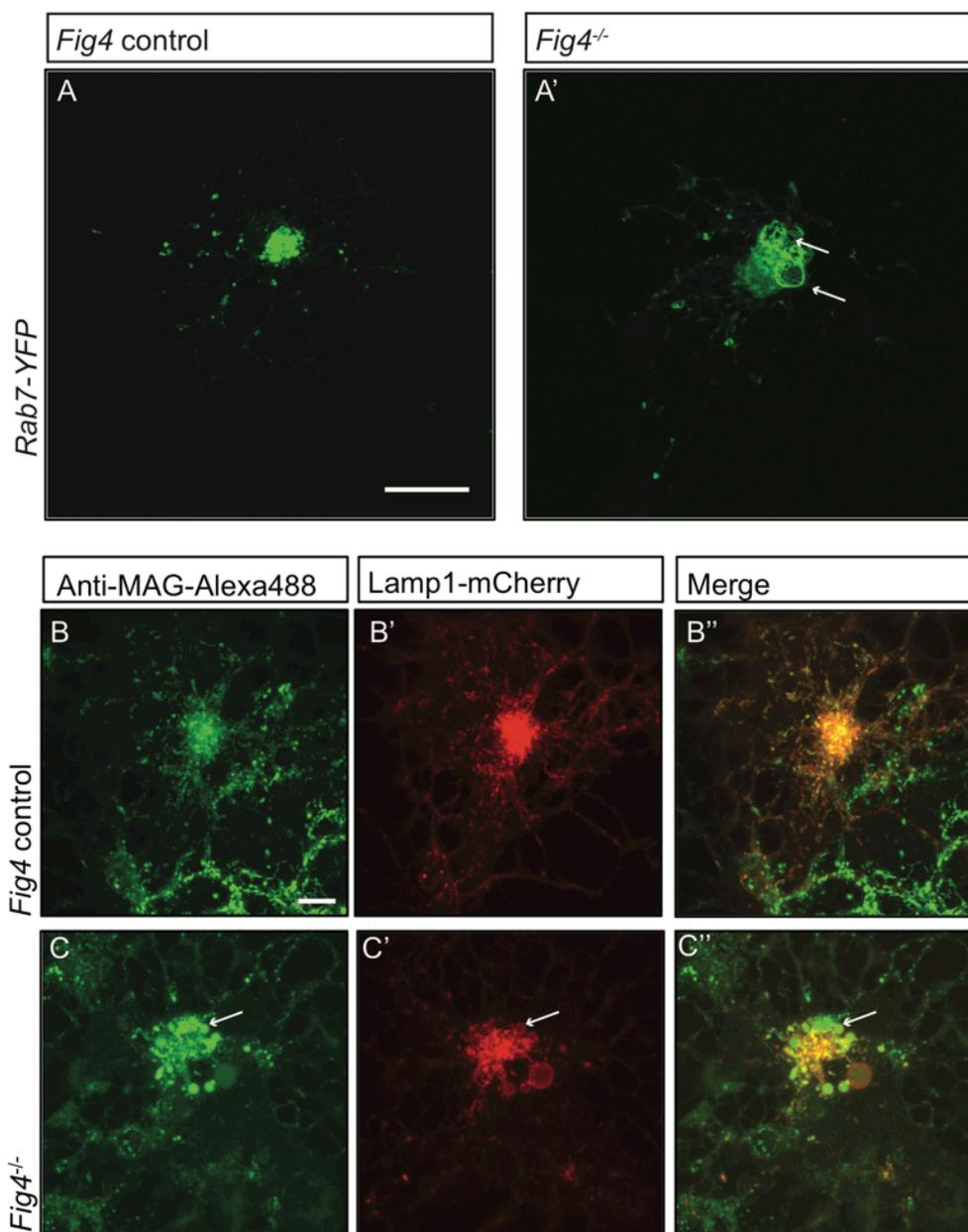
Figure 2.16 In *Fig4^{-/-}* OLs, PM derived MAG is transported to enlarged vesicles in the LE/Lys compartment. Representative confocal images of (**A**) *Fig4* control OLs and (**A'**) *Fig4^{-/-}* OLs transfected with a *Rab7-YFP* expression construct. Large perinuclear Rab7-YFP$^+$ vesicular structures are observed in *Fig4^{-/-}* OLs (arrows). Scale bar = 20 μm. Confocal images of (**B-B"**) *Fig4* control (*Fig4^{+/+}* or *Fig4^{+/-}*) and (**C-C"**) *Fig4^{-/-}* OL cultures transfected with a *LAMP-1mCherry* expression construct and incubated in bath applied anti-MAG-Alexa488 antibody. (**B"**) In *Fig4* control cultures MAG is localized to LAMP1$^+$ vesicles with a diameter of less than 1 μm. (**C"**) In *Fig4^{-/-}* cultures, MAG labeling is frequently observed in enlarged perinuclear and LAMP1$^+$ vesicles (arrows). Scale bar = 20 μm.
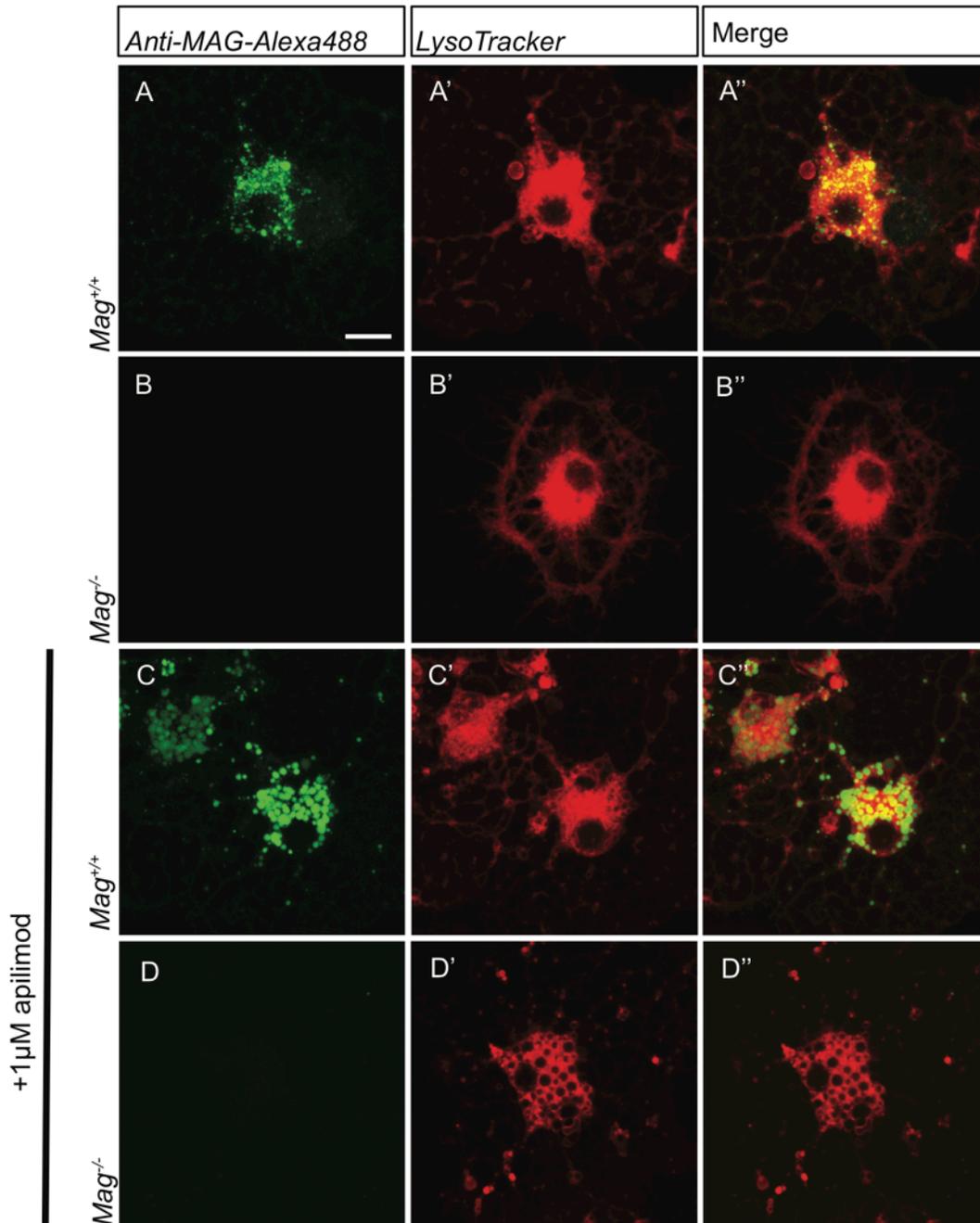
Figure 2.17 Specificity control for anti-MAG-Alexa488 antibody. Live-cell imaging of primary OLs prepared from *Mag*$^{+/+}$ and *Mag*$^{-/-}$ pups following bath application of anti-MAG-Alexa488 (green) and LysoTracker Deep Red. Representative confocal Z-stack images are shown. (**A-A"**) Anti-MAG-488 labeling of intracellular vesicles is robust in *Mag*$^{+/+}$ OLs. (**B-B"**) No signal is detected in parallel processed *Mag*$^{-/-}$ OLs. Independent of *MAG* genotype, prominent LysoTracker staining is observed. (**C-D"**) To rule out the possibility that large vacuoles are non-specifically labeled by anti-MAG-Alexa488, *Mag*$^{+/+}$ and *Mag*$^{-/-}$ OL cultures

were treated with the PIKfyve kinase inhibitor apilimod. Apilimod leads to accumulation of enlarged perinuclear vacuoles in $Mag^{+/+}$ and $Mag^{-/-}$ cultures. (**C-C''**) In $Mag^{+/+}$ cultures, vacuoles are strongly labeled with anti-MAG-Alexa488. (**D-D''**) In $Mag^{-/-}$ cultures, no labeling with anti-MAG-Alexa488 was observed. Scale bar in A-D" = 7.5 µm.
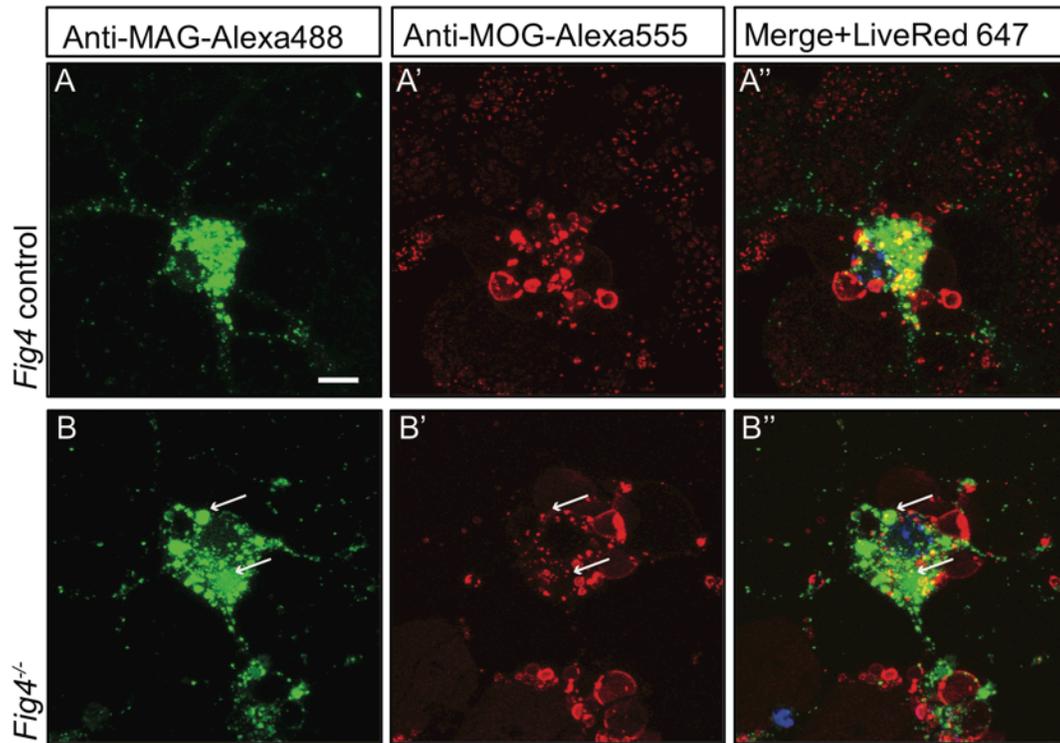
Figure 2.18 Live imaging of primary OLs reveals distinct trafficking routes for PM-derived MAG and MOG. Confocal images of (**A-A"**) *Fig4* control and (**B-B"**) *Fig4*^{-/-} OLs simultaneously incubated with anti-MAG-Alexa488 and anti-MOG-Alexa555 antibodies. Independent of *Fig4* genotype, there is little overlap among MAG$^+$ (green) and MOG$^+$ (red) structures. In *Fig4*^{-/-} OLs, enlarged MAG$^+$ vesicular structures (arrows) are MOG$^-$. Scale bar A-B' = 7.5 μm.
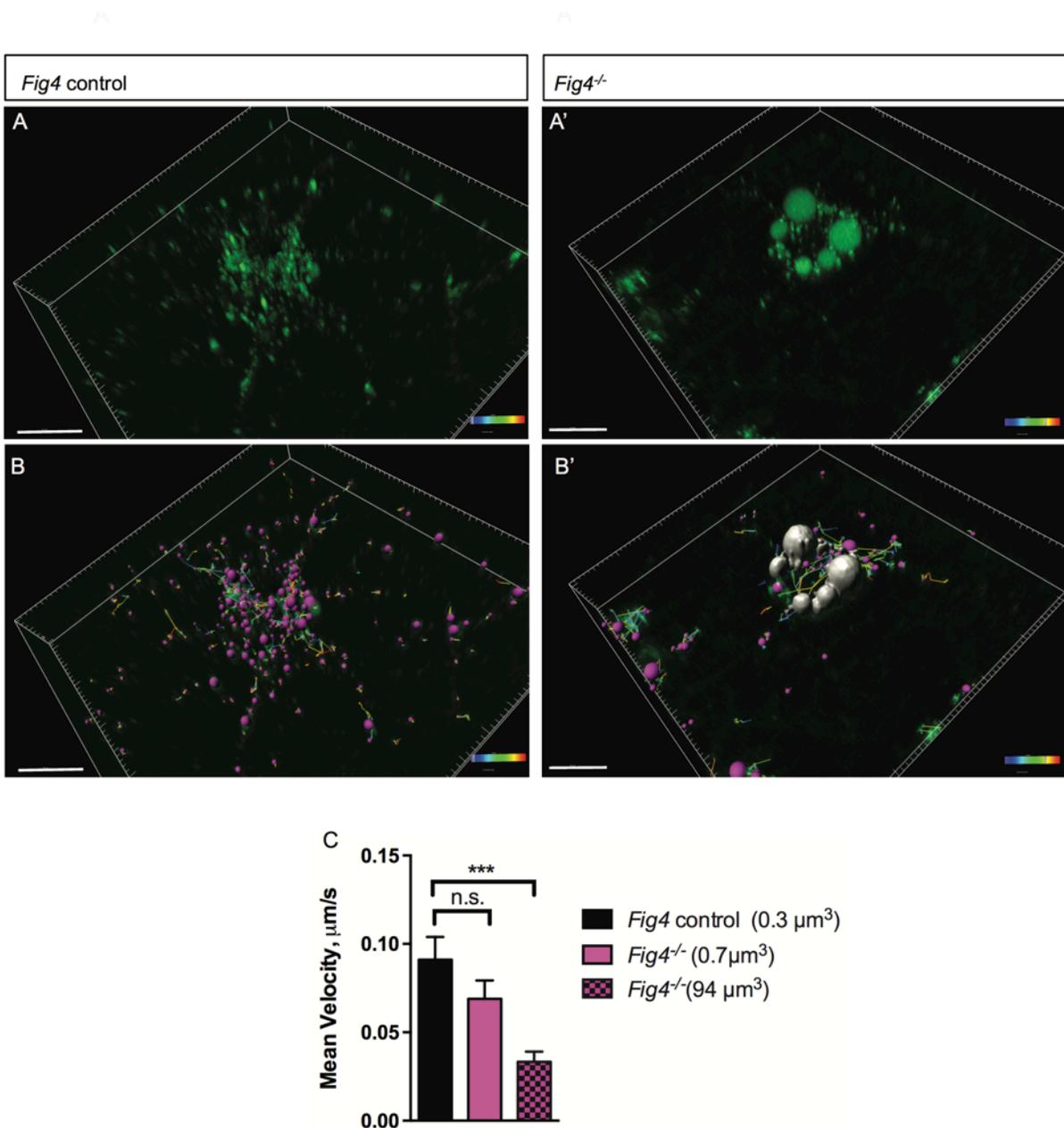
Figure 2.19 In *Fig4^{-/-}* OLs, vesicular trafficking through the LE/Lys compartment is defective. Representative confocal images of live, anti-MAG-Alex488 labeled **(A)** *Fig4* control OLs and **(A')** *Fig4^{-/-}* OLs. Time-lapse imaging was used to track movement of MAG$^+$ vesicles. **(B)** Using Imaris software, MAG$^+$ vesicles were labeled with pink spheres and vesicular movement was tracked (yellow lines) in *Fig4* control cultures. **(B')** Imaris software was used to track movement of large vesicles (white color) and small vesicles (purple color) in *Fig4^{-/-}* OLs: tracks of individual vesicles are shown. **(C)** Quantification of mean velocity of MAG$^+$ vesicles in *Fig4* control OLs and *Fig4^{-/-}* OLs. In *Fig4^{-/-}* OLs, movement of small vesicles (0.7 μm^3) and large vesicles (94 μm^3) was assessed separately. The velocity is shown as mean value ± SEM. N= 4 independent experiments and a total of 9 cells per genotype were analyzed. One-way ANOVA with Dunnett posthoc, ***p= 0.001. (n.s. = not significant).
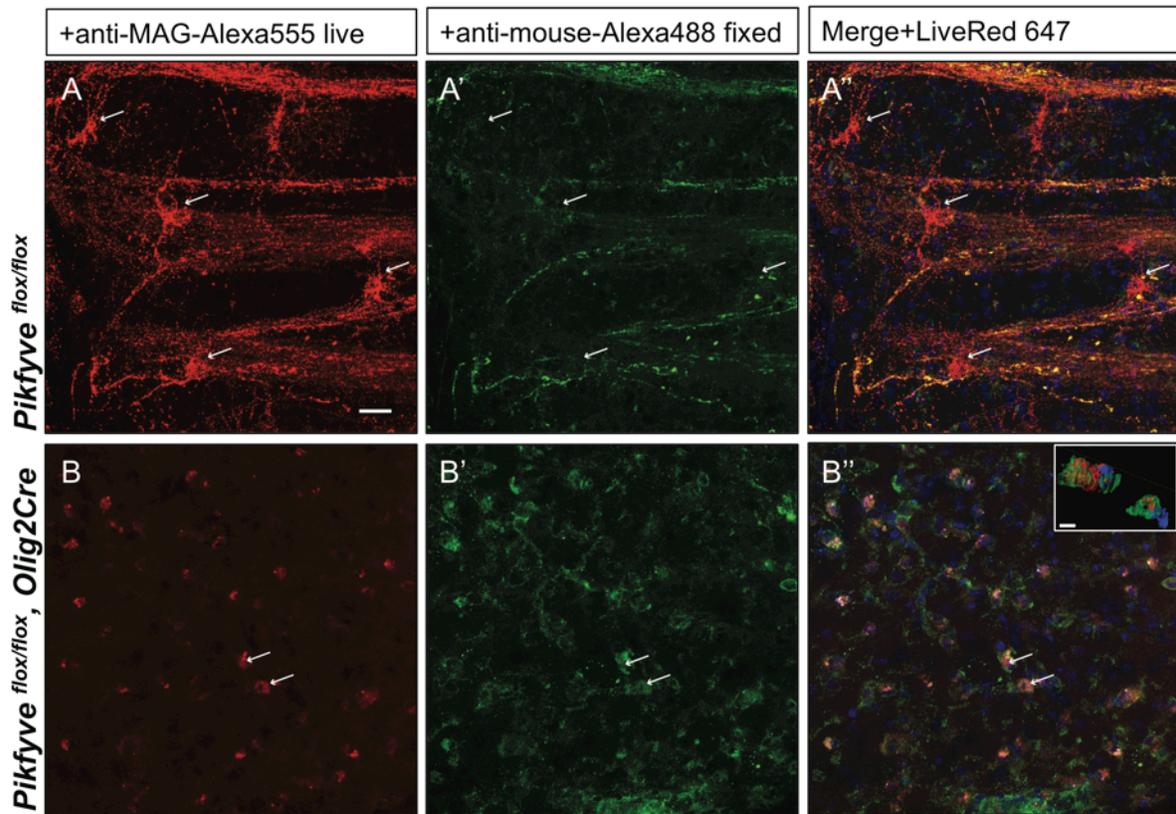
Figure 2.20 Impaired trafficking of MAG in *Pikfyve^flox/flox,Olig2Cre* brain slices.
Confocal images of acute brain slices in oxygenated ACSF treated with bath-applied anti-MAG-Alexa555 antibody, fixed and stained with anti-mouse-Alexa488 secondary antibody to distinguish between endocytosed MAG (red) and PM localized MAG (green). **(A)** OLs in the striatum of *Pikfyve* control mice (P13) show punctate MAG labeling in the cell soma (arrows) and along processes that form internodes. Only few MAG$^+$ structures are also stained with anti-mouse-Alexa488, and thus, localized on the PM. (**B-B"**) Limited perinuclear MAG labeling is observed in the *Pikfyve^flox/flox,Olig2Cre* striatum. Many MAG$^+$ structures are labeled red and green, and thus localized to the PM, however intracellular MAG is observed in some cells. Scale bar = 20 μm. Small inset shows a 3D view of the two cells labeled with arrows (B-B"). MAG$^+$ vesicles (red) only partially overlap with PM localized MAG (green). Alexa488$^+$ isosurface transparency is adjusted to 50% to demonstrate intracellular Alexa555$^+$ (red) and LiveNuc 647$^+$ (blue) structures. Scale bar = 10 μm.
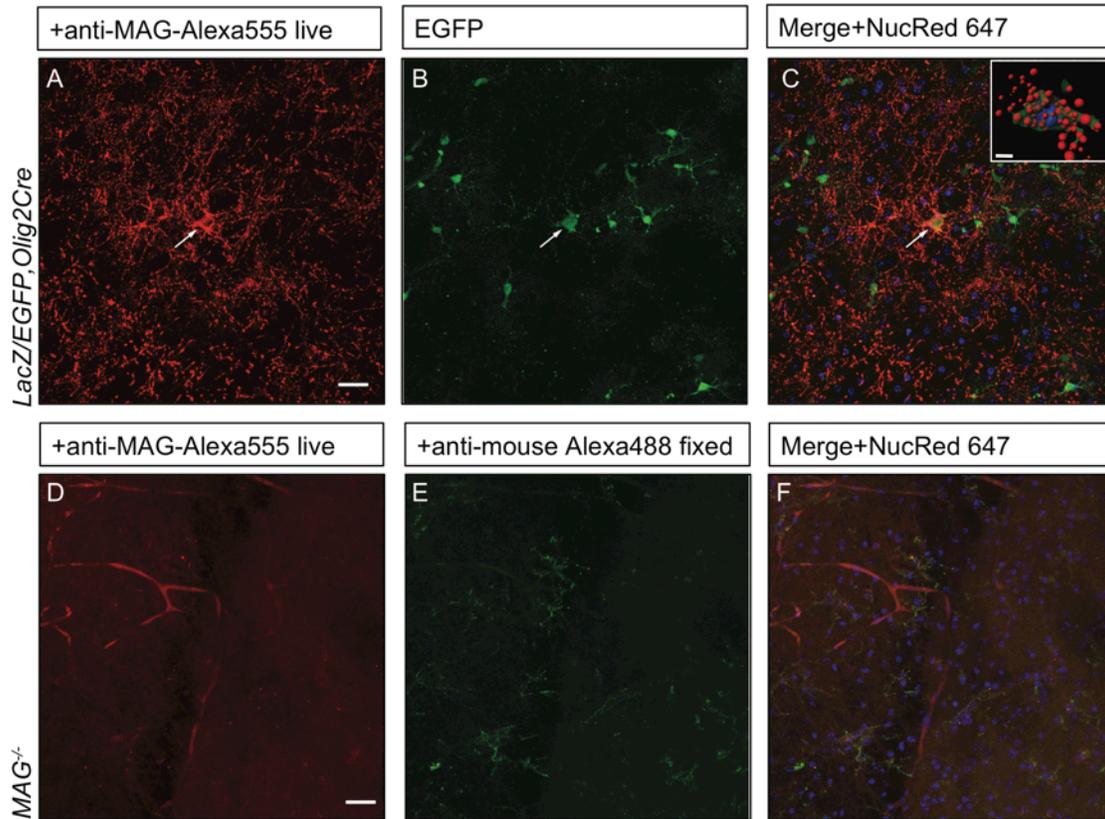
Figure 2.21 Anti-MAG labeling of EGFP⁺ OLs and specificity control for anti-MAG antibody in acute brain slices. (A-C) The *LacZ/EGFP,Olig2Cre* reporter mouse was used for genetic labeling of cells in the OL lineage. In acute brain slices, punctate anti-MAG-Alexa555 labeling is observed in the soma and processes of EGFP⁺ OLs in the developing neocortex of P14 mice (arrow). For nuclear staining slices were incubated with NucRed 647. Insert: Isosurface rendering of the MAG⁺/EGFP⁺ cell labeled with the arrow. EGFP⁺ isosurface transparency is increased to 50% to demonstrate intracellular Alexa555⁺ (red) and LiveNuc 647⁺ (blue) structures. Scale bar = 10 µm. (**D-F**) Parallel processed brain slices from *Mag⁻ᐟ⁻* pups labeled live with mouse anti-MAG-Alexa555 antibody, fixed and incubated with anti-mouse Alexa488, show no staining above background. Scale bar = 20 µm.

2.8 References

Arroyo EJ, Scherer SS (2000) On the molecular architecture of myelinated fibers. Histochemistry and cell biology 113:1-18.

Barres BA, Raff MC (1993) Proliferation of oligodendrocyte precursor cells depends on electrical activity in axons. Nature 361:258-260.

Baulac S, Lenk GM, Dufresnois B, Ouled Amar Bencheikh B, Couarch P, Renard J, Larson PA, Ferguson CJ, Noe E, Poirier K, Hubans C, Ferreira S, Guerrini R, Ouazzani R, El Hachimi KH, Meisler MH, Leguern E (2014) Role of the phosphoinositide phosphatase FIG4 gene in familial epilepsy with polymicrogyria. Neurology 82:1068-1075.

Behnia R, Munro S (2005) Organelle identity and the signposts for membrane traffic. Nature 438:597-604.

Bercury KK, Macklin WB (2015) Dynamics and mechanisms of CNS myelination. Developmental cell 32:447-458.

Bharadwaj R, Cunningham KM, Zhang K, Lloyd TE (2016) FIG4 regulates lysosome membrane homeostasis independent of phosphatase function. Human molecular genetics 25:681-692.

Bucci C, Thomsen P, Nicoziani P, McCarthy J, van Deurs B (2000) Rab7: a key to lysosome biogenesis. Molecular biology of the cell 11:467-480.

Cai X, Xu Y, Cheung AK, Tomlinson RC, Alcazar-Roman A, Murphy L, Billich A, Zhang B, Feng Y, Klumpp M, Rondeau JM, Fazal AN, Wilson CJ, Myer V, Joberty G, Bouwmeester T, Labow MA, Finan PM, Porter JA, Ploegh HL, Baird D, De Camilli P, Tallarico JA, Huang Q (2013) PIKfyve, a class III PI kinase, is the target of the small molecular IL-12/IL-23 inhibitor apilimod and a player in Toll-like receptor signaling. Chemistry & biology 20:912-921.

Campeau PM, Lenk GM, Lu JT, Bae Y, Burrage L, Turnpenny P, Roman Corona-Rivera J, Morandi L, Mora M, Reutter H, Vulto-van Silfhout AT, Faivre L, Haan E, Gibbs RA, Meisler MH, Lee BH (2013) Yunis-Varon syndrome is caused by mutations in FIG4, encoding a phosphoinositide phosphatase. American journal of human genetics 92:781-791.

Carbajal KS, Mironova Y, Ulrich-Lewis JT, Kulkarni D, Grifka-Walk HM, Huber AK, Shrager P, Giger RJ, Segal BM (2015) Th Cell Diversity in Experimental Autoimmune Encephalomyelitis and Multiple Sclerosis. Journal of immunology 195:2552-2559.

Chen C, Westenbroek RE, Xu X, Edwards CA, Sorenson DR, Chen Y, McEwen DP, O'Malley HA, Bharucha V, Meadows LS, Knudsen GA, Vilaythong A, Noebels JL, Saunders TL, Scheuer T, Shrager P, Catterall WA, Isom LL (2004) Mice lacking sodium channel beta1 subunits display defects in neuronal excitability, sodium channel expression, and nodal architecture. The Journal of neuroscience : the official journal of the Society for Neuroscience 24:4030-4042.

Chow CY, Zhang Y, Dowling JJ, Jin N, Adamska M, Shiga K, Szigeti K, Shy ME, Li J, Zhang X, Lupski JR, Weisman LS, Meisler MH (2007) Mutation of FIG4 causes neurodegeneration in the pale tremor mouse and patients with CMT4J. Nature 448:68-72.

Christian KM, Song H, Ming GL (2014) Functions and dysfunctions of adult hippocampal neurogenesis. Annual review of neuroscience 37:243-262.

Coman I, Barbin G, Charles P, Zalc B, Lubetzki C (2005) Axonal signals in central nervous system myelination, demyelination and remyelination. Journal of the neurological sciences 233:67-71.

Dessaud E, Yang LL, Hill K, Cox B, Ulloa F, Ribeiro A, Mynett A, Novitch BG, Briscoe J (2007) Interpretation of the sonic hedgehog morphogen gradient by a temporal adaptation mechanism. Nature 450:717-720.

Dong XP, Shen D, Wang X, Dawson T, Li X, Zhang Q, Cheng X, Zhang Y, Weisman LS, Delling M, Xu H (2010) PI(3,5)P(2) controls membrane trafficking by direct activation of mucolipin Ca(2+) release channels in the endolysosome. Nature communications 1:38.

Duan Y, Wang SH, Song J, Mironova Y, Ming GL, Kolodkin AL, Giger RJ (2014) Semaphorin 5A inhibits synaptogenesis in early postnatal- and adult-born hippocampal dentate granule cells. eLife 3.

Dugas JC, Emery B (2013) Purification and culture of oligodendrocyte lineage cells. Cold Spring Harbor protocols 2013:810-814.

Egami Y, Taguchi T, Maekawa M, Arai H, Araki N (2014) Small GTPases and phosphoinositides in the regulatory mechanisms of macropinosome formation and maturation. Frontiers in physiology 5:374.

Emery B, Agalliu D, Cahoy JD, Watkins TA, Dugas JC, Mulinyawe SB, Ibrahim A, Ligon KL, Rowitch DH, Barres BA (2009) Myelin gene regulatory factor is a critical transcriptional regulator required for CNS myelination. Cell 138:172-185.

Emery B, Dugas JC (2013) Purification of oligodendrocyte lineage cells from mouse cortices by immunopanning. Cold Spring Harbor protocols 2013:854-868.

Faust PL, Kaye EM, Powers JM (2010) Myelin lesions associated with lysosomal and peroxisomal disorders. Expert review of neurotherapeutics 10:1449-1466.

Ferguson CJ, Lenk GM, Jones JM, Grant AE, Winters JJ, Dowling JJ, Giger RJ, Meisler MH (2012a) Neuronal expression of Fig4 is both necessary and sufficient to prevent spongiform neurodegeneration. Human molecular genetics 21:3525-3534.

Ferguson CJ, Lenk GM, Jones JM, Grant AE, Winters JJ, Dowling JJ, Giger RJ, Meisler MH (2012b) Neuronal expression of Fig4 is necessary and sufficient to prevent spongiform neurodegeneration. Hum Mol Genet.

Ferguson CJ, Lenk GM, Meisler MH (2009) Defective autophagy in neurons and astrocytes from mice deficient in PI(3,5)P2. Human molecular genetics 18:4868-4878.

Fields RD (2008) White matter in learning, cognition and psychiatric disorders. Trends in neurosciences 31:361-370.

Folkerth RD (1999) Abnormalities of developing white matter in lysosomal storage diseases. J Neuropathol Exp Neurol 58:887-902.

Fruhbeis C, Frohlich D, Kramer-Albers EM (2012) Emerging roles of exosomes in neuron-glia communication. Frontiers in physiology 3:119.

Grishchuk Y, Sri S, Rudinskiy N, Ma W, Stember KG, Cottle MW, Sapp E, Difiglia M, Muzikansky A, Betensky RA, Wong AM, Bacskai BJ, Hyman BT, Kelleher RJ, 3rd, Cooper JD, Slaugenhaupt SA (2014) Behavioral deficits, early gliosis, dysmyelination and synaptic dysfunction in a mouse model of mucolipidosis IV. Acta neuropathologica communications 2:133.

Hofmann I, Munro S (2006) An N-terminally acetylated Arf-like GTPase is localised to lysosomes and affects their motility. Journal of cell science 119:1494-1503.

Hutagalung AH, Novick PJ (2011) Role of Rab GTPases in membrane traffic and cell physiology. Physiological reviews 91:119-149.

Ikonomov OC, Sbrissa D, Delvecchio K, Xie Y, Jin JP, Rappolee D, Shisheva A (2011) The phosphoinositide kinase PIKfyve is vital in early embryonic development:

preimplantation lethality of *Pikfyve*^{-/-} embryos but normality of *Pikfyve*^{+/-} mice. The Journal of biological chemistry 286:13404-13413.

Inoue K (2005) PLP1-related inherited dysmyelinating disorders: Pelizaeus-Merzbacher disease and spastic paraplegia type 2. Neurogenetics 6:1-16.

Ishibashi T, Dakin KA, Stevens B, Lee PR, Kozlov SV, Stewart CL, Fields RD (2006) Astrocytes promote myelination in response to electrical impulses. Neuron 49:823-832.

Jean S, Cox S, Nassari S, Kiger AA (2015) Starvation-induced MTMR13 and RAB21 activity regulates VAMP8 to promote autophagosome-lysosome fusion. EMBO reports 16:297-311.

Jean S, Kiger AA (2012) Coordination between RAB GTPase and phosphoinositide regulation and functions. Nature reviews Molecular cell biology 13:463-470.

Jin N, Chow CY, Liu L, Zolov SN, Bronson R, Davisson M, Petersen JL, Zhang Y, Park S, Duex JE, Goldowitz D, Meisler MH, Weisman LS (2008) VAC14 nucleates a protein complex essential for the acute interconversion of PI3P and PI(3,5)P(2) in yeast and mouse. The EMBO journal 27:3221-3234.

Kang SH, Fukaya M, Yang JK, Rothstein JD, Bergles DE (2010) NG2+ CNS glial progenitors remain committed to the oligodendrocyte lineage in postnatal life and following neurodegeneration. Neuron 68:668-681.

Karim SA, Barrie JA, McCulloch MC, Montague P, Edgar JM, Kirkham D, Anderson TJ, Nave KA, Griffiths IR, McLaughlin M (2007) PLP overexpression perturbs myelin protein composition and myelination in a mouse model of Pelizaeus-Merzbacher disease. Glia 55:341-351.

Lee H, Raiker SJ, Venkatesh K, Geary R, Robak LA, Zhang Y, Yeh HH, Shrager P, Giger RJ (2008) Synaptic function for the Nogo-66 receptor NgR1: regulation of dendritic spine morphology and activity-dependent synaptic strength. The Journal of neuroscience : the official journal of the Society for Neuroscience 28:2753-2765.

Lenk GM, Meisler MH (2014) Mouse models of PI(3,5)P2 deficiency with impaired lysosome function. Methods in enzymology 534:245-260.

Maier O, Hoekstra D, Baron W (2008) Polarity development in oligodendrocytes: sorting and trafficking of myelin components. Journal of molecular neuroscience : MN 35:35-53.

Makinodan M, Rosen KM, Ito S, Corfas G (2012) A critical period for social experience-dependent oligodendrocyte maturation and myelination. Science 337:1357-1360.

Marinelli C, Bertalot T, Zusso M, Skaper SD, Giusti P (2016) Systematic Review of Pharmacological Properties of the Oligodendrocyte Lineage. Frontiers in cellular neuroscience 10:27.

Masaki T (2012) Polarization and myelination in myelinating glia. ISRN neurology 2012:769412.

Mayinger P (2012) Phosphoinositides and vesicular membrane traffic. Biochimica et biophysica acta 1821:1104-1113.

McCartney AJ, Zhang Y, Weisman LS (2014) Phosphatidylinositol 3,5-bisphosphate: low abundance, high significance. BioEssays : news and reviews in molecular, cellular and developmental biology 36:52-64.

Mizuguchi R, Sugimori M, Takebayashi H, Kosako H, Nagao M, Yoshida S, Nabeshima Y, Shimamura K, Nakafuku M (2001) Combinatorial roles of olig2 and neurogenin2 in the coordinated induction of pan-neuronal and subtype-specific properties of motoneurons. Neuron 31:757-771.

Muller C, Bauer NM, Schafer I, White R (2013) Making myelin basic protein -from mRNA transport to localized translation. Frontiers in cellular neuroscience 7:169.

Nave KA, Trapp BD (2008) Axon-glial signaling and the glial support of axon function. Annual review of neuroscience 31:535-561.

Nicholson G, Lenk GM, Reddel SW, Grant AE, Towne CF, Ferguson CJ, Simpson E, Scheuerle A, Yasick M, Hoffman S, Blouin R, Brandt C, Coppola G, Biesecker LG, Batish SD, Meisler MH (2011) Distinctive genetic and clinical features of CMT4J: a severe neuropathy caused by mutations in the PI(3,5)P(2) phosphatase FIG4. Brain 134:1959-1971.

Ohno M, Hiraoka Y, Matsuoka T, Tomimoto H, Takao K, Miyakawa T, Oshima N, Kiyonari H, Kimura T, Kita T, Nishi E (2009) Nardilysin regulates axonal maturation and myelination in the central and peripheral nervous system. Nature neuroscience 12:1506-1513.

Pan B, Fromholt SE, Hess EJ, Crawford TO, Griffin JW, Sheikh KA, Schnaar RL (2005) Myelin-associated glycoprotein and complementary axonal ligands, gangliosides, mediate axon stability in the CNS and PNS: neuropathology and behavioral deficits in single- and double-null mice. Experimental neurology 195:208-217.

Perlman SJ, Mar S (2012) Leukodystrophies. Advances in experimental medicine and biology 724:154-171.

Prolo LM, Vogel H, Reimer RJ (2009) The lysosomal sialic acid transporter sialin is required for normal CNS myelination. The Journal of neuroscience : the official journal of the Society for Neuroscience 29:15355-15365.

Pusic AD, Kraig RP (2014) Youth and environmental enrichment generate serum exosomes containing miR-219 that promote CNS myelination. Glia 62:284-299.

Raiker SJ, Lee H, Baldwin KT, Duan Y, Shrager P, Giger RJ (2010) Oligodendrocyte-myelin glycoprotein and Nogo negatively regulate activity-dependent synaptic plasticity. The Journal of neuroscience : the official journal of the Society for Neuroscience 30:12432-12445.

Rempe D, Vangeison G, Hamilton J, Li Y, Jepson M, Federoff HJ (2006) Synapsin I Cre transgene expression in male mice produces germline recombination in progeny. Genesis 44:44-49.

Salzer JL (2003) Polarized domains of myelinated axons. Neuron 40:297-318.

Schardt A, Brinkmann BG, Mitkovski M, Sereda MW, Werner HB, Nave KA (2009) The SNARE protein SNAP-29 interacts with the GTPase Rab3A: Implications for membrane trafficking in myelinating glia. Journal of neuroscience research 87:3465-3479.

Schuller U, Heine VM, Mao J, Kho AT, Dillon AK, Han YG, Huillard E, Sun T, Ligon AH, Qian Y, Ma Q, Alvarez-Buylla A, McMahon AP, Rowitch DH, Ligon KL (2008) Acquisition of granule neuron precursor identity is a critical determinant of progenitor cell competence to form Shh-induced medulloblastoma. Cancer cell 14:123-134.

Schulze U, Vollenbroker B, Braun DA, Van Le T, Granado D, Kremerskothen J, Franzel B, Klosowski R, Barth J, Fufezan C, Wolters DA, Pavenstadt H, Weide T (2014) The Vac14-interaction network is linked to regulators of the endolysosomal and autophagic pathway. Molecular & cellular proteomics : MCP 13:1397-1411.

Schweitzer JK, Krivda JP, D'Souza-Schorey C (2009) Neurodegeneration in Niemann-Pick Type C disease and Huntington's disease: impact of defects in membrane trafficking. Curr Drug Targets 10:653-665.

Simons M, Lyons DA (2013) Axonal selection and myelin sheath generation in the central nervous system. Current opinion in cell biology 25:512-519.

Simons M, Trajkovic K (2006) Neuron-glia communication in the control of oligodendrocyte function and myelin biogenesis. Journal of cell science 119:4381-4389.

Stenmark H (2009) Rab GTPases as coordinators of vesicle traffic. Nature reviews Molecular cell biology 10:513-525.

Toth AB, Terauchi A, Zhang LY, Johnson-Venkatesh EM, Larsen DJ, Sutton MA, Umemori H (2013) Synapse maturation by activity-dependent ectodomain shedding of SIRPalpha. Nature neuroscience 16:1417-1425.

Trajkovic K, Dhaunchak AS, Goncalves JT, Wenzel D, Schneider A, Bunt G, Nave KA, Simons M (2006) Neuron to glia signaling triggers myelin membrane exocytosis from endosomal storage sites. The Journal of cell biology 172:937-948.

Vaccari I, Carbone A, Previtali SC, Mironova YA, Alberizzi V, Noseda R, Rivellini C, Bianchi F, Del Carro U, D'Antonio M, Lenk GM, Wrabetz L, Giger RJ, Meisler MH, Bolino A (2015) Loss of Fig4 in both Schwann cells and motor neurons contributes to CMT4J neuropathy. Hum Mol Genet 24:383-396.

Wang W, Zhang X, Gao Q, Xu H (2014) TRPML1: an ion channel in the lysosome. Handb Exp Pharmacol 222:631-645.

Wang X, Zhang X, Dong XP, Samie M, Li X, Cheng X, Goschka A, Shen D, Zhou Y, Harlow J, Zhu MX, Clapham DE, Ren D, Xu H (2012) TPC proteins are phosphoinositide-activated sodium-selective ion channels in endosomes and lysosomes. Cell 151:372-383.

White R, Kramer-Albers EM (2014) Axon-glia interaction and membrane traffic in myelin formation. Frontiers in cellular neuroscience 7:284.

Winters JJ, Ferguson CJ, Lenk GM, Giger-Mateeva VI, Shrager P, Meisler MH, Giger RJ (2011) Congenital CNS hypomyelination in the Fig4 null mouse is rescued by neuronal expression of the PI(3,5)P(2) phosphatase Fig4. J Neurosci 31:17736-17751.

Winterstein C, Trotter J, Kramer-Albers EM (2008) Distinct endocytic recycling of myelin proteins promotes oligodendroglial membrane remodeling. Journal of cell science 121:834-842.

Yaghootfam A, Gieselmann V, Eckhardt M (2005) Delay of myelin formation in arylsulphatase A-deficient mice. Eur J Neurosci 21:711-720.

Yao D, McGonigal R, Barrie JA, Cappell J, Cunningham ME, Meehan GR, Fewou SN, Edgar JM, Rowan E, Ohmi Y, Furukawa K, Furukawa K, Brophy PJ, Willison HJ (2014) Neuronal expression of GalNAc transferase is sufficient to prevent the age-related neurodegenerative phenotype of complex ganglioside-deficient mice. The Journal of neuroscience : the official journal of the Society for Neuroscience 34:880-891.

Ye F, Chen Y, Hoang T, Montgomery RL, Zhao XH, Bu H, Hu T, Taketo MM, van Es JH, Clevers H, Hsieh J, Bassel-Duby R, Olson EN, Lu QR (2009) HDAC1 and HDAC2 regulate oligodendrocyte differentiation by disrupting the beta-catenin-TCF interaction. Nature neuroscience 12:829-838.

Yu T, Lieberman AP (2013) Npc1 acting in neurons and glia is essential for the formation and maintenance of CNS myelin. PLoS genetics 9:e1003462.

Zhang Y, Chen K, Sloan SA, Bennett ML, Scholze AR, O'Keeffe S, Phatnani HP, Guarnieri P, Caneda C, Ruderisch N, Deng S, Liddelow SA, Zhang C, Daneman R, Maniatis T, Barres BA, Wu JQ (2014) An RNA-sequencing transcriptome and splicing database of glia, neurons, and vascular cells of the cerebral cortex. J Neurosci 34:11929-11947.

Zhang Y, Zolov SN, Chow CY, Slutsky SG, Richardson SC, Piper RC, Yang B, Nau JJ, Westrick RJ, Morrison SJ, Meisler MH, Weisman LS (2007) Loss of Vac14, a regulator of the signaling lipid phosphatidylinositol 3,5-bisphosphate, results in neurodegeneration in mice. Proceedings of the National Academy of Sciences of the United States of America 104:17518-17523.

Zou J, Hu B, Arpag S, Yan Q, Hamilton A, Zeng YS, Vanoye CG, Li J (2015) Reactivation of Lysosomal Ca2+ Efflux Rescues Abnormal Lysosomal Storage in FIG4-Deficient Cells. J Neurosci 35:6801-6812.

Zuchero JB, Barres BA (2013) Intrinsic and extrinsic control of oligodendrocyte development. Current opinion in neurobiology 23:914-920.

Zuchero JB, Fu MM, Sloan SA, Ibrahim A, Olson A, Zaremba A, Dugas JC, Wienbar S, Caprariello AV, Kantor C, Leonoudakis D, Lariosa-Willingham K, Kronenberg G, Gertz K, Soderling SH, Miller RH, Barres BA (2015) CNS myelin wrapping is driven by actin disassembly. Developmental cell 34:152-167.

CHAPTER III:

Myelinated Fibers in the Adult PNS and CNS Differ in Vulnerability to Reduced Levels of the Signaling Lipid PI(3,5)P₂

3.1 Abstract

The signaling lipid phosphatidylinositol 3,5-bisphosphate, $PI(P3,5)P_2$, is essential for proper vesicular trafficking in eukaryotic cells. $PI(P3,5)P_2$ levels are regulated by an enzyme complex that includes the kinase PIKFYVE, the phosphatase FIG4, and scaffold protein VAC14. Impaired function of any of these components of the $PI(P3,5)P_2$ biosynthetic complex results in reduction of $PI(3,5)P_2$, deleterious enlargement of vesicles, and defects in trafficking through the endolysosomal compartment. Mutations in human FIG4 cause inherited disorders including Charcot-Marie-Tooth disease type 4J, polymicrogyria with epilepsy, and Yunis-Varon syndrome. *Fig4*$^{-/-}$ mice present with tremor, reduced lifespan, spongiform neural tissue degeneration, and severe myelination defects in the central and peripheral nervous systems (CNS and PNS). Conditional *Fig4* deletion in neurons or myelinating glia in the CNS and PNS results in a severe hypomyelination phenotype, suggesting both intrinsic and extrinsic regulation of myelination by $PI(3,5)P_2$ during development. To test whether $PI(3,5)P_2$ biosynthesis is required for adult maintenance and repair of myelin, we generated a tamoxifen-inducible global *Fig4* knockout mouse using the *CMVCreER* transgene (*Fig4*$^{-/flox}$*,CMVCreER*). Strikingly, adult *Fig4* deletion leads to rapid deterioration in mice, including severe motor impairment, tremor, weight loss, and death within two months of *Cre* induction. Ultrastructural analysis of sciatic nerves isolated from

Fig4^{-/flox},CMVCreER mice 60 days after tamoxifen administration reveals a robust degenerative phenotype, with axonal dropout and abnormal myelin folding. Dorsal root ganglia present with severe spongiform degeneration similar to *Fig4^{-/-}* germline mutants. In the same animals, the CNS is only mildly affected and spongiform degeneration is limited. Optic nerve and corpus callosum display no obvious ultrastructural, functional, or biochemical abnormalities, suggesting that in adulthood *Fig4* is dispensable for CNS myelin stability within the two months of survival after tamoxifen. Early induction of global *Fig4* deletion at P3 to P4 does result in CNS hypomyelination, enlarged late endosome/lysosome (LE/Lys) accumulation in cultured oligodendrocyte precursors/oligodendrocytes (OPCs/OLs), and region-specific spongiform degeneration. These data are consistent with our previously published results indicating that *Fig4* is critical for OL differentiation *in vitro* and *in vivo*. Preliminary evidence suggests that inducible *Fig4* loss in the adult CNS thwarts myelin repair in the lysophosphatidylcholine model of reversible myelin lesion. Taken together, these data suggest a differential demand for PI(3,5)P$_2$ biosynthesis in the adult CNS and PNS.

3.2 Introduction

In higher vertebrates, myelination is critically important for proper CNS and PNS function. Myelin accelerates propagation of action potentials along the axon and thereby greatly facilitates neuron-neuron communication. In the CNS, myelin is produced by oligodendrocytes (OLs). Oligodendrocyte precursors (OPCs) arise and get specified early in development, undergo extensive migration and are present in the brain and spinal cord throughout life (Bergles and Richardson, 2015). After differentiation, myelinating oligodendrocytes are committed to the axons they are ensheathing and are incapable of repairing damaged myelin in the adult CNS

(Crawford et al., 2016a). Instead, myelin repair is carried out by differentiating OPCs, thus partially recapitulating the developmental program (Franklin and Ffrench-Constant, 2008). In the PNS, murine Schwann precursors cells arise from neural crest cells at E13, undergo differentiation into immature Schwann cells, and perform radial fiber sorting in nerve trunks. Myelinating Schwann cells ensheath axons at a 1:1 ratio and nonmyelinating Schwann cells associate with small caliber fibers as Remak bundles (Woodhoo and Sommer, 2008). Schwann cells, unlike OLs, are capable of de-differentiation and remyelination of damaged axons after injury (Hall, 2005). In both CNS and PNS, myelinating glia not only ensure saltatory axonal conduction, but also provide axons with metabolic support. In the absence of either function, neurodegeneration may occur (Nave and Trapp, 2008).

The phosphatidylinositol-3,5-bisphosphate generating biosynthetic complex consists of the kinase PIKFYVE, phosphatase FIG4, and a scaffold protein VAC14 that are highly conserved in all eukaryotic cells. The complex is localized to the early and late endosomes, where $PI(3,5)P_2$ specifies the identity of LE/Lys organelles, maintains their ionic homeostasis, vesicle fission, nutrient sensing, and autophagy (McCartney et al., 2014a, Jin et al., 2016). Human patients with a missense I41T mutation in *FIG4* combined with a null *FIG4* allele present with severe Charcot Marie Tooth type 4J peripheral neuropathy (Chow et al., 2007). Interestingly, pathological manifestations of CMT4J in human patients suggest both demyelinating and neurodegenerative contributions. The presence of "onion bulbs" and reduced sciatic nerve conduction velocity categorize CMT4J as a demyelinating neuropathy, but upper and lower motor neuron function impairment, proximal muscle weakness, and sensory deficits indicate nerve damage (Zhang et al., 2008, Nicholson et al., 2011). Strikingly, CMT4J human patients do not bear any cognitive impairment and to date there is no evidence of affected CNS

white matter. These observations suggest differential requirement for properly functioning PI(3,5)P$_2$ for CNS and PNS myelin and axonal maintenance. More severe *FIG4* mutations do affect the central nervous system and manifest as anatomical CNS defects (polymycrogiria), psychotic behaviors, calossal dysplasia, neurodegeneration, and death (Campeau et al., 2013, Baulac et al., 2014).

Previously, we extensively characterized the PI(3,5)P$_2$ biosynthetic complex in the developing CNS and PNS focusing on myelination. Loss of any component of the complex in neurons, oligodendrocytes, or Schwann cells results in CNS and PNS hypomyelination (Chow et al., 2007, Winters et al., 2011, Ferguson et al., 2012b, Vaccari et al., 2015). However, whether these phenotypes are strictly developmental or develop postnatally is not known. Furthermore, while PI(3,5)P$_2$ is critical for myelination, it is unclear whether it is necessary for myelin stability, turnover, and repair. Here, we demonstrate for the first time that FIG4 is essential in adulthood. Strikingly, loss of *Fig4* severely affects PNS axons and glial cells but only causes mild region-specific spongiform degeneration in the CNS. CNS myelin stability is not affected by inducible deletion of *Fig4* in the adult - however, CNS remyelination is impaired. These data suggest differential vulnerability of PNS and CNS to PI(3,5)P$_2$ levels in the adult organism.

3.3 Results

Inducible *Fig4* ablation in adult mice causes rapid health deterioration and death

Fig4 germline ablation in mice results in severe multi-organ defects, including CNS and PNS neurodegeneration, decreased spleen size, and skeletal abnormalities (Chow et al., 2007). To test whether loss of *Fig4* function in adult animals would lead to a similar pathology, tamoxifen-inducible *CreER* under the ubiquitously expressed *chicken beta actin* (*CAG*) promoter

(otherwise known and hereafter referred to as *CMVCreER*) was used to ablate *Fig4* globally in adult mice (Hayashi and McMahon, 2002). Without tamoxifen, *Fig4$^{-/flox}$,CMVCreER* animals showed limited *Fig4 floxed* allele recombination in tail and brain biopsies (as reported elsewhere, (Mirantes et al., 2013), but were otherwise morphologically indistinguishable from their control littermates and had normal lifespan (data not shown). To induce *Fig4* deletion, intraperitoneal tamoxifen administration was performed for five consecutive days in P60-P90 mice. As early as 10 days after the first tamoxifen dose (10 days post-injection, dpi), animals presented with abnormal hindlimb clasping (Figure 3.1A). At 30 dpi *Fig4*-deficient mice were subjected to tail suspension. While *Fig4* control littermates splayed their hindlimbs for the majority of the test duration, *Fig4$^{-/flox}$,CMVCreER* animals presented with abnormal hindlimb clasping and truncal twisting (Figure 3.2A-A'). Germline *Fig4$^{-/-}$* mice are significantly smaller than control littermates by body size and weight (Chow et al., 2007). *Fig4^{flox,}CMCVreER* animals began significantly lagging in weight compared to control littermates as early as 20 dpi. At 60 dpi, the average weight of a *Fig4$^{-/flox}$,CMVCreER* knockout was 16±0.8g compared 33±1g of littermate controls (Figure 3.2C), males in both groups were heavier than females. Furthermore, at 60 dpi *Fig4* inducible knockout animals became moribund with severely compromised gait, tremor, and hunched posture (Video 3.1, Figure 3.1B-B'). *Fig4*-deficient animals also gradually displayed variable degrees of fur discoloration, from white patches on the rump and abdomen to an almost completely white fur (Figure 3.1B-B'). At 60-63 dpi animals had gait impairment, demonstrating limited limb control and "swimming-like" limb movement (Supplementary video 3.1). At 60-63 dpi adult inducible *Fig4* knockout mice became progressively lethargic and non-responsive, and died or were terminated. An independent cohort of animals received tamoxifen administration at P21. They demonstrated a virtually identical trajectory of deterioration over 53

days (Figure 3.1C, 3.2D). Taken together, these data demonstrate that FIG4 is necessary for postnatal mammalian survival.

Adult inducible *Fig4* deletion causes mild spongiform degeneration of the CNS

A hallmark of germline *Fig4* deletion is a region-specific spongiform degeneration of the CNS. In particular, deep cortical layers, deep cerebellar nuclei, thalamus, dorsal root ganglia, and spinal motor neurons are severely affected (Chow et al., 2007), Chapter II, Figure 3.3.A'-E'). Neuronal conditional *Fig4$^{-/flox}$,SynCre* mice also present with similar pattern of spongiform degeneration, suggesting that this phenotype is predominantly neuron-specific (Ferguson et al., 2012a). To test whether spongiform degeneration occurs in adult mice within 2 months following inducible *Fig4* deletion in adult mice, nervous system tissue was isolated from P120-P150 *Fig4$^{-/flox}$,CMVCreER* animals and stained with hematoxylin and eosin (H&E). H&E staining in *Fig4* inducible knockouts at 60 dpi revealed mild vacuolation in the cortical layers 4&5, brainstem, cerebellum, and ventral spinal cord (Figure 3.3.A''-D''). Strikingly, the dorsal root ganglia demonstrated extensive vacuolation, comparable in severity to the P30 *Fig4* germline mutant, suggesting an increased vulnerability of this cell population to *Fig4* loss (Figure 3.3E-E''). A similar pathology was observed in mice injected with tamoxifen at P21. Taken together, these data indicate that spongiform degeneration can develop in the adult CNS and PNS and therefore is not restricted to developmental and early postnatal period.

To assess the extent of *CMVCre* activity, *CMVCreER* mice were crossed with *Rosa26$^{LacZ/LacZ}$* reporter animals (Soriano, 1999), and *Rosa26$^{LacZ/+}$, CMVCreER* progeny were injected with tamoxifen at 21 days and various tissues were stained for β-galactosidase 2 weeks after injection. Staining demonstrated robust reporter signal in the brain, notably in the cortex,

118

hippocampus, and cerebellum (Figure 3.4A-B). Dorsal root ganglia were intensely β-gal positive. Limited signal was observed in the spinal cord grey matter, retina, and sciatic nerve. While the *LacZ* reporter activity does not represent recombination at the *Fig4* locus, it indicates where *Cre* may be most active. Genotyping DNA from retinal tissue isolated from *Fig4⁻/flox,CMVCreER* mice at 60 dpi revealed robust recombination of the *Fig4 floxed* allele, demonstrating that *Cre* was active in that tissue (Figure 3.4F).

Severe PNS anatomical defects in adult inducible *Fig4* knockout mice

Patients with Charcot-Marie-Tooth disease type 4J, in which *Fig4* function is significantly impaired, present with intact CNS, but develop progressive and severe peripheral neuropathy (Chow et al., 2007). To examine whether loss of *Fig4* function in adulthood results in PNS damage, sciatic nerves were isolated from P120-P150 *Fig4* control and *Fig4⁻flox,CMVCreER* mice and processed for ultrastructural analysis. Toluidine blue staining of *Fig4* control sciatic nerve demonstrated structurally intact nerve architecture with robustly myelinated large caliber fibers (Figure 3.5A-A''). In contrast, *Fig4⁻/flox,CMVCre*ER sciatic nerves presented with gross histological abnormalities. Toluidine blue staining revealed reduced fiber density throughout the sciatic nerve main trunk and auxiliary branches (Figure 3.5B-B''). When imaged at high magnification with transmission electron microscope (TEM), sciatic nerve fibers in adult induced *Fig4* mutants exhibited myelin folding, abnormal aggregation of axonal mitochondria, and electron-dense inclusion bodies suggestive of impaired lysosomal transport and autophagy (Figure 3.6B-B'). These data indicate both axonal pathology and demyelination, but it is unclear which begins first. Similar pathology was observed in sciatic nerves isolated from P74 *Fig4⁻/flox,CMVCreER* mice when tamoxifen was administered at P21 (Figure 3.7). To assess the

functional significance of sciatic nerve pathology, compound action potentials (CAPs) from acutely isolated sciatic nerves were recorded. A significant decrease in sciatic nerve CAP amplitude, but not velocity, was observed, potentially indicative of axonal conduction blockage (Figure 3.8). Of note, the variability of CAP recordings in the *Fig4$^{-/flox}$,CMVCreER* group was high, ranging from electrically dead nerves to relatively normal responses. Taken together, these data indicate that adult PNS fibers are exquisitely sensitive to reduced PI(3,5)P$_2$ levels, both morphologically and functionally.

Adult inducible *Fig4* loss does not lead to demyelination in the brain after 60 days

    Fig4$^{-/-}$ mice present with severe CNS dysmyelination that does not improve with age (Chow et al., 2007), Chapter II). Likewise, the CNS in both neuron-specific (*Fig4$^{-/flox}$,SynCre*) and OL-specific (*Fig4$^{-/flox}$,Olig2Cre*) mutants remains hypomyelinated regardless of the animals' age, suggesting that myelin formation in these mice is permanently impaired (Chapter II). To test whether FIG4 is necessary for myelin stability and/or turnover, whole brain membrane preparations were carried out on P120-P150 *Fig4$^{-/flox}$,CMV-CreER* mice at 60 dpi and probed with antibodies against FIG4 and myelin markers including myelin-associated glycoprotein (MAG), myelin basic protein (MBP), proteolipid protein (PLP), and 2'3'-cyclic nucleotide 3'-phosphodiesterase (CNPase: Figure 3.9). A significant reduction in FIG4 protein levels was observed (27±5% compared to *Fig4* control set as 100%) in *Fig4$^{-/flox}$,CMVCreER* brain membrane preparations, indicating successful recombination at the *Fig4* locus. Nonetheless, no significant changes were observed in protein levels of MAG, MBP, CNPase, or PLP (Figure 3.9B). Similar results were recorded in juvenile inducible *Fig4* mutants (Figure 3.10). These data suggest that FIG4 may be dispensable for CNS myelin stability and turnover in adult mice for at

least 2 months. Consistent with these data, conditional *Fig4* deletion in the OL lineage does not result in rapid deterioration in mice, and OL lineage-specific mutant (*Fig4^{-/flox}*,*PDGFRaCreER)* mice are currently alive in our colony for over 5 months after tamoxifen administration. Similarly, *Fig4^{-/flox,}Olig2Cre* mice have a normal lifespan (Chapter II), suggesting that longevity and CNS myelination defects in *Fig4*-deficient mice are uncoupled.

Normal optic nerve ultrastructure and conduction in *Fig4^{-/flox}*,*CMVCreER* mice

The severe hypomyelination phenotype in *Fig4^{-/-}* germline mutants is associated with a drastic decrease in the density of myelinated fibers and reduced myelin thickness in the optic nerve at P21 (Chapter II). To examine whether adult inducible *Fig4* deletion leads to demyelination in the CNS, optic nerves from *Fig4* control and *Fig4^{-/flox}*,*CMVCReER* mice at 60 dpi were imaged using TEM. No obvious defects in compact myelin structure, axonal integrity, or number of myelinated axons were observed (Figure 3.11A-A'). There was no significant decrease in myelinated fiber density in juvenile inducible *Fig4* knockouts (3.12A-A'). Consistent with their ultrastructural pathology, *Fig4^{-/-}* mice demonstrate significant impairment of optic nerve conduction (Winters et al., 2011), Chapter II). To test whether inducible *Fig4* ablation in the adult CNS interferes with optic nerve function, we performed CAP recordings in P120-P150 *Fig4* inducible knockout mutants at 60 dpi. A mature optic nerve fires a multi-peak compound action potential with the peaks corresponding to myelinated axonal populations of different diameter (3.11C). The conduction velocity and amplitude of each peak can be resolved by fitting the CAP as a sum of three of four Gaussians (Carbajal et al., 2015). In *Fig4^{-/-}* germline mutants, there is a significant increase in the population of slowly conducting fibers with a concomitant decrease in fast conducting populations (Winters et al., 2011). Strikingly, optic nerves isolated

from *Fig4^{-/flox}, CMVCreER* mutants exhibited normal conduction, with no significant change in conduction velocity or amplitude of any of the CAP components (Figure 3.11B-E). These data were consistent with normal biochemical levels of myelin-associated proteins in the adult inducible *Fig4* knockout brains and the optic nerve ultrastructural analysis. Optic nerves from juvenile inducible *Fig4* knockout mice and control animals exhibited similar CV and amplitude of fast conducting populations. Interestingly, some of the recorded *Fig4^{-/flox,}CMVCreER* optic nerves had a small, but identifiable, slowly conducting peak (peak 4, CV~0.5-0.6 m/s), which was not observed in control nerves (Figure 3.14C-E'). While most of the optic nerve is myelinated by P21, the density of myelinated fibers increases between P21 and P75 (Zuchero et al., 2015), Chapter II), indicating some additional myelination. Therefore, interfering with FIG4 function at P21 and onward may impair later stages of optic nerve myelination, thus leaving some populations unmyelinated. Taken together, these data indicate that despite the loss of *Fig4* function, optic nerve myelinated fibers are not affected structurally and functionally for at least 2 months.

Early postnatal global *Fig4* deletion recapitulates some neurological defects observed in *Fig4^{-/-}* germline mutants

    Fig4^{-/-} germline mutants present with multiple neurological defects, including tremor, hydrocephalus, spongiform degeneration, CNS and PNS hypomyelination, and reactive gliosis (Chow et al., 2007, Winters et al., 2011), Chapter II). All these phenotypes are readily observed in *Fig4^{-/-}* mice at P10 until death at 4-6 weeks (Chow et al., 2007). To test whether *Fig4* ablation in early postnatal *Fig4^{flox,}CMVCreER* pups mimics the phenotype of constitutive mutants, 4-hydroxytamoxifen was administered to pups at P3 and P4 before onset of CNS myelination. Pups

were morphologically indistinguishable prior to tamoxifen administration. By P22, *Fig4$^-$/flox,CMVCreER* pups were comparable to their control littermates weight- and size-wise, however, they displayed some abdominal fur discoloration (Figure 3.1D). There were no obvious gait defects, but juvenile inducible *Fig4* knockouts displayed a mild propensity for limb clasping during tail suspension (supplementary video 3.2). Hydrocephalus was not observed (data not shown). To examine whether inducible *Fig4* knockout in early postnatal mice had any histological defects, sagittal brain sections were stained with Fluoromyelin Green. Massive spongiform degeneration, a hallmark of germline *Fig4*-deficiency was observed in cortical layers 4 and 5 (Figure 3.13A-B). Thinning of myelin-rich structures in the striatum, corpus callosum, and brain stem was evident, suggesting impaired CNS myelination. For a more quantitative assessment of myelin defects in young *Fig4* inducible knockouts, cerebellum/brainstem and forebrain homogenates were probed with antibodies against FIG4 and myelin-associated proteins MAG and MBP. A substantial decrease in FIG4 signal intensity was observed in both cortical and cerebellar lysates of *Fig4$^-$/flox,CMVCReER* knockouts, indicating a rapid FIG4 knockdown (Figure 3.13C). Interestingly, there was a noticeable reduction in myelin-associated markers MAG and MBP. As was previously reported (Chapter II) germline and conditional *Fig4* deletion results in significantly impairmed of OL terminal differentiation. The peak of OPC proliferation, differentiation, and myelination occurs during the first 2-3 postnatal weeks in mice, and therefore disrupting FIG4 function during this critical period may potentially interfere with myelinating events and thus lead to hypomyelination (Hill et al., 2014b).

Neonatal *Fig4* deletion results in enlarged LAMP1$^+$ structures in cultured OPCs/OLs

Fig4 germline-deficient OLs display abnormal accumulation of enlarged LAMP1$^+$ vacuoles *in vitro* (Chapter II). To examine whether global *Fig4* deletion happens in the OL lineage and results in a similar LE/Lys compartment abnormality, primary OPCs (PDGFRα$^+$), postmitotic OLs (O4$^+$), and myelinating OLs (MOG$^+$) were isolated from *Fig4$^{-/flox,}$CMVCreER* pups at P10, seven days after 4-hydroxytamoxifen administration. Immediately after OPCs/OLs isolation and for the next several days *in vitro*, *Fig4$^{-/flox}$,CMVCreER* OPCs/OLs were morphologically indistinguishable from littermate control cultures (data not shown). However, after 4 days *in vitro* (DIV4), abnormally large vacuoles could be detected by phase-contrast microscopy in *Fig4*-deficient cultures. When fixed and stained with the OL marker MAG and LE/Lys marker LAMP1, *Fig4$^{-/flox}$,CMVCreER*, but not control cultures, exhibited substantially enlarged LAMP1$^+$ structures, similar to what was documented in *Fig4$^{-/-}$* and *Fig4$^{-/flox}$,Olig2Cre* OLs (Chapter II; Figure 3.14A-C'). To assess the efficacy of *Fig4* deletion in isolated OPCs/OLs, parallel cultures were lysed and probed for FIG4. FIG4 protein levels were drastically decreased in *Fig4$^{-/flox}$,CMVCreER* OPCs and postmitotic OLs (Figure 3.14D). These data indicate that early global neonatal *Fig4* deletion is efficient in OPCs/OLs and leads to rapid impairment of the LE/Lys transport. These results may also indicate that lack of demyelination in the CNS of adult inducible *Fig4* knockout mice is not due to inefficient *Cre* activity in the OL lineage.

Global adult inducible Fig4 deletion prevents myelin repair after LPC injection

Remyelination in the adult CNS occurs in response to white matter damage associated with stroke, trauma, or autoimmune attack. Myelin repair is preceded by active migration of

124

OPCs to the damaged myelin, their differentiation into immature OLs and myelination of naked axons. To an extent, this process recapitulates developmental myelination, although the ability of OPCs to differentiate and myelinate decreases with age (Crawford et al., 2016b). Here, we used a well-established model of reversible myelin lesion via stereotaxic brain injection of lysophosphatidylcholine (LPC; (Gregson and Hall, 1973). P60-P90 control littermate and *Fig4⁻/flox,CMVCreER* mice were injected with tamoxifen, and at 10 dpi LPC was injected stereotactically into the corpus callosum. This timeline was selected due to early pathological manifestations in adult inducible *Fig4*-deficient mice and their rapid health deterioration afterwards. At 21 days after LPC injection, the corpus callosum is typically remyelinated and the resulting myelin, while thinner than established developmentally, is electrophysiologically competent (Brill et al., 1977). Toluidine blue staining in *Fig4* control littermates at 21 days after LPC injection demonstrated an identifiable lesion site, but with a robust toluidine blue signal within lesion borders, suggesting remyelination (Figure 3.15A). Preliminary studies in *Fig4*-deficient animals revealed that the lesion site had notable absence of toluidine blue signal, indicating a lack of myelinated structures (3.15B). TEM imaging of intact corpus callosum regions revealed no difference in myelin structure and axonal integrity in *Fig4⁻/flox,CMVCreER* mutants, consistent with the optic nerve ultrastructural analysis (Figure 3.15A'-B'). There were multiple thinly myelinated fibers in the lesion core of control littermate mice, but very little evidence of remyelination in *Fig4*-deficient mutants (Figure 3.15A''-B''). These data suggest that while *Fig4* may be dispensable for myelin stability and turnover in the CSN, it is necessary for remyelination. Cerebellum lysates collected from the animals at the same tamoxifen dpi demonstrated a robust decrease in FIG4 protein levels, indicating successful *Fig4* deletion by Cre (Figure 3.15C).

3.4 Discussion and future directions

PI(3,5)P$_2$ homeostasis is essential for normal physiology in the adult mammalian organism. As early as 10 days after tamoxifen administration, *Fig4*-deficient mice showed motor defects such as abnormal hindlimb clasping. Furthermore, both juvenile and adult global inducible *Fig4* deletion led to severe weight loss, loss of fur pigmentation, "swimming" gait, and reduced lifespan. At 60 dpi, FIG4 protein levels in the brain were less than 30% of wildtype levels, demonstrating efficient *Cre* activity. Region-specific spongiform degeneration was observed in adult inducible *Fig4* knockouts at 60 dpi. Ultrastructural analysis of sciatic nerves in *Fig4$^{-/flox,}$CMVCreER* mice revealed severe PNS degeneration with both axonal pathology and demyelination. Remarkably, in the same animals, CNS myelin in the brain was largely intact with no signs of demyelination or impaired electrophysiological properties. Neonatal *Fig4* genetic deletion, however, did result in CNS hypomyelination, suggesting that *Fig4* may be essential during the critical period of OPC differentiation and myelination in the first postnatal weeks. *Fig4$^{-/flox}$,CMVCreER* OLs displayed enlarged vacuolation similar to germline *Fig4$^{-/-}$* cells and robust decrease in FIG4 protein levels, indicating successful *Fig4* deletion in the OL lineage. Interestingly, CNS white matter lesion remyelination appears to be impaired in adult inducible *Fig4* mice. Taken together, our data indicate differential demand for *Fig4* function in the adult mouse organism depending on the organ system and physiological conditions.

Genetic *Fig4* deletion leads to a severely shortened lifespan

Germline inactivation of any component of the PI(3,5)P$_2$ biosynthetic complex in mice results in decreased survival. Depending on genetic background, germline *Fig4* null mutants live up to 6 weeks, *Vac14* null mutants die neonatally, and *Pikfyve* null mice do not survive past E3.5

in utero (Chow et al., 2007, Zhang et al., 2007, Ikonomov et al., 2011). Here, we demonstrated that inducible *Fig4* deletion in adult mice on a genetic background similar to well-characterized *Fig4* germline mutants ((C57BL/6J x C3H) F1, Chapter II) leads to a severely shortened lifespan. The ultimate cause of death in both germline and inducible *Fig4* knockouts is not clearly understood. The animals are still capable of eating and drinking, despite continuous reduction in weight. Muscle atrophy in $Fig4^{-/-}$ germline mutants was shown to be secondary to neurodegeneration (Reifler et al., 2013). Both germline and adult *Fig4* inducible knockouts may die due to breathing impairment, since animals were observed gasping for air shortly before their death (data not shown). Among tissue-specific conditional *Fig4* mutants, it is notable that neuron-specific knockouts ($Fig4^{-/flox}$,*SynCre*) have a shorter lifespan than the OPC and the OL lineage-specific *Fig4* mutants (Chapter II). Conversely, a significant lifespan increase in transgenic $Fig4^{-/-}$,*NSE-Fig4* mice compared to germline *Fig4* mutants suggests that FIG4 function in neurons is essential for survival. Of note, FIG4 is enriched in DRGs (Guo et al., 2012). DRGs are among the earliest and most severely affected neuronal populations in germline null, *SynCre*, and global adult inducible *Fig4* knockouts, whereas these cells are completely intact in the *Olig2Cre Fig4* conditional mutants (Chapter II). It may be of interest to examine DRGs more closely to determine what makes them so vulnerable to impaired $PI(3,5)P_2$ biosynthesis and whether their degeneration contributes to reduced lifespan in mutant mice. Interestingly, $Fig4^{-/flox}$,*Olig2Cre* conditional knockouts display severe spongiform degeneration in the spinal cord (Vaccari et al., 2015), Chapter II), yet have a normal lifespan and do exhibit any obvious gait abnormalities.

Notably, some CMT4J patients have died due to respiratory complications in adulthood (Zhang et al., 2008). Yunis-Varon patients die in infancy due to multi-organ failure. Two of the

reported polymycrogyria patients died of seizures, and two more committed suicide (Campeau et al., 2013, Baulac et al., 2014). Taken together, the observations in mouse mutants and human patients strongly suggest that there is a minimal requirement for PI(3,5)P$_2$ level that is needed to maintain normal physiology. Our new data indicate that even an adult mammalian organism is vulnerable to *Fig4* loss of function.

***Fig4* is necessary in the adult PNS**

The most striking observation in *Fig4$^{-/flox}$,CMVCreER* mutants is a devastating effect of adult inducible *Fig4* deletion on sciatic nerve fibers. Drastic deterioration of sciatic nerves is consistent with the human CMT4J phenotype where peripheral nerves are greatly affected. As in human patients, PNS pathology in *Fig4* adult inducible knockout mice exhibits signs of both neuronal and Schwann cell contribution. With the current data, it is difficult to establish whether axons or Schwann cells first develop pathology. Abnormal mitochondrial accumulation is suggestive of axonal defects, as is reduced CAP amplitude in recorded sciatic nerves. However, the accumulation of myelin debris and misfolded myelin indicate demyelination and abnormal Schwann cell function. Since PI(3,5)P$_2$ regulates autophagy (Ferguson et al., 2009, 2010), it would be interesting to examine the effect of adult inducible *Fig4* deletion on autophagic processes in neurons and Schwan cells, which may contribute to PNS abnormalities (see Chapter IV for a more detailed discussion). A previous study used conditional knockout to dissect the neuron-glia contribution to the sciatic nerve pathology in *Fig4* germline mutants (Vaccari et al., 2015). Selective *Fig4* loss in motor neurons resulted in mild hypomyelination of motor-specific nerves (quadriceps) and eventual motor neurodgeneration and axonal dropout. *Fig4* deletion in Schwann cells caused significant hypomyelination in sciatic nerve, impaired SC autophagy, and

128

additional demyelination in aged animals. Sensory nerve pathology was not characterized in depth. Both mice and human patients have sensory neuron abnormalities (as described above), but they are relatively mild in human CMT4J patients compared to their motor defects. Interestingly, a recent genome-wide association study in prostate cancer patients identified an intronic *VAC14* SNP as a potential predictor of docetaxel-induced peripheral neuropathy (Hertz et al., 2016). These data further support PNS dependence on properly functioning PI(3,5)P$_2$ biosynthesis.

Axon-glia interactions necessary for myelin formation and repair after injury in the PNS are well described. In particular, Neuregulin 1 type III (NRG1) signaling has been shown as a major regulator of PNS myelination and repair, but as dispensable for maintenance of Schwann cells and myelin in the adult PNS (Atanasoski et al., 2006). Interestingly, it was recently demonstrated that during PNS repair, Schwann cells themselves produce NRG1 type III and NRGI type I to compensate for the absence of neuronal-derived NRG1 and thus ensure effective remyelination (Stassart et al., 2013). It is possible that in the absence of *Fig4,* some aspect of NRG1 signaling is altered, thus leading to impaired communication in the axoglial unit and its degeneration. Currently, we have no direct evidence of altered NRG1 levels in the absence of *Fig4* in either PNS cell population. It would be possible to use biochemistry, *in situ* hybridization, and immunostaining to directly test an effect of PI(3,5)P$_2$ deficiency on NRG1 levels Further dissection of the PNS phenotype in adult inducible *Fig4* knockout mice can be achieved by employing cell-type specific inducible *Cre* lines.

Clasping and gait abnormalities in adult inducible *Fig4* knockout mice

At 60 dpi, adult inducible *Fig4* knockout mice demonstrate severely impaired locomotion, with tremor and impaired gait. Furthermore, the animals show abnormal behaviors during tail suspension, such as hindlimb clasping and truncal twisting as early as 10 dpi. These phenotypic manifestations may be partially due to impaired PNS and secondary muscle loss. Abnormal behavior during tail suspension, however, suggests neurological defects, but it may originate from multiple neuronal populations. Abnormal twisting and clasping are reported in mouse models of Huntington's disease, dystonia, ALS, and peroneal muscular atrophy, among other conditions (Lin et al., 2001, Li et al., 2005, McGoldrick et al., 2013, Liang et al., 2014, Pappas et al., 2014, Pappas et al., 2015, Weisheit and Dauer, 2015). Neurodegeneration is relatively region-specific in all these disorders, but nonetheless they converge onto a similar phenotypical manifestation. Spongiform degeneration in adult inducible *Fig4* knockout mice is subtle compared to germline mutants, but it may be sufficient to result in degeneration of neuronal populations that contribute to abnormal tail suspension behavior. Of note, neuron-specific *Fig4* mutants progressively exhibit abnormal clasping (Ferguson et al., 2012a), whereas *Fig4^{flox},Olig2Cre* mice do not, despite some CNS spongiform degeneration and robust hypomyelination (Chapter II). Closely examining neuronal populations whose neurodegeneration contributes to abnormal clasping phenotypes, such as basal ganglia, cortex, and spinal cord will provide additional insight into cell-type specific vulnerability to impaired PI(3,5)P$_2$ biosynthesis.

Is FIG4-mediated intracellular trafficking dispensable for myelin stability and turnover?

Despite a robust FIG4 knockdown in the brain at 60 dpi, adult *Fig4*$^{-/flox}$*,CMVCReER* mutants do not demonstrate a decrease in myelin-associated proteins in the CNS. While there is mild spongiform degeneration in the CNS, optic nerve and corpus callosum myelin show no signs of demyelination or degeneration, and optic nerve electrophysiological properties are not altered. *LacZ* reporter activity is limited in the retina and little signal is detected in the RGC layer. However, genomic DNA from retina demonstrates robust *Fig*^{flox} recombination, indicating that at least in some retinal populations *Cre* was active. Furthermore, brain lysates and ultrastructural imaging of the corpus callosum reveal relatively intact myelin in the adult inducible *Fig4* mutants, suggesting that observations made in the optic nerve are likely representative of the CNS myelin state. A potential caveat is insufficient Fig4 knockdown specifically in mature myelinating OLs which may lead to underestimating the role of FIG4 in adult myelin stability.

Myelin in the mature CNS has long been considered static, given the long high half-life of myelin associated proteins (Savas et al., 2012) and somewhat reduced OPC proliferative capacity (Crawford et al., 2016b). However, recent advances in monitoring oligodendrocytes in the living adult CNS suggest active myelin remodeling. It is possible that loss of FIG4 function for just two months is not sufficient to cause demyelination. Genetic deletion of myelin regulatory factor (*Myrf*) in all OPCs/OLs of the adult CNS, however, is devastating for myelin stability, as it leads to decreased myelin protein synthesis, demyelination, and OL death. These events transpire fairly rapidly, with animals displaying phenotypical manifestations of demyelination as early as 5 weeks after tamoxifen administration, and profound myelin defects at 8 wpi (Koenning et al., 2012). Therefore, it is possible to cause destabilization of mature myelin

within 6 weeks. Studies assessing long-term *Fig4* deletion specifically in the OL lineage would be essential to truly establish whether *Fig4* is dispensable for myelin maintenance. It is important to differentiate between myelin maintenance by existing OLs, and myelin turnover, which involves adult OPC migration and differentiation into myelinating OLs. We are currently addressing the role of FIG4 in myelin turnover in adult inducible OPC-specific *Fig4* conditional mutants (*Fig4*$^{-/flox,}$*PDGFRCreER*). The use of myelinating OL-specific *Cre* lines such as *MBPCreER* or *PlpCreER* would permit assessing the importance of *Fig4* for myelin stability. Importantly, thus far, our observations on the FIG4 function in the CNS myelin stability are restricted to the brain. Weakness and impaired gait in *Fig4* adult inducible knockouts is reminiscent of pathological conditions where white matter of the spinal cord is compromised (Koenning et al., 2012). Therefore, it would be critical to determine whether global *Fig4* inducible ablation impairs myelin stability and turnover in the spinal cord white matter.

Strikingly, genetically deleting *Fig4* in the early neonatal pups results in impaired myelination at P22. Hypomyelination in inducible *Fig4* knockouts is milder than in *Fig4* germline mutants, which could be partially due to *Cre* efficacy and timing of tamoxifen injection. It may also suggest the importance of FIG4 in some developmental aspects of the OL lineage, such as OPC specification, migration, and initiation of axoglial contact, which haven't been addressed extensively. It is possible that 4-hydroxytamofixen administered shortly after birth may have different efficacy on *Cre* recombination specifically in the OL lineage when compared to the IP administration in the adult animals. Isolation of adult OPCs and examining their FIG4 protein levels would serve as an excellent way of addressing that caveat. Nonetheless, hypomyelination in neonatally induced *Fig4* mutants versus intact myelin in adult inducible *Fig4* knockouts strongly suggests the importance of FIG4 during the critical postnatal period of OPC

differentiation and myelination. These results are consistent with our published data on neonatal OPC-specific *Fig4* deletion, which also led to a mild, but significant CNS myelination defects in mice (*Fig4⁻/flox, PDGFRaCreER*). Our studies of constitutive *Fig4* mutants demonstrated that FIG4 is critical for terminal OL differentiation (Winters et al., 2011), chapter II). Precise mechanisms are not well understood. Notably, FIG4 is not the only protein that presumably affects OPC differentiation, but not myelin stability. For example, Arp2/3 actin nucleation complex is critical for initiation of myelin assembly, but is dispensable in the adult CNS (Zuchero et al., 2015). Similarly, perturbation of mTORC1 signaling at different OPC stages yields distinct effects on their maturation and myelination (Tyler et al., 2009, Zou et al., 2014).

FIG4 positively regulates CNS myelin repair

While CNS myelin is largely intact in global adult inducible *Fig4* knockout mice at 60 dpi, our preliminary data suggest that FIG4 may be necessary for myelin repair. These observations would indicate recapitulation of FIG4-depenent development-like events during remyelination. Notably, OPCs have to undergo proliferation and differentiation to repair damaged myelin. Given the critical role of PI(3,5)P$_2$ biosynthetic complex for OPC differentiation, one possibility is that adult inducible *Fig4* deletion may be arresting OPC differentiation at the lesion site. We are currently in the process of examining myelin repair in OPC-specific inducible *Fig4* knockouts, which would gain additional insights into cell-autonomous aspects of remyelination.

A traditional approach to measuring the extent of remyelination after LPC lesion in the corpus callosum is quantification of thinly myelinated axons by TEM or blinded ranking of lesion remyelination on toluidine blue sections (Gautier et al., 2015). However, this protocol has

its limitations as it is challenging to definitively delineate the lesion border at high TEM magnification. In addition, calossal projections run both lateral/medial and rostral/caudal and only 30% of them are myelinated, making scoring the extent of remyelination difficult. We propose a low-throughput, unbiased approach by employing *Mbp in situ* hybridization as the readout of lesion repair. As *Mbp* is translated locally, the *Mbp* mRNA signal is robust and homogenous throughout the corpus callosum. In contrast, in lesioned white matter the *Mbp* signal is reduced, and a sharp border can be observed between the intact and damaged myelin. As remyelination takes place, the *Mbp* signal can be observed gradually filling the lesion site, and remyelinated lesion becomes darker due to excessive *Mbp* production. Studies applying this approach to our *Fig4* knockouts are currently in progress.

3.5 Methods

Mouse genetics - All mice were housed and cared for in accordance with NIH guidelines, and all research conducted was done with the approval of the University of Michigan Committee on Use and Care of Animals. Both male and female mice were used in experiments. For global *Fig4* inducible deletion, $Fig4^{+/-}$ mice on congenic C57BL background were crossed with the *CMVCreER* tamoxifen inducible line (#004682, Jackson Laboratories). Their $Fig4^{+/-}$,*CMVCreER* progeny were crossed with $Fig4^{flox/flox}$ mice on C3HeB background. OPC-specific *Fig4* deletion was performed as previously described (Chapter II). For reporter studies, $Rosa26^{LacZ/LacZ}$ mice (#003474, Jackson Laboratories) were crossed with *CMVCreER* mice. For all experiments, *Fig4* control animals contained at least one WT *Fig4* allele and in most cases received tamoxifen treatment to account for any toxicity effects.

Cre induction - Tamoxifen (Sigma-Aldrich) was dissolved in 910:90 Sunflower seed oil/100% Ethanol mixture at 10mg/ml. P21 and P60-P90 mice received 75mg/kg of tamoxifen IP injections for 5 days. For early postnatal studies, 4-hydroxytamofixen was dissolved at 10mg/ml in pure ethanol and was administered to P3 pups for 2 days as described previously (Chapter II).

Tail suspension test. Tail suspension test was performed as described previously (Weisheit and Dauer, 2015).

H&E staining. H&E staining of tissue was performed as described previously (Ferguson et al., 2012b).

Toluidine blue staining and TEM - Transmission electron microscopy was performed as described previously (Winters et al., 2011). The main trunk of the sciatic nerve was used for ultrastructural analysis. Toluidine blue images were taken using 40x oil objective on Zeiss Axio Examiner inverted microscope (Zeiss) and tiled images were stitched using ZEN. TEM was performed using Jeol JEM-1400 microscope.

Beta-galactosidase staining - β-gal staining was performed as described previously (Holtz et al., 2015).

Optic and sciatic nerve recordings - CAP recordings of acutely isolated optic and sciatic nerves were performed as reported previously (Chen et al., 2004, Carbajal et al., 2015).

Membrane purification - Membrane purification was performed as described previously (Winters et al., 2011). For brain region-specific biochemistry in juvenile inducible *Fig4* knockout mice cerebellum/brainstem and forebrains were lysed in RIPA buffer as described previously (Chapter II). For early postnatal induced *Fig4* knockouts, region-specific homogenates were collected in low sucrose buffer as described previously (Winters et al 2011).

Western blotting - Western blotting was performed as described previously (Chapter II).

OPC culture - Primary OPCs/OLs were isolated from P10 (7 days after the first 4-hydroxytamoxifen injection) *Fig4$^{+/flox,}$ CMVCreER* and *Fig4$^{-/flox,}$CMVCreER* pups as reported previously (Chapter II). PDGFR$^+$, O4$^+$, and MOG$^+$ OLs were allowed to differentiate in T3 supplemented culture medium for 4 days. Cells were fixed and stained for lysosomal marker LAMP1 (Abcam) and MAG (Millipore) as described previously. Cells were imaged using Zeiss Axio Examiner inverted microscope (Zeiss, Germany) equipped with Axiocam 503 and Apotome. Z-stacks and apotome optical sections were collected and maximum intensity projections were generated with ZEN and FIJI.

OPC biochemistry - PDGFRα$^+$ and O4$^+$ OPCs/OLs were plated at a high density (80,000-100,000 cells/12 well plate well) and allowed to proliferate for 5 days. The day after cells spontaneously differentiated due to high confluency, they were lysed directly in the loading buffer, boiled and loaded at equal volume for Western blotting as described previously (Chapter II). Lysates were probed with anti-FIG4 (Neuromab) and CNPase (Abcam) antibodies.

Immunohistochemistry - For Fluoromyelin Green staining, animals were perfused with cold PBS and brains were rapidly dissected and post-fixed in 4% PFA for 2 hours at 4C. Following the cryoprotection in 30%sucrose, 40 μm sagittal free-floating sections were collected on a freezing cryostat (Leica). Fluoromyelin Green staining was performed according to manufacturer's instructions (Thermo Scientific). Brain sections were imaged using Zeiss Axio Examiner and tiled images were stitched together with ZEN.

LPC injection - Mice were injected with tamoxifen as descried above. 10 days after the first tamoxifen dose, P70-P90 mice were used for stereotaxic injection of L-A-Lysophosphatidylcholine (LPC) (Sigma, L4129) into the corpus callosum. Mice were anesthetized with 4% isoflurane, secured in stereotaxic stage (Stoelting), and kept under 2%

isoflurane anesthesia during surgery. A 5µl Hamilton syringe was loaded with 1% LPC in PBS (Gibco) and mounted on a motorized stereotaxic pump (Stoelting). Injections were performed at the following coordinates: AP - 1.25mm, LR - ±1mm, D - 2.25mm. Over a time period of 1 min, 0.5µl of 1%LPC solution was injected at the ipsilateral site and 0.5µl 1XPBS on the contralateral side as the control. After the injection, the needle was kept in place for 2 min before retraction. Following surgery, mice were treated with 3 doses of 70µl of buprenorphine (0.3mg/ml) every 12 hours. Brains were harvested at 21 days post LPC injection.

Statistical analysis. Statistical analysis was performed using Graphad Prism and Microsoft Excel. For Western blotting, intensity of the control sample was set as 1. For electrophysiological studies, the analysis was performed using Clampfit (Molecular Devices) and Origin Pro. For TEM quantification, 10 images were taken at random and percentage of myelinated fibers was quantified.

3.6 Author contributions

Roman Giger, Yevgeniya Mironova, and Miriam Meisler designed the study. Jing-Ping Lin established the *Mbp* remyelination protocol. Guy Lenk, J.P.L., Travis Dickendesher, and Y.M. performed the experiments. Y.M. performed data analysis and wrote the manuscript, J.P.L. contributed the LPC methods description.

3.7 Acknowledgments

We would like to thank Jonah Chan and Bradley Zuchero for providing us with O4 and MOG hybridomas, respectively, University of Michigan Microscopy and Imaging Core for the
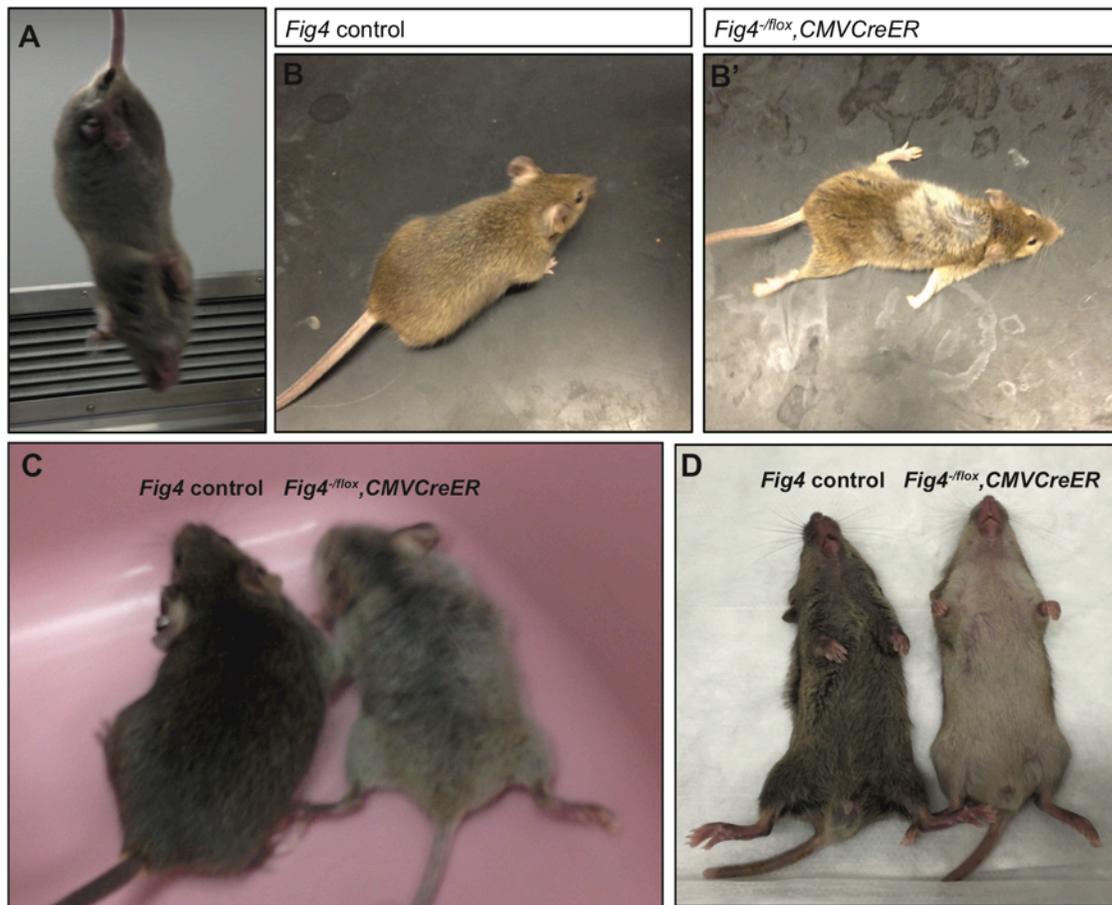
Figure 3.1 Global adult inducible *Fig4* knockout mice at different ages. (A) P70-110 *Fig4⁻/flox,CMVCreER* mice display abnormal hindlimb clasping 10 days after first tamoxifen administration (10 dpi). **(B-B')** P120-150 *Fig4* control and *Fig4⁻/flox,CMVCreER* at 60 dpi. *Fig4⁻/flox,CMVCreER* mouse shows patchy fur discoloration, weight loss, and "swimming" gait. **(C)** P74 *Fig4⁻/flox,CMVCreER* mice at 53 dpi. Inducible global *Fig4* knockout displays complete fur discoloration and motor defects. **(D)** P22 *Fig4* control and *Fig4⁻/flox,CMVCreER* mutant mice at 19 dpi. Belly fur of the *Fig4⁻/flox,CMVCreER* mouse is notably lighter than control littermate's, but there are no obvious size differences.
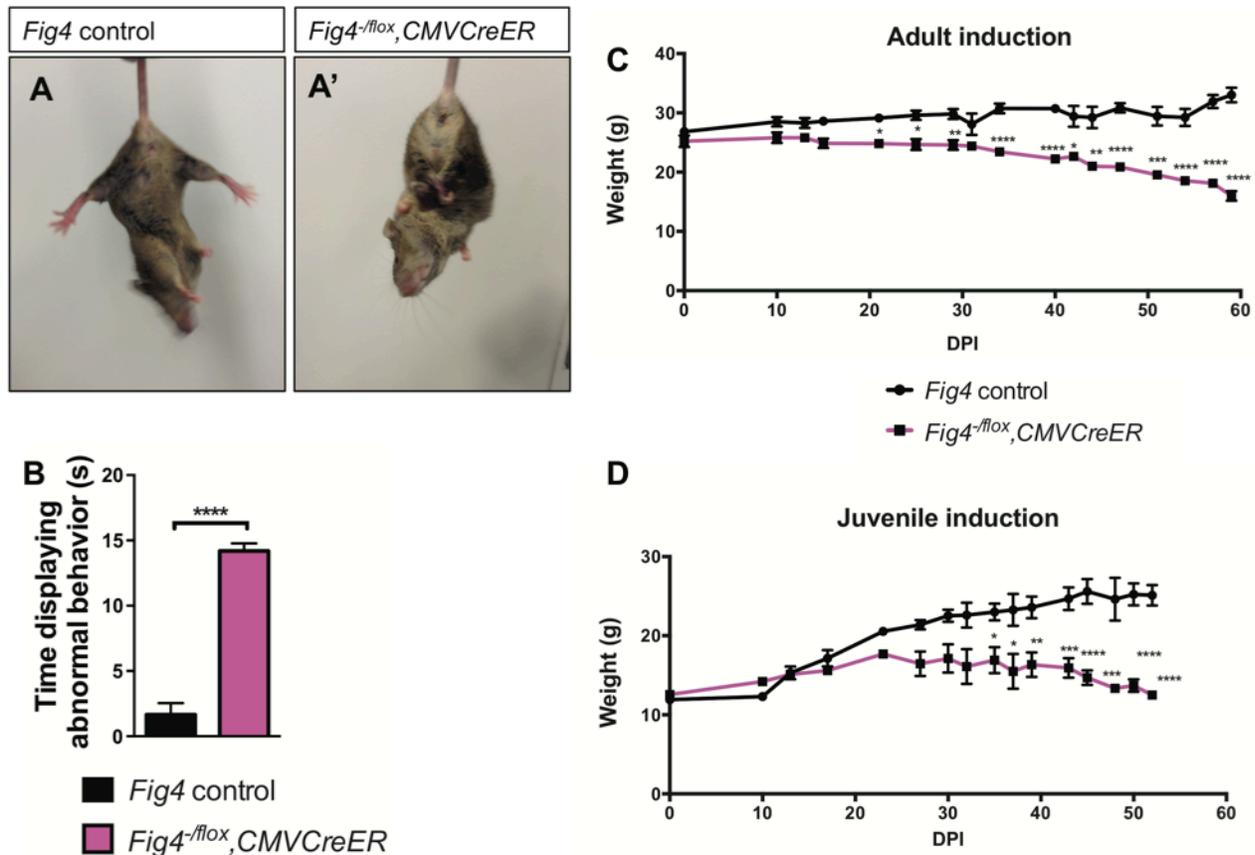
Figure 3.2 Global adult inducible *Fig4* deletion results in motor defects and weight loss in mice. **(A-A')** P90-120 *Fig4* control and global inducible *Fig4* knockout mice during the tail suspension test at 30 dpi. Control mice display typical hindlimb spreading, whereas *Fig4⁻/flox*,*CMVCreER* mice show abnormal clasping. **(B)** Tail suspension quantification. Animals were held by their tails for 15s and time displaying abnormal behavior was recorded. Data presented as mean±SEM, ****p<0.0001, unpaired Student *t*-test. **(C-D)** Weight loss chart in adult (**C**, at P60-90) and juvenile (**D**, at P21) inducible *Fig4* mutants. Day 0 denotes the first tamoxifen injection. *p<0.05, **p<0.01, ***p<0.001, ****p<0.0001. n=10 (day 0) and 8 (day 60) for control, n=5 (day 0) and n=3 (day 60) for *Fig4⁻/flox*,*CMVCreER* adult inducible mutants. N=5 for control and n=3 for juvenile inducible knockouts. 2-way ANOVA with Sidak correction.
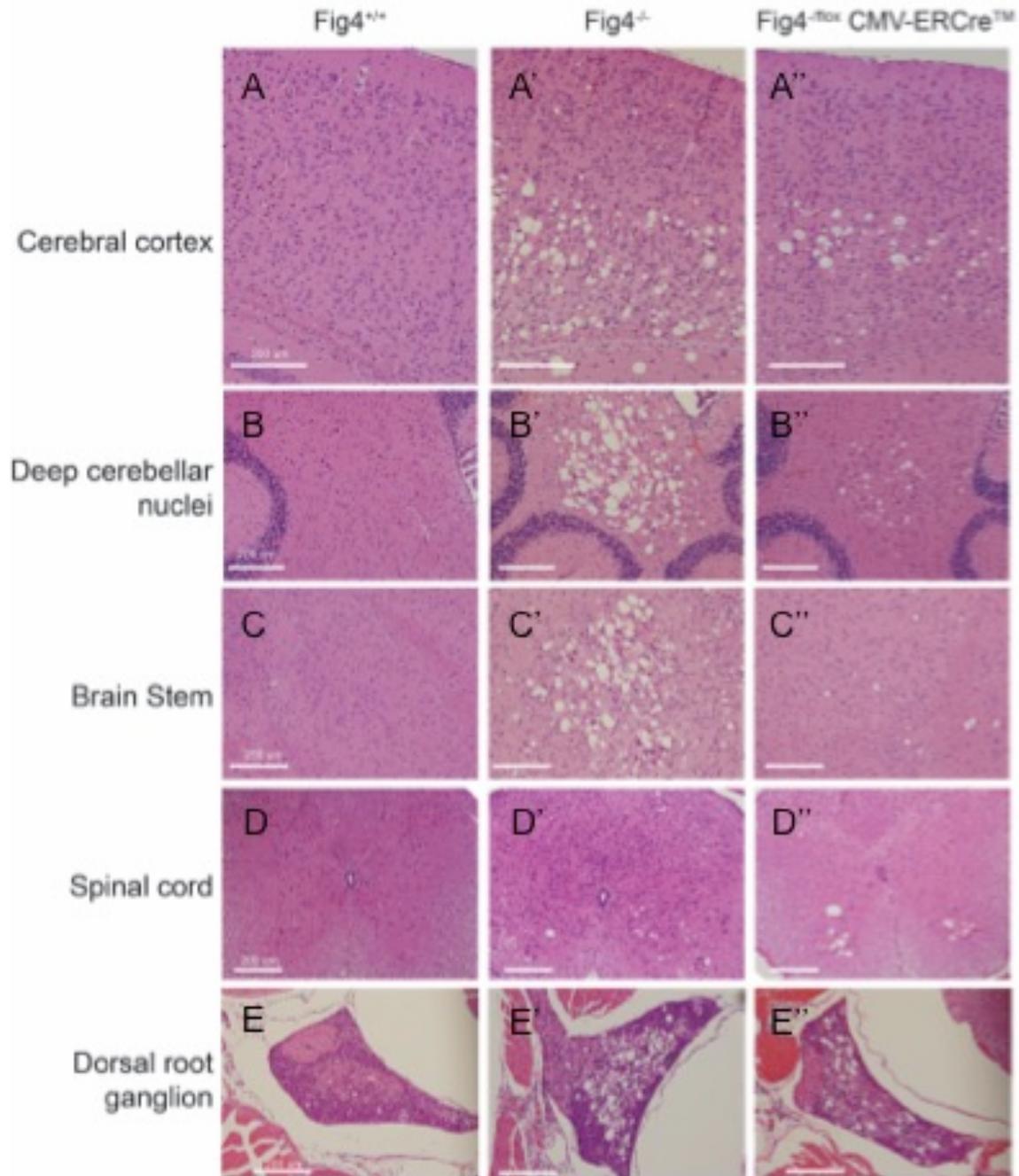
Figure 3.3 Spongiform degeneration in global adult inducible *Fig4* knockout mice. H&E staining of the cerebral cortex **(A-A'')**, deep cerebellar nuclei **(B-B'')**, brain stem **(C-C'')**, and spinal cord **(D-D'')** reveals mild spongiform degeneration in P120 *Fig4^{-/flox;}CMVCreER* mice at 60 dpi compared to severe vacuolation in P30 *Fig4^{-/-}* global mutants. **(E-E'')** Comparable degeneration, however, is observed in the dorsal root ganglia. N=3, scale bars as indicated. Image courtesy Guy Lenk
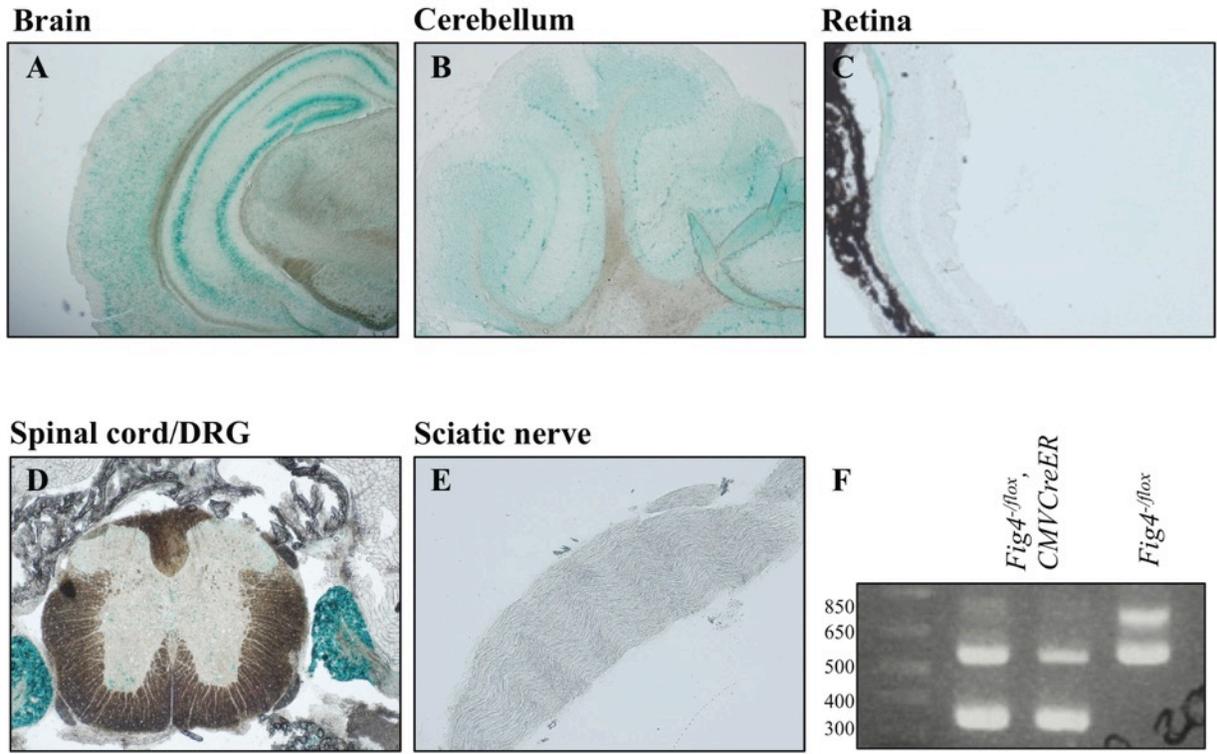
Figure 3.4 *LacZ* **reporter expression in** *CMVCreER* **mice.** Representative neural tissue sections from P34 *Rosa26^{LacZ/+},CMVCreER* mice at 21 dpi stained for LacZ demonstrate robust signal in the cortex and hippocampus **(A),** cerebellum **(B)**, and dorsal root ganglia **(D).** Sparse and restricted signal is observed in the retina **(C)**, spinal cord grey matter **(D)**, and sciatic nerve **(E)**. Scale bar = 200μm. **(F)** *Fig4^{flox}* genotyping PCR of the retinas isolated from *Fig4^{-/flox},CMVCreER* mice at 53 dpi (first 2 lanes) and *Fig4^{-/flox}* control littermate. 282 kb products indicating deletion of the *floxed Fig4* allele are observed only in *Fig4^{-/flox},CMVCReER* and *Fig4^{+/flox},CMVCreER* mice. Images courtesy Travis Dickednesher.
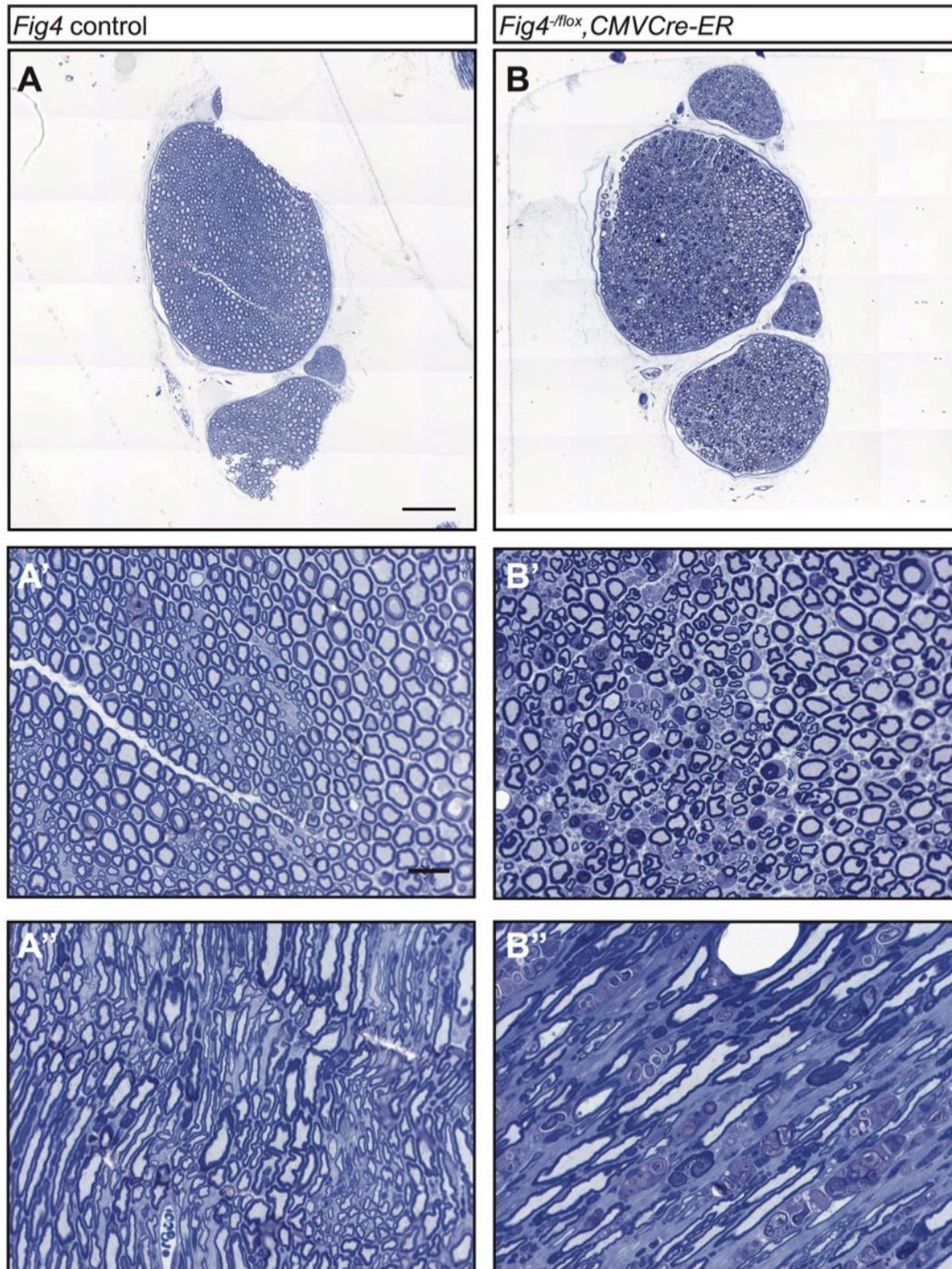
Figure 3.5 Robust PNS neurodegenerative phenotype in *Fig4$^{-/flox}$,CMVCreER* mice. (A-B) Representative toluidine blue staining of the sciatic nerve main trunk cross section isolated from P120-150 *Fig4* control and *Fig^{-flox},CMVCReER* mice at 60 dpi. Scale bar = 50μm. **(B-B')** High magnification images of **(A-B)** reveal axonal dropout and abnormal myelin folding in *Fig4$^{-/flox,}$CMVCreER* mice. **(A''-B'')** Longitudinal sciatic nerve sections reveal increased interstitial space and abnormal accumulations in *Fig4$^{-/flox}$,CMVCreER* mice compared to the normal architecture of the *Fig4* control nerve. N=4. Scale bar = 20μm.
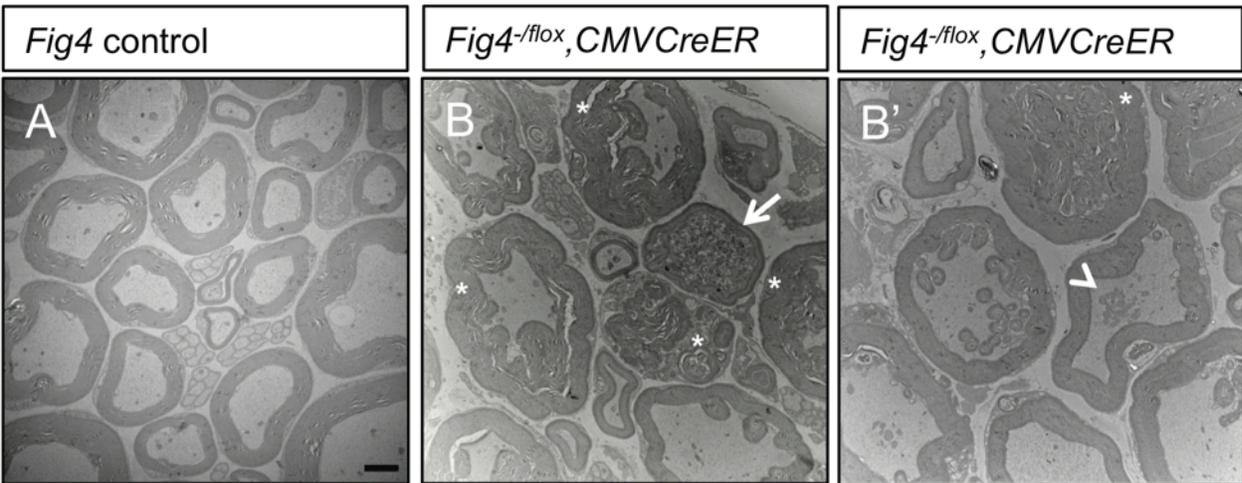
Figure 3.6 Ultrastructural defects in *Fig4^{-/flox,}CMVCReER* sciatic nerves. Representative TEM micrographs of cross sciatic nerve main trunk sections isolated from P120-150 mice at 60 dpi. **(A)** *Fig4* control nerves demonstrate robust myelination of large caliber fibers and well-defined Remak bundles. **(B-B')** Sciatic nerves isolated from *Fig4^{-/flox,}CMVCreER* mice at 60 dpi reveal abnormal myelin folding (asterisks), accumulation of neurodegenerative axonal material (arrow), and abnormal mitochondrial aggregation in axons (arrowhead). Scale bar = 2μm. N=4.
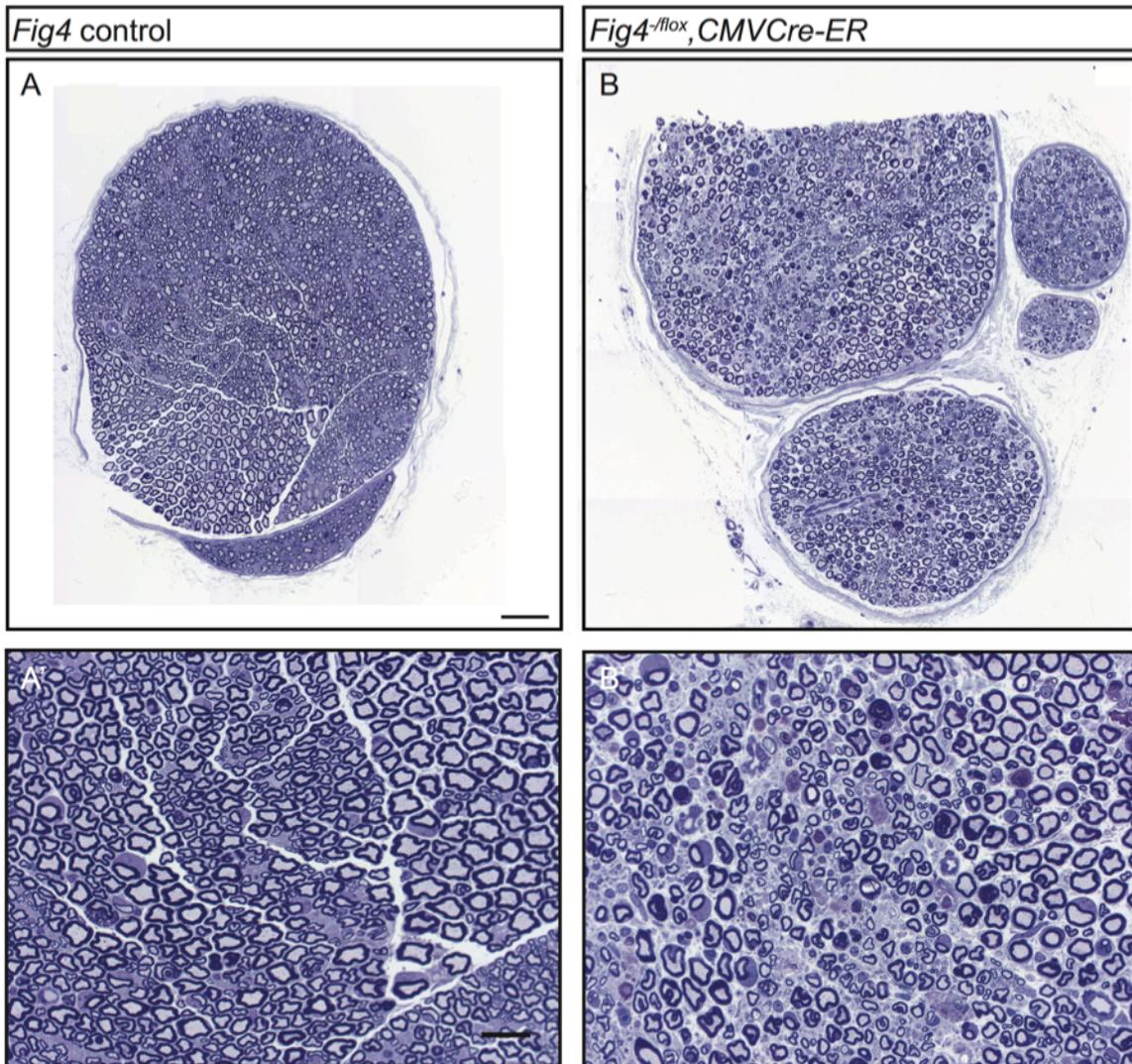
Figure 3.7 Sciatic nerve ultrastructural defects in juvenile global inducible *Fig4* knockout mice. (**A-B**) Toluidine blue sciatic nerve main trunk cross sections. Scale bar = 50 μm. (**A'-B'**) Higher magnification images of (**A**) and (**B**), scale bar = 2μm. N=3.
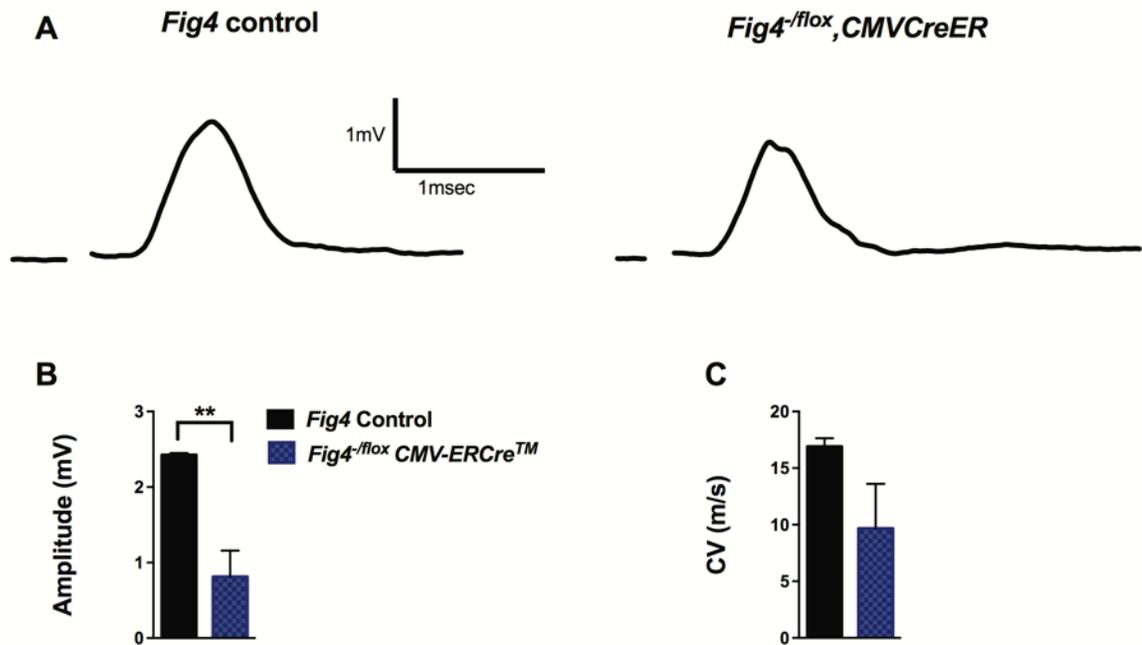
Figure 3.8 Impaired sciatic nerve conduction in juvenile global inducible *Fig4* knockout mice after 53 days. (A) Representative compound action potential traces of acutely isolated sciatic nerve recordings from P74 *Fig4* control and *Fig4$^{-/flox}$,CMVCReER* mutant at 53 dpi. **(B)** *Fig$^{-/flox}$,CMVCreER* mutants reveal a significant decrease in CAP amplitude, but not conduction velocity (CV). **$p=0.0046$ n= 4 nerves (control), n=5 nerves (*Fig4$^{-/flox,}$CMVCreER*). Mean ± SEM, unpaired Student *t*-test.
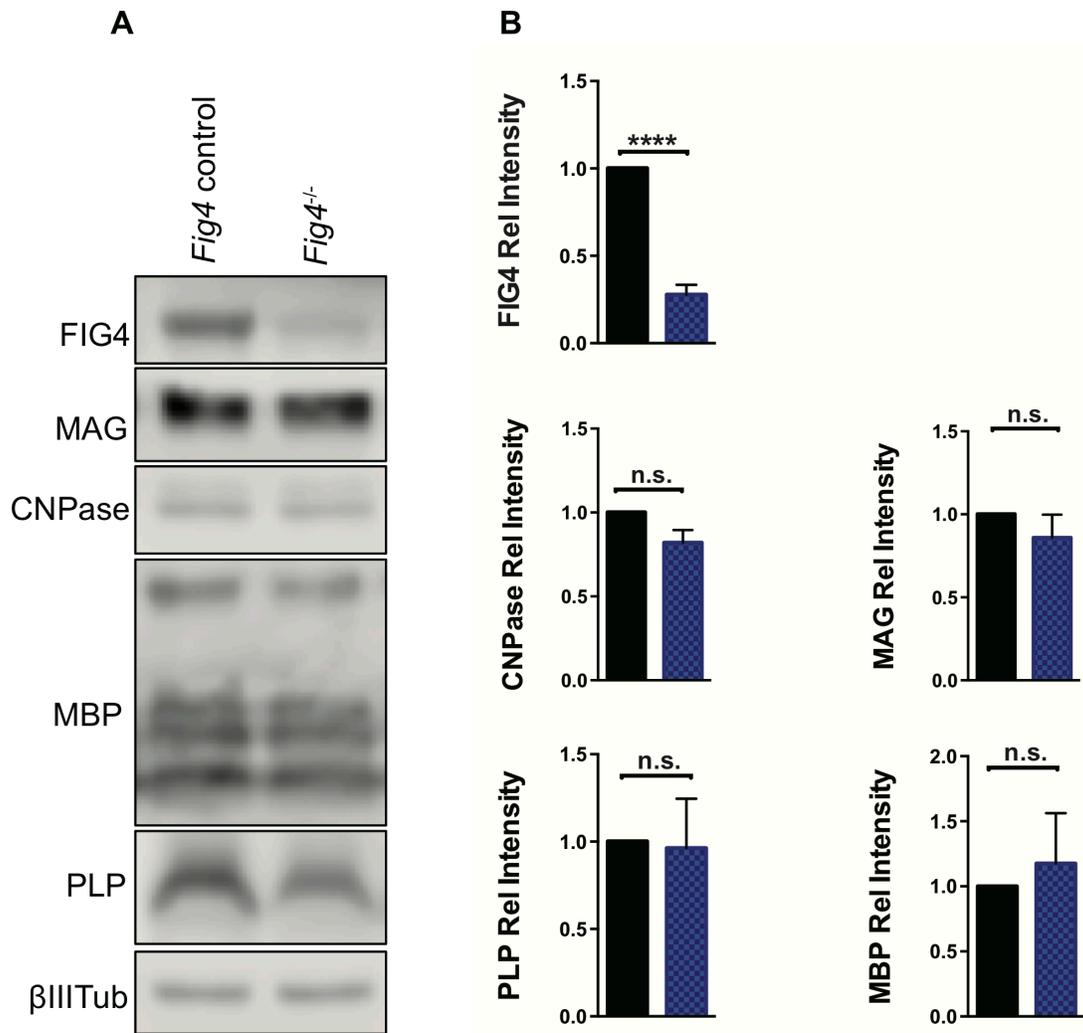
Figure 3.9 Myelin protein abundance is not affected by adult inducible _Fig4_ deletion after 60 days. **(A)** Representative Western blots of P120-150 brain membranes isolated from adult inducible _Fig4_ control and _Fig4$^{-/flox}$,CMVCreER_ animals at 60 dpi and probed with antibodies specific for FIG4 and myelin proteins MAG, CNPase, MBP, and PLP. Neuronal marker βIIItub was used as loading control. **(B)** Quantification of FIG4 and myelin protein signals is normalized to βIII Tub. Relative protein intensities compared to _Fig4_ control brains are shown as mean value ± SEM. N=4 brains each group. Unpaired Student _t_-test, ****p<0.0001.

Figure 3.10 Myelin protein abundance is not affected by juvenile inducible *Fig4* deletion after 53 days. Representative Western blots of P74 cerebellum/brainstem and cerebral cortex homogenates isolated from juvenile inducible *Fig4* control and *Fig4*⁻/flox,*CMVCreER* animals at 53 dpi and probed with antibodies specific for myelin proteins MAG and MBP. Neuronal marker βIIItub was used as loading control.

Figure 3.11 Optic nerve ultrastructure and function are not affected by adult inducible *Fig4* deletion after 60 days. (A-A') Representative TEM optic nerve cross section micrographs of P120 *Fig4* control and *Fig4^{-/flox,}CMVCreER* mice at 60 dpi. Scale bar = 1μm, n=4 animals/group. **(B-C)** Representative optic nerve CAP traces recorded from P1201-150 *Fig4* control and *Fig4^{-/flox},CMVCreER* mice at 60 dpi. **(D)** Quantification of conduction velocities and **(E)** amplitudes for each peak within CAP traces identified by Gaussian fit. Multiple unpaired student *t*-tests, n=5 nerves (*Fig4* control), n=6 nerves (*Fig4^{-/flox,}CMVCreER*). Mean ± SEM.
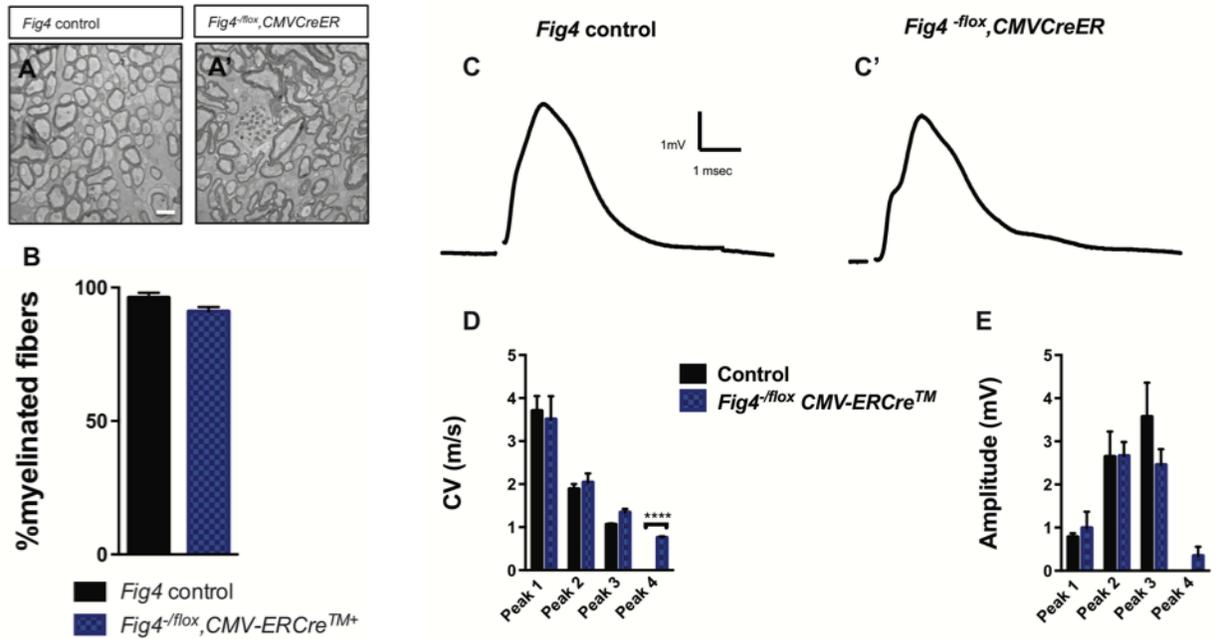
Figure 3.12 Optic nerve ultrastructure and function are not affected by global juvenile inducible *Fig4* deletion at 53 days. **(A-A')** Representative TEM optic nerve cross section micrographs of P74 *Fig4* control and *Fig4^-/flox,CMVCreER* mice at 53dpi. **(B)** Quantification of percentage of myelinated fibers in the optic nerves at P74 (53 dpi). Unpaired Student *t*-test, n=2 animals/group. Scale bar = 1 μm. **(C-C')** Representative optic nerve CAP traces recorded from *Fig4* control and *Fig4^-/flox,CMVCreER* mice at 53 dpi. **(D)** Quantification of conduction velocities and **(E)** amplitudes for each peak within CAP traces identified via Gaussian fit. Multiple unpaired student *t*-tests, n=3 nerves (Fig4 control), n=5 nerves (*Fig4^-/flox,CMVCreER*) ****p<0.0001. Mean ± SEM.
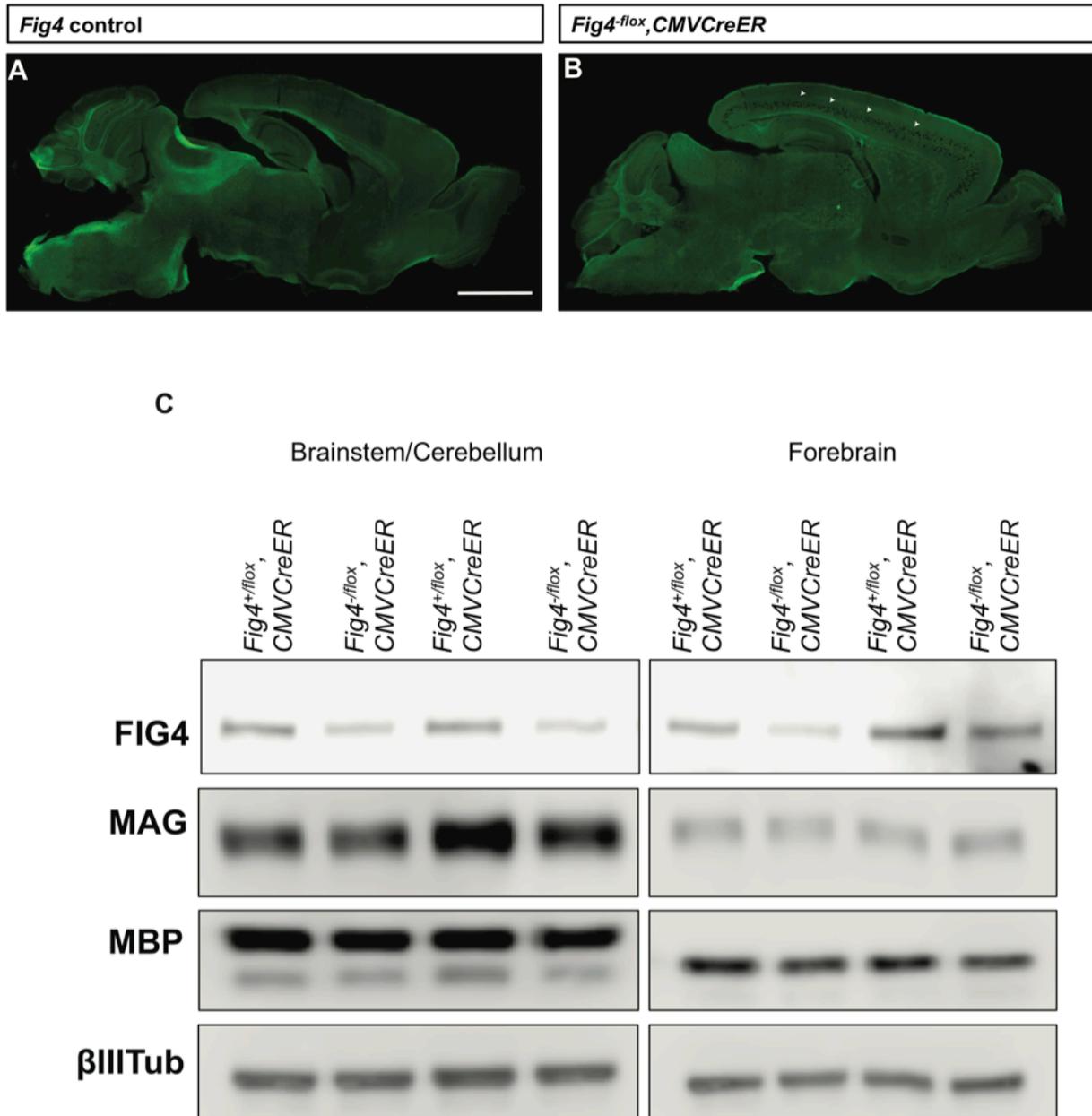
Figure 3.13 Hypomyelination and spongiform degeneration in neonatal inducible *Fig4⁻/flox*,*CMVCreER* mutants. (A-B) Representative sagittal brain sections of P22 *Fig4* control and *Fig4⁻/flox*,*CMVCreER* mice at 19 dpi stained with Fluoromyelin Green. Cortical spongiform degeneration in *Fig4⁻/flox*,*CMVCreER* knockout is indicated by arrowheads Scale bar = 200μm, n=2. **(C)** Western blots of cerebellum and forebrain homogenates isolated from P22 *Fig4* control and *Fig4⁻/flox*,*CMVCreER* mice at 19 dpi and probed with antibodies specific for FIG4 and myelin proteins MBP and MAG. βIII Tub is shown as a loading control. Each lane represents a different animal (n=2).
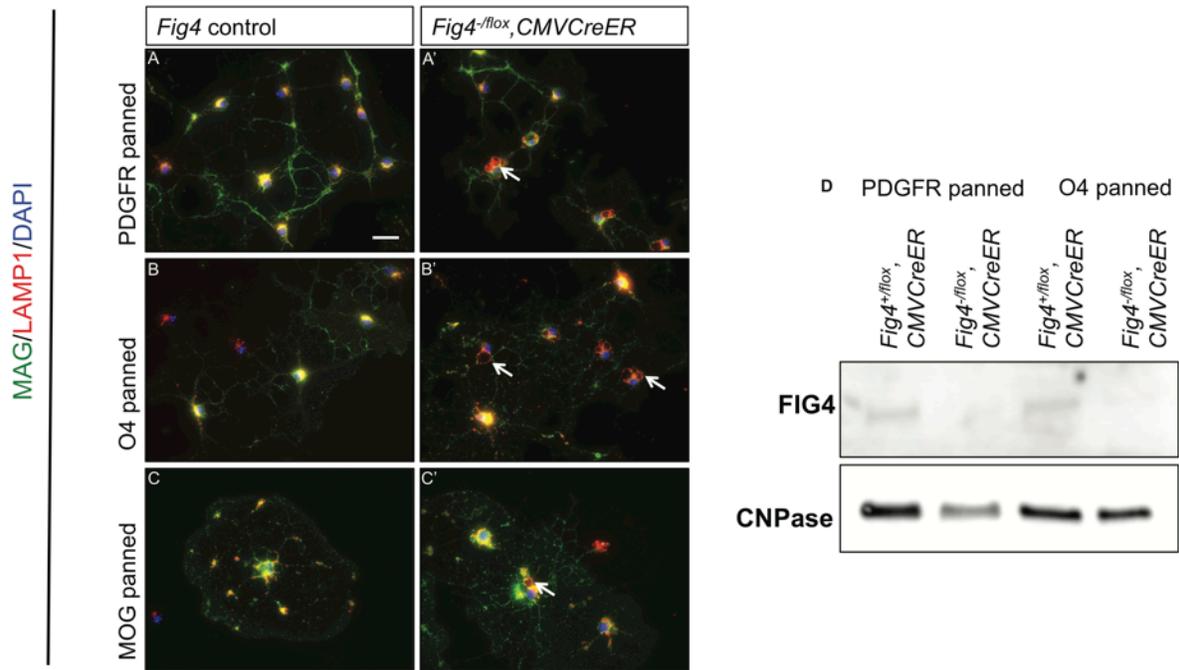
Figure 3.14 Abnormal endolysosomal trafficking in *Fig4^-/flox^,CMVCreER* OPCs/OLs. (A-C') Representative images of DIV4 *Fig4* control and *Fig4^-/flox^,CMVCreER* OLs isolated at the OPC (PDGFRα$^+$, **A-A'**), immature OL (O4$^+$, **B-B'**), and myelinating OL (MOG$^+$, **C-C'**) stages, stained with MAG and LAMP1. Enlarged LAMP1$^+$ structures in *Fig4^-/flox^,CMVCreER* are marked by arrows. **(D)** Western blots of DIV3 OPC/OL lysates probed with antibodies specific for FIG4 and CNPase. Scale bar = 20μm. N=1.
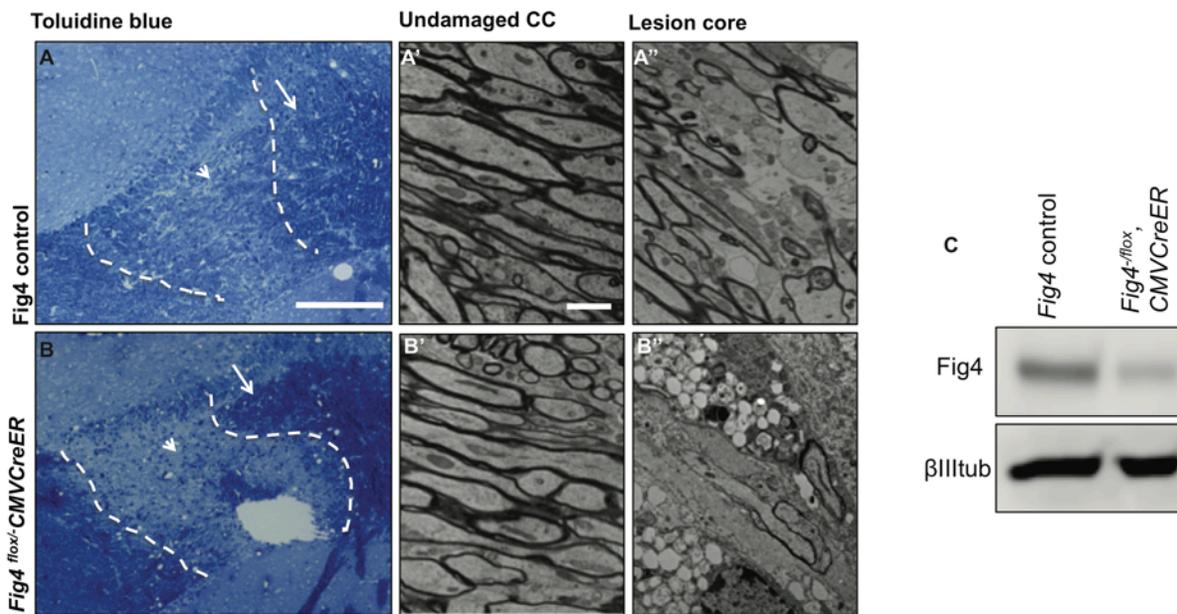
Figure 3.15 Adult inducible *Fig4* deletion thwarts myelin repair. (A-B) Representative coronal brain sections of P91 *Fig4* control and *Fig4$^{-/flox}$,CMVCreER* mice at 31 dpi, 21 days after LPC injection. Dashed line demarcates the lesion site in the corpus callosum. Arrowheads indicate the lesion core, arrows denote the intact corpus callosum. Scale bar = 200μm. **(A'-A")** TEM micrographs of the intact calossal myelin indicated by arrows in (**A** and **B**). *Fig4$^{-/flox}$,CMVCreER* TEM micrographs of the lesion core (arrowheads in **A** and **B**). Scale bar = 2μm. **(C)** Western blots of cerebellum homogenates isolated from P91 *Fig4* control and *Fig4$^{-/flox}$,CMVCreER* probed with antibodies specific for FIG4 and βIIITub. N=4.

3.9 References

Atanasoski S, Scherer SS, Sirkowski E, Leone D, Garratt AN, Birchmeier C, Suter U (2006) ErbB2 signaling in Schwann cells is mostly dispensable for maintenance of myelinated peripheral nerves and proliferation of adult Schwann cells after injury. J Neurosci 26:2124-2131.

Baulac S, Lenk GM, Dufresnois B, Ouled Amar Bencheikh B, Couarch P, Renard J, Larson PA, Ferguson CJ, Noe E, Poirier K, Hubans C, Ferreira S, Guerrini R, Ouazzani R, El Hachimi KH, Meisler MH, Leguern E (2014) Role of the phosphoinositide phosphatase FIG4 gene in familial epilepsy with polymicrogyria. Neurology 82:1068-1075.

Bergles DE, Richardson WD (2015) Oligodendrocyte Development and Plasticity. Cold Spring Harb Perspect Biol 8.

Brill MH, Waxman SG, Moore JW, Joyner RW (1977) Conduction velocity and spike configuration in myelinated fibres: computed dependence on internode distance. J Neurol Neurosurg Psychiatry 40:769-774.

Campeau PM, Lenk GM, Lu JT, Bae Y, Burrage L, Turnpenny P, Roman Corona-Rivera J, Morandi L, Mora M, Reutter H, Vulto-van Silfhout AT, Faivre L, Haan E, Gibbs RA, Meisler MH, Lee BH (2013) Yunis-Varon syndrome is caused by mutations in FIG4, encoding a phosphoinositide phosphatase. American journal of human genetics 92:781-791.

Carbajal KS, Mironova Y, Ulrich-Lewis JT, Kulkarni D, Grifka-Walk HM, Huber AK, Shrager P, Giger RJ, Segal BM (2015) Th Cell Diversity in Experimental Autoimmune Encephalomyelitis and Multiple Sclerosis. Journal of immunology 195:2552-2559.

Chen C, Westenbroek RE, Xu X, Edwards CA, Sorenson DR, Chen Y, McEwen DP, O'Malley HA, Bharucha V, Meadows LS, Knudsen GA, Vilaythong A, Noebels JL, Saunders TL, Scheuer T, Shrager P, Catterall WA, Isom LL (2004) Mice lacking sodium channel beta1 subunits display defects in neuronal excitability, sodium channel expression, and nodal architecture. J Neurosci 24:4030-4042.

Chow CY, Zhang Y, Dowling JJ, Jin N, Adamska M, Shiga K, Szigeti K, Shy ME, Li J, Zhang X, Lupski JR, Weisman LS, Meisler MH (2007) Mutation of FIG4 causes neurodegeneration in the pale tremor mouse and patients with CMT4J. Nature 448:68-72.

Crawford AH, Tripathi RB, Foerster S, McKenzie I, Kougioumtzidou E, Grist M, Richardson WD, Franklin RJ (2016a) Pre-Existing Mature Oligodendrocytes Do Not Contribute to Remyelination following Toxin-Induced Spinal Cord Demyelination. Am J Pathol 186:511-516.

Crawford Abbe H, Tripathi Richa B, Richardson William D, Franklin Robin JM (2016b) Developmental Origin of Oligodendrocyte Lineage Cells Determines Response to Demyelination and Susceptibility to Age-Associated Functional Decline. Cell Reports 15:761-773.

Ferguson CJ, Lenk GM, Jones JM, Grant AE, Winters JJ, Dowling JJ, Giger RJ, Meisler MH (2012a) Neuronal expression of Fig4 is both necessary and sufficient to prevent spongiform neurodegeneration. Hum Mol Genet 21:3525-3534.

Ferguson CJ, Lenk GM, Jones JM, Grant AE, Winters JJ, Dowling JJ, Giger RJ, Meisler MH (2012b) Neuronal expression of Fig4 is necessary and sufficient to prevent spongiform neurodegeneration. Hum Mol Genet.

Ferguson CJ, Lenk GM, Meisler MH (2009) Defective autophagy in neurons and astrocytes from mice deficient in PI(3,5)P2. Hum Mol Genet 18:4868-4878.

Ferguson CJ, Lenk GM, Meisler MH (2010) PtdIns(3,5)P2 and autophagy in mouse models of neurodegeneration. Autophagy 6:170-171.

Franklin RJ, Ffrench-Constant C (2008) Remyelination in the CNS: from biology to therapy. Nat Rev Neurosci 9:839-855.

Gautier HO, Evans KA, Volbracht K, James R, Sitnikov S, Lundgaard I, James F, Lao-Peregrin C, Reynolds R, Franklin RJ, Karadottir RT (2015) Neuronal activity regulates remyelination via glutamate signalling to oligodendrocyte progenitors. Nat Commun 6:8518.

Gregson NA, Hall SM (1973) A quantitative analysis of the effects of the intraneural injection of lysophosphatidyl choline. Journal of cell science 13:257-277.

Guo J, Ma YH, Yan Q, Wang L, Zeng YS, Wu JL, Li J (2012) Fig4 expression in the rodent nervous system and its potential role in preventing abnormal lysosomal accumulation. J Neuropathol Exp Neurol 71:28-39.

Hall S (2005) The response to injury in the peripheral nervous system. J Bone Joint Surg Br 87:1309-1319.

Hayashi S, McMahon AP (2002) Efficient recombination in diverse tissues by a tamoxifen-inducible form of Cre: a tool for temporally regulated gene activation/inactivation in the mouse. Dev Biol 244:305-318.

Hertz DL, Owzar K, Lessans S, Wing C, Jiang C, Kelly WK, Patel JN, Halabi S, Furukawa Y, Wheeler HE, Sibley A, Lassiter C, Weisman LS, Watson D, Krens SD, Mulkey F, Renn CL, Small EJ, Febbo PG, Shterev I, Kroetz D, Friedman PN, Mahoney JF, Carducci MA, Kelley MJ, Nakamura Y, Kubo M, Dorsey SG, Dolan ME, Morris MJ, Ratain MJ, McLeod HL (2016) Pharmacogenetic Discovery in CALGB (Alliance) 90401 and Mechanistic Validation of a VAC14 Polymorphism That Increases Risk of Docetaxel-Induced Neuropathy. Clin Cancer Res.

Hill RA, Patel KD, Goncalves CM, Grutzendler J, Nishiyama A (2014) Modulation of oligodendrocyte generation during a critical temporal window after NG2 cell division. Nat Neurosci 17:1518-1527.

Holtz AM, Griffiths SC, Davis SJ, Bishop B, Siebold C, Allen BL (2015) Secreted HHIP1 interacts with heparan sulfate and regulates Hedgehog ligand localization and function. The Journal of cell biology 209:739-757.

Ikonomov OC, Sbrissa D, Delvecchio K, Xie Y, Jin JP, Rappolee D, Shisheva A (2011) The phosphoinositide kinase PIKfyve is vital in early embryonic development: preimplantation lethality of PIKfyve-/- embryos but normality of PIKfyve+/- mice. J Biol Chem 286:13404-13413.

Jin N, Lang MJ, Weisman LS (2016) Phosphatidylinositol 3,5-bisphosphate: regulation of cellular events in space and time. Biochem Soc Trans 44:177-184.

Koenning M, Jackson S, Hay CM, Faux C, Kilpatrick TJ, Willingham M, Emery B (2012) Myelin gene regulatory factor is required for maintenance of myelin and mature oligodendrocyte identity in the adult CNS. J Neurosci 32:12528-12542.

Li JY, Popovic N, Brundin P (2005) The use of the R6 transgenic mouse models of Huntington's disease in attempts to develop novel therapeutic strategies. NeuroRx 2:447-464.

Liang CC, Tanabe LM, Jou S, Chi F, Dauer WT (2014) TorsinA hypofunction causes abnormal twisting movements and sensorimotor circuit neurodegeneration. J Clin Invest 124:3080-3092.

Lin CH, Tallaksen-Greene S, Chien WM, Cearley JA, Jackson WS, Crouse AB, Ren S, Li XJ, Albin RL, Detloff PJ (2001) Neurological abnormalities in a knock-in mouse model of Huntington's disease. Hum Mol Genet 10:137-144.

McCartney AJ, Zhang Y, Weisman LS (2014) Phosphatidylinositol 3,5-bisphosphate: low abundance, high significance. BioEssays : news and reviews in molecular, cellular and developmental biology 36:52-64.

McGoldrick P, Joyce PI, Fisher EM, Greensmith L (2013) Rodent models of amyotrophic lateral sclerosis. Biochimica et biophysica acta 1832:1421-1436.

Mirantes C, Eritja N, Dosil MA, Santacana M, Pallares J, Gatius S, Bergada L, Maiques O, Matias-Guiu X, Dolcet X (2013) An inducible knockout mouse to model the cell-autonomous role of PTEN in initiating endometrial, prostate and thyroid neoplasias. Dis Model Mech 6:710-720.

Nave KA, Trapp BD (2008) Axon-glial signaling and the glial support of axon function. Annual review of neuroscience 31:535-561.

Nicholson G, Lenk GM, Reddel SW, Grant AE, Towne CF, Ferguson CJ, Simpson E, Scheuerle A, Yasick M, Hoffman S, Blouin R, Brandt C, Coppola G, Biesecker LG, Batish SD, Meisler MH (2011) Distinctive genetic and clinical features of CMT4J: a severe neuropathy caused by mutations in the PI(3,5)P(2) phosphatase FIG4. Brain : a journal of neurology 134:1959-1971.

Pappas SS, Darr K, Holley SM, Cepeda C, Mabrouk OS, Wong JM, LeWitt TM, Paudel R, Houlden H, Kennedy RT, Levine MS, Dauer WT (2015) Forebrain deletion of the dystonia protein torsinA causes dystonic-like movements and loss of striatal cholinergic neurons. eLife 4:e08352.

Pappas SS, Leventhal DK, Albin RL, Dauer WT (2014) Mouse models of neurodevelopmental disease of the basal ganglia and associated circuits. Curr Top Dev Biol 109:97-169.

Reifler A, Lenk GM, Li X, Groom L, Brooks SV, Wilson D, Bowerson M, Dirksen RT, Meisler MH, Dowling JJ (2013) Murine Fig4 is dispensable for muscle development but required for muscle function. Skelet Muscle 3:21.

Savas JN, Toyama BH, Xu T, Yates JR, 3rd, Hetzer MW (2012) Extremely long-lived nuclear pore proteins in the rat brain. Science 335:942.

Soriano P (1999) Generalized lacZ expression with the ROSA26 Cre reporter strain. Nat Genet 21:70-71.

Stassart RM, Fledrich R, Velanac V, Brinkmann BG, Schwab MH, Meijer D, Sereda MW, Nave KA (2013) A role for Schwann cell-derived neuregulin-1 in remyelination. Nat Neurosci 16:48-54.

Tyler WA, Gangoli N, Gokina P, Kim HA, Covey M, Levison SW, Wood TL (2009) Activation of the mammalian target of rapamycin (mTOR) is essential for oligodendrocyte differentiation. J Neurosci 29:6367-6378.

Vaccari I, Carbone A, Previtali SC, Mironova YA, Alberizzi V, Noseda R, Rivellini C, Bianchi F, Del Carro U, D'Antonio M, Lenk GM, Wrabetz L, Giger RJ, Meisler MH, Bolino A (2015) Loss of Fig4 in both Schwann cells and motor neurons contributes to CMT4J neuropathy. Hum Mol Genet 24:383-396.

Weisheit CE, Dauer WT (2015) A novel conditional knock-in approach defines molecular and circuit effects of the DYT1 dystonia mutation. Hum Mol Genet 24:6459-6472.

Winters JJ, Ferguson CJ, Lenk GM, Giger-Mateeva VI, Shrager P, Meisler MH, Giger RJ (2011) Congenital CNS hypomyelination in the Fig4 null mouse is rescued by neuronal expression of the PI(3,5)P(2) phosphatase Fig4. J Neurosci 31:17736-17751.

Woodhoo A, Sommer L (2008) Development of the Schwann cell lineage: from the neural crest to the myelinated nerve. Glia 56:1481-1490.

Zhang X, Chow CY, Sahenk Z, Shy ME, Meisler MH, Li J (2008) Mutation of FIG4 causes a rapidly progressive, asymmetric neuronal degeneration. Brain : a journal of neurology 131:1990-2001.

Zhang Y, Zolov SN, Chow CY, Slutsky SG, Richardson SC, Piper RC, Yang B, Nau JJ, Westrick RJ, Morrison SJ, Meisler MH, Weisman LS (2007) Loss of Vac14, a regulator of the signaling lipid phosphatidylinositol 3,5-bisphosphate, results in neurodegeneration in mice. Proc Natl Acad Sci U S A 104:17518-17523.

Zou Y, Jiang W, Wang J, Li Z, Zhang J, Bu J, Zou J, Zhou L, Yu S, Cui Y, Yang W, Luo L, Lu QR, Liu Y, Chen M, Worley PF, Xiao B (2014) Oligodendrocyte precursor cell-intrinsic effect of Rheb1 controls differentiation and mediates mTORC1-dependent myelination in brain. J Neurosci 34:15764-15778.

Zuchero JB, Fu MM, Sloan SA, Ibrahim A, Olson A, Zaremba A, Dugas JC, Wienbar S, Caprariello AV, Kantor C, Leonoudakis D, Lariosa-Willingham K, Kronenberg G, Gertz K, Soderling SH, Miller RH, Barres BA (2015) CNS myelin wrapping is driven by actin disassembly. Developmental cell 34:152-167.

Chapter IV:

Discussion and Future Directions

4.1 Abstract

Overall, the work presented in this dissertation provides novel insights into the role of intracellular membrane trafficking in the OL lineage and how defects in the LE/lys compartment influence myelin formation, stability, and repair. Furthermore, this research suggests a differential demand for properly functioning intracellular trafficking in the adult central vs. peripheral nervous systems. Specifically, this thesis work contributes the following to our general knowledge on vesicular trafficking and myelination: 1) the $PI(3,5)P_2$ biosynthetic complex is a critical regulator of myelination that functions intrinsically and extrinsically; 2) $PI(3,5)P_2$ biosynthesis is essential for terminal differentiation of the OL lineage in the CNS; 3) $PI(3,5)P_2$ biosynthetic complex is necessary for intracellular trafficking of myelin building blocks; 4) $PI(3,5)P_2$ phosphatase FIG4 is necessary for adult mammalian organism homeostasis and stability of PNS myelinated fibers; 5) FIG4 is dispensable for CNS myelin stability for at least 2 months , but 6) FIG4 is likely necessary for CNS myelin repair. Here I discuss these findings in the context of other known $PI(3,5)P_2$ molecular functions and propose future experiments to further elucidate the role of intracellular trafficking in myelination.

4.2 How can impaired trafficking interfere with myelination?

Differential demand for PI(3,5)P$_2$ biosynthesis during OL maturation

We have demonstrated that impaired PI(3,5)P$_2$ biosynthesis results in abnormal accumulation of LE/Lys material in cultured OPCs/OLs. However, there were distinct differences in vesicle accumulation depending on the severity of PI(3,5)P$_2$ biosynthesis impairment and the OL developmental stage. We showed that at the OPC stage enlarged vacuoles are rarely present in *Fig4$^{-/-}$* cultured cells. In contrast, as OLs undergo differentiation and arborization, abnormally enlarged LAMP1$^+$ vacuoles accumulate perinuclearly. Time-lapse imaging indicates that enlarged vacuoles in *Fig4$^{-/-}$* OLs are dynamic, with some disappearing and reappearing within hours. It is therefore possible that all *Fig4$^{-/-}$* cells have increased vacuolation at a certain point of their lifespan. Staining mature (DIV6 under differentiative conditions) OL *Fig4$^{-/-}$* cultures reveals that cells with abnormally enlarged LAMP1$^+$ vesicles have impaired terminal maturation, as indicated by incomplete actin disassembly and reduced MOG$^+$ and MBP$^+$ expansion. However, there are many "escaper" cells with normal LE/Lys compartment and fully formed membrane sheet. Interestingly, the overall severity of terminal differentiation impairment in cultured OPCs/OLs is markedly milder than what is observed *in vivo*. *In vitro*, *Fig4$^{-/-}$* OLs demonstrate an approximately 30% decrease in the number of MAG$^+$ and MBP$^+$ mature OLs, whereas *in vivo* there is an almost 3-fold decrease in the density of *Plp1* and *Mag* OLs in the optic nerve. One explanation is that in the *in vitro* setting, cells are supplied with excessive amounts of reagents necessary for survival and differentiation (insulin, growth factors, serum) which *Fig4$^{-/-}$* OPCs/OL *in vivo* may otherwise not have access to or incapable of metabolizing in their microenvironment. Another explanation could be that *in vivo* the OL lineage receives

additional prohibitive cues from other cells (neurons, astrocytes, microglia) that render differentiation less likely. A third explanation suggests differential vulnerability of spatially distinct OPC populations to impaired PI(3,5)P$_2$ homeostasis. For *in vitro* cultures, OPCs/OLs are isolated from the entire brain, and therefore our observations may be biased by clonal division of OPC populations less susceptible to impaired PI(3,5)P$_2$ biosynthesis. For example, it's been shown that white matter NG2 glia are more responsive to PDGF than their gray matter counterparts (Hill et al., 2013). Isolating *Fig4$^{-/-}$* OPCs from various brain regions and culturing them separately will allow establishing any region-specific vulnerability in the OL lineage.

In marked contrast, *Pikfyve*-deficient OPCs are vacuolated at every stage of their development *in vitro*. The phenotype is so severe that vacuoles can be easily identified in *Pikfyve$^{flox/flox}$,Olig2Cre* mice semi-thin optic nerve preparations. Unlike *Fig4$^{-/-}$* and *Fig4$^{-/flox,}$Olig2Cre* mice that develop some CNS myelin, *Pikfyve*-deficient animals demonstrate a virtual absence of terminally differentiated OLs and white matter. Taking these observations together, it is possible to speculate that as the OL lineage cell undergoes expansive membrane trafficking, its demand for PI(3,5)P$_2$ biosynthesis increases. In case of *Fig4$^{-/-}$* OPCs/OLs, PI(3,5)P$_2$ levels would presumably be 50% of normal values, based on measurement in fibroblasts (Chow et al., 2007, (Zolov et al., 2012). It is possible that the remaining PI(3,5)P$_2$ is sufficient for normal OPC proliferation, however, it permits only limited differentiation and myelination. *Pikfyve*-deficient OPCs presumably would have no PI(3,5)P$_2$ at all, and thus their proliferation is impaired and differentiation is completely impossible, resulting in no myelin. It is worth noting that PIKFYVE is also responsible for all of the PI5P pool, which may have an additional contribution to hypomyelination phenotype (Zolov et al., 2012). It would be of great interest to monitor dynamic changes of PI(3,5)P$_2$ levels in the OL lineage as it undergoes

maturation (Figure 4.1). Inositol labeling and PIP measurement are technically challenging, but they have been was performed successfully in cultured hippocampal neurons (McCartney et al., 2014). Given that OPC cultures can be expanded *in vitro*, acquiring a sufficient amount of cellular material is technically possible. Dong et al. and Li et al. identified TRPML1 channel as the direct binding partner of PI(3,5)P_2 and employed its N-terminus as a fluorescently tagged biosensor for monitoring PI(3,5)P_2 localization and activity (Dong et al., 2010, Li et al., 2013). Using this tool in OPCs/OLs *in vitro* would gain additional insights into PI(3,5)P_2 dynamics, although introducing foreign DNA to OPCs/OLs has its technical limitations (see Appendix for more details).

Monitoring PI(3,5)P$_2$-deficient OL dynamics ex vivo

As discussed in Chapter I, significant progress was made in monitoring myelin dynamics in a living adult brain. These studies are beginning to fill critical knowledge gaps in our understanding of myelin formation and remodeling. Early postnatal studies in organotypic slice cultures revealed that the majority of cortical OPCs differentiate into myelinating OLs (Hill et al., 2014b) during a critical early postnatal period P3-P8. Myelin observations in the adult CNS revealed limited turnover of myelinating oligodendrocytes and high motility and homeostatic self-repulsion of the progenitor population (Hughes et al., 2013, Schain et al., 2014). Now that the tools are in place, it would be of great scientific interest to apply these imaging paradigms towards more mechanistic inquiries. We established that reduced PI(3,5)P_2 biosynthesis results in impaired OPC differentiation. Temporal *in vivo* dynamics of *Fig4* and *Pikfyve*-deficient OL lineage have not been examined. Immature CNPase$^+$, O4$^+$, MOG$^-$, MBP$^-$ premyelinating OLs are considered a short-lived population that does not exist *in vivo* unless it commits to ensheathing

axons. Therefore, it is possible that either $Fig4^{-/-}$ OPCs do not differentiate at all, or they die off in a caspase-3 independent manner (Winters et al., 2011). *Ex vivo* organotypic slice cortical preparations from *Fig4* mutants crossed with OL reporter mice (*Fig4$^{-/flox}$,Olig2Cre, LacZ/EGFP* or *Fig4$^{-/flox}$,PdgfrαCreER, LacZ/EGFP*) can reveal the $Fig4^{-/-}$ OL lineage dynamics during the critical postnatal OPC differentiation/myelination period. This experimental set up would also permit additional pharmacological and genetic manipulations of the OL lineage in its natural habitat to further dissect mechanistic aspects of intracellular trafficking in myelination (Hill et al., 2014a) (Figure 4.2). Ideally, monitoring *Fig4*-deficient OL dynamics in a living brain would be most physiologically relevant, but this approach requires sophisticated imaging.

PI(3,5)P₂ regulates trafficking of myelin building blocks

Reduced levels of PI(3,5)P$_2$ have profound effects on the endolysosomal axis in all eukaryotic cells. We have demonstrated that in *Fig4* and *Pikfyve*-deficient OLs trafficking of some myelin blocks is impaired. It would be of interest to examine whether impaired myelin trafficking is associated with disruption of the protein network that oversees organelle identity and cargo delivery. In polarized cells, apical trafficking of transport vesicles and fusion with the plasma membrane is mediated by the soluble N-ethylmaleimide-sensitive factor attachment protein receptor (SNARE) complex which comprises vesicular (v)-SNARE such as vesicle-associated membrane proteins (VAMPs) and target (t)-SNARE such as syntaxins (Jahn and Scheller, 2006, Sudhof and Rothman, 2009). Apical and basolateral-destined vesicles harbor different v-SNAREs and fuse with different t-SNAREs localized to the apical (syntaxin-3) or basolateral (syntaxin-4) plasma membrane (Masaki, 2012). Regulation of SNAREs is achieved, at least in part, through Rab GTPase family members (Schardt et al., 2009). Interestingly, in

162

myelinating OLs PLP insertion into the myelin sheath is t-SNARE (SNAP29)-dependent (Schardt et al., 2009). *In vitro*, at least two SNARE-dependent trafficking pathways participate in surface expression of PLP, a VAMP-3 dependent pathway from recycling endosomes to the PM and a VAMP-7 dependent pathway that regulates exocytosis of LE/Lys delivered cargo to the developing myelin sheath (Feldmann et al., 2011). Loss of the adaptor protein AP-3δ in *mocha* mice results in mislocalization of VAMP7 (Martinez-Arca et al., 2003, Kent et al., 2012). *Mocha* mice suffer from impaired secretion of lysosome-related organelles, and exhibit mild CNS dysmyelination, neurodegeneration, seizures, and altered fur pigmentation (Kantheti et al., 1998, Danglot and Galli, 2007, Feldmann et al., 2011), phenotypes that are reminiscent of, but less severe than, those in *Fig4* global mutants (Chow et al., 2007, Winters et al., 2011).

Does PI(3,5)P$_2$ participate in mTOR-mediated myelination?

Myelination is an energetically costly process, and proper function of signaling pathways regulating nutrient sensing, growth, and survival are critical in the OL lineage at all stages. For example, insulin signaling is essential for OPC survival (Barres et al., 1993). PI3K/mTOR signaling is necessary for white matter NG2 glia proliferation in response to PDGF (Hill et al., 2013). Inhibition of mTOR with rapamycin *in vitro* significantly decreases the number of O4$^+$ OLs, thus suggesting the importance of the mTOR signaling in early OL differentiation (Tyler et al., 2009). Inhibiting mTOR signaling *in vitro* decreases transcription of myelin-associated genes *Mbp* and *Plp*. In particular, mTORC2 serves to reduce inhibition of myelin-associated genes by repressing the transcriptional activity of negative myelination regulators Id2, Id4, and Tc4 (Chen et al., 2012). Furthermore, the mTORC1 downstream targets, such as 4E-BP1 may also be regulating expression of myelin-associated genes (Tyler et al., 2009). Interestingly, rapamycin

does not have a significant effect on OLs when added to mature cultures (DIV3 and DIV5), potentially indicating reduced demand for active mTOR signaling when the myelin sheath is already established. The reports on the role of mTORC signaling in myelination *in vivo* are somewhat variable. In general, studies agree on the importance of mTORC signaling for OPC terminal differentiation and myelination, however there are some spatial and temporal discrepancies in the evidence presented by different groups. For example, conditional deletion of the mTORC1 effector *Raptor* in the OL lineage was shown to cause significant downregulation of select myelin-associated genes and hypomyelination in the spinal cord, but only limited defects in the corpus callosum (Bercury et al., 2014). *Rictor* deletion leads to small and transient changes in myelination. Conditional ablation of the mTORC1 activating GTPase *Rheb1* results in impaired OPC differentiation in the brain, but is dispensable for myelin maintenance (Zou et al., 2014). Intriguingly, conditional OL lineage-specific deletion of the mTOR negative regulator *Tsc1* also impairs myelination, suggesting that mTOR levels have to be precisely calibrated for proper OL differentiation and myelination (Lebrun-Julien et al 2014).

$PI(3,5)P_2$ is an important regulator of mTORC1 (Bridges et al., 2012, Jin et al., 2014, Jin et al., 2016). $PI(3,5)P_2$ binds the mTORC1 adaptor protein Raptor and recruits it to the lysosomal membrane (Bridges et al., 2012, Jin et al., 2014). Furthermore, $PI(3,5)P_2$ indirectly regulates mTROC1 activity through binding and recruitment of its downstream target S6 kinase (Bridges et al., 2012). The $PI(3,5)P_2$–mTORC1 interaction negatively regulates autophagy (Bridges et al., 2012). As mTORC1 downstream targets induce transcriptional activation, it would be interesting to test whether mTORC misregulation in the absence of $PI(3,5)P_2$ results in impaired expression of myelin-associated genes. Furthermore, mTORC regulates local mRNA synthesis in neurons (Takei et al., 2004). It has not been tested directly, but it is possible that mTORC may be

playing a role in local *Mbp* mRNA translation. Thus far, there is no direct evidence that constitutive loss of *Fig4* results in altered mTORC signaling in the nervous system (Ferguson et al., 2009). In cultured OPCs, S6 is robustly phosphorylated in *Fig4^{-/-}* OPCs/OLs, and rapamycin treatment impairs their differentiation similar to control cultures (Mironova et al., unpublished observations). However, standard OPC culture conditions require insulin supplement, thus possibly saturating basal mTORC signaling for immunocytochemical observations. Furthermore, constitutive *Fig4* deletion in germline or conditional mutants may result in compensatory mechanisms that distort an accurate readout of the mTOR activity during CNS myelination. Optimization of cultured conditions combined with acute manipulation of PI(3,5)P$_2$ biosynthesis in the OL via PIKFYVE inhibition or siRNA knockdown would be a feasible approach for assessing mTORC signaling with reduced PI(3,5)P$_2$ levels.

Lysosomal gene network in the OL lineage

Lysosomal gene network (Coordinated Lysosomal Expression and Regulation or CLEAR) is mediated by the master regulator transcription factor EB (TFEB). The discovery of both CLEAR and TFEB identified the endolysosomal compartment as an important hub of gene regulation in response to cellular energy changes (Sardiello et al., 2009, Settembre et al., 2011). Transgenic or viral *Tfeb* overexpression has been shown to successfully abate pathological processes associated with impaired lysosomal clearance and autophagy (Medina et al., 2011). TFEB is now tested extensively as a potential therapeutic target in many lysosomal storage disease (LSD) mouse models, such as Huntington's disease, Alzheimer's disease, and non-neuronal LSDs (Spampanato et al., 2013, Polito et al., 2014, Martini-Stoica et al., 2016). TFEB phosphorylation and transcriptional activity are directly regulated by mTOR, thus ensuring a

tight feedback between lysosomal and autophagy gene networks and altered energy states in the cell (Settembre et al., 2012). Interestingly, the PI(3,5)P$_2$ biosynthetic complex scaffold *Vac14* gene expression is up-regulated in response to *Tfeb* overexpression (Sardiello et al., 2009). Given its role as a regulator of mTOR at the lysosome, PI(3,5)P$_2$ may play a complex role in mediating mTORC-TFEB signaling. It would be of interest to examine whether any pathological changes in *Fig4*-deficient OL lineage could be traced back to impaired TFEB function and alterations in lysosomal network gene expression. RNA sequencing data on *Fig4$^{-/-}$* forebrain tissue and gene expression array on acutely isolated *Pikfyve*-deficient OPCs/OLs demonstrate profound transcriptional changes in the mutant groups compared to controls (Appendix A1). Notably, there are significant changes in the lysosomal pathway genes, severe downregulation of myelin-associated genes, and genes associated with chromatin structure. There is an exciting possibility that the lysosomal gene network may be involved in regulating myelin-specific gene expression, and our observations prime the field for potentially making this connection.

PI(3,5)P$_2$ and actin dynamics during myelination

Actin dynamics are essential for OPC differentiation and myelination. Specifically, actin nucleation factor Arp2/3 drives actin assembly critical for OPC differentiation and initiation of myelination. Conditional *Arp2/3* deletion in the OL lineage at the initiation of ensheathment stage results in profound CNS hypomyelination and aberrant myelin outfoldings. In contrast, Arp2/3 function is dispensable for myelin wrapping. Instead, MBP-dependent actin disassembly drives myelin sheath formation (Nawaz et al., 2015, Zuchero et al., 2015). MBP competes with actin disassembly factors gelsolin and cofilin for binding to PI(4,5)P$_2$ at the plasma membrane, thus leading to actin disassembly at the leading edge of myelinating OL. Actin-modifying factors

are also present at the endoslysosomal membrane and play an important role in actin dynamics (Girao et al., 2008). It is currently unknown whether endosomal actin dynamics are involved in myelin formation. Our *in vitro* experiments demonstrated that in *Fig4*$^{-/-}$ OLs, full actin disassembly is impaired (Chapter II). We employed characterization of actin morphology and MBP expansion as a tool for staging the OL terminal differentiation, however, there is a possibility that impaired actin disassembly in *Fig4*$^{-/-}$ OLs is not just a correlative observation. $PI(3,5)P_2$ recently has been shown to interact directly with the branched actin regulator contractin (Hong et al., 2015). $PI(3,5)P_2$ interaction with contractin promotes actin turnover at the endosomal membrane. Given the critical importance of properly timed actin assembly and disassembly in the OL lineage maturation and myelination, it is possible that disrupting net actin turnover via reduced levels of $PI(3,5)P_2$ may lead to impaired OL lineage dynamics. It would be intriguing to apply pharmacological modulators of actin assembly and disassembly to examine if they have any effect on differentiation in cultured *Fig4*$^{-/-}$ and *Pikfyve*-deficient OLs.

4.3 Can *Fig4*$^{-/-}$ OPCs become astrocytes?

One of the hallmarks of *Fig4*$^{-/-}$ CNS is reactive gliosis, with a prominent increase in the number of GFAP^{+} astrocytes. This observation may be accompanied by elevated autophagy in astrocytes themselves and their reactive response to neuronal degeneration, but the mechanisms of this phenomenon are not well understood (Chow et al., 2007, Ferguson et al., 2009). Neuron-specific *Fig4* overexpression rescues neurodegeneration and decreases reactive gliosis, suggesting a non-cell-autonomous *Fig4* effect on astrocyte dynamics (Ferguson et al., 2012). Intriguingly*, in vitro*, many *Pikfyve*-deficient OLs assume an astrocytic morphology and become robustly GFAP^{+} (Mironova et al., unpublished observations). Gene expression arrays of acutely

isolated *Pikfyve*-deficient OPCs/OLs and RNAseq of *Fig4*-deficient P10 forebrain tissue revealed significantly up-regulated *Gfap* gene expression (Appendix A1). It was previously thought that astrocyte and OL progenitors are fate-specified early in development and there is no possibility of switch between the two (Rowitch and Kriegstein, 2010). However, a recent study identified histone deacetylase 3 (HDAC3) as a critical regulator of fate switching between astrocytes and OPCs (Zhang et al., 2016). Conditional OL lineage *Hdac3* deletion results in severely impaired CNS myelination and a drastic decrease in the number of Olig2$^+$ cells. In contrast, there is a concomitant rise in the number of GFAP$^+$ and Aldh1l1$^+$ cells. Fate-mapping studies demonstrated that these ectopic astrocytes arise from OPCs (Zhang et al., 2016). HDAC3 acts as a suppressor of astrocyte-specific genes, and *Hdac*3 deletion leads to up-regulation of the pro-astrocytic Jak-Stat3 pathway. Given a significant decrease in the number of Olig2$^+$ cells and terminally differentiated OLs in *Fig4* and *Pikfyve*-deficient brains with no evidence of increased cell death, it may be interesting to examine whether OPCs with impaired PI(3,5)P$_2$ biosynthesis may commit to an astrocytic fate. Fate-mapping analysis employing conditional *Fig4* knockout + reporter strategy (*Fig4$^{-/flox}$,PdgfrαCreER,LacZ/EGFP*) combined with immunohistochemistry for OL and astrocytic markers is a feasible first step to addressing that hypothesis.

4.4 Does altered synaptic strength in PI(3,5)P$_2$-deficient neurons influence myelination?

Several studies indicate that impaired PI(3,5)P$_2$ homeostasis results in altered synaptic strength in glutamatergic neurons (Zhang et al., 2012, McCartney et al., 2014b). Specifically, PI(3,5)P$_2$ biosynthesis dynamically regulates AMPA endocytosis and increases presynaptic release probability. Increased PIKFYVE activity decreases synaptic depression in cultured hippocampal neurons. Conversely, loss of PI(3,5)P$_2$ inhibits chemical LTD, thus identifying it as

a negative regulator of synaptic strength (McCartney et al., 2014b). It is unknown whether these alterations of synaptic strength occur *in vivo* and in all neuronal populations with reduced PI(3,5)P$_2$. Intriguingly, *Mcoln1$^{-/-}$* mutants also present with CNS hypomyelination and enhanced long-term potentiation (LTP), providing an independent evidence for the importance of intracellular trafficking in mediating synaptic strength and myelination (Grishchuk et al., 2014). These observations are especially intriguing considering a direct molecular interaction between TRPML1 (Mcoln1) and PI(3,5)P$_2$ (Dong et al., 2010, Li et al., 2013). Any potential consequences of altered glutamatergic signaling in *Fig4* or *Vac14*-deficient CNS on myelination have not been addressed. The hypomyelination phenotype in *Fig4$^{-/flox}$,SynCre* mice and rescue thereof in *Fig4$^{-/-}$,NSE-Fig4* mutants suggest a possibility of neuronal FIG4 actively regulating CNS myelination. It is unknown whether impaired PI(3,5)P$_2$ biosynthesis alters electrophysiological properties of OPCs/OLs themselves. Given that glutamatergic signaling does alter OPC dynamics *in vivo* (Hughes and Appel, 2016), it may be of interest to examine the electrophysiological aspects of axoglial interaction in *Fig4*–deficient CNS. One approach is a heterogeneous neuron-OL co-culture, which permits pharmacological modulation of neuronal electrophysiological properties in the presence or absence of *Fig4*, *Pikfyve*, or *Vact14* in neurons and OLs (Lundgaard et al., 2013). Our first attempt at that approach is described in the Appendix. It is also possible to examine the OL-neuron dynamics in a more physiologically relevant context of the organotypic slice culture as described above. Excitingly, independently isolated OPCs can be injected into organotypic cerebellar slices *ex vivo*, thus generating a genetically heterologous system suitable for testing cell-autonomous aspects of myelination in greater detail (Najim et al 2013). A true "pie in the sky" experiment would be to employ optogenetics in *Fig4$^{-/-}$* deficient animals to examine whether repeated electrical stimulation in the

CNS can elicit enhanced OPC proliferation and increase myelin thickness (as described by (Gibson et al., 2014).

4.5 Why is the PNS more vulnerable to impaired PI(3,5)P$_2$ homeostasis?

We have demonstrated that within the same time period, myelinated PNS fibers show increased vulnerability to impaired PI(3,5)P$_2$ biosynthesis compared to the CNS when *Fig4* is globally ablated in adult mice. While the actual underlying mechanisms are yet to be established, our current knowledge of the CNS vs. PNS biology and PI(3,5)P$_2$ homeostasis allows us to make certain predictions. PI(3,5)P$_2$ regulates autophagy, and *Fig4$^{-/-}$* brains demonstrate increased levels of p62 and CL3-II, with defects in completion of basal autophagy (Ferguson et al., 2009, 2010). Neurons are highly vulnerable to impaired autophagy. Aggregation of misfolded proteins or aberrations in autophagy itself leads to formation of inclusion bodies, which are highly toxic to neurons. Thus far, no evidence of impaired autophagy was found in the *Fig4$^{-/-}$* OL lineage (Ferguson et al 2009, Mironova et al, unpublished observations). In contrast, Schwann cells employ autophagy for myelin debris clearance during axonal regeneration and myelin repair in the PNS (Gomez-Sanchez et al., 2015). *Fig4$^{-/flox}$,P0Cr*e sciatic nerves demonstrate elevated levels of p62, ubiquitin, and CL3-II, suggesting impaired autophagy (Vaccari et al., 2015). It is possible that in adult inducible *Fig$^{-/flox}$,CMVCreER* mice reduced PI(3,5)P$_2$ leads to endolysosomal trafficking defects in PNS neurons and Schwann cells, and failure of autophagic degradation of myelin perpetuates the phenotype. It will be important to examine whether *Fig4$^{-/flox}$,CMVCreER* sciatic nerves and isolated Schwann cells display defective autophagy. Attempting to pharmacologically enhance autophagy in *Fig4*-deficient Schwann cells may

alleviate some of the pathology associated with impaired PI(3,5)P$_2$ function in the adult PNS (Renna et al., 2010).

4.6 Is gene therapy feasible for correcting impaired PI(3,5)P$_2$ biosynthesis?

Previous studies demonstrated that transgenic *Fig4* overexpression rescues neurodegeneration, hypomyelinaton, and reduced lifespan in *Fig4*$^{-/-}$ mice (Winters et al., 2011, Ferguson et al., 2012b). The *NSE* promoter is first expressed at E12.5 (Forss-Petter et al., 1990), therefore rescue of *Fig4*-associated pathologies in transgenic mice can be embryonic, postnatal, or both. Interestingly, multiple *in vitro* experiments demonstrated that transfecting *WT-Fig4* in *Fig4*$^{-/-}$ fibroblasts and neurons can rescue their vacuolation phenotype, suggesting corrected endolysosomal trafficking in postnatally isolated populations (Lenk et al., 2011, Campeau et al., 2013, Lenk et al., 2016a). It is not clear, however, whether LE/Lys clearance actually leads to functional improvements. We have demonstrated that adult inducible *Fig4* deletion causes rapid and devastating defects in mice including reduced survival, strongly suggesting the importance of FIG4 and PI(3,5)P$_2$ for normal physiology (Chapter III). A reverse experiment of introducing *Fig4* postnatally to *Fig4*-deficient mice at different ages has not been done, but is of great importance. *Fig4* viral delivery to the neural tissue is a potentially more clinically relevant approach than a transgenic *Fig4* knock-in. For example, it would be intriguing to assess whether adenoviral *Fig4* delivery to retinal ganglion cells (RGCs) can non-cell-autonomously rescue optic nerve hypomyelination observed in *Fig4* germline or conditional mutants. Furthermore, given the extreme vulnerability of DRGs to FIG4 loss of function at all developmental and postnatal stages, it would be exciting to examine whether overexpressing *Fig4* in that cell

population would lead to lysosomal clearance, regeneration and remyelination of peripheral fibers, and restoration of functional deficits.

4.7 Concluding remarks

Myelin constitutes up to 50% of adult human brain, and increased white matter volume is evolutionarily correlated with cognitive superiority of higher vertebrates. Significant progress has been made in studying myelin formation, maintenance, and repair, but many questions remain unanswered. Our contribution to the field of myelin biology is identifying the low abundant, but highly significant phosphoinositide $PI(3,5)P_2$, as a critical regulator of myelin dynamics. In particular, the characterization of cultured OPCs from $PI(3,5)P_2$-deficient mice has provided new insight into the role of $PI(3,5)P_2$ in myelin biosynthesis. Revealing the precise mechanisms of $PI(3,5)P_2$ –mediated axoglial interaction is of great interest, as it will provide additional insights into neuropathology of myelin and neurodegenerative disorders.

4.8 Author contributions

The *PI(3,5)P₂ regulates trafficking of myelin building blocks* paragraph was written together with Roman J. Giger.

WT OL lineage (100% PI(3,5)P$_2$)

Fig4$^{-/-}$ OL lineage (50% PI(3,5)P$_2$)

Pikfyve$^{-/-}$ OL lineage (0% PI(3,5)P$_2$)

PI(3,5)P$_2$ Turnover demand
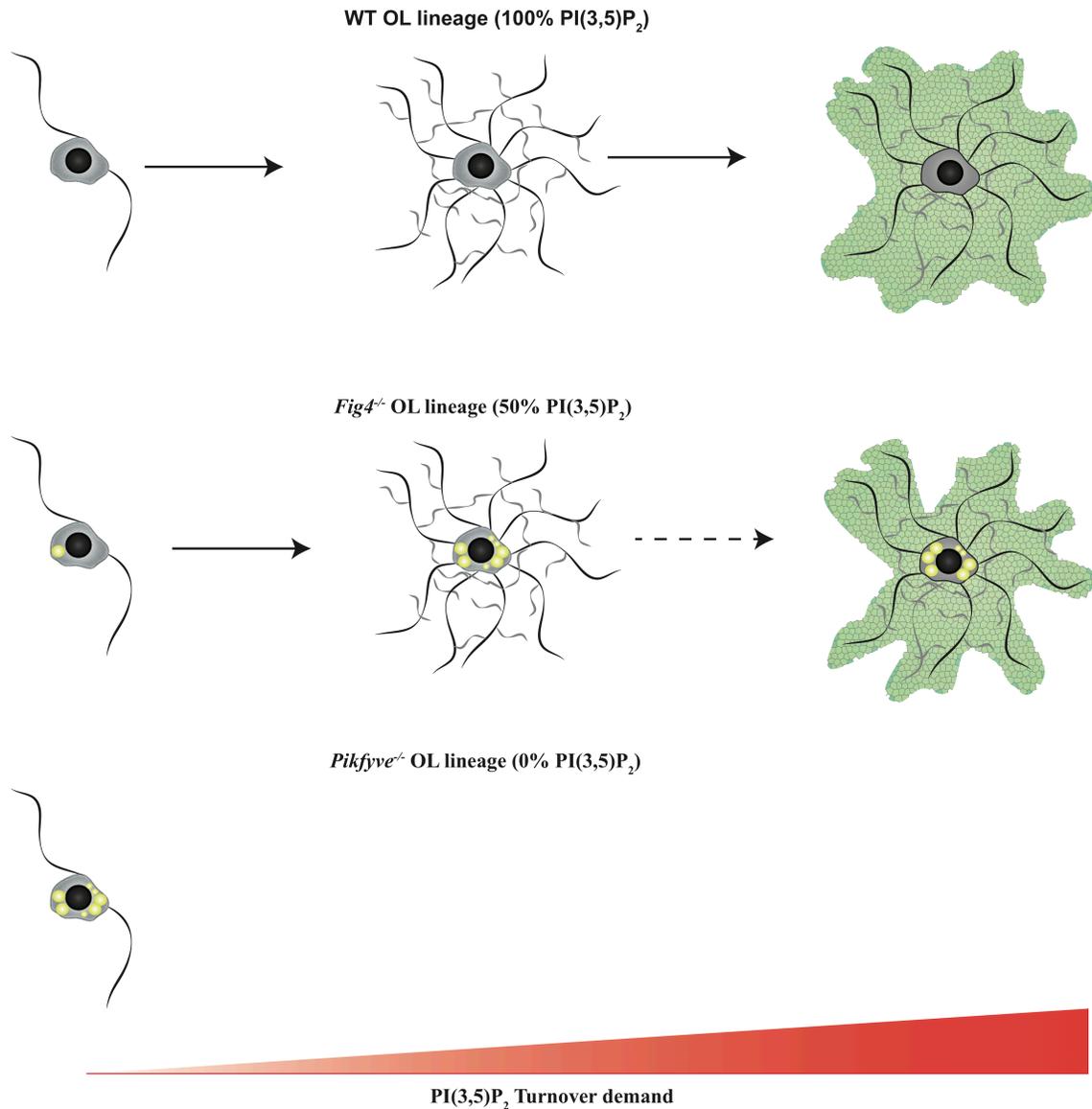
Figure 4.1 Correlation between PI(3,5)P$_2$ levels and OL dynamics. OPC differentiation and maturation requires extensive membrane expansion and trafficking of myelin building blocks. Theoretically, as the OL matures and generates myelin, its demand for properly functioning PI(3,5)P$_2$ would increase. In *Fig4$^{-/-}$* OPCs, PI(3,5)P$_2$ levels are presumably reduced to 50% of the WT value. At the OPC stage, even reduced PI(3,5)P$_2$ may be sufficient for normal OL lineage proliferation. As a *Fig4$^{-/-}$* OPC/OL undergoes differentiation and begins generating myelin sheath, its supply of PI(3,5)P$_2$ is no longer adequate to its demand, thus resulting in impaired differentiation and hypomyelination. In *Pikfyve*-deficient OPCs, there is no PI(3,5)P$_2$, and therefore even at the precursor stage OPCs have impaired proliferation and are completely incapable of differentiation.
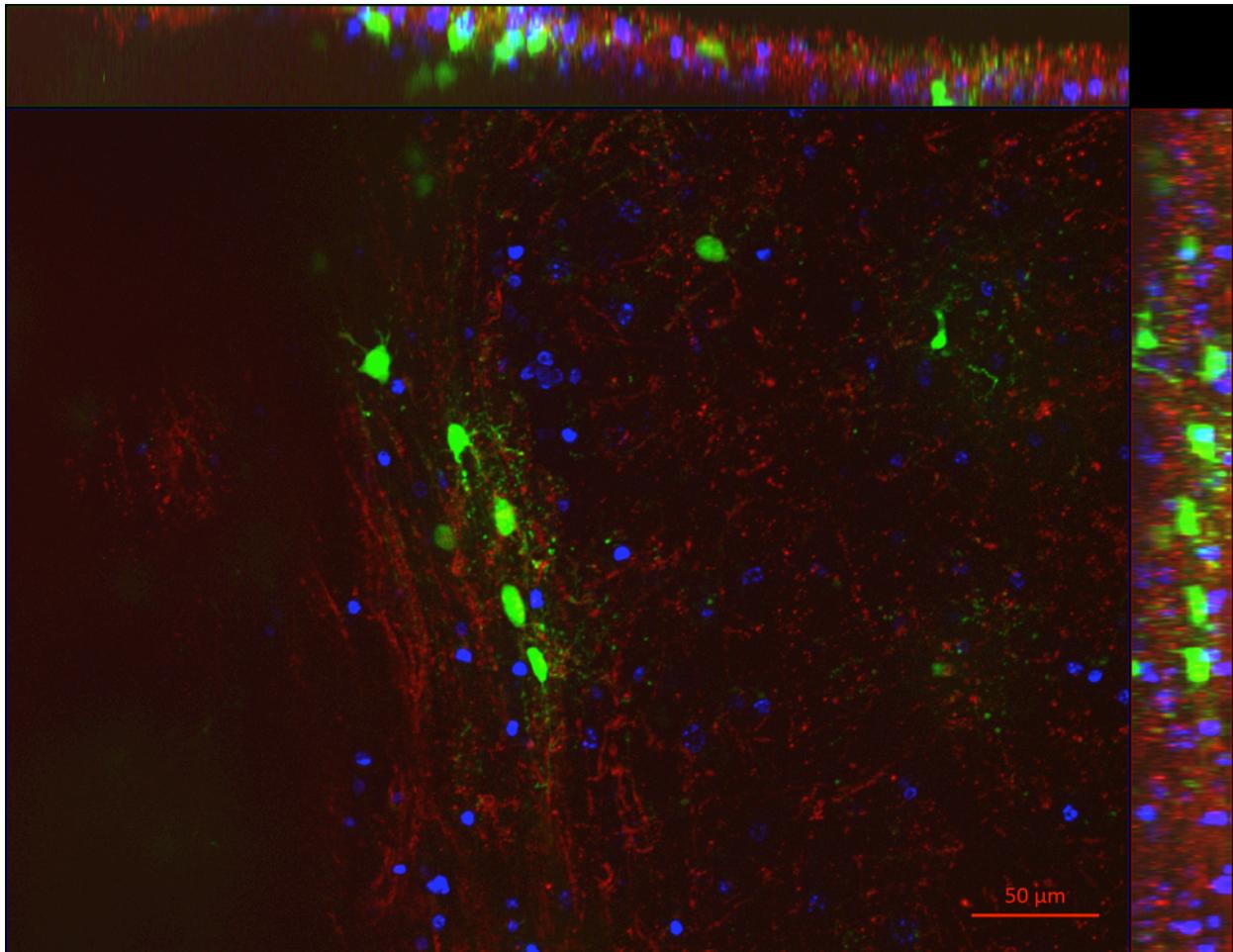
Figure 4.2 Live imaging of GFP⁺ OL lineage cells in acutely isolated cortical slices. A representative image of white matter OPCs/OLs in acute *PdgfrαCreER,LacZ/EGFP* mouse cortical slice preparation. Red, anti-MAG-Alexa-555; blue, Hoechst; Green, GFP. Scale bar as indicated. XZ (top) and YZ (right) projections.

4.9 References

Barres BA, Schmid R, Sendnter M, Raff MC (1993) Multiple extracellular signals are required for long-term oligodendrocyte survival. Development 118:283-295.

Bercury KK, Dai J, Sachs HH, Ahrendsen JT, Wood TL, Macklin WB (2014) Conditional ablation of raptor or rictor has differential impact on oligodendrocyte differentiation and CNS myelination. J Neurosci 34:4466-4480.

Bridges D, Ma JT, Park S, Inoki K, Weisman LS, Saltiel AR (2012) Phosphatidylinositol 3,5-bisphosphate plays a role in the activation and subcellular localization of mechanistic target of rapamycin 1. Molecular biology of the cell 23:2955-2962.

Campeau PM, Lenk GM, Lu JT, Bae Y, Burrage L, Turnpenny P, Roman Corona-Rivera J, Morandi L, Mora M, Reutter H, Vulto-van Silfhout AT, Faivre L, Haan E, Gibbs RA, Meisler MH, Lee BH (2013) Yunis-Varon syndrome is caused by mutations in FIG4, encoding a phosphoinositide phosphatase. American journal of human genetics 92:781-791.

Chen XS, Zhang YH, Cai QY, Yao ZX (2012) ID2: A negative transcription factor regulating oligodendroglia differentiation. Journal of neuroscience research 90:925-932.

Chow CY, Zhang Y, Dowling JJ, Jin N, Adamska M, Shiga K, Szigeti K, Shy ME, Li J, Zhang X, Lupski JR, Weisman LS, Meisler MH (2007) Mutation of FIG4 causes neurodegeneration in the pale tremor mouse and patients with CMT4J. Nature 448:68-72.

Danglot L, Galli T (2007) What is the function of neuronal AP-3? Biology of the cell / under the auspices of the European Cell Biology Organization 99:349-361.

Dong XP, Shen D, Wang X, Dawson T, Li X, Zhang Q, Cheng X, Zhang Y, Weisman LS, Delling M, Xu H (2010) PI(3,5)P(2) controls membrane trafficking by direct activation of mucolipin Ca(2+) release channels in the endolysosome. Nat Commun 1:38.

Feldmann A, Amphornrat J, Schonherr M, Winterstein C, Mobius W, Ruhwedel T, Danglot L, Nave KA, Galli T, Bruns D, Trotter J, Kramer-Albers EM (2011) Transport of the major myelin proteolipid protein is directed by VAMP3 and VAMP7. The Journal of neuroscience : the official journal of the Society for Neuroscience 31:5659-5672.

Ferguson CJ, Lenk GM, Jones JM, Grant AE, Winters JJ, Dowling JJ, Giger RJ, Meisler MH (2012) Neuronal expression of Fig4 is necessary and sufficient to prevent spongiform neurodegeneration. Hum Mol Genet.

Ferguson CJ, Lenk GM, Meisler MH (2009) Defective autophagy in neurons and astrocytes from mice deficient in PI(3,5)P2. Hum Mol Genet 18:4868-4878.

Ferguson CJ, Lenk GM, Meisler MH (2010) PtdIns(3,5)P2 and autophagy in mouse models of neurodegeneration. Autophagy 6:170-171.

Forss-Petter S, Danielson PE, Catsicas S, Battenberg E, Price J, Nerenberg M, Sutcliffe JG (1990) Transgenic mice expressing beta-galactosidase in mature neurons under neuron-specific enolase promoter control. Neuron 5:187-197.

Gibson EM, Purger D, Mount CW, Goldstein AK, Lin GL, Wood LS, Inema I, Miller SE, Bieri G, Zuchero JB, Barres BA, Woo PJ, Vogel H, Monje M (2014) Neuronal activity promotes oligodendrogenesis and adaptive myelination in the mammalian brain. Science 344:1252304.

Girao H, Geli MI, Idrissi FZ (2008) Actin in the endocytic pathway: from yeast to mammals. FEBS Lett 582:2112-2119.

175

Gomez-Sanchez JA, Carty L, Iruarrizaga-Lejarreta M, Palomo-Irigoyen M, Varela-Rey M, Griffith M, Hantke J, Macias-Camara N, Azkargorta M, Aurrekoetxea I, De Juan VG, Jefferies HB, Aspichueta P, Elortza F, Aransay AM, Martinez-Chantar ML, Baas F, Mato JM, Mirsky R, Woodhoo A, Jessen KR (2015) Schwann cell autophagy, myelinophagy, initiates myelin clearance from injured nerves. The Journal of cell biology 210:153-168.

Grishchuk Y, Sri S, Rudinskiy N, Ma W, Stember KG, Cottle MW, Sapp E, Difiglia M, Muzikansky A, Betensky RA, Wong AM, Bacskai BJ, Hyman BT, Kelleher RJ, 3rd, Cooper JD, Slaugenhaupt SA (2014) Behavioral deficits, early gliosis, dysmyelination and synaptic dysfunction in a mouse model of mucolipidosis IV. Acta neuropathologica communications 2:133.

Hill RA, Medved J, Patel KD, Nishiyama A (2014a) Organotypic slice cultures to study oligodendrocyte dynamics and myelination. J Vis Exp e51835.

Hill RA, Patel KD, Goncalves CM, Grutzendler J, Nishiyama A (2014b) Modulation of oligodendrocyte generation during a critical temporal window after NG2 cell division. Nat Neurosci 17:1518-1527.

Hill RA, Patel KD, Medved J, Reiss AM, Nishiyama A (2013) NG2 cells in white matter but not gray matter proliferate in response to PDGF. J Neurosci 33:14558-14566.

Hong NH, Qi A, Weaver AM (2015) PI(3,5)P2 controls endosomal branched actin dynamics by regulating cortactin-actin interactions. The Journal of cell biology 210:753-769.

Hughes EG, Appel B (2016) The cell biology of CNS myelination. Current opinion in neurobiology 39:93-100.

Hughes EG, Kang SH, Fukaya M, Bergles DE (2013) Oligodendrocyte progenitors balance growth with self-repulsion to achieve homeostasis in the adult brain. Nat Neurosci 16:668-676.

Jahn R, Scheller RH (2006) SNAREs--engines for membrane fusion. Nature reviews Molecular cell biology 7:631-643.

Jin N, Lang MJ, Weisman LS (2016) Phosphatidylinositol 3,5-bisphosphate: regulation of cellular events in space and time. Biochem Soc Trans 44:177-184.

Jin N, Mao K, Jin Y, Tevzadze G, Kauffman EJ, Park S, Bridges D, Loewith R, Saltiel AR, Klionsky DJ, Weisman LS (2014) Roles for PI(3,5)P2 in nutrient sensing through TORC1. Molecular biology of the cell 25:1171-1185.

Kantheti P, Qiao X, Diaz ME, Peden AA, Meyer GE, Carskadon SL, Kapfhamer D, Sufalko D, Robinson MS, Noebels JL, Burmeister M (1998) Mutation in AP-3 delta in the mocha mouse links endosomal transport to storage deficiency in platelets, melanosomes, and synaptic vesicles. Neuron 21:111-122.

Kent HM, Evans PR, Schafer IB, Gray SR, Sanderson CM, Luzio JP, Peden AA, Owen DJ (2012) Structural basis of the intracellular sorting of the SNARE VAMP7 by the AP3 adaptor complex. Developmental cell 22:979-988.

Lenk GM, Ferguson CJ, Chow CY, Jin N, Jones JM, Grant AE, Zolov SN, Winters JJ, Giger RJ, Dowling JJ, Weisman LS, Meisler MH (2011) Pathogenic mechanism of the FIG4 mutation responsible for Charcot-Marie-Tooth disease CMT4J. PLoS genetics 7:e1002104.

Lenk GM, Frei CM, Miller AC, Wallen RC, Mironova YA, Giger RJ, Meisler MH (2016) Rescue of neurodegeneration in the Fig4 null mouse by a catalytically inactive FIG4 transgene. Hum Mol Genet 25:340-347.

Li X, Wang X, Zhang X, Zhao M, Tsang WL, Zhang Y, Yau RG, Weisman LS, Xu H (2013) Genetically encoded fluorescent probe to visualize intracellular phosphatidylinositol 3,5-bisphosphate localization and dynamics. Proc Natl Acad Sci U S A 110:21165-21170.

Lundgaard I, Luzhynskaya A, Stockley JH, Wang Z, Evans KA, Swire M, Volbracht K, Gautier HO, Franklin RJ, Charles F-C, Attwell D, Karadottir RT (2013) Neuregulin and BDNF induce a switch to NMDA receptor-dependent myelination by oligodendrocytes. PLoS Biol 11:e1001743.

Martinez-Arca S, Rudge R, Vacca M, Raposo G, Camonis J, Proux-Gillardeaux V, Daviet L, Formstecher E, Hamburger A, Filippini F, D'Esposito M, Galli T (2003) A dual mechanism controlling the localization and function of exocytic v-SNAREs. Proceedings of the National Academy of Sciences of the United States of America 100:9011-9016.

Martini-Stoica H, Xu Y, Ballabio A, Zheng H (2016) The Autophagy-Lysosomal Pathway in Neurodegeneration: A TFEB Perspective. Trends Neurosci 39:221-234.

Masaki T (2012) Polarization and myelination in myelinating glia. ISRN neurology 2012:769412.

McCartney AJ, Zolov SN, Kauffman EJ, Zhang Y, Strunk BS, Weisman LS, Sutton MA (2014) Activity-dependent PI(3,5)P2 synthesis controls AMPA receptor trafficking during synaptic depression. Proc Natl Acad Sci U S A 111:E4896-4905.

Medina DL, Fraldi A, Bouche V, Annunziata F, Mansueto G, Spampanato C, Puri C, Pignata A, Martina JA, Sardiello M, Palmieri M, Polishchuk R, Puertollano R, Ballabio A (2011) Transcriptional activation of lysosomal exocytosis promotes cellular clearance. Developmental cell 21:421-430.

Nawaz S, Sanchez P, Schmitt S, Snaidero N, Mitkovski M, Velte C, Bruckner BR, Alexopoulos I, Czopka T, Jung SY, Rhee JS, Janshoff A, Witke W, Schaap IA, Lyons DA, Simons M (2015) Actin filament turnover drives leading edge growth during myelin sheath formation in the central nervous system. Developmental cell 34:139-151.

Polito VA, Li H, Martini-Stoica H, Wang B, Yang L, Xu Y, Swartzlander DB, Palmieri M, di Ronza A, Lee VM, Sardiello M, Ballabio A, Zheng H (2014) Selective clearance of aberrant tau proteins and rescue of neurotoxicity by transcription factor EB. EMBO Mol Med 6:1142-1160.

Renna M, Jimenez-Sanchez M, Sarkar S, Rubinsztein DC (2010) Chemical inducers of autophagy that enhance the clearance of mutant proteins in neurodegenerative diseases. J Biol Chem 285:11061-11067.

Rowitch DH, Kriegstein AR (2010) Developmental genetics of vertebrate glial-cell specification. Nature 468:214-222.

Sardiello M, Palmieri M, di Ronza A, Medina DL, Valenza M, Gennarino VA, Di Malta C, Donaudy F, Embrione V, Polishchuk RS, Banfi S, Parenti G, Cattaneo E, Ballabio A (2009) A gene network regulating lysosomal biogenesis and function. Science 325:473-477.

Schain AJ, Hill RA, Grutzendler J (2014) Label-free in vivo imaging of myelinated axons in health and disease with spectral confocal reflectance microscopy. Nat Med 20:443-449.

Schardt A, Brinkmann BG, Mitkovski M, Sereda MW, Werner HB, Nave KA (2009) The SNARE protein SNAP-29 interacts with the GTPase Rab3A: Implications for membrane trafficking in myelinating glia. Journal of neuroscience research 87:3465-3479.

Settembre C, Di Malta C, Polito VA, Garcia Arencibia M, Vetrini F, Erdin S, Erdin SU, Huynh T, Medina D, Colella P, Sardiello M, Rubinsztein DC, Ballabio A (2011) TFEB links autophagy to lysosomal biogenesis. Science 332:1429-1433.

Settembre C, Zoncu R, Medina DL, Vetrini F, Erdin S, Erdin S, Huynh T, Ferron M, Karsenty G, Vellard MC, Facchinetti V, Sabatini DM, Ballabio A (2012) A lysosome-to-nucleus signalling mechanism senses and regulates the lysosome via mTOR and TFEB. EMBO J 31:1095-1108.

Spampanato C, Feeney E, Li L, Cardone M, Lim JA, Annunziata F, Zare H, Polishchuk R, Puertollano R, Parenti G, Ballabio A, Raben N (2013) Transcription factor EB (TFEB) is a new therapeutic target for Pompe disease. EMBO Mol Med 5:691-706.

Sudhof TC, Rothman JE (2009) Membrane fusion: grappling with SNARE and SM proteins. Science 323:474-477.

Takei N, Inamura N, Kawamura M, Namba H, Hara K, Yonezawa K, Nawa H (2004) Brain-derived neurotrophic factor induces mammalian target of rapamycin-dependent local activation of translation machinery and protein synthesis in neuronal dendrites. J Neurosci 24:9760-9769.

Tyler WA, Gangoli N, Gokina P, Kim HA, Covey M, Levison SW, Wood TL (2009) Activation of the mammalian target of rapamycin (mTOR) is essential for oligodendrocyte differentiation. J Neurosci 29:6367-6378.

Vaccari I, Carbone A, Previtali SC, Mironova YA, Alberizzi V, Noseda R, Rivellini C, Bianchi F, Del Carro U, D'Antonio M, Lenk GM, Wrabetz L, Giger RJ, Meisler MH, Bolino A (2015) Loss of Fig4 in both Schwann cells and motor neurons contributes to CMT4J neuropathy. Hum Mol Genet 24:383-396.

Winters JJ, Ferguson CJ, Lenk GM, Giger-Mateeva VI, Shrager P, Meisler MH, Giger RJ (2011) Congenital CNS hypomyelination in the Fig4 null mouse is rescued by neuronal expression of the PI(3,5)P(2) phosphatase Fig4. J Neurosci 31:17736-17751.

Zhang L, He X, Liu L, Jiang M, Zhao C, Wang H, He D, Zheng T, Zhou X, Hassan A, Ma Z, Xin M, Sun Z, Lazar MA, Goldman SA, Olson EN, Lu QR (2016) Hdac3 Interaction with p300 Histone Acetyltransferase Regulates the Oligodendrocyte and Astrocyte Lineage Fate Switch. Developmental cell 36:316-330.

Zhang Y, McCartney AJ, Zolov SN, Ferguson CJ, Meisler MH, Sutton MA, Weisman LS (2012) Modulation of synaptic function by VAC14, a protein that regulates the phosphoinositides PI(3,5)P(2) and PI(5)P. EMBO J 31:3442-3456.

Zolov SN, Bridges D, Zhang Y, Lee WW, Riehle E, Verma R, Lenk GM, Converso-Baran K, Weide T, Albin RL, Saltiel AR, Meisler MH, Russell MW, Weisman LS (2012) In vivo, Pikfyve generates PI(3,5)P2, which serves as both a signaling lipid and the major precursor for PI5P. Proc Natl Acad Sci U S A 109:17472-17477.

Zou Y, Jiang W, Wang J, Li Z, Zhang J, Bu J, Zou J, Zhou L, Yu S, Cui Y, Yang W, Luo L, Lu QR, Liu Y, Chen M, Worley PF, Xiao B (2014) Oligodendrocyte precursor cell-intrinsic effect of Rheb1 controls differentiation and mediates mTORC1-dependent myelination in brain. J Neurosci 34:15764-15778.

Zuchero JB, Fu MM, Sloan SA, Ibrahim A, Olson A, Zaremba A, Dugas JC, Wienbar S, Caprariello AV, Kantor C, Leonoudakis D, Lariosa-Willingham K, Kronenberg G, Gertz K, Soderling SH, Miller RH, Barres BA (2015) CNS myelin wrapping is driven by actin disassembly. Developmental cell 34:152-167.

APPENDIX

Searching for Mechanistic Clues in PI(3,5)P$_2$-Mediated Aspects of Myelination

A1. A high-throughput analysis of gene expression in PI(3,5)P$_2$ deficiency mutants

RNA-seq of Fig4$^{-/-}$ forebrain tissue reveals a selective reduction of mature OL enriched transcripts.

We employed multiple strategies to demonstrate that PI(3,5)P$_2$ biosynthesis is critical for the OL terminal differentiation (Chapter II). To more accurately determine the stage of OL lineage differentiation at which *Fig4* function is required, we dissected the neocortex and hippocampus from *Fig4$^{+/+}$* and *Fig4$^{-/-}$* pups and subjected samples to RNA sequencing and gene ontology (GO) analysis (Figure A1). We chose P10 brain tissue because this represents an OL developmental stage *in vivo* that is comparable to the primary OLs studied *in vitro*. Of note, transcripts of genes implicated in PI(3,5)P$_2$ synthesis or signaling are not significantly altered in *Fig4$^{-/-}$* forebrain (Table A1). However, many OL specific transcripts are significantly reduced in *Fig4$^{-/-}$* tissue, the majority encoding proteins enriched in the myelin sheath. The strongest reduction was observed for *Mobp* (-15 fold), *Opalin* (-11 fold), *Mag* (-6 fold), *Plp1* (-3 fold), *Mbp* (-3 fold) and *transmembrane protein 125* (-3 fold). GO analysis further revealed that several genes associated with chromatin structure are significantly reduced in *Fig4$^{-/-}$* mice (Figure A1.B). In addition, a striking increase in immune response genes was found in *Fig4$^{-/-}$* brain tissue (Figure A1.B). To assess the effect of *Fig4* deficiency on expression of neural cell type-specific genes, we compared our RNA-seq data with the recently reported cell-type

specificity of neural gene expression (Zhang et al., 2014). Of 37 genes highly enriched in OPCs, including *Pdgfrα* and *NG2/Cspg4*, none were significantly altered (false discovery rate or FDR <0.1) in *Fig4⁻ᐟ⁻* mutants (Table A2). Of 33 genes enriched in newly formed OLs (NFOs), the transcripts of only two genes, *Kif19a* and *Enpp6,* were significantly reduced in *Fig4⁻ᐟ⁻* mutants (Table A3). Of 45 genes enriched in mature OLs, the transcripts of 9 genes were significantly reduced in *Fig4⁻ᐟ⁻* mutants: *Mbp, Mag, Plp1, Cnp, Cldn11, Ugt8a, Opalin/Tmem10, Mobp,* and the Rab11a GAP *Tbc1d9b* (Table A4). Together, these studies indicate that OL lineage progression from OPC to NFO is largely intact in *Fig4⁻ᐟ⁻* deficient brains, but differentiation from NFO to mature myelin forming OL is severely compromised. Interestingly, a virtually identical list of OL genes is reduced by selective ablation of maturing OLs in transgenic mice by expression of diphtheria toxin under the control of the *CNPase* promoter (Golan et al., 2008). Moreover, reorganization of chromatin structure is known to play a critical role in OL differentiation and CNS myelination (Liu and Casaccia, 2010). In contrast, expression of neuron specific genes is minimally affected by *Fig4* deficiency (Table A5). With regard to astrocyte-enriched genes, *Gfap* transcripts are significantly increased (4-fold) in *Fig4⁻ᐟ⁻* tissue, as previously observed (Ferguson et al., 2009), while expression of 47 other astrocyte-enriched genes changed minimally, if at all (Table A6). Of 50 microglia-enriched genes examined, 20 were significantly upregulated in *Fig4⁻ᐟ⁻* tissue (Table A7). This is consistent with the previously reported microgliosis detected by anti-Iba1 immunocytochemistry (Ferguson et al., 2009). In particular, transcripts encoding the CC chemokine ligands CCL2, CCL3, CCL4, CCL12, several cathepsin family members of the lysosomal proteolytic system, and the pattern recognition receptor CLEC7A/dectin-1 are significantly up-regulated in *Fig4⁻ᐟ⁻* tissue. Overall, *Fig4* inactivation induced a limited number of gene expression changes in functional categories

related to late-stage OL differentiation, chromatin structure, lysosomal proteolysis, innate immune response and chemokine receptor binding.

Robust differential gene expression in Pikfyve-deficient OPCs/OLs

Pikfyve-deficient OPCs present with an extremely severe vacuolation phenotype, reduced proliferation, and completely impaired differentiation (Chapter II). To test whether these phenotypes are associated with transcriptional changes in the *Pikfyve$^{flox/flox}$,Olig2Cre* OL lineage, the Affymetrix gene expression array was performed on acutely isolated control and *Pikfyve*-deficient PDGFRα$^+$ OPCs and O4$^+$ immature OLs (see Appendix.. for methods). The variability between samples was low and samples from the same genotype and condition clustered with high fidelity (n=4 animals/genotype with the exception of n=3 for control O4. *Pifkyve$^{flox/flox}$* pups were used as control). Strikingly, there were 1282 genes with at least 1.5 fold change ratio between PDGFRα$^+$ *Pikyve* control and *Pikfyve$^{flox/flox}$,Olig2Cre* OPCs and 2831 genes between control and *Pikfyve$^{flox/flox}$,Olig2Cre* O4$^+$ cells. Notably, the highest fold change of gene expression in both OPC and OL groups included *bona fide* myelin markers *Opalin*, *Plp1*, *Mag*, *Mog*, and *Mbp*, and *Mal* (Tables A8 and A9) Interestingly, *Pikfyve$^{flox/flox}$,Olig2Cre* OPCs also demonstrated significant downregulation of OPC genes such as *Pdgfrα* and *Cspg4*, which was not observed in *Fig4$^{-/-}$* tissue (included in raw data analysis). The gene ontology (GO) analysis using logistic regression path (LR path (Kim et al., 2012, Lee et al., 2016) revealed significant down-regulation of myelin-specific genes and both OPC and OL groups (Tables A10 and A11). Consistent with the function of PIKFYE as a major regulator of intracellular trafficking, both PDGFRα$^+$ and O4$^+$ *Pikfyve*-deficient cells demonstrated significant upregulation in pathways associated with vesicular transport. Interestingly, *Pikfyve*-deficient OLs also showed significant

upregulation of pathways associated with chromatin regulation and gene transcription. These data pose an intriguing possibility that profound alterations in intracellular transport due to reduced $PI(3,5)P_2$ biosynthesis may lead to transcriptional changes in multiple pathways. Interestingly, *Pikfyve*-deficient OPCs and OL had significant increase in gene expression of astrocyte markers including *Gfap* and *Aldh1l1*. These data may be indicative of astrocyte contamination during purification process. It is, however, a possibility that impaired intracellular trafficking may result in preferential silencing of OL-specific genes with a concomitant up-regulation of astrocyte genes (Chapter IV).

A2. Ganglioside levels are not altered in *Fig4*$^{-/-}$ brain

Gangliosides have been shown to regulate CNS myelination (Pan et al., 2005, Yao et al., 2014) and can be transferred between cells by membrane shedding and uptake (Heffer-Lauc et al., 2005, Lauc and Heffer-Lauc, 2006). Ganglioside transfer from neurons is a potential oligodendrocyte-extrinsic function during myelin development that could be compromised by *Fig4* deficiency (Yao et al., 2014). We therefore examined P10 brain tissue for total ganglioside levels and composition of individual ganglioside species. High performance thin-layer chromatography was used for comparison of *Fig4* mutant and wildtype littermate tissue. As shown in Table A12, *Fig4* deficiency does not alter total levels or composition of ganglioside species in the developing brain (Figure A2).

A3. Hypomyelination in *Fig4$^{flox/-}$,Olig2Cre* mice is rescued by neuron-specific overexpression of transgenic *Fig4*

Previously we reported that transgenic overexpression of recombinant *Fig4* specifically in neurons (*Fig4$^{-/-}$,NSE-Fig4*) on a *Fig4$^{-/-}$* background largely rescues defects in CNS myelination (Winters et al., 2011). This finding stands in apparent conflict with the hypomyelination phenotype identified in *Fig4$^{-/flox}$,Olig2cre* mice (Chapter II). One interpretation of these data is that overexpression of recombinant Fig4 in neurons is sufficient to compensate [through an unknown mechanism] for the absence of *Fig4* in the OL-linage. A potential caveat that we investigated was "leakiness" of the *NSE* promoter resulting in some expression of *Fig4* transcript in the OL-lineage. To address this possibility, primary OPC/OL cultures from *NSE-Fig4* transgenic pups were analyzed by RT-PCR for NSE promoter activity resulting in transgene expression. As positive control, strong *NSE* promoter activity was detected in a neuron-enriched fraction from the same brains (Figure A3.1A). There was a very low level of *NSE* promoter activity, in primary OLs, likely due to co-purification of a small number of neurons, as shown by the *tubb3* signal in OPC/OL cultures. To control for the presence of OPCs in purified fraction, we used RT-PCR for *Cspg4* (Figure A3.1B). Surprisingly, cultured *Fig4$^{-/-}$,NSE-Fig4* OPCs differentiated normally *in vitro*, and did not show enlarged vacuolation at any stage (Figure A3C-C'''', A3E-E'). Furthermore, *Fig4$^{-/-}$,NSE-Fig4* OL lysates probed with anti-FIG4 antibody demonstrated similar FIG4 levels to control cultures despite the low level of *NSE* promoter activity (Figure A3.1D).

In parallel, we performed *Fig4 in situ* hybridization of optic nerve cross sections of *Fig4$^{-/-}$,NSE-Fig4* mice. Few *Fig4^{+}* cells were observed in optic nerve cross sections. Double-labeling with the OL-lineage marker Olig2 revealed minimal, if any, overlap with *Fig4^{+}* cells (Figure

A3.1B-B'). Collectively, these experiments show selective expression of transgenic *Fig4* in OPCs/OLs of *Fig4^-/-,NSE-Fig4* mice. To demonstrate that the *NSE-Fig4* transgene is sufficient to rescue CNS myelination, *NSE* transgenic animals were crossed onto a *Fig4^-/flox,Olig2cre* background, resulting in *Fig4^-/flox,Olig2cre, NSE-Fig4* mice (Figure A3.2A). These mice present with apparent normal myelin, as assessed by immunoblotting of brain lysates for MAG, CNPase, and MBP (Fig A3.2B-2C). Electrophysiological studies further showed that defects in optic nerve conduction observed in *Fig4^-/flox;Olig2cre* mice (Chapter II) are fully rescued by the *NSE-Fig4* transgene (Fig A3.2D-2F).

Collectively, neuron specific *Fig4* gain-of-function (Winters et al., 2011, Ferguson et al., 2012b) and loss-of-function studies (Chapter II) indicate that FIG4-dependent mechanism(s) extrinsic to the OL lineage are critical for proper CNS myelination and propagation of electrical impulses. Transgenic overexpression of neuronal *Fig4* presumably leads to overproduction of a pro-myelination signal and, strikingly, this is sufficient to compensate for loss of *Fig4* in the OL lineage. Other instances of neuron-specific overexpression modulating the OL lineage non-cell-autonomously have been reported (Stritt et al., 2009, Yao et al., 2014). However, important caveats associated with mouse genetics models of transgenic overexpression have to be considered. *Fig4 mRNA* levels are below detection level by RT-PCR in the OL enriched samples and ISH in the optic nerve, but it cannot be ruled out that even minimal *NSE* promoter driven expression of *Fig4* in the OL lineage is sufficient to provide enough *Fig4* transcript for fully functioning OLs. Another possibility may be that FIG4 or PI(3,5)P$_2$ itself through an unknown mechanism are shared between neurons and the OLs. The latter hypothesis is somewhat unlikely given that FIG4 protein has a short half-life and is rapidly degraded by proteasome (Ikonomov et al., 2010), and cultured OLs would therefore presumably "run out" of externally supplied FIG4

in vitro. As increased VAC14 levels stabilize FIG4 *in vitro*, it would be of interest to examine whether VAC14 levels change homeostatically in response to low FIG4 levels. As a future direction, cell-type specific neuronal *Fig4* expression in RGCs via adenoviral or AAV-mediated delivery may serve as an additional assessment of the non-cell-autonomous FIG4 function in myelination of the optic nerve. Furthermore, more sensitive methods of mRNA detection should be employed to fully assess *NSE* expression in the OL lineage, such as digital droplet PCR.

A4. *Fig4*-deficient OLs ensheath nanofibers

Isolated primary oligodendrocyte culture is a powerful tool for studying the OL dynamics *in vitro*. However, the mature OL morphology drastically differs *in vitro* vs. *in vivo* (chapter I, Figure 1.2). Fully mature OLs expressing MBP, MOG and other myelin markers *in vivo* are always associated with axons and are not observed as an independent entity. It has been shown that *in vitro* OLs are fairly promiscuous and are capable of enwrapping fixed axons and even polymer fibers, micropillars, and beads (Lee et al., 2013, Mei et al., 2014). To examine whether *Fig4* deficiency in primary OLs attenuates ensheathing of axon-like structures, we employed polystyrene nanofibers with a diameter of 1-1.5 µm (Lee et al., 2013). Although MBP$^+$ OLs were significantly reduced in *Fig4$^{-/-}$* cultures, they did retain the ability to ensheath the nanofibers (Figure Figure A4A-B). This observation is consistent with the hypomyelination phenotype in *Fig4$^{-/flox}$,Olig2* mice, where the number of mature OLs is significantly reduced, but mature OLs that are present are capable of wrapping axons. This result indicates that the molecular programs necessary for fiber enseathment are largely intact in *Fig4$^{-/-}$* OLs.

A5. Monitoring PLP intracellular trafficking in *Fig4⁻/⁻* OLs.

Proteolipid protein (PLP) is the essential component of compact myelin, necessary for stabilization of myelin leaflets and maintaining the tightly wrapped structure of the sheath (Chapter I). PLP is associated with cholesterol-rich lipid rafts and is trafficked to the nascent myelin sheath via the endosome/lysosomal pathway (Trajkovic et al., 2006). We have demonstrated that loss of Fig4 function results in accumulation of MAG in the enlarged LE/Lys compartment of maturing *Fig4⁻/⁻* OLs, suggesting that myelin building blocks may be transported via LE/Lys compartment in a PI(3,5)P$_2$-dependent manner (Chapter II). We have also confirmed previous reports that MOG and MAG have distinct localization in living OLs and demonstrated that MOG is not present in enlarged LAMP1$^+$ structures observed in *Fig4⁻/⁻* OLs (Winterstein et al., 2008). Given that PLP, like MAG, is also trafficked via the LE/Lys compartment, we set to examine whether it accumulates in enlarged LAMP1$^+$ vesicles. OLs were co-transfected with *PLP-YFP* and *LAMP1-mCherry* expression constructs. Consistent with previous studies, recombinant PLP formed aggregates (Simons et al., 2002). In *Fig4⁻/⁻* OLs, PLP-YFP and LAMP1-mCherry localized to membranes of enlarged vesicles (Figure A5.1A'-C'). This suggests that in the absence of *Fig4*, myelin building blocks trafficked through the LE/Lys compartment associate with enlarged vesicles.

Since PLP overexpression does not represent a physiologically relevant PLP distribution in the maturing OLs, rabbit anti-PLP antibody was conjugated to Alexa555 and bath-applied it to WT and *Fig4⁻/flox,CMVCreER* OLs in culture medium as described before (Chapter II). PLP application resulted in bright punctate accumulation of Alexa555$^+$ signal in immature and mature WT and *Fig4*-deficient OLs that partially overlapped with anti-MAG-Alexa488 (Figure A5.2A-B"). Enlarged perinuclear structures in *Fig4⁻/flox,CMVCreER* cells were Alexa555 and Alexa488-

positive (Figure A5.2B-B'', arrows). Since rabbit PLP antibody was supplied as a whole serum, goat serum was put through the identical Alexa555 conjugation protocol and applied to OL cultures in parallel as a nonspecific control. Surprisingly, tagged serum had a similar intracellular distribution in WT and *Fig4$^{-/flox}$,CMVCreER* OLs, however, the observed signal was considerably dimmer (Figure A5.2C-D''). These experiments suggest that a higher purity anti-PLP antibody and ideally, *Plp1$^{-/-}$* OLs would be necessary to test whether the signal observed was specific.

A6. Myelin regulatory factor in *Fig4$^{-/-}$* OL lineage

The identity, proliferation, and differentiation of the OL lineage are tightly regulated by a network of transcription factors (TF) (Emery and Lu, 2015). Noted transcriptional regulators of the OL lineage at various stages are Olig2, Olig1, AscI, and Sox10. Recent discovery of myelin regulatory factor (MRF) (Emery et al., 2009) identified it as a critical regulator of later stages of myelination. MRF is expressed exclusively by maturing OLs in the CNS and its expression is directly regulated by Sox10 (Hornig et al., 2013). Full-length MRF is an ER transmembrane protein, but upon autoproteolitic cleavage its N-terminus is transported to the nucleus, where it binds directly to the enhancer sequence of late stage myelin markers *Mag*, *Plp1* and *Mbp*, among others (Bujalka et al., 2013). In the absence of *Myrf*, OLs fail to terminally mature past the arborized early postmitotic stage *in vitro* and express virtually none of the *Myrf* target genes (Emery et al., 2009). *Myrf*-deficient mutants present with severe hypomyelitation phenotype *in vivo* and increased OL cell death. Furthermore, inducible *Myrf* inactivation in the adult CNS results in severe demyelination within 8 weeks, decreased expression of MAG, MBP, and PLP and OL death, suggesting the necessity of MRF function for myelin stability (Koenning et al.,

2012, McKenzie et al., 2014). Overexpression of *Myrf* in WT OPCs at DIV2 results in precocious expression of the mature OL marker MOG, suggesting that timing of *Myrf* expression is critical for the OL terminal differentiation (Bujalka et. al 2013).

Impaired $PI(3,5)P_2$ biosynthesis results in a significant decrease in gene expression of myelin-associated machinery. Given this observation, we hypothesized that reduced $PI(3,5)P_2$ levels may be leading, directly or indirectly, to impaired *Myrf* expression and/or its failure to induce myelin-specific gene expression.

Myrf gene expression in Fig4- and Pikfyve-deficient brain and OL samples

RNA sequencing analysis revealed a small but significant decrease in *Myrf* levels (LogFC 0.8) in *Fig4^{-/-}* P10 forebrain samples compared to WT. FDR, however, was 0.4, which together with a small fold change suggested minimal difference in *Myrf* gene expression in *Fig4^{-/-}* forebrain. In contrast, gene expression array in *Pikfyve*-deficient OPCs and OLs demonstrated an almost 5-fold decrease in *Myrf* expression (Table A8). It would be of interest to examine a mechanistic relationship between *Myrf* expression and $PI(3,5)P_2$ biosynthesis.

Myrf endogenous expression in Fig4^{-/-} OLs

To assess the endogenous localization and expression of MRF in *Fig4*-deficient OLs, *Fig4* control and *Fig4^{-/-}* OLs were cultured in T3 medium for 4 days and stained with the N-terminus rabbit anti-MRF and anti-MBP antibodies. As reported previously, *Fig4^{-/-}* OLs had reduced MBP expansion and expression (Chapter II) and displayed hallmark enlarged perinuclear vacuolation. MRF staining, however was observed faintly throughout the membrane portion of the OL and brightly in the nucleus and appeared compatible to WT OLs (Figure A6A-

B'''). These data suggest that in the absence of *Fig4*, MRF can still successfully translocate to the nucleus. To test whether loss of *Fig4* function results in impaired MRF cleavage, lysates isolated from cultured WT, *Fig4^{-/-}*, *Fig4^{+flox},Olig2Cre,* and *Fig4^{-/flox},Olig2Cre* OLs were probed with antibodies against N and C terminal MRF. As reported elsewhere (Bujalka et al., 2013), a faint band representing a full length MRF was observed at ~140 kDa and 75 and 70 kDa bands were detected using anti N- and C-terminus antibodies, respectively. The OL-specific marker CNPase was used as a loading control. No notable differences in protein levels of either cleaved MRF form were observed in *Fig4*-deficient OLs, suggesting its normal processing in the absence of *Fig4* (Figure A6C). As was discussed previously (Chapter IV), *in vitro Fig4*-deficient OLs demonstrate a milder terminal differentiation phenotype compared to a severe decrease in the density of mature OLs and profound hypomyelination observed *in vivo.* It would be therefore interesting to examine MRF protein levels and processing in acutely isolated immature and myelinating *Fig4*-deficient OLs.

Myrf overexpression induces precocious differentiation in Fig4^{-/-} OLs.

     Myrf expression coincides with the OL maturation and onset of myelination. When *Myrf* is overexpressed in OPCs *in vitro,* it induces precocious differentiation as evidenced by increased OL arborization and premature MOG expression (Bujalka et al., 2013). *Fig4^{-/-}* and *Pikfyve*-deficient OLs present with impaired trafficking and reduced levels of major myelin building blocks. To test whether *Fig4^{-/-}* OPCs can still respond to *Myrf* overexpression *in vitro*, the cells were cultured for 1 day in the presence of PDGF and NT3 and co-transfected with *Myc-Myrf-Flag* and *GFP* plasmids. *GFP* only plasmid was used as a control. As reported previously, *Myrf* and *GFP* co-transfected OPCs presented with arborized morphology as early as the following

day after transfection (Figure A6E), whereas *GFP* only transfected OPCs remained in a simple bipolar state (Figure A6D). Similarly, *Fig4*$^{-/-}$ OPCs also have undergone arborization (Figure A6D'-E'), suggesting that *Fig4*-deficient OPCs were still intrinsically capable of responding to *Myrf*-induced differentiation. In our hands, transfection interferes with the ability of OLs to undergo terminal differentiation (more on that below), therefore at this point we cannot conclude whether *Myrf* overexpression rescues impaired terminal differentiation in *Fig4*-deficient OLs. Overexpressing *Myrf* using lentiviral infection may be a better strategy.

A7. Transfecting and infecting OPCs/OLs *in vitro*

The OL lineage is notoriously difficult to manipulate *in vitro* without impeding on its ability to terminally differentiate (Ben Emery, personal correspondence). Among widely utilized methods for introducing DNA to OPCs, Amaxa electroporation results in approximately 30% transfection efficacy with limited cell death (Emery et al., 2009, Bujalka et al., 2013). However, Amaxa electroporation only works for large cell quantities in suspension, which is not always feasible. Another commonly used way to introduce DNA to cells is Lipofectamine-mediated transfection, which in proliferating cells can lead to high transfection efficiency. Using Lipofectamine in post-mitotic populations, however, results in cell death and low transfection efficiency (Duan et al., 2014). Adeno- and lentiviral infection is arguably the safest and the most effective way of delivering genetic material to the OPC lineage. When titrated to a correct amount, viruses can be used efficiently to overexpress a gene of interest and/or introduce a desired reporter. Here, we discuss some of the troubleshooting steps encountered during establishing an optimal infection and transfection protocols for cultured OPCs and OLs in our lab.

Transfecting OPCs and OLs with Lipofectamine-2000

Given that OPCs actively divide *in vitro*, we reasoned that they would be receptive to transfection with Lipofectamine. 1μg DNA transfection with 4 μl of Lipofectamine (LF) of 10,000-20000 OPCs yielded a fairly large number of GFP$^+$ cells a day after transfection (Figure A7.1A-A'). However, when compared to control cells in a parallel culture, transfected populations did not undergo differentiation as readily when placed in T3 supplemented medium (data not shown). This phenomenon was observed regardless of whether the cells in transfected cultures were GFP-positive or not, suggesting that transfection protocol itself may impede on the OL maturation. To sacrifice transfection efficiency in favor of more robust cell health, the amount of both DNA and LF was decreased by 75%. Switching to a lower DNA/LF2000 concentration improved the culture health, however, transfected cells still did not generate a fully expanded membrane sheet (Chapter II). Interestingly, it is feasible to transfect postmitotic premyelinating OLs (MAG$^+$, O4$^+$, MOG$^-$, Chapter II) as late as DIV5. Transfection efficiency is extremely low (less than 1%) and causes substantial cell death, however, this approach is suitable for short-term (24-48 hours post-transfection) reporter studies.

OPC infection with Lenti-RSV-GFP-VSVG

Lenti-and adenoviral gene delivery has been successfully tested in various neuronal postmitotic cells both *in vitro* and *in vivo* in our lab. We therefore aimed to establish the appropriate viral titer that would permit genetic labeling of OPCs/OLs without disrupting their differentiative program. Lenti-RSV-GFP-VSVG stock virus was obtained from the University of Michigan Viral Core. GFP expression was under the CMV promoter. Suggested stock

191

concentration was 10x and was successfully used as such in hippocampal neurons (Baldwin, Mironova, unpublished observations). OPCs were isolated from postnatal pups as described previously and cultured in proliferative conditions for one day. The following day, the GFP virus was diluted to 1x in 1.5ml of PDGF medium and added to OPCs. While the GFP signal typically takes approximately 72 hours to become detectable in neuronal cultures, primary OPCs were brightly green the following day and infection efficacy was fairly high (Figure A7.1C'). However, the overall health of infected culture was poor compared to uninfected controls (Figure A7.1B-C'). Not all infected cells perished and surviving OPCs were expanded under proliferative conditions, passaged and differentiated in T3 supplemented medium (Figure A7.1D-D'). To test whether lowering the viral concentration would improve cell survival, OPC cultures were passaged and infected with the GFP virus at higher dilutions (diluting the original stock as 20x and 50x). Cells were less brightly GFP$^+$ the following day compared to the 10x infected population, however, cell health was more robust (Figure A7.1E-F'). Differentiating OLs remained GFP$^+$ even at the membrane sheet stage. Altogether, these data suggested that the Lenti-RSV-GFP-VSVG virus can be safely used in cultured OPCs at fairly low concentrations, which makes it a powerful and easily attainable tool for genetic manipulation in the OL lineage.

OPC infection with Lenti 3.7.-RSV-dsREd

Aiming to find a suitable alternative to the GFP reporter virus, we tested Lenti-3.7.-RSV-dsRed available as a stock virus at the University of Michigan Vector Core. Similar to Lenti-RSV-GFP-VSVG, the dsRed virus infection was highly efficient and dsRed signal was readily detectable one day after infection of OPCs when used as instructed (diluted 10x, data not shown). However, the 10x concentration was detrimental to OPC health. Therefore, 20x, 50x,

and 100x dilutions were tested. All three higher dilutions resulted in bright dsRed fluorescence in OPCs that decreased somewhat in ramified/membrane sheet OLs (Figure A7.2A-C). dsRed$^+$ OLs were capable of surviving for multiple weeks in neuronal co-culture, however, it is possible that their myelinating capability was compromised by viral infection (see Appendix A9).

Infection of OPCs by AAV2-CBA-UFF1

AAV viral vectors are extremely useful in biological research, as their cell-type specific isotypes allow preferential *in vivo* infection (Zincarelli et al., 2008). Here, we tested AAV2-CBA-UFF1 virus obtained from the University of Florida Vector Core. This virus demonstrated high efficacy of neuronal infection *in vivo* (data not shown). Surprisingly, AAV2 infection of primary OPCs was robust and could be readily observed throughout the maturing/mature OL structure (Figure A7.2D-E). AAV2 viruses therefore can be employed as a useful tool for studying OLs *in vitro*.

A8. *SynapsinCre* expression in the OL lineage

Our data demonstrate that conditional *Fig4* deletion using *SynapsinCre* (*Fig4$^{-/flox,}$SynCre*) results in severe CNS hypomyelination (Chapter II, (Ferguson et al., 2012b). *Fig4$^{-/flox,}$SynCre* mice show progressive tremor, spongiform degeneration, and early lethality (Ferguson et al., 2012b). When crossed with the *Rosa26LacZ/+* reporter mouse line, *SynapsinCre* expression is robust in neurons (hippocampus, cortex) and is rarely observed in white matter structures (Yu and Lieberman, 2013). Furthermore, transgenic *Fig4* overexpression in neurons using the *NSE* promoter rescues CNS hypomyelination in *Fig4*-deficient mice, suggesting the possibility of non-cell autonomous *Fig4* function in myelination (Winters et al., 2011, Ferguson et al., 2012b).

Similarly, conditional deletion of *Npc1* in neurons results in severe CNS hypomyelination (Yu and Lieberman, 2013), providing more evidence of endolysoomal transport in neurons non-cell-autonomously regulating CNS myelination. However, there are some caveats associated with using *SynapsinCre* for assessing neuronal contribution to myelination. It has been demonstrated previously that *Syn1* is expressed in the OL lineage at detectable levels (Zhang et al., 2014). Therefore, endogenous *Syn1* expression in the OL lineage suggests a possibility that *SynCre* may be active in the OL lineage *in vivo* at some point during development, and thus may contribute to the hypomyelination phenotype observed in *Fig4$^{-/flox}$,SynCre* mice. Here, we aimed to examine *SynCre* expression in the *Fig4$^{-/-}$* and WT OL lineage *in vivo* and *in vitro*.

Fig4$^{-/flox}$,SynCre OLs demonstrate reduced FIG4 protein levels and abnormal vacuolation in vitro.

 In vivo, *Fig4$^{-/flox}$,SynCre* mice display impaired terminal OL differentiation in the optic nerve (Chapter II). However, the level of anatomical resolution does not permit to further examine the morphology of *Fig4$^{-/flox}$,SynCre* OLs *in vivo*. To examine whether *Fig4$^{-/flox}$,SynCre* derived primary OPCs/OLs display abnormalities in the LE/Lys compartment, *Fig4^{flox},SynCre* OPCs were isolated by immunopanning as described previously and cultured for several days. Similar to *Fig4$^{-/-}$* and *Fig4$^{-/flox}$,Olig2Cre* OPCs, *Fig4^{flox},SynCre* OPCs demonstrated limited perinuclear vacuolation at the bipolar OPC stage (data not shown). Strikingly, under differentiative conditions, *Fig4^{flox},SynCre* OLs presented with substantially enlarged vacuoles, suggesting defects in intracellular trafficking (A8.1B-B'). To assess the endogenous FIG4 levels in *Fig4^{flox},SynCre* OLs, cells were lysed and probed with an antibody against FIG4. Compared to control cultures, *Fig4^{flox},SynCre* OLs showed drastic decrease in FIG4 protein levels (Figure

A8.1A). Multiple attempts to probe OLs for Cre expression the using Millipore anti-Cre antibody were not successful.

Fig4 floxed allele recombination in Fig4$^{+/flox}$,SynCre optic nerves

The optic nerve is a homogenous bundle of RGC axons and glial cells, most abundantly OLs (Butt et al., 2004). As has been previously shown, neuronal genomic DNA is not present in axons (Kim and Jung, 2015). Therefore, any genomic DNA isolated from the optic nerve would be non-neuronal and mostly from the OL lineage. To test tissue-specific *SynCre* activity, nerves, brains, and tail tissue were isolated from *Fig4$^{+/flox}$,SynCre* and *Fig4$^{+/flox}$,Olig2Cre* animals and standard genotyping PCR was performed on genomic DNA retrieved from those specimen. As expected, *Fig4$^{+/flox}$,Olig2Cre* optic nerves and brains demonstrated robust *Fig4 floxed* recombination, as evidenced by a smaller (deleted) 282bp product and a faint (*floxed*) 679bp product, whereas no recombination was detected in the tail tissue (Figure A8.2). Strong *Fig4^{flox}* recombination was detected in *Fig4$^{+/flox}$,SynCre* brain tissue and no 282 bp product was detected in the tail. Unexpectedly, the *deleted* product was also detected in *SynCre* optic nerves, suggesting *Cre* activity in that tissue. To ensure *Cre* specificity, *SynCre*-specific primers were used and the predicted 300 bp product was detected only in *SynCre+*, but not *Olig2Cre+* positive tissues. The presence or absence of *Cre* was shown in all tissues using the generic Cre PCR protocol.

LacZ/EGFP, SynCre OLs are GFP-positive

To test whether *SynCre* activity in the OLs can be detected with a genetic reporter, *SynCre* mice were crossed with a *LacZ/EGFP* line (Chapter II). *LacZ/EGFP,SynCre* OPCs were

isolated and cultured, and the purification fraction (CD45⁻,PDGFR⁻,O4⁻) containing neurons was plated in parallel as a positive control. *LacZ/EGFP* only OPCs, OLs, and neurons were GFP-negative at all stages (Figure A8.3C-D'). In contrast, *LacZ/EGFP,SynCre* OPCs and OLs had detectable levels of GFP expression (Figure A8.3A-B', E). A putative neuronal culture presented with faint but detectable GFP levels, although the signal appeared less robust than what was observed in the OPC enriched cultures.

Discussion

Overall, our data provide several lines of evidence suggesting that *SynCre* is active in non-neuronal cell types. However, at this point our data are largely correlative and more rigorous investigation is required. Due to the logistics of mouse breeding, *Fig4⁻/flox,SynCre* OPCs/OLs were isolated and cultured only once and therefore it is critical to repeat this experiment to confirm or refute the original observations. As was reported previously, in male mice, *SynCre* is mis-expressed in the germline, thus rendering this *Cre* line non-specific in subsequent generations (Rempe et al., 2006). It is, however, unlikely that in our hands the *SynCre* line ever became germline, as *SynCre* conditional knockout and *Fig4* global mutants are phenotypically distinct even at earlier stages of their development, and *deleted Fig4* product is not detected in the tail tissue.

Conventional genotyping in the optic nerve of *Fig4⁺/flox,SynCre* mice strongly suggests *Cre* recombination, presumably in non-neuronal cell types. Given the qualitative nature of the experiment, however, it is difficult to gauge the level or recombination observed and it is impossible to identify its cellular origin. While a great care was exercised at the optic nerve dissection to ensure no RGC/brain tissue contamination, neuronal DNA could still have ended up

in the final samples. A digital droplet PCR technology is becoming increasingly popular for quantitative assessment of *Cre* off target expression and would be a more efficient approach here than conventional PCR.

LacZ/EGFP is a conservative reporter and has been shown to under- rather than over-estimate the level of recombination in the tissue of interest (Dwight Bergles, personal communications). Detectable GFP signal in *LacZ/EGFP,SynCre* OLs strongly indicates that *Cre* recombination did take place at the *floxed* sites of *LacZ/EGFP* in these cells but it does not necessarily mean the same event occurs at the *Fig4* locus in *Fig4^{-flox},SynCre* animals. It is also not possible at this point to distinguish between Cre mis-expresion or Cre non-cell autonomous transfer to non-neuronal cell types by either mRNA or protein delivery, which would be independent of the promoter activity (Fruhbeis et al., 2013).

Given the robust hypomyelination phenotype observed in the OL specific *Fig4* knockouts, it is reasonable to assume that in the event of cell-autonomous *SynCre* function in the OL lineage in *Fig4$^{-/flox}$,SynCre* mice the resulting hypomyelination phenotype would be at least partially due to reduced FIG4 levels in OPCs/OLs. Nonetheless, even in that case it is not possible to conclusively rule out the necessity of neuronal FIG4 contribution to OPC differentiation. *Fig4$^{-/-}$* neurons present with altered electrical properties (Zhang et al., 2012, McCartney et. al, 2014), accumulate LE/Lys vacuoles and eventually degenerate. Given a highly interactive relationship between OL lineage and neurons it is possible that disrupting neuronal trafficking may alter the OL lineage dynamics. There are several additional experiments that may aid us in further dissecting neuronal contribution of PI(3,5)P$_2$ biosynthesis to myelination. To confidently establish the cell-autonomous *Fig4* function in the OL lineage, we employed two independent OPC/OL specific Cre lines (*Olig2Cre* and *PdgfraCreER*). An additional highly

specific neuronal *Cre* line may provide critical evidence for neuronal contribution to myelination in *Fig4*^{-/-} mice. *Nex-CreERT* line is highly specific to a particular subset of cortical and hippocampal neurons (Goebbels et al., 2006), and the ultrastructural analysis of *Fig4*[/flox]*,NEXCreERT* CNS may gain potential insights into the cell-autonomy of FIG4 function in myelination. As a less time-consuming approach, neuron-specific viral *Cre* delivery can be tested in *Fig4*[flox/flox] animals. For example, Bei et al recently reported high level of specificity and recombination efficacy of *AAV2-Cre* in RGCs (Bei et al., 2016). Furthermore, as was attempted and described below, reciprocal *Fig4* WT-KO and KO-WT neuron-OL co-cultures can serve as a powerful tool for assessing neuronal FIG4 contribution to OL myelinating properties *in vitro*.

A9. Heterogeneous neuronal-OL co-cultures

Isolation and culture of primary OPCs/OLs is a powerful tool for studying lineage dynamics and monitoring its gene and protein expression. However, in a living brain, myelinating oligodendrocytes do not exist unless they are wrapping axons (Hughes et al., 2013). The absence of axoglial communication profoundly changes the OL behavior *in vitro*. For example, cultured mature OLs in the membrane sheet stage (MBP[+], MOG[+], Figure 1.2) rarely survive past 7 days after differentiation. In contrast, when co-cultured with neurons, myelinating OLs survive for multiple weeks (Zuchero et al., 2015). Similarly, myelinatng OLs *in vivo* are stable and can be observed over many weeks (Hughes et al., 2013, Hill et al., 2014).

Our data demonstrate that conditional *Fig4* ablation in either neurons or OL lineage results in a severe hypomyelination phenotype. However, given a well-documented mis-expression of employed *Cre* lines (Zhang et al., 2014), there is a risk of incorrect interpretation of observed phenotypes *vis a vis* their cell origin. Therefore, we aimed to establish an *in vitro*

system where OLs and neurons can be isolated from genetically different animals and examine the effect of differential neuron/OL *Fig4* genotypes on the OL myelinating properties. Ideally, we aimed to isolate neurons from *Fig4$^{-/flox}$,SynCre* animals, culture them with either WT or *Fig4$^{-/-}$* OLs, and then perform a complementary experiment with WT neurons. However, timely generation of cultures from these mutants is logistically very difficult. Instead, we took advantage of lentiviral Cre-mediated *Fig4$^{flox/flox}$* recombination in neurons, which allowed setting up control and experimental cultures from the same cohort of *Fig4$^{flox/flox}$* pups, thus greatly increasing neuronal yields. A classical co-culture experiment employs dorsal root ganglia neurons (DRGs), as they do not possess dendrites and can be readily myelinated by both Schwann cells and OLs. However, DRG isolation is somewhat difficult and neuronal yields are limited. To further increase the available cell numbers, instead, a hippocampal neuronal/OL co-culture was attempted as described by Gardner et al, with modifications (Gardner et al., 2012). To avoid overlap between characterizing endogenous OLs present in the hippocampal culture and differentiate them from the exogenously introduced ones, a dual reporter strategy was employed. First, prior to the OL seeding, *Fig4$^{flox/flox}$* and *Pikfyve$^{flox/flox}$* neurons were infected with neuron-specific viruses Lenti-SynCre-IRES-GFP and Lenti-SynGFP. Second, prior to-culture, exogenously introduced WT and *Fig4$^{-/flox}$,Olig2Cre* OLs were infected with Lenti-3.7-RSV-dsRed reporter virus. This system permits genotype-specific analysis based on reporter activity.

At the time of co-culture seeding at DIV15, *Fig4$^{flox/flox}$* and *Pikfyve$^{flox/flox}$* neurons treated with the Cre lentivirus demonstrated vacuolation indicating successful Cre recombination (data not shown). Shortly after, *Pikfyve$^{flox/flox}$* cells treated with the Cre virus rapidly deteriorated and the co-cultures had to be fixed and stained at DIV21, well before the optimal 3 weeks of co-

culture. After prolonged culture, all neurons, regardless of the genotype, tended to form aggregates, most likely due to suboptimal substrate conditions (Figure A9A).

While cultured under proliferative conditions, OPCs maintained their bright dsRed signal. However, under differentiative conditions or in the presence of neurons dsRed fluorescence noticeably decreased, mostly likely due to metabolic demands of myelinating OL and their preferential distribution of protein material in the membrane sheet. In contrast, morphologically non-OL dsRed cells (most likely astrocytes) remained brightly dsRed-positive (Figure A9A). At DIV33, multiple MBP$^+$ OLs were observed in the co-culture, indicating OL terminal differentiation. Some, but not all, were dsRed-positive, suggesting that MBP$^+$/dsREd$^-$ cells were either present in the original neuronal culture, or were exogenously introduced OLs that did not get infected. A large number of dsRed$^+$/MBP$^-$ cells were observed on neuronal somal aggregations, however, the identity of those cells could not be easily established (Figure A9A). Somewhat surprisingly, a very limited number of MBP+ cells were associated with GFP+ neuronal processes and internode-like colocalization of GFP and MBP signals was rarely observed (Figure A9B). Qualitatively, the number of MBP$^+$ cells and their morphology (membrane sheet expansion) was the highest in *Fig4$^{flox/flox}$*/Lenti-SynGFP + *Fig4* control OLs co-culture conditions, with less so in the *Fig4$^{flox/flox}$*/Lenti-SynCre-GFP+ *Fig4* control OLs co-cultures (A9C). A notably low number of MBP$^+$ OLs was documented in all co-cultures where OLs were *Fig4$^{-/flox}$,Olig2Cre*, consistent with previous observations (Chapter II; Figure A9D-E).

A significant amount of optimization was necessary to arrive at the described protocol. In particular, optimal conditions necessary for robust neuronal cultures and myelinating OLs were not completely compatible, and favoring one over the other resulted in respective cell death. Given the differential osmolarity of Neurobasal and DMEM, any substantial (over 25%) medium

200

changes resulted in neuronal blebbing and death. An attempt to "acclimate" neurons by preparing their medium with a 50:50 mix of Neurobasal:DMEM did not meet much success, as culture health declined under those conditions. The Gardner et al. protocol suggests Ara-C treatment to thwart proliferation of mitotic populations present in mixed hippocampal cultures. However, both Ara-C and FrdU treatments in postnatal hippocampal cultures were greatly detrimental to neuronal health and cells had to be discarded (data not shown). The OL health and survival declined gradually over the course of the culture. It may be indicative of suboptimal medium conditions. As per Gardner et al., a fairly large volume (400 μl) of neuronal medium has to be substituted for myelin medium in the first week of the co-culture, whereas under our conditions that would result in rapid neuronal death. A lack of truly myelianting OLs can therefore also be attributed to less-than-ideal culture conditions. In contrast, when a co-culture was performed with WT rat hippocampal neurons isolated from rats at E18.5, multiple myelinating OLs were readily observed (data not shown). Rat neurons were more receptive to substantial media changes and were in general more robust than postnatal mouse culture. In addition, in rat cultures there was no additional burden of viral infection. As hippocampal neurons get polarized in culture and develop dendritic and axonal components that fasciculate together, it perturbs the ability of OLs to efficiently myelinate axons. It is also possible that Lenti-dsRed infection even at low doses can affect the OL ability to myelinate. Taken together, our experiment, while theoretically presenting an ideal and efficient system to asses differential contribution of neuronal and OL $PI(3,5)P_2$ to myelination, in practice encountered an exorbitant amount of logistical issues. The DRG-OL co-culture, while less efficient neuronal yield-wise may be a more feasible option.

A10. Enhanced Long-term Potentiation in the *Fig4*^{-/-} CA3-CA1 circuit.

Intracellular trafficking is essential for proper synaptic function in neurons (Man et al., 2000). At the presynaptic site, vesicular formation, transport and neurotransmitter release into the synaptic cleft has to be done in a rapid and timely manner. At the postsynaptic site, endocytosis and recycling of various synaptic receptors, such as AMPAR, are necessary for maintaining synaptic strength. Recent evidence identified that Vac14 – a scaffold protein for the $PI(3,5)P_2$ biosynthetic complex – is enriched at excitatory synapses (Zhang et al., 2012). Genetic deletion of pharmacological inhibition of *Fig4* or *Pikfyve* results in increased frequency of miniature postsynaptic currents, indicating the potential importance of $PI(3,5)P_2$ for regulation of synaptic strength. Excitingly, McCartney et al. also demonstrated that dynamic regulation of $PI(35,)P_2$ levels has direct consequences on synaptic strength. In particular, reduced $PI(3,5)P_2$ biosynthesis results in impaired chemical long-term depression (LTD) (McCartney et al., 2014b). Here, we investigated whether impaired PI(3,5)P2 biosynthesis changes another form of Hebbian synaptic plasticity, long-term potentiation (LTP). Unlike the *in vitro* whole cell recording experiments performed by McCartney et al., we employed hippocampal field recordings in a well-studied CA3-CA1 circuit *ex vivo*.

To evoke long-term potentiation in *Fig4*^{-/-} mice, acute hippocampal slices from P19 WT and *Fig4*^{-/-} animals were prepared and recorded from in oxygenated aCSF. When Schaffer collaterals were stimulated and field excitatory postsynaptic potentials (fEPSPs) were recorded in the CA1, no obvious differences in the input/output curve were detected in WT and *Fig4*^{-/-}. Furthermore, baseline recordings collected at 50% of maximum stimulus intensity were compatible (Figure A10). In contrast, with high frequency stimulation of 2 100Hz trains, *Fig4*^{-/-} slices demonstrated a dramatic post-tetanic-potentiation (PTP, highest value 240%) and

sustained LTP at 172.7±0.8% relative to baseline, whereas in WT slices maximum PTP was 195% and LTP averaged 152.3±0.5% relative to baseline. These data suggest a possibility that FIG4 (or more likely, PI(3,5)P$_2$) may be serving as a negative regulator of synaptic potentiation and are consistent with impaired chemical LTD as reported previously (McCartney et al., 2014). An important caveat for this study is a small sample size – a higher number of recorded slices (at least 6-8/group) would be more representative of any potential phenotype.

A11. Methods

RNA-sequencing: Brains from three *Fig4$^{-/-}$* pups and three *Fig4$^{+/+}$* littermates at P10 were extracted, rinsed in ice cold PBS and the cortex and hippocampus carefully dissected. Each tissue sample was transferred into a separate tube with TRIzol (Invitrogen, MA) and processed separately for RNA extraction. Total RNA was processed with Ribo-Zero Gold kit (Epicentre, WI) to remove ribosomal RNAs. Sequencing libraries were prepared using the Illumina TruSeq RNA sample prep kit following the manufacturer's protocol. After library preparation, amplified double-stranded cDNA was fragmented into 125-bp (Covaris-S2, Woburn, MA) DNA fragments, and 200 ng aliquotes were end-repaired to generate blunt ends with 5'- phosphates and 3'- hydroxyls followed by ligation of adapters. The purified cDNA library products were evaluated using the Agilent Bioanalyzer (Santa Rosa, CA) and diluted to 10 nM for cluster generation *in situ* on the HiSeq paired-end flow cell using the CBot automated cluster generation system. All samples were multiplexed into a single pool in order to avoid batch effects (Auer and Doerge, 2010) and sequenced using an Illumina HiSeq 2500 sequencer (Illumina, San Diego, CA) across 2 lanes of 69-bp-paired-end sequencing, corresponding to 3 samples per lane and yielding between 52 and 65 million reads per sample. Quality control was performed on base

qualities and nucleotide composition of sequences. Alignment to the *M. musculus* (mm10) refSeq (refFlat) reference gene annotation was performed using the STAR spliced read aligner (Dobin et al., 2013) with default parameters. Additional QC was performed after the alignment to examine: the level of mismatch rate, mapping rate to the whole genome, repeats, chromosomes, key transcriptomic regions (exons, introns, UTRs, genes), insert sizes, AT/GC dropout, transcript coverage and GC bias. Between 89 and 92% (average 90.4%) of the reads mapped uniquely to the mouse genome. Total counts of read-fragments aligned to candidate gene regions were derived using HTSeq program (www.huber.embl.de/users/anders/HTSeq/doc/overview.html) with mouse mm10 (Dec.2011) refSeq (refFlat table) as a reference and used as a basis for the quantification of gene expression. Only uniquely mapped reads were used for subsequent analyses. Differential expression analysis was conducted with R-project and the Bioconductor package edgeR (Robinson et al., 2010) and limma-voom (Law et al., 2014). Statistical significance of the differential expression was determined at false discovery rate (FDR) <0.1. RNAseq data has been deposited within the Gene Expression Omnibus (GEO) repository (www.ncbi.nlm.nih.gov/geo).

Affymetrix assay: 2 litters of P10 control littermates (*PIKfyve$^{flox/flox}$*, n=4) and *PIKfyve $^{flox/flox}$, Olig2Cre* (n=4) were processed for OPCs and OL immunopanning as described previously (Chapter II). PDGFRα^+ and O4$^+$ cells were collected directly off the panning plates using a cell scraper and RNA was isolated using the RNAEasy kit (Qagen) according to manufacturer's instructions. Total RNA was collected in 1.5 ml Eppendorf tubes and frozen at -80C. The following day, RNA samples were submitted to the University of Michigan Sequencing Core for the Affymetrix Gene Array. Only the probesets with ratio change of 1.5 or greater and p<0.05 were used in the final analysis.

Fibers: Fig4 control and *Fig4$^{-/-}$* OPCs were isolated and cultured as described previously (Chapter II). Polysterne fibers were kindly generated and provided by Samuel Tuck as described (Lee et al., 2013). OPCs were cultured under proliferative conditions for 7 days. Afterwards, they were gently passaged onto PDL coated fibers at a high density (150K/coverslip). OPCs were allowed to adhere to the fibers overnight in a drop of medium overnight, after which the wells were flooded with extra medium. OLs were allowed to differentiate and wrap the fibers for 7 days. Afterwards, they were fixed and stained for MBP as described previously (Lee et al., 2013). For quantification, at least 10 non-overlapping images of OLs on fibers in the middle of the well were taken per coverslip. Whenever possible, two coverslips/genotype were analyzed. Four independent experiments were used for quantification.

OPC Infection/transfection: OPC transfection was performed as described previously (Chapter II). For OPC infection, the medium was aspirated from DIV1 OPCs and fresh proliferative medium containing the viral stock diluted to indicated concentrations was applied for 48 hours, after which the medium was replaced completely. The next day, cells were switched into differentiative medium and cultured for a desired amount of time.

Brain gangliosides: Gangliosides were isolated and purified from lyophilized P10 brain from *Fig4$^{+/+}$* and *Fig4$^{-/-}$* mice using previously described procedures (Hauser et al., 2004, Baek et al., 2009). The resorcinol assay was used to estimate the amount of ganglioside sialic acid in tissue samples as described (Hauser et al., 2004). Individual ganglioside species were analyzed qualitatively and quantitatively by high-performance thin-layer chromatograph (HPTLC) and densitometric scanning according to previously described methods (Ando et al., 1978, Baek et al., 2009, Arthur et al., 2011).

MRF *experiments:* OPCs were transfected as described previously (Chapter II). For anti-MRF westerns, DIV3 OLs were lysed in RIPA buffer and triturated ten times using a 21G syringe. Lysates were centrifuged at 14,000g for 15 minutes, supernatants were collected and boiled with 2x Laemmli buffer and BME. Equal protein amounts were using for Western blotting as described previously.

RT-PCR - To assess potential leakiness of the transgenic *NSE* promoter in the OL lineage, primary OPCs from *Fig4$^{-/-}$,NSE-Fig4* and *Fig4$^{+/+}$,NSE-Fig4* littermates were isolated by immunopanning, as described above. The cellular fraction containing neurons (cells not captured by anti-PDGFRα panning) was spun down at 220g for 15 min, resuspended in TRIzol and stored at -80°C. OPCs were cultured for 3 days in PDGF supplemented culture medium and then suspended in TRIzol and processed for RNA isolation and qRT-PCR as described (Winters et al., 2011).

Co-culture: <u>*Neuronal culture:*</u> For rat neurons, hippocampal cultures were isolated from E18.5 pups as described previously (Raiker et al., 2010). For mouse neurons, P0-P2 hippocampal cultures form *Fig4$^{flox/flox}$* and *Pikfyve$^{flox/flox}$* pups were established as described previously (Duan et al., 2014). Cells were cultured on 12mm glass coverslips (coated with 5 μg/ml laminin and 100μg/ml PDL) at 60,000 cells/coverslip density in 600μl of standard neuronal culture medium (Neurobasal/1x Pen/Strep/1x B27). Five days after plating, Lenti-SynGFP and LentiSynGFP-Cre viruses were added to the culture medium. At 72 hours post-infection, ½ medium was replaced with fresh neuronal medium. <u>*OPC culture:*</u> *Fig4* control and *Fig4$^{-/flox}$,Olig2Cre* OPCs were isolated as described previously (Chapter II) and plated at 30,000 cells/well of a 12 well plate. At DIV1, OPCs were infected with Lentilox-3.7.-dsRed virus at 0.1x concentration of the core supplied stock virus. As tested previously, this virus concentration provided high infection rate

without impeding on the OPC ability to successfully differentiate. OPCs were kept in proliferation medium to prevent them from differentiating. <u>*Myelinating co-culture*</u>: Two days before starting a co-culture, 1/3 of neuronal medium was replaced. At neuronal DIV15, OPCs were gently trypsinized off the culture plates, spun down at 300rcf for 15min and plated onto neuronal cultures at 60,000 cells/well in 100 μl of neuronal medium. The following day, 250 μl of the medium was removed and 150 μl myelin medium (see (Gardner et al., 2012) for the recipe) was added. For subsequent days, 200 μl of medium was replaced with myelin medium every third day. At DIV34, cells were fixed with 4% PFA for 14 min and stained with anti-MBP, anti-dsRed, and anti-GFP as described previously (Chapter II).

Slice electrophysiology: *Fig4*$^{+/+}$ and *Fig4*$^{-/-}$ P18-P19 animals were sacrificed and their brains rapidly dissected in oxygenated ACSF as described previously (Toth et al., 2013). Transverse hippocampal sections were collected and allowed to rest in oxygenated aCSF for at least 2 hours prior to recording session. Stable baseline recordings were obtained at the 50% stimulus intensity of Schaffer collaterals in the CA1 region. LTP was induced as described previously (Lee et al., 2008). After potentiation, LTP recordings were performed for at least an hour. Slices with unstable baseline or fiber volley PTP change exceeding 10% were excluded from analysis.

A12. Author contributions

Giovanni Coppola and Riki Kawaguchi at the University of California, Los Angeles performed the RNA sequencing experiments and analysis and wrote the RNAseq methods. Thomas Seyfried and Kevin Santos at Boston College performed ganglioside experiments and wrote respective methods and figure legends. Samuel Tuck and Joseph Corey at the University of Michigan generated polysterene fibers. Guy Lenk generated *Fig4*$^{-/flox}$*, Olig2Cre,NSE-Fig4*

mice and performed *NSE-Fig4* RT-PCR. Roman J. Giger did optic nerve ISH and staining. A1-A5 were written together with Roman J. Giger.

A13. Acknowledgements
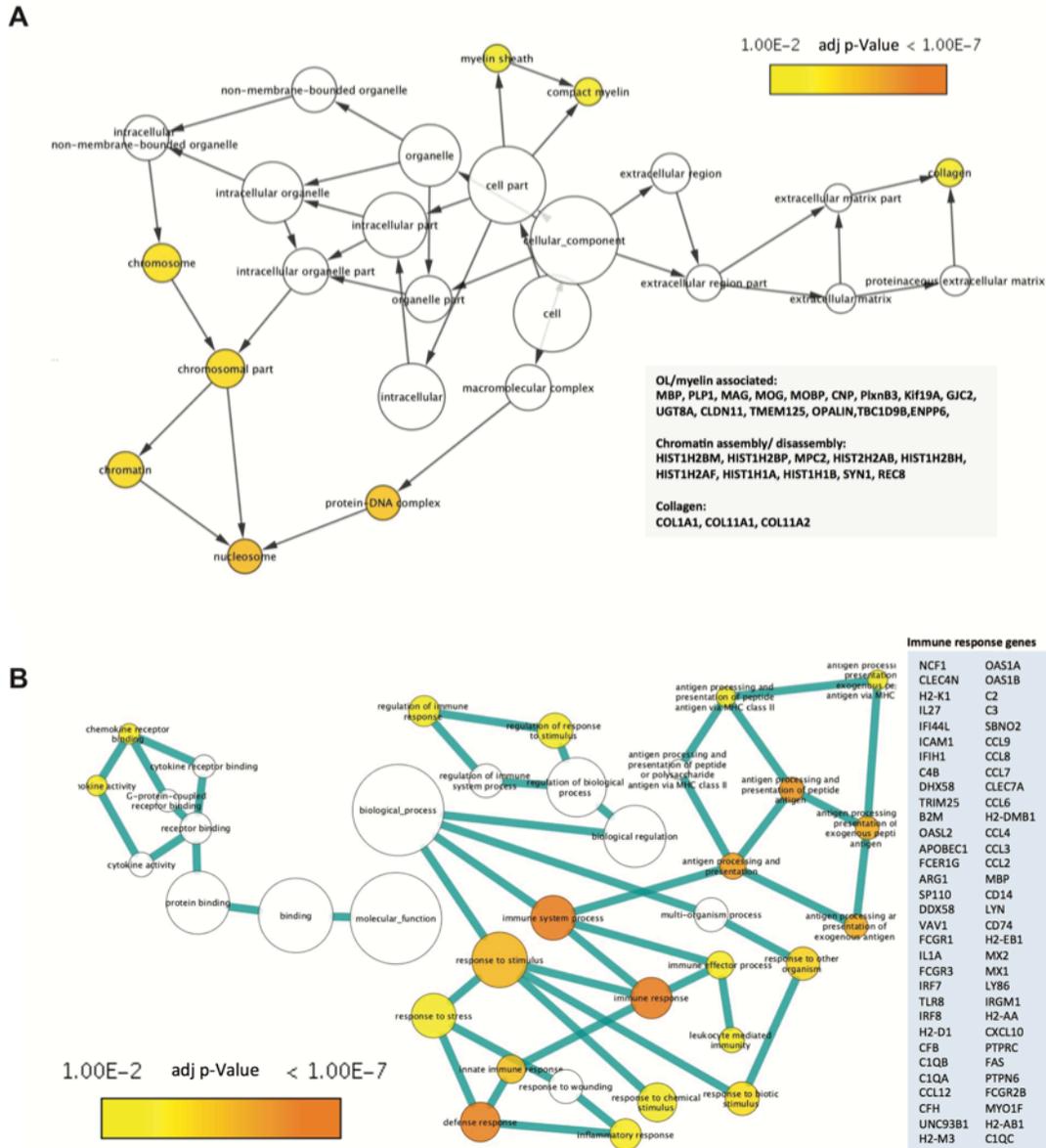
Figure A1. Profiling of *Fig4*-dependent gene expression in the developing mouse.
(A) Graphic representation of GO enrichments for genes that are down-regulated in *Fig4*$^{-/-}$
forebrain tissue prepared from P10 pups. Genes associated with late-stage OL development are
significantly reduced. In addition, genes associated with chromatin structure are down-regulated.
A total of 6 littermate mice were subjected to RNA-sequencing, *Fig4*$^{-/-}$ pups (n= 3) and *Fig4*$^{+/+}$
pups (n= 3). Statistical analysis: BiNGO, FDR <0.01. The size of the circle is proportional to
the number of genes in the category. **(B)** Graphic representation of GO enrichments for genes
upregulated in P10 forebrain tissue of *Fig4*$^{-/-}$ mice. The majority of genes fall into "immune
system processes", suggesting that loss of *Fig4* triggers a strong neuro-inflammatory response.
Statistical analysis: BiNGO, FDR <0.01. The size of the circle is proportional to the number of
genes in the category. Data/Image credit: Drs. Riki Kawaguchi and Giovanni Coppola, UCLA.
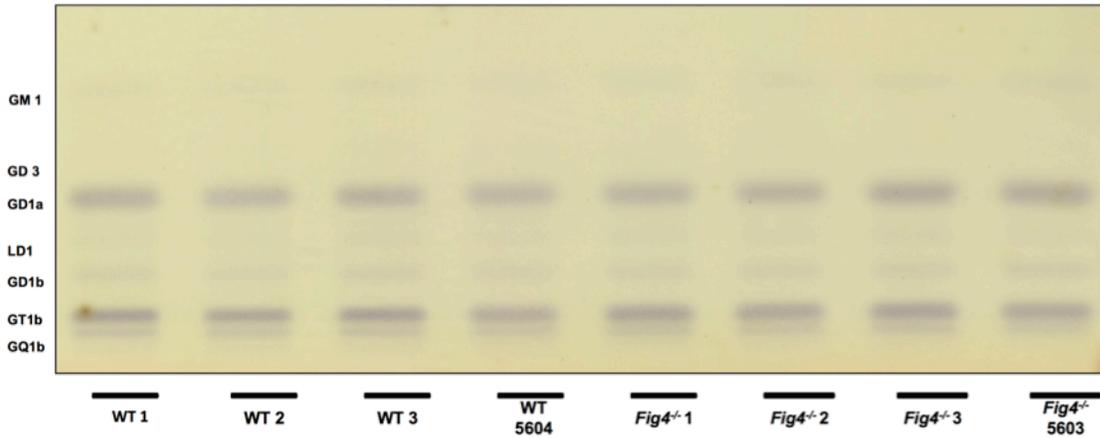
Figure A2. High Performance thin-layer chromatogram of whole brain ganglioside distribution in WT and *Fig4^-/-* mice. Approximately 1.5 μg of gangiloside sialic acid was spotted for each sample. The plate was developed by one ascending run with chloroform:methanol:water: (55:45:10 by vol) that contained 0.02%CaCl$_2$:H$_2$O. The bands were visualized by the resorcinol-HCL spray and heating at 95ºC for 10 min. Data/image credit: Dr. Thomas Seyfried and Kevin Santos.

211
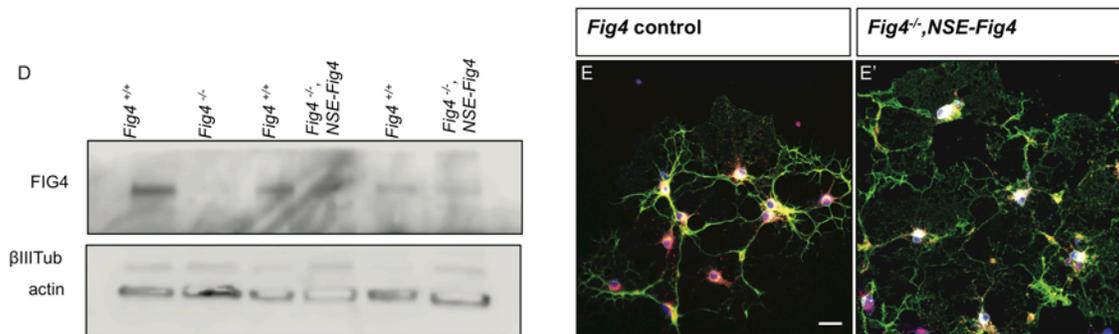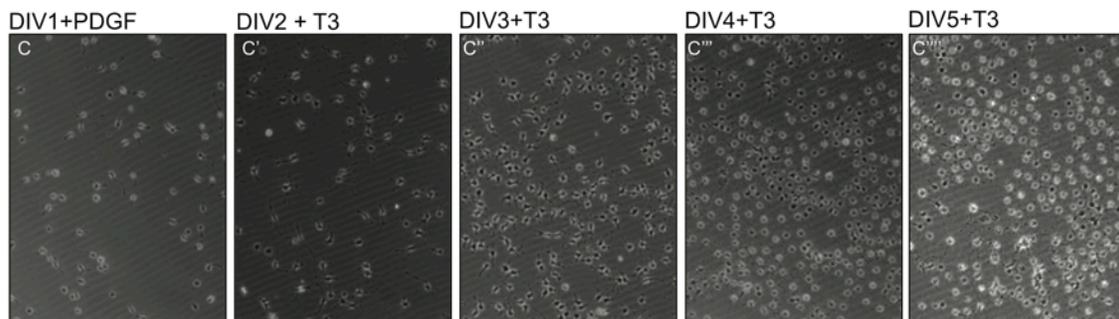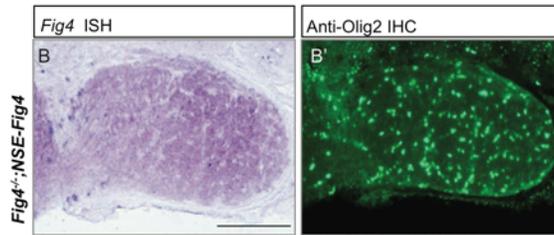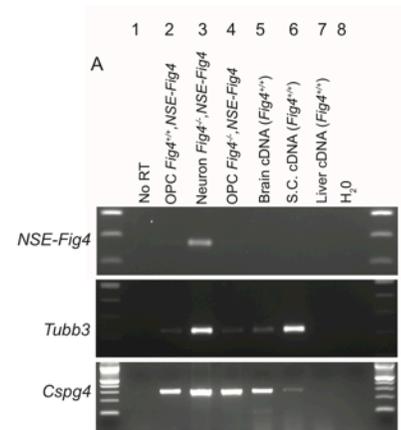
Figure A3.1 Abundance of the *NSE-Fig4* mRNA in OLs is below detection limit, but *$Fig4^{-/-}$,NSE-Fig4* OPCs/OLs display normal morphology and detectable FIG4 protein. (A) RT-PCR analysis of primary OPCs prepared from *$Fig4^{+/+}$,NSE-Fig4* and *$Fig4^{-/-}$,NSE-Fig4* pups using the anti-PDGFRα immunopanning method. *NSE* promoter-driven transgene expression was detected with a forward primer in exon 1 of the *NSE* gene and a reverse primer in exon 2 of the *Fig4* gene. As a positive control for the *NSE-Fig4* RT-PCR, we used cells not captured by the anti-PDGFRα immunopanning (Neuron *$Fig4^{-/-}$,NSE-Fig4* lane) and obtained a 228-bp product. In OPCs from *$Fig4^{+/+}$,NSE-Fig4* or *$Fig4^{-/-}$,NSE-Fig4* mice transgene expression is greatly decreased and near the detection limit. The small amount of *NSE-Fig4* in OPC cultures is likely the result of a small amount of neuronal contamination, as assessed by RT-PCR for *Tubb3* transcript (228-bp product). cDNA prepared from wildtype brain, spinal cord (s.c) and liver served as negative controls. As positive control for neuronal expression, RT-PCR for tubb3 was performed. As positive control for OPCs, we used PCR primers specific for *Cspg4* (336-bp product). **(B)** Coronal view of optic nerve section from a P21 *$Fig4^{-/-}$,NSE-Fig4* mice. Distribution of *Fig4* expression was independently assessed by *Fig4 in situ* hybridization on optic nerve cross-sections of P21 *$Fig4^{-/-}$,NSE-Fig4* mice. A small number of labeled cells are found in the optic nerve. **(B')** The same section was stained with anti-Olig2 to assess distribution of OPCs/OLs. The vast majority of Olig2$^+$ cells do not express *Fig4* mRNA. **(C-C'''')** Phase contrast images of *$Fig4^{-/-}$,NSE Fig4* OPCs/OLs at different stages of maturation. The OPCs/OLs are from the same preparation used for RT-PCR in **(A).** Unlike *$Fig4^{-/-}$* OPCs/OLs, *$Fig4^{-/-}$,NSE-Fig4* OLs do not demonstrate abnormal vesicular accumulation in proliferative (PDGF$^+$) or differentiative (T3$^+$) culture conditions. **(D)** Western blot analysis of *$Fig4^{+/+}$*, *$Fig4^{-/-}$,* and *$Fig4^{-/-}$,NSE-Fig4* OLs probed with anti-FIG4, anti-actin, and anti βIIITub. *$Fig4^{-/-}$,NSE-Fig4* lanes are duplicates of the same sample. **(E)** Representative images of mature *Fig4* control and *$Fig4^{-/-}$,NSE* Fig4 OLs stained with anti-LAMP1 (red), anti-MAG (green), and nuclear marker TO-Pro-3. Abnormal LAMP1 structures are not observed in *$Fig4^{-/-}$,NSE-Fig4* OLs. Scale bar = 20µm. n=1 experiments for biochemistry and n=2 for cell culture. Data/image credit: Figure **A**: Dr. Guy Lenk, Figure **B-B'**: Dr. Roman Giger.
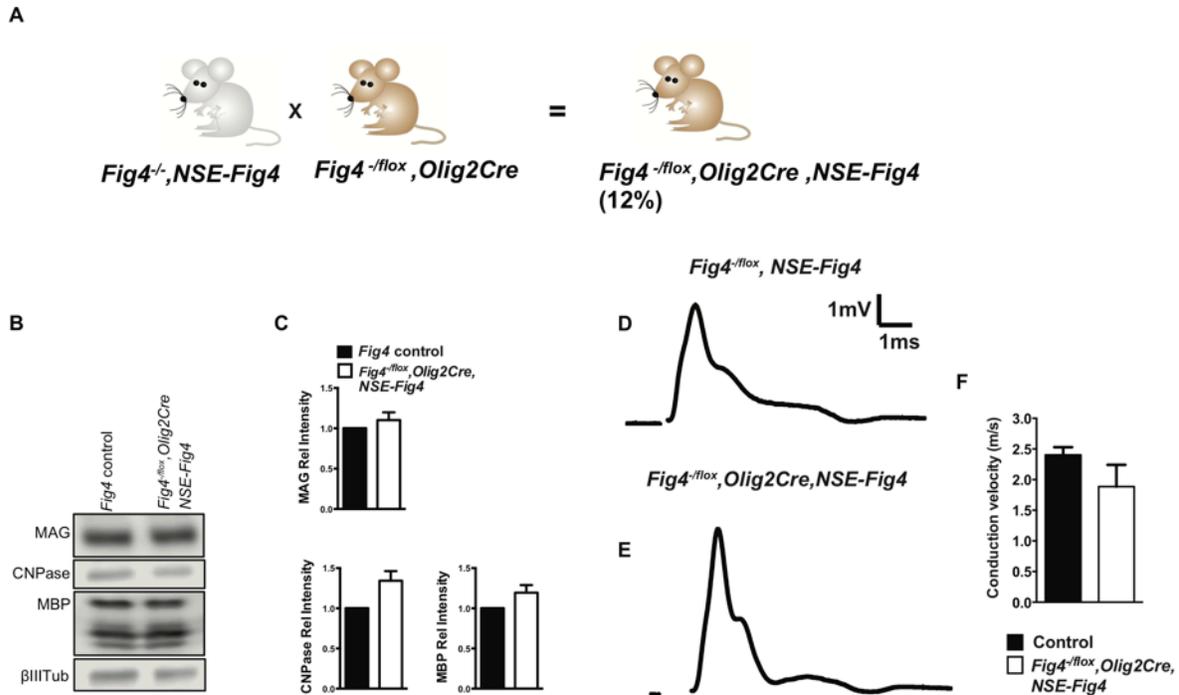
Figure A3.2 Overexpression of recombinant *Fig4* in neurons rescues the hypo-myelination phenotype in *Fig4⁻/flox,Olig2Cre* mice. (A) Breeding strategy for generating *Fig⁻/flox,Olig2Cre,NSE-Fig4* mice. **(B)** Western blot analysis of P26-P48 brain membranes prepared from control mice (*Fig4⁻/flox,* and *Fig4⁺/flox*, n= 3 brains) and *Fig4⁻/flox,Olig2Cre,NSE-Fig4* mice (n = 4 brains) probed with anti-MAG, anti-CNPase, anti-MBP and the neuronal marker class III β-tubulin (βIII Tub). **(C)** Quantification of relative protein signals for MAG, CNPase, and MBP normalized to βIII Tub. Results are shown as mean value ±SEM, unpaired two-tailed Student's *t*-test revealed no significant differences. **(D and E)** Representative CAP traces recorded from P36 (control) *NSE-Fig4,Fig4⁻/flox* (n= 4 nerves, 2 animals) and *NSE-Fig4,Fig4⁻/flox,Olig2Cre* (n= 6 nerves, 3 animals) littermates reveal no difference in the population of fast conducting fibers. **(F)** Quantification of average conduction velocity of largest amplitude peaks identified in **D** and **E**. Results are shown as mean value ±SEM, Unpaired Student's *t*-test. *P*-value = 0.29.
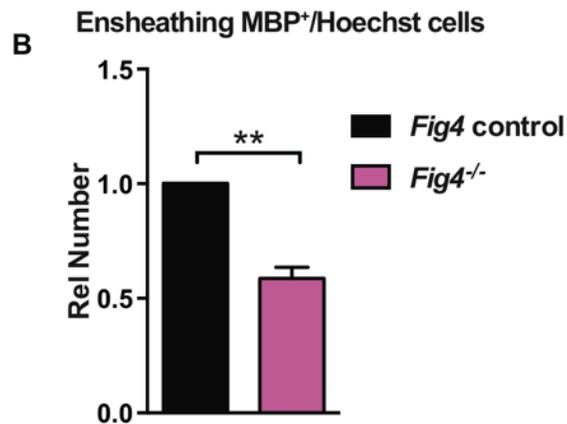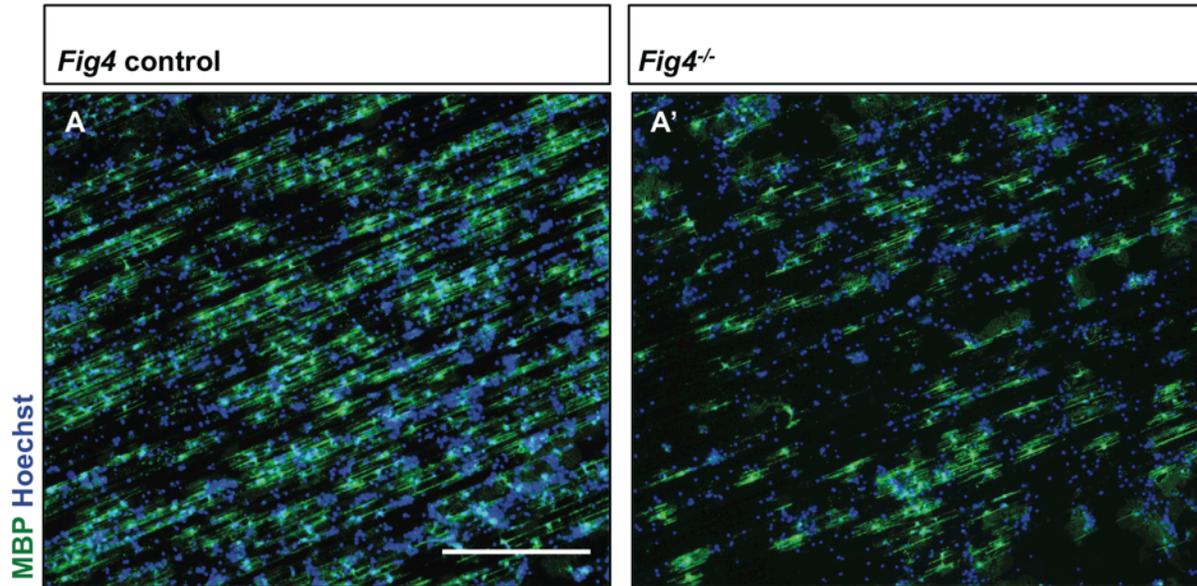
Figure A4. Primary OLs from *Fig4*^{-/-} mice do ensheath nanofibers. (A-A') Primary OLs from *Fig4* control *(Fig4^{+/+}* or *Fig4^{+/-})* and *Fig4^{-/-}* pups were plated on 1-1.5 μm polystyrene fibers and cultured for 7 days. To visualize mature OLs, cultures were fixed and stained with anti-MBP (green) and Hoechst 33342 dye to monitor total cell density. (**B**) Quantification of the number of MBP$^+$ cells ensheathing nanofibers normalized to total number of Hoechst$^+$ cells per region of interest. While the number of MBP$^+$ cells in *Fig4^{-/-}* cultures is reduced, these cells do ensheath fibers. Results are shown as mean value ±SEM, unpaired Student's *t*-test. **p-value = 0.0011.
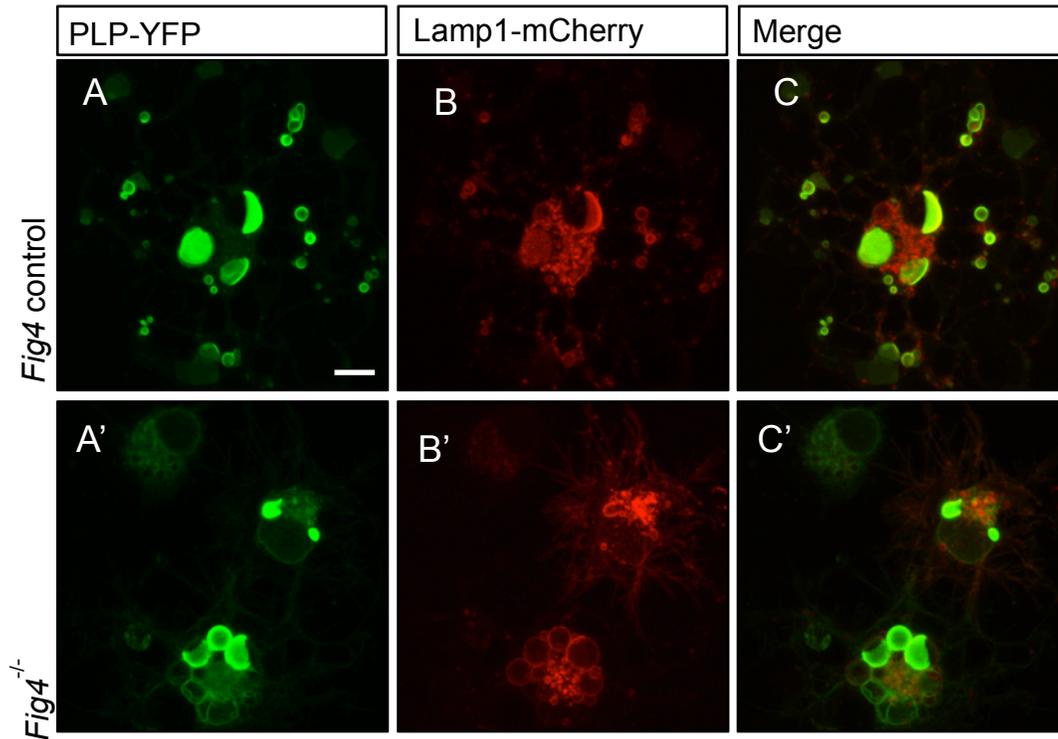
Figure A5.1 In *Fig4⁻ᐟ⁻* OLs, PLP-YFP is present in LAMP1-mCherry positive vacuoles. Representative confocal images of (**A-C**) *Fig4* control (*Fig4⁺ᐟ⁺* or *Fig4⁺⁻* OLs) and (**B'-C'**) *Fig4⁻ᐟ⁻* OLs transfected with *PLP-YFP* and *Lamp1-mCherry* expression constructs. In *Fig4⁺ᐟ⁺* and in *Fig4⁻ᐟ⁻* OLs, PLP-YFP shows co-localization with LAMP1-mCherry. In *Fig4* control and mutant OLs, PLP-YFP forms aggregates. In *Fig4⁻ᐟ⁻* OLs, this includes large perinuclear vacuoles. Scale bar = 7.5 μm.
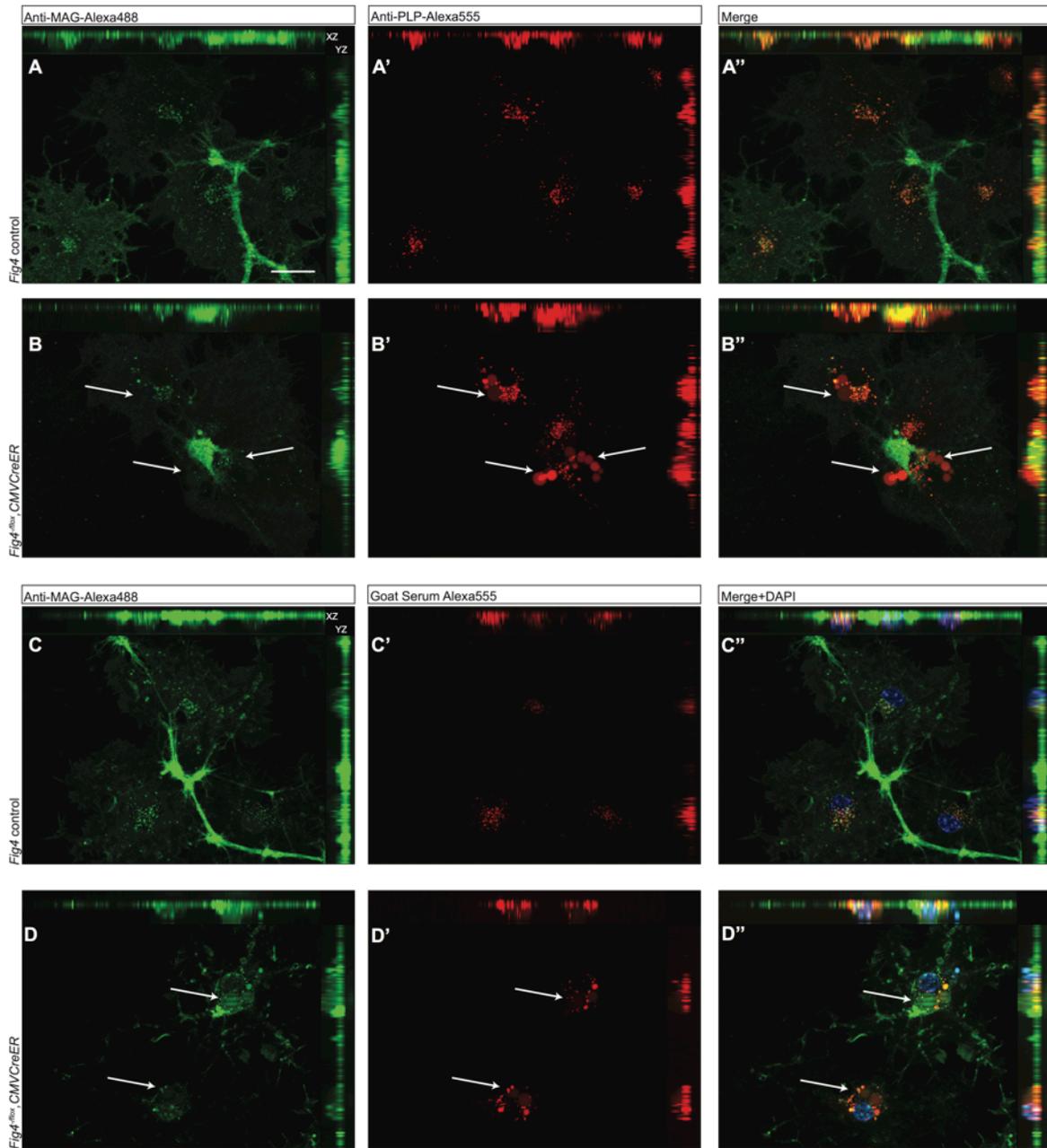
Figure A5.2 Labeled PLP antibody trafficking in WT and *Fig4*-deficient OLs. **(A-B''')** Representative images of live *Fig4* control and *Fig4⁻/flox,CMVCreER* DIV3 OLs incubated with anti-MAG-Alexa488 and anti-PLP-Alexa555. Large vacuoles intensely positive for PLP are observed in *Fig⁻/flox,CMVCreER* OLs, but in not control cells (arrows) **(C-D")** Representative images of the same cell cohort incubated with anti-MAG-Alexa488 and goat serum conjugated to Alexa555. Some Alexa555 signal is observed in both control and *Fig4⁻/flox,CMVCreER* cells, albeit at diminished intensity compared to anti-PLP-Alexa555. All images are maximum Z stack projections with XZ and YZ orthogonal sections shown as indicated. Scale bar = 20μm. N=1.

A6. Myelin regulatory factor (Myrf or MRF) is expressed and processed normally in *Fig4*^{-/-}
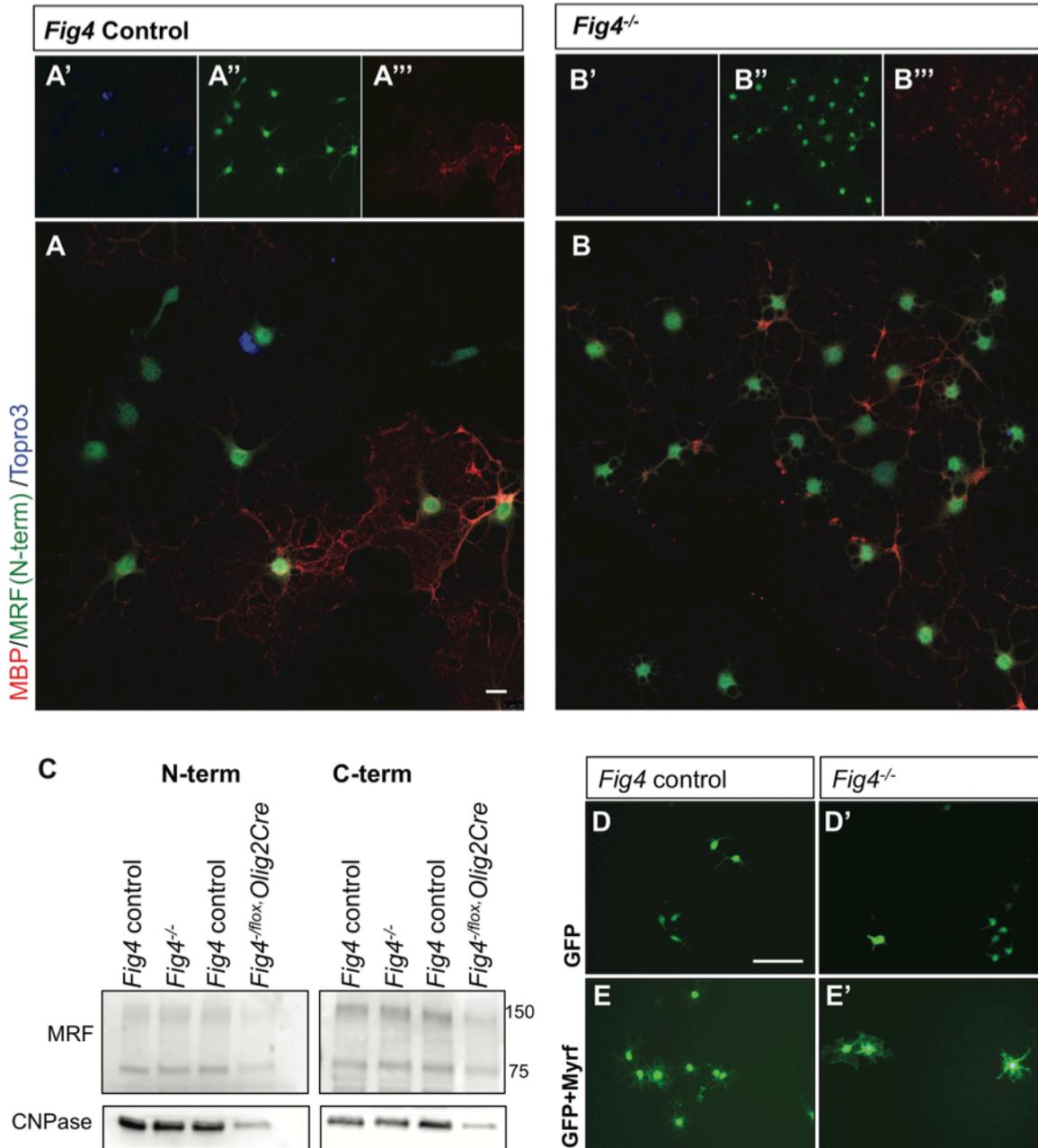
A6. Myelin regulatory factor (Myrf or MRF) is expressed and processed normally in *Fig4*$^{-/-}$ OLs. **(A-B''')** Representative confocal images of DIV4 *Fig4* control and *Fig4*$^{-/-}$ OLs stained with antibodies against MBP, MRF N-terminus and nuclear marker To-Pro-3. The anti-MRF antibody recognizes full length MRF localized to the ER and the cleaved N-terminus portion that gets transported to the nucleus. A similar MRF signal distribution is observed in *Fig4* control and *Fig4*$^{-/-}$ OLs despite their altered morphology and diminished MBP signal. Scale bar = 10 μm, N=2. **(C)** Western blots of *Fig4* control, *Fig4*$^{-/-}$, and *Fig4*$^{-/flox,}$*Olig2Cre* DIV3 OL lysates probed with antibodies against N- and C-terminus MRF and CNPase as a loading control. Full-length MRF is detected by both antibodies at 140 kDa and both cleaved forms are ~70-75kDa. No

obvious differences in MRF cleavage and expression levels are observed in *Fig4*-deficient OLs when accounted for CNPase levels. **(D-E')** Representative images of *Fig4* control and *Fig4*$^{-/-}$ OPCs transfected with either *GFP* or *GFP+Flag-Myrf-Myc* at 24 hours post-infection (DIV2). With GFP transfection only, both *Fig4* control and *Fig4*$^{-/-}$ OPCs maintain simple morphology. *Myrf* co-expression induces precocious differentiation and ramified morphology in both *Fig4* control and *Fig4*$^{-/-}$ OPCs. Scale bar = 50 μm. N=2.
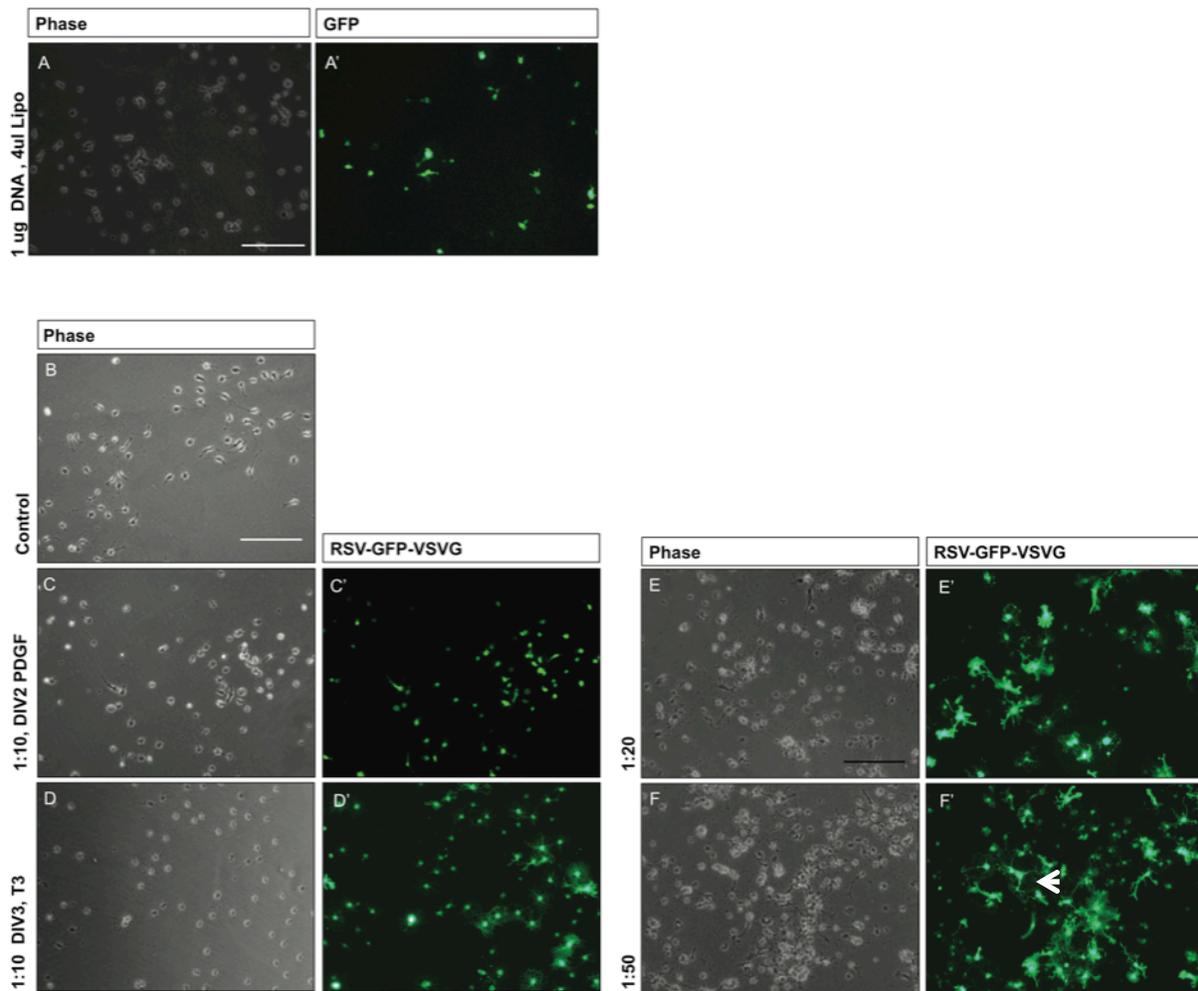
A7.1 Transfection and infection strategies for cultured OPCs/OLs *in vitro*. (A-A') DIV2 OPCs transfected with 1 μg GFP DNA and 4 μl Lipofectamine-2000. A high percentage of GFP⁺ cells is observed as early as the following day after transfection. Scale bar = 200 μm. **(B-C')** Control (**B**, no virus), and Lenti-RSV-GFP-VSVG (**C-C'**) infected cells at DIV2, 24 hours post-infection. A high number of GFP⁺ cells is observed, but cell health is poor compared to the control cultures. **(D-D')** Cells pictured in **(C-C')** were passaged and allowed to differentiate in T3 medium for 3 days. Ramified GFP⁺ cells are easily observed. **(E-F')** Passaged OPCs were infected with diluted GFP virus stock and allowed to differentiate in T3 medium for 3 days. Robust GFP expression is observed at lower viral titer, and GFP⁺ cells are capable of making membrane sheets (**F'**, arrow). Scale bar = 200 μm.
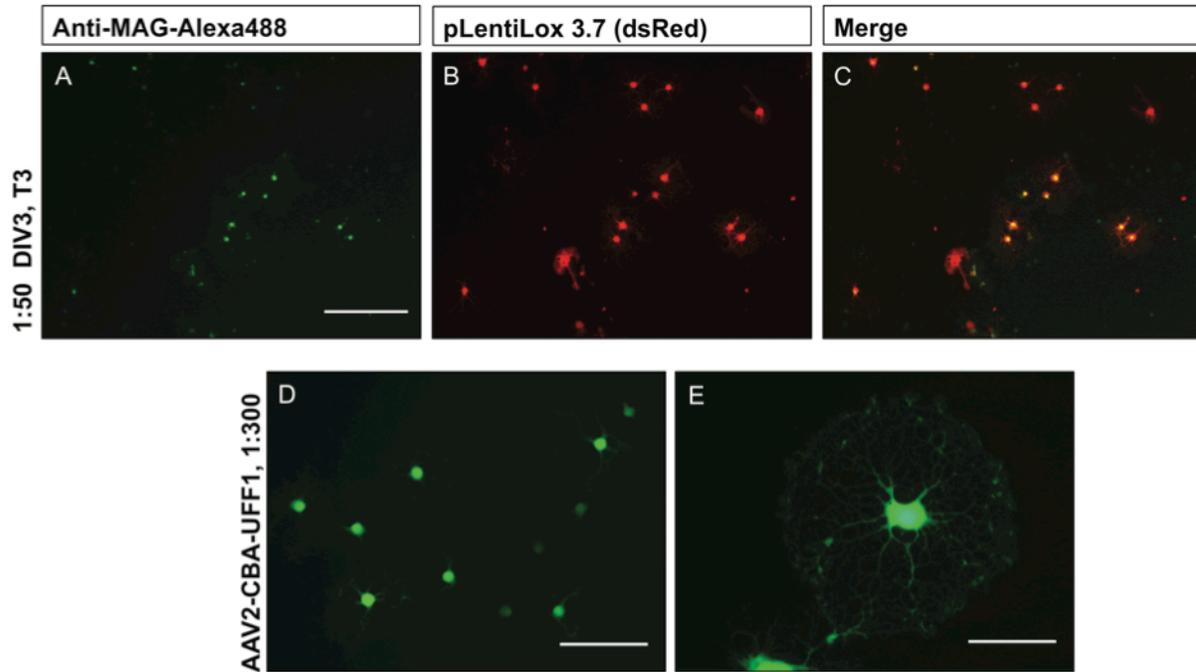
A7.2 Transfection and infection strategies for cultured OPCs/OLs *in vitro*. (A-C) Passaged OPCs were infected with Lentilox-3.7.-dsRed, cultured in T3 medium for 3 days and treated with anti-MAG-Alexa488 antibody. Scale bar = 200 µm. **(D-E)** Representative images of OLs treated with AAV2-CBA-UFF1 virus 3 days after infection. A robust GFP signal is observed even in fully flattened, mature OLs **(E)**. Scale bar = 100 µm **(D)**, 50 µm **(E)**.
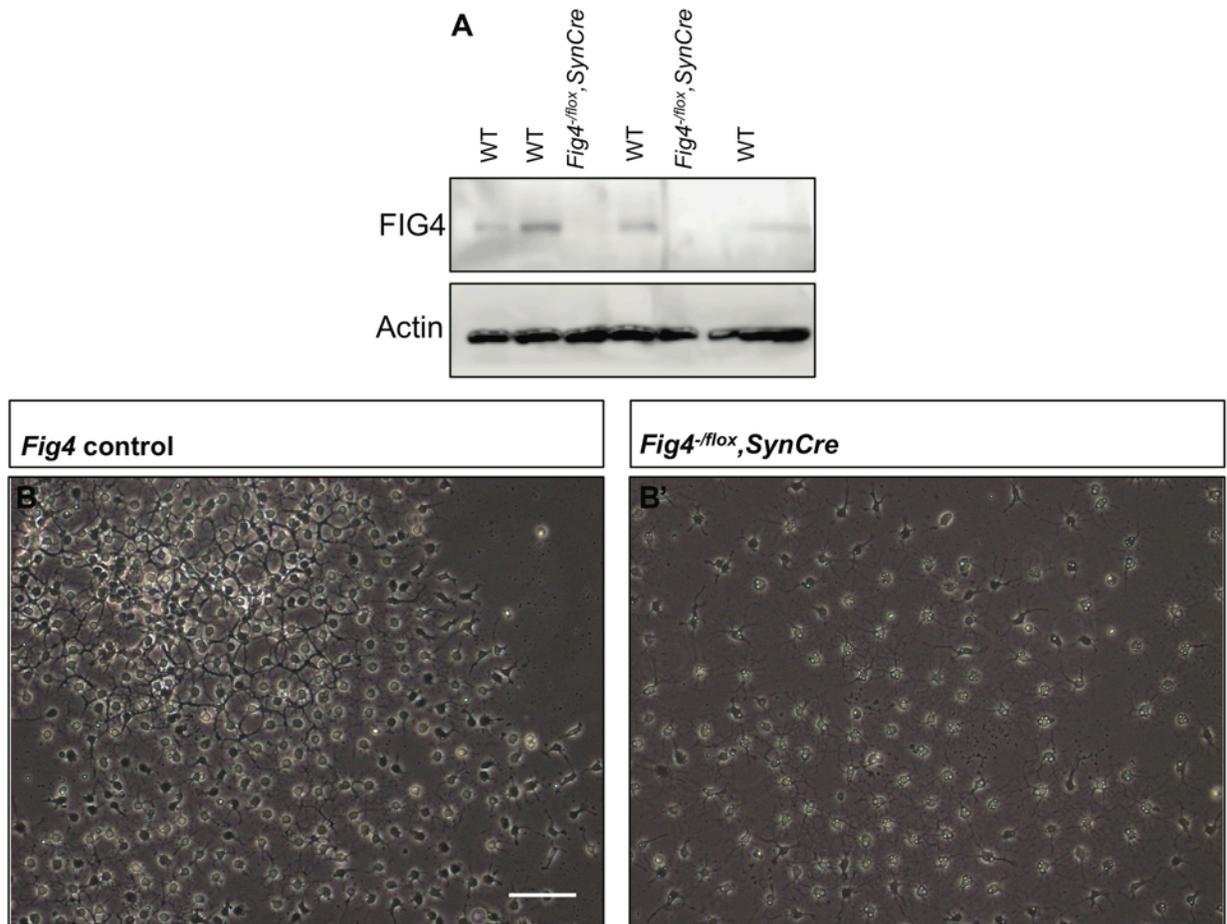
Figure A8.1 *SynapsinCre* expression in the OL lineage. (A) Western blots of *Fig4* control (WT) and *Fig4^{-/flox}*,*SynCre* DIV3 OL lysates probed with anti-FIG4 and anti-actin as a loading control. Duplicate wells were loaded for *Fig4^{-/flox}*,*SynCre* OLs. No detectable FIG4 100kDa band is observed in *Fig4^{-/flox}*,*SynCre* cultures. N=1. **(B-B')** Representative phase contrast images of *Fig4* control and *Fig4^{-/flox,}SynCre* OLs at DIV3. Increased vacuolation is observed in *Fig4^{-/flox}*,*SynCre*, but not control, cultures. Scale bar = 200 μm. N=1.
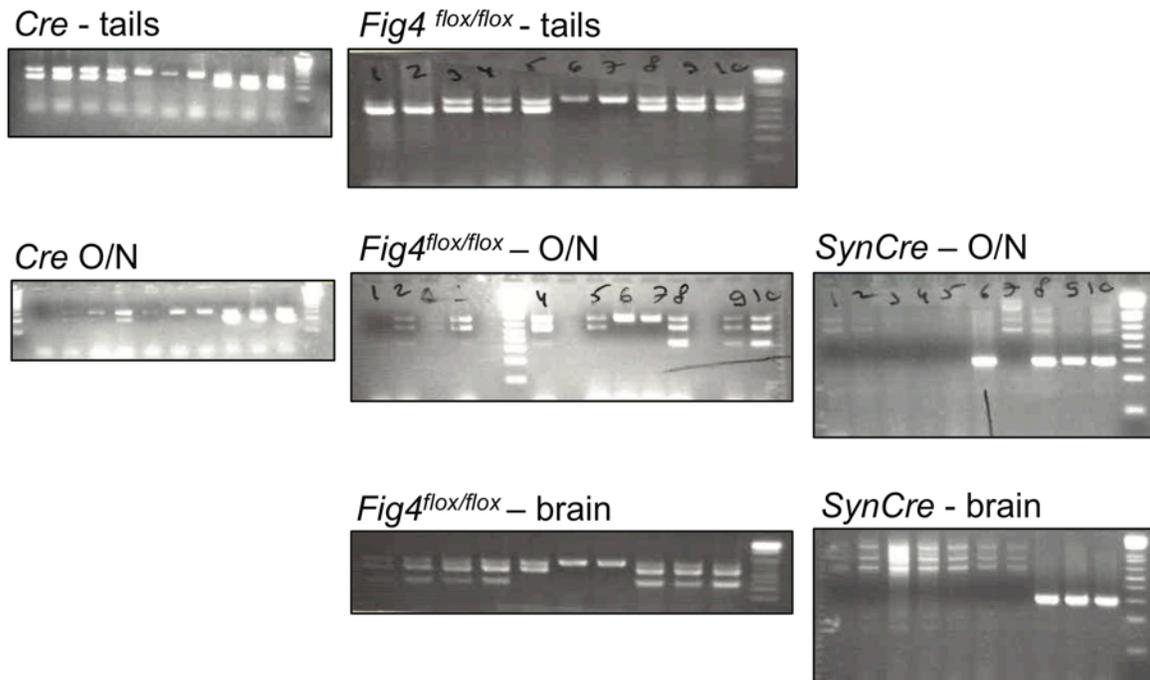
Figure A8.2 *Fig4 floxed* allele recombination in various tissues. Representative genotyping PCR of tail, brain, and whole optic nerve biopsies isolated from *Fig4$^{+/flox}$,Olig2Cre* (1-4), *Fig4$^{flox/+}$* (5), *Fig4$^{flox/flox}$* (6-7), and *Fig4$^{+/flox}$,SynCre* (8-10) mice. The *Cre* genotyping product at 200 bp is readily observed in the tail tissue and somewhat less robustly in the optic nerve samples. *Fig4 floxed* (679 bp) and *WT* (558 bp) products are detected in tail biopsies. In the optic nerves and brain tissue, "*deleted*" *Fig4* product (282 bp) was observed in both *Olig2Cre* and *SynCre* samples. *SynCre*-specific 300 bp product was observed only in the *SynCre$^+$* tissue (with the exception of the animal #6 most likely due to contamination).
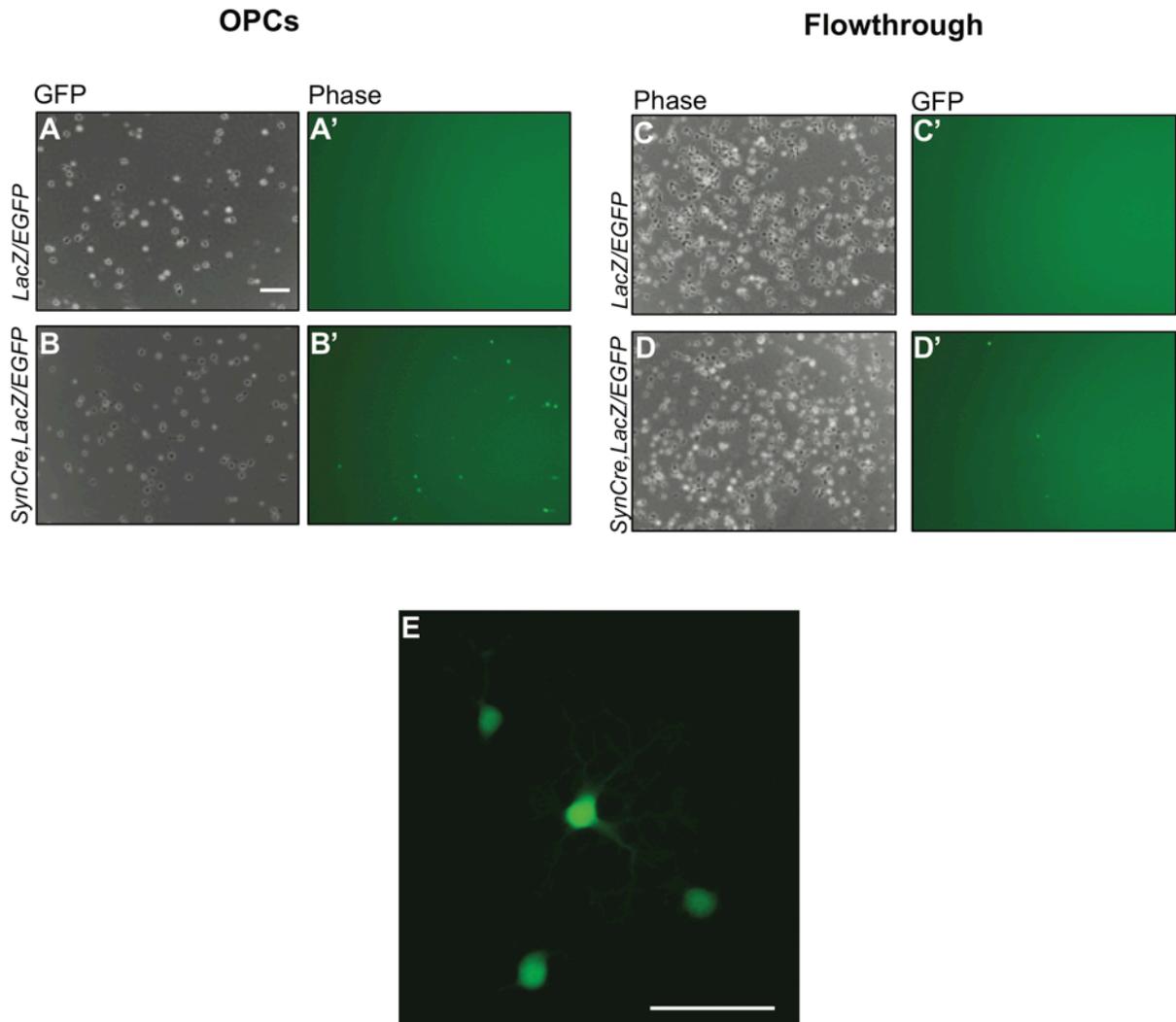
Figure A8.3 Reporter expression in *LacZ/EGFP,SynCre* OL lineage. (A-B') Representative images of cultured DIV1 OPCs isolated from *LacZ/EGFP* and *LacZ/EGFP,SynCre* pups. Faint GFP signal is detected in *LacZ/EGFP,SynCre* cultures. **(C-D")** Representative images of the "flowthrough" culture (PDGFRα⁻, O4⁻), presumably containing neurons. Faint GFP signal is detected in *LacZ/EGFP,SynCre* cultures. Scale bar = 200 μm. **(E)** A higher magnification image of *LacZ/EGFP,SynCre* OLs expressing GFP at DIV2. Scale bar = 50 μm. N=1.
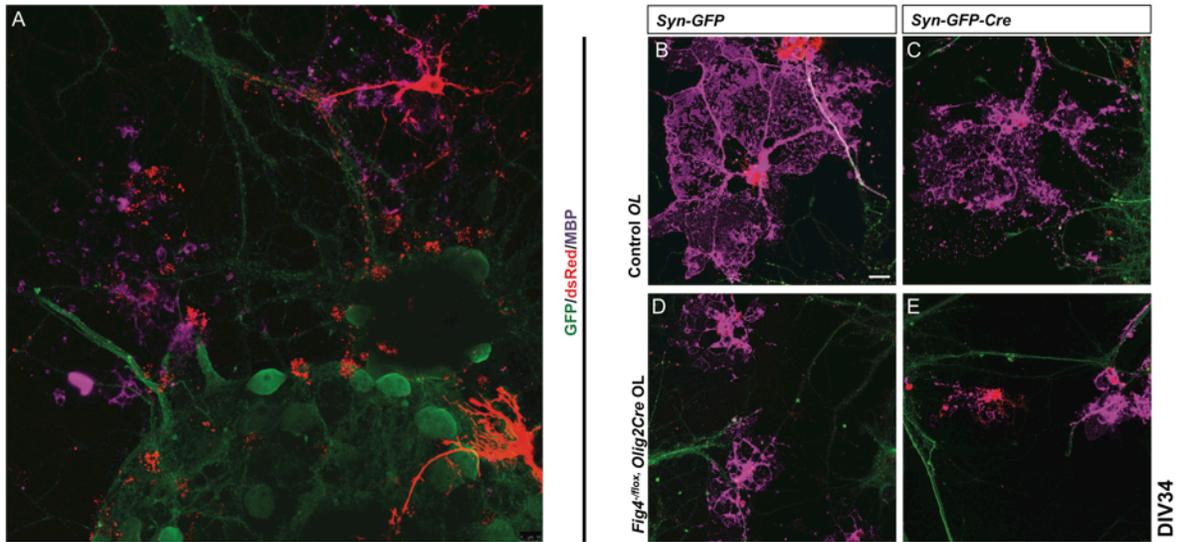
Figure A9. Differential *Fig4* expression in neuron-OL co-cultures. (A) A representative image of a hippocampal neuron – OL co-culture at DIV34. Lenti-Synapsin-GFP neurons are robustly GFP-positive and dsREd$^+$ cells are observed with or without MBP expression (magenta). Scale bar = 10μm. **(B-E)** Representative confocal images of neuron-OL co-cultures with *Fig4$^{flox/flox}$* neurons either infected with Lenti-Synapsin-GFP or Lenti-Synapsin-GFPCre, and dsRed infected OLs are either *Fig4* control, or *Fig4$^{-/flox,}$Olig2Cre*. **(B)** A robust, fully mature MBP$^+$ OL is observed making myelinating contact with a GFP$^+$ axon. **(C)** Qualitatively, fewer MBP$^+$/dsRed$^+$ OLs are observed in cultures where neurons are infected with Lenti-Synapsin-GFPCre. *Fig4^{flox,}Olig2Cre* OLs display reduced membrane MBP$^+$ sheet expansion regardless of neuronal genotype . Scale bar =10μm.
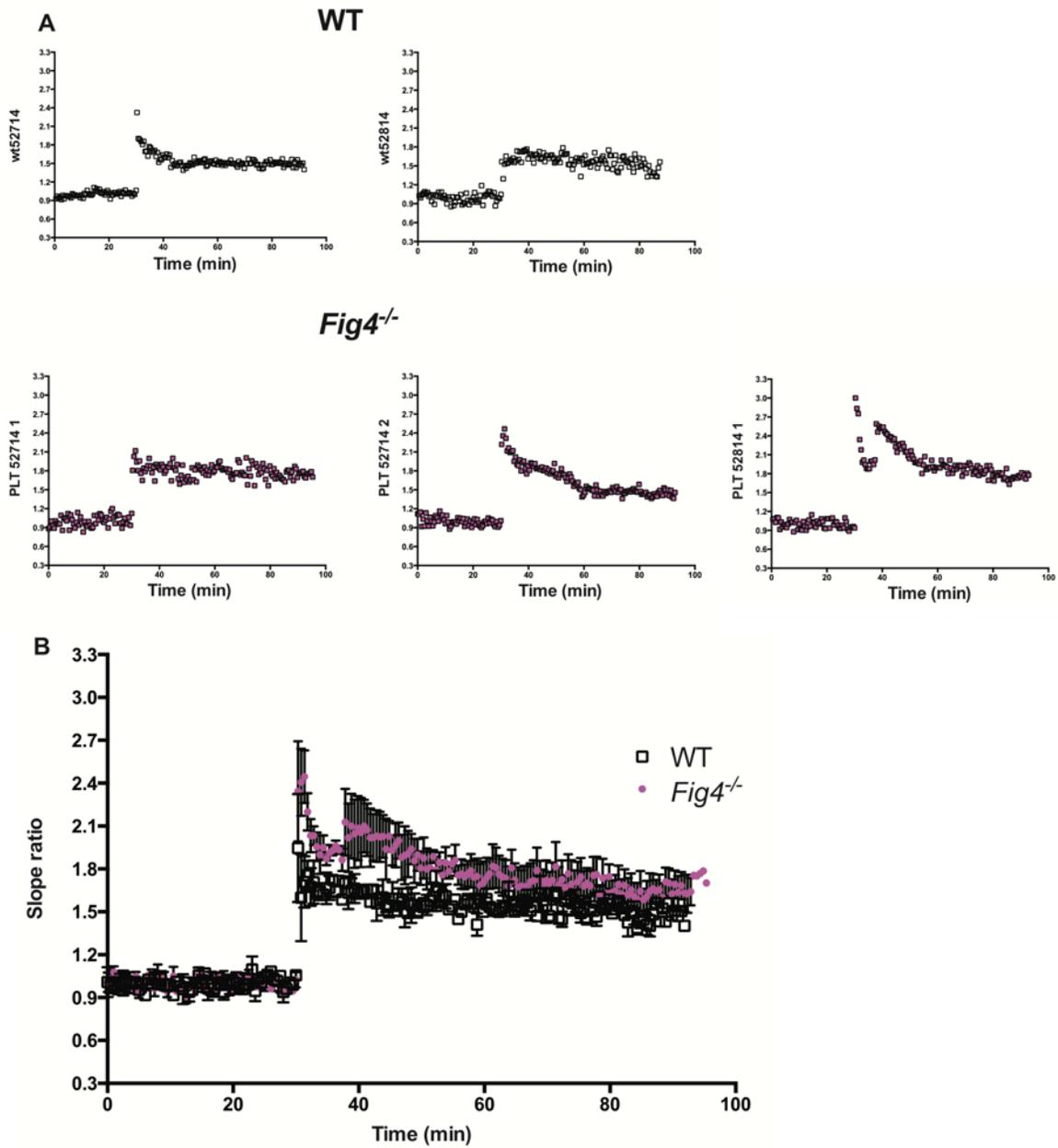
A10. Enhanced hippocampal LTP in *Fig4*^-/- juvenile CA3-CA1. (A) Raw data traces of WT and *Fig4*^-/- hippocampal LTP, individual slice recordings. **(B)** Averaged traces demonstrating a trend towards enhanced LTP in *Fig4*^-/- slices. Data collected from two animals/genotype.

gene	refSeq	PI(3,5)P2 metabolism and signaling	rank	logFC_Fig4-/-_vs_WT	p Value	FDR_WT_vs_Fig4-/-
Fig4	NM_133999	FIG4 homolog (S. cerevisiae)	4797	-1.03	3.97E-28	7.44E-25
Pikfyve	NM_011086	phosphoinositide kinase, FYVE finger containing	2031	0.06	0.5	0.9
Vac14	NM_146216	Vac14 homolog (S. cerevisiae)	8541	-0.31	0.01	0.22
Mcoln1	NM_053177	mucolipin 1 (TRPML1)	5141	-0.09	0.38	0.85
Tpcn1	NM_145853	two pore channel 1	8542	0.03	0.8	0.98
Tpcn2	NM_146206	two pore segment channel 2	12485	-0.56	0.01	0.23
Rab7	NM_009005	RAB7, member RAS oncogene family	1429	-0.12	0.17	0.74
Cttn	NM_007803	cortactin	1026	-0.13	0.14	0.69
Dnm1	NM_010065	dynamin 1	604	0.08	0.46	0.9
Rabepk	NM_145522	Rab9 effector protein with kelch motifs	7915	0.02	0.85	0.99
Mcoln3	NM_134160	mucolipin 3 (TRPML3)	16969	-0.78	0.18	0.74
Snx10	NM_028035	sorting nexin 10	915	0.04	0.61	0.94
Snx11	NM_028965	sorting nexin 11	6392	0.02	0.83	0.98
Wipi1	NM_145940	WD repeat domain, phosphoinositide interacting 1	9573	0.11	0.38	0.85
Wipi2	NM_178398	WD repeat domain, phosphoinositide interacting 2	2451	0.04	0.65	0.95

Table A1. Expression of gene products previously implicated in PI(3,5)P$_2$ metabolism or signaling is not regulated in *Fig4$^{-/-}$* forebrain tissue. As expected, *Fig4* transcript levels are significantly reduced in *Fig4$^{-/-}$* tissue. However other components of the PI(3,5)P$_2$ biosynthetic complex or molecules implicated in PI(3,5)P$_2$ signaling are not regulated at the transcriptional level in the absence of Fig4. The log$_2$ fold-change in gene expression of *Fig4$^{-/-}$* versus WT tissue is shown (logFC *Fig4$^{-/-}$* vs WT). *p* values and false discovery rates (FDR) were calculated. Genes with an FDR of < 0.1 are highlighted in pink. The "rank" indicates the relative abundance of expression in WT forebrain tissue.

gene	refSeq	protein (OPC enriched)	rank	logFC_Fig4-/-_vs_WT	p Value	FDR_WT_vs_Fig4-/-
Pdgfra	NM_011058	platelet derived growth factor receptor, alpha polypeptide	1162	-0.149577332	0.087334573	0.631836029
Lnx1	NM_010727	ligand of numb-protein X 1	5524	-0.193003247	0.075603121	0.59838446
Dcn	NM_007833	decorin	4732	-0.013877283	0.879034987	0.995262602
Mmp15	NM_008609	matrix metallopeptidase 15	7311	-0.089748328	0.466922545	0.897057322
Cdo1	NM_033037	cysteine dioxygenase 1, cytosolic	3100	0.053854238	0.529312495	0.925433698
Kcnk1	NM_008430	potassium channel, subfamily K, member 1	5111	-0.308907438	0.026902952	0.434332716
Rasgrf1	NM_011245	RAS protein-specific guanine nucleotide-releasing factor 1	4620	-0.055507748	0.668972198	0.952562845
Pcdh15	NM_023115	protocadherin 15	4461	-0.00491355	0.955148939	0.999799332
Chrna4	NM_015730	cholinergic receptor, nicotinic, alpha polypeptide 4	8757	-0.067562474	0.623788204	0.94471845
Dll3	NM_007866	delta-like 3 (Drosophila)	12827	0.090585272	0.667634081	0.951999637
Sstr1	NM_009216	somatostatin receptor 1	3727	-0.080041296	0.348065459	0.837129829
Pnlip	NM_026925	pancreatic lipase	13737	0.040424765	0.868503245	0.992568182
Cspg4	NM_139001	chondroitin sulfate proteoglycan 4	7509	0.160175498	0.212190019	0.767885729
Ppapdc1a	NM_001080963	phosphatidic acid phosphatase type 2 domain containing 1A	13098	-0.009413526	0.966007224	0.999799332
Nxph1	NM_008751	neurexophilin 1	5460	-0.011327519	0.901477643	0.999799332
Ugdh	NM_009466	UDP-glucose dehydrogenase	6061	0.122137811	0.284936764	0.780599739
Slitrk1	NM_199065	SLIT and NTRK-like family, member 1	4131	-0.019255053	0.831880333	0.985921406
Shc4	NM_199022	SHC (Src homology 2 domain containing) family, member 4	10510	0.249952997	0.058596179	0.573310467
Smoc1	NM_022316	SPARC related modular calcium binding 1	10178	0.371866357	0.01230459	0.298027918
Emid1	NM_080595	EMI domain containing 1	6710	-0.065405106	0.606800218	0.942050545
Rlbp1	NM_020599	retinaldehyde binding protein 1	5980	0.139230796	0.186385838	0.766480217
Dcaf12l1	NM_178739	DDB1 and CUL4 associated factor 12-like 1	6861	-0.301258933	0.015274092	0.336366993
Lhfpl3	NM_029990	lipoma HMGIC fusion partner-like 3	3526	-0.016462791	0.852121758	0.988988046
Myt1	NM_008665	myelin transcription factor 1	5321	0.044588394	0.624696548	0.945099571
C1ql1	NM_011795	complement component 1, q subcomponent-like 1	11295	-0.25288273	0.17052568	0.742763299
Tmem179	NM_178915	transmembrane protein 179	2922	-0.152981459	0.099098144	0.668726535
Megf11	NM_172522	multiple EGF-like-domains 11	8812	-0.10034292	0.437021658	0.88185921
Ncald	NM_134094	neurocalcin delta	135	-0.112025475	0.23488542	0.767885729
Sdc3	NM_011520	syndecan 3	1112	-0.055095071	0.552969155	0.933364902
Rprm	NM_023396	reprimo, TP53 dependent G2 arrest mediator candidate	4299	0.130538723	0.176772232	0.751327239
Cacng4	NM_019431	calcium channel, voltage-dependent, gamma subunit 4	8837	0.007743716	0.955880731	0.999799332
Grin3a	NM_001033351	glutamate receptor ionotropic, NMDA3A	2094	-0.176802422	0.059780544	0.577662867
Gsx1	NM_008178	GS homeobox 1	16099	-0.760412425	0.042443877	0.497990475
Sox3	NM_009237	SRY-box containing gene 3	14711	-0.265905167	0.346502135	0.836412692
Sox6	NM_011445	SRY-box containing gene 6	5359	0.069337678	0.484576251	0.907338758
Nkx2-2	NM_010919	NK2 transcription factor related, locus 2 (Drosophila)	13941	-0.077876732	0.780945206	0.976203223

Table A2. Analysis of OPC enriched transcripts. RNA-sequencing was performed on P10 forebrain tissue from $Fig4^{+/+}$ (WT) and $Fig4^{-/-}$ littermate pups. $Fig4$ dependent changes in gene expression were compared to transcripts enriched in oligodendrocyte progenitor cells (OPC) described by Zhang and colleagues (Zhang et al., 2014). A heat-map with $\log_2$ fold-change in gene expression of $Fig4^{-/-}$ versus WT tissue is shown (logFC $Fig4^{-/-}$ vs WT). p values and false discovery rates (FDR) were calculated. Changes in gene expression with p values < 0.05 are shown in red (if increased) or in green (if decreased). The "rank" indicates the relative abundance of expression in WT forebrain.

gene	refSeq	protein (Newly formed OL enriched)	logFC_Fig4-/-_vs_WT	p Value	FDR_WT_vs_Fig4-/-
Gp1bb	NM_010327	glycoprotein Ib, beta polypeptide	-0.266697557	0.080490501	0.608565581
Tmem108	NM_178638	transmembrane protein 108	-0.003026536	0.976818738	0.999799332
Fyn	NM_008054	Fyn proto-oncogene	-0.023469436	0.788544398	0.976907244
Ust	NM_177387	uronyl-2-sulfotransferase	-0.311858173	0.019860292	0.379220086
Mical3	NM_153396	microtubule associated monoxygenase, calponin and LIM domain containing 3	-0.060883965	0.526143553	0.924423497
Kif19a	NM_001102615	kinesin family member 19A	-0.872292852	0.000799499	0.049406169
Nfasc	NM_182716	neurofascin	-0.266672271	0.040309254	0.490718526
Ssh3	NM_198113	slingshot homolog 3 (Drosophila)	-0.074418352	0.493528754	0.910673605
Pik3r3	NM_181585	phosphatidylinositol 3 kinase, regulatory subunit, polypeptide 3 (p55)	-0.149301037	0.137710231	0.674815011
Enpp6	NM_177304	ectonucleotide pyrophosphatase/phosphodiesterase 6	-1.143235776	1.87E-06	0.000266117
Tns3	NM_001083587	tensin 3	-0.185788131	0.195323139	0.767885729
Bmp4	NM_007554	bone morphogenetic protein 4	-0.148436181	0.384051588	0.855791479
Mcl1	NM_008562	myeloid cell leukemia sequence 1	0.053139904	0.540635321	0.929022643
Cdv3	NM_175833	carnitine deficiency-associated gene expressed in ventricle 3	-0.043426919	0.619033189	0.943948194
Tmem163	NM_028135	transmembrane protein 163	-0.199668188	0.108968554	0.672580358
Rap2a	NM_029519	RAS related protein 2a	-0.097721396	0.278676157	0.774963336
Cnksr3	NM_172546	Cnksr family member 3	-0.738745969	0.0088561	0.246687869
Cyfip2	NM_133769	cytoplasmic FMR1 interacting protein 2	-0.172845062	0.102990192	0.672580358
Slc12a2	NM_009194	solute carrier family 12, member 2	-0.028749483	0.779336747	0.975775226
Itpr2	NM_019923	inositol 1,4,5-triphosphate receptor 2	-0.037576178	0.740621756	0.966661307
Rnf122	NM_175136	ring finger protein 122	-0.43195846	0.02886012	0.444631786
Lims2	NM_144862	LIM and senescent cell antigen like domains 2	-0.180200096	0.430427924	0.879408626
Samd4b	NM_175021	sterile alpha motif domain containing 4B	-0.171416664	0.284310078	0.780143855
Chn2	NM_023543	chimerin (chimaerin) 2	-0.002655231	0.976852219	0.999799332
Ppp2r3a	NM_172144	protein phosphatase 2, regulatory subunit B'', alpha	0.039961369	0.712168412	0.962549772
Glrb	NM_010298	glycine receptor, beta subunit	-0.09261223	0.311668237	0.806458583
Rras2	NM_025846	related RAS viral (r-ras) oncogene homolog 2	-0.176427497	0.07324619	0.594968244
Fmnl2	NM_172409	formin-like 2	0.017422652	0.841154059	0.987732955
Sema5a	NM_009154	sema domain, seven thrombospondin repeats (type 1 and type 1-like), semaphorin 5A	-0.313992858	0.017247506	0.353818056
Strn4	NM_133789	striatin, calmodulin binding protein 4	-0.013544579	0.892325944	0.99943707
Elovl6	NM_130450	ELOVL family member 6, elongation of long chain fatty acids (yeast)	-0.039498169	0.670617092	0.953091607
Atrn	NM_009730	attractin	0.049713886	0.572021753	0.937480045
Lrrc42	NM_029985	leucine rich repeat containing 42	0.046092498	0.659833416	0.951192367

Table A3. Analysis of newly formed OL enriched transcripts. RNA-sequencing was performed on P10 forebrain tissue from *Fig4*$^{+/+}$ (WT) and *Fig4*$^{-/-}$ littermate pups. *Fig4* dependent changes in gene expression were compared to transcripts enriched in newly formed oligodendrocytes, (Zhang et al., 2014). A heat-map with log$_2$ fold-change in gene expression of *Fig4*$^{-/-}$ versus WT tissue is shown (logFC *Fig4*$^{-/-}$ vs WT). *p* values and false discovery rates (FDR) were calculated. Changes in gene expression with p-values < 0.05 are shown in red (if increased) or in green (if decreased). Genes with an FDR of < 0.1 are highlighted in pink. The "rank" indicates the relative abundance of expression in WT forebrain.

gene	refSeq	protein (OL enriched)	rank	logFC_Fig4-/-_vs_WT	p Value	FDR_WT_vs_Fig4-/-
Mbp	NM_010777	myelin basic protein	1078	-1.551940523	6.55E-09	1.63E-06
Mog	NM_010814	myelin oligodendrocyte glycoprotein	11242	-0.361762791	0.025858052	0.426439679
Mag	NM_010758	myelin-associated glycoprotein	10548	-2.574492455	3.31E-09	8.85E-07
Plp1	NM_011123	proteolipid protein (myelin) 1	1976	-1.707899966	6.10E-09	1.56E-06
Cnp	NM_009923	2',3'-cyclic nucleotide 3' phosphodiesterase	3439	-0.744427394	8.67E-06	0.001059257
Cldn11	NM_008770	claudin 11	9495	-0.851146267	2.54E-05	0.002703539
Tmem125	NM_172383	transmembrane protein 125	16181	-1.446070169	0.008444821	0.239071388
Ugt8a	NM_011674	UDP galactosyltransferase 8A	8437	-0.997889992	1.34E-06	0.000193688
Mog	NM_010814	myelin oligodendrocyte glycoprotein	11242	-0.361762791	0.025858052	0.426439679
Mal	NM_010762	myelin and lymphocyte protein, T-cell differentiation protein	11987	-0.402879217	0.110981944	0.672580358
Opalin	NM_153520	oligodendrocytic myelin paranodal and inner loop protein	17605	-3.437946348	0.000486624	0.034397279
Ppp1r14a	NM_026731	protein phosphatase 1, regulatory (inhibitor) subunit 14A	15316	-0.713218773	0.043231225	0.50116115
Adssl1	NM_007421	adenylosuccinate synthetase like 1	13616	0.302404996	0.204497976	0.767885729
Mobp	NM_008614	myelin-associated oligodendrocytic basic protein	11754	-3.947874241	1.17E-05	0.001367585
Acy3	NM_027857	aspartoacylase (aminoacylase) 3	15292	0.114343885	0.704052543	0.960317821
Trp53inp2	NM_178111	transformation related protein 53 inducible nuclear protein 2	4178	-0.302564698	0.017017619	0.353205946
Pla2g16	NM_139269	phospholipase A2, group XVI	10263	0.08004603	0.58418569	0.937480045
Efhd1	NM_028889	EF hand domain containing 1	11718	-0.495289853	0.008605816	0.241500049
Itgb4	NM_133663	integrin beta 4	11868	0.149542733	0.379928246	0.853367981
Hapln2	NM_022031	hyaluronan and proteoglycan link protein 2	15734	-0.22304574	0.587412863	0.939156127
Hcn2	NM_008226	hyperpolarization-activated, cyclic nucleotide-gated K+ 2	6643	-0.238019918	0.085048256	0.622641706
Cdc42ep2	NM_026772	CDC42 effector protein (Rho GTPase binding) 2	9071	0.017462938	0.887750286	0.998223064
Slco3a1	NM_023908	solute carrier organic anion transporter family, member 3a1	5205	0.020050442	0.825346414	0.984477214
Apod	NM_007470	apolipoprotein D	7116	0.468192811	0.000626371	0.041289025
Gsn	NM_146120	gelsolin	7341	-0.036922435	0.793381998	0.978126176
Pdlim2	NM_145978	PDZ and LIM domain 2	13465	-0.03278042	0.895743396	0.999799332
Prr18	NR_028280	proline rich region 18	9857	0.033978024	0.810759286	0.981284471
Inf2	NM_198411	inverted formin, FH2 and WH2 domain containing	7973	-0.023942819	0.908491509	0.999799332
Tppp3	NM_026481	tubulin polymerization-promoting protein family member 3	3203	0.042233379	0.654169844	0.950860818
Tbc1d9b	NM_029745	TBC1 domain family, member 9B	2433	-0.354979664	0.001742577	0.086838261
Nol3	NM_030152	nucleolar protein 3 (apoptosis repressor with CARD domain)	12695	0.064329461	0.767633426	0.972931321
Slc45a3	NM_145977	solute carrier family 45, member 3	15886	-0.513247772	0.141143391	0.682087675
Arsg	NM_028710	arylsulfatase G	11238	0.136577783	0.384802931	0.856424859
Rftn1	NM_181397	raftlin lipid raft linker 1	9784	0.044999275	0.73346027	0.966040464
Adap1	NM_172723	ArfGAP with dual PH domains 1	771	-0.181605518	0.092530438	0.650727428
Plekhb1	NM_013746	pleckstrin homology domain containing, family B (evectins) member 1	6970	-0.129515232	0.379854735	0.853367981
Trf	NM_133977	transferrin	8532	0.136007882	0.54105505	0.929022643
Insc	NM_173767	inscuteable homolog (Drosophila)	15066	-0.129659834	0.665365267	0.951949619
Cryab	NM_009964	crystallin, alpha B	8261	-0.145339466	0.306388803	0.80267263
Kif5a	NM_008447	kinesin family member 5A	61	-0.119711334	0.217722895	0.767885729
Hapln2	NM_022031	hyaluronan and proteoglycan link protein 2	15734	-0.22304574	0.587412863	0.939156127
Trak2	NM_172406	trafficking protein, kinesin binding 2	817	-0.102233787	0.307105088	0.803358599
Sp7	NM_130458	Sp7 transcription factor 7	15766	-0.692963902	0.080168439	0.607561083
Gjb1	NM_008124	gap junction protein, beta 1	14831	0.157090784	0.559326993	0.935416451
Ndrg1	NM_008681	N-myc downstream regulated gene 1	4666	0.325791964	0.028342754	0.441396156

Table A4. Analysis of mature OL enriched transcripts. RNA-sequencing was performed on P10 forebrain tissue from *Fig4*$^{+/+}$ (WT) and *Fig4*$^{-/-}$ littermate pups. *Fig4* dependent changes in gene expression were compared to transcripts enriched in oligodendrocytes, (Zhang et al., 2014). A heat-map with log$_2$ fold-change in gene expression of *Fig4*$^{-/-}$ versus WT tissue is shown (logFC *Fig4*$^{-/-}$ vs WT). *p* values and false discovery rates (FDR) were calculated. Changes in gene expression with p-values < 0.05 are shown in red (if increased) or in green (if decreased). Genes with an FDR of < 0.1 are highlighted in pink. The "rank" indicates the relative abundance of expression in WT forebrain.

gene	refSeq	protein (neuron enriched)	rank	logFC_Fig4-/-_vs_WT	p Value	FDR_WT_vs_Fig4-/-
Tubb3	NM_023279	tubulin, beta 3	26	-0.054181487	0.624363202	0.945066093
Reln	NM_011261	reelin	681	0.012049237	0.914320365	0.999799332
Nhlh2	NM_178777	nescient helix loop helix 2	13209	-0.341915888	0.151352714	0.70793986
Slc17a6	NM_080853	solute carrier family 17 (sodium-dependent inorganic phosphate cotransporter), member 6	3706	-0.084359423	0.426958016	0.87757519
Trp73	NM_011642	transformation related protein 73	14122	-0.161656434	0.502679126	0.915426054
Lhx5	NM_008499	LIM homeobox protein 5	15482	0.193023291	0.564630045	0.937480045
Sstr5	NM_011425	somatostatin receptor 5	15730	0.310294848	0.371324373	0.849483497
Snhg11	NM_175692	small nucleolar RNA host gene 11	20	-0.115540438	0.210957425	0.767885729
Mrap2	NM_001177731	melanocortin 2 receptor accessory protein 2	12625	-0.07390303	0.709056464	0.961986124
Dlx1as	NR_002854	distal-less homeobox 1, antisense	7042	0.072889945	0.547670635	0.932404796
Islr2	NM_177193	immunoglobulin superfamily containing leucine-rich repeat 2	1052	0.139121217	0.181491458	0.758847654
Gdf5	NM_008109	growth differentiation factor 5	14756	0.327099937	0.280854599	0.776418695
Stmn2	NM_025285	stathmin-like 2	53	0.0818011	0.402594097	0.865402134
Ecel1	NM_021306	endothelin converting enzyme-like 1	11324	-0.011811186	0.941955223	0.999799332
Robo2	NM_175549	roundabout homolog 2 (Drosophila)	341	0.017981012	0.833649014	0.986458336
Dlx1as	NR_002854	distal-less homeobox 1, antisense	7042	0.072889945	0.547670635	0.932404796
Nxph4	NM_183297	neurexophilin 4	15369	-0.237231091	0.46480034	0.896835553
Grm2	NM_001160353	glutamate receptor, metabotropic 2	10015	-0.224392055	0.166026972	0.735721728
Npy	NM_023456	neuropeptide Y	3958	0.366222537	3.30E-05	0.003399523
Tbr1	NM_009322	T-box brain gene 1	7785	-0.232084869	0.043447108	0.502068138
Slc32a1	NM_009508	solute carrier family 32 (GABA vesicular transporter), member 1	6314	0.029276318	0.786696029	0.976801723
Dlx2	NM_010054	distal-less homeobox 2	13208	-0.123846294	0.601730772	0.940329832
Npas4	NM_153553	neuronal PAS domain protein 4	11577	-0.031461672	0.868365201	0.992568182
Ebf3	NM_010096	early B-cell factor 3	14408	-0.267238359	0.346015801	0.836121449
Bcl11a	NM_016707	B-cell CLL/lymphoma 11A (zinc finger protein)	3683	0.023196939	0.783103284	0.976308074
Cacna2d2	NM_020263	calcium channel, voltage-dependent, alpha 2/delta subunit 2	6333	-0.06292388	0.629902583	0.945844884
Clstn2	NM_022319	calsyntenin 2	4802	-0.009872962	0.939721027	0.999799332
Dpysl5	NM_023047	dihydropyrimidinase-like 5	1679	-0.089259117	0.361402636	0.846467546
Nppc	NM_010933	natriuretic peptide type C	12249	-0.202500136	0.32726581	0.820180775
Tmem130	NM_177735	transmembrane protein 130	2147	-0.016323595	0.861744183	0.990862826
Vgf	NM_001039385	VGF nerve growth factor inducible	6094	-0.181650017	0.192033461	0.767885729
Bhlhe22	NM_021560	basic helix-loop-helix family, member e22	1577	-0.013195399	0.916079779	0.999799332
Ebf3	NM_010096	early B-cell factor 3	14408	-0.267238359	0.346015801	0.836121449

Table A5. Analysis of neuron enriched transcripts. RNA-sequencing was performed on P10 forebrain tissue from *Fig4*$^{+/+}$ (WT) and *Fig4*$^{-/-}$ littermate pups. *Fig4* dependent changes in gene expression were compared to transcripts enriched in neurons, (Zhang et al., 2014). A heat-map with log$_2$ fold-change in gene expression of *Fig4*$^{-/-}$ versus WT tissue is shown (logFC *Fig4*$^{-/-}$ vs WT). *p* values and false discovery rates (FDR) were calculated. Changes in gene expression with p-values < 0.05 are shown in red (if increased) or in green (if decreased). Genes with an FDR of < 0.1 are highlighted in pink. The "rank" indicates the relative abundance of expression in WT forebrain. In *Fig4*$^{-/-}$ forebrain tissue, there was a 2-fold reduction in *Fig4* transcripts, consistent with the mutational mechanism described for the pale tremor (plt) mouse. This *Fig4* null allele was inactivated by insertion of an ETn2b transposon into intron 18, but partial transcripts are produced (Chow et al., 2007).

gene	refSeq	Protein (astrocyte enriched)	rank	logFC_Fig4-/-_vs_WT	p Value	FDR_WT_vs_Fig4-/-
Gfap	NM_010277	glial fibrillary acidic protein	212	2.150275204	4.14E-65	9.30E-61
Hgs	NM_008244	HGF-regulated tyrosine kinase substrate	4568	0.13978733	0.119791461	0.672580358
Aqp4	NM_009700	aquaporin 4	275	0.404021589	0.002853596	0.125924539
Itih3	NM_008407	inter-alpha trypsin inhibitor, heavy chain 3	8569	0.356557965	0.029767866	0.451499389
Bmpr1b	NM_007560	bone morphogenetic protein receptor, type 1B	6430	0.145599827	0.215229715	0.767885729
Itga7	NM_008398	integrin alpha 7	9225	0.327860485	0.042497887	0.498097157
Plcd4	NM_148937	phospholipase C, delta 4	9210	0.101170876	0.437839167	0.881967136
Grm3	NM_181850	glutamate receptor, metabotropic 3	1181	-0.148913393	0.120089262	0.672580358
Slc14a1	NM_028122	solute carrier family 14 (urea transporter), member 1	8930	0.329316239	0.046446684	0.51557746
Phkg1	NM_011079	phosphorylase kinase gamma 1	10296	-0.170834007	0.370317384	0.849483497
Pla2g3	NM_172791	phospholipase A2, group III	8996	-0.151433272	0.501967385	0.915239466
Cbs	NM_178224	cystathionine beta-synthase	7507	-0.212202103	0.066493493	0.581482995
Paqr6	NM_198410	progestin and adipoQ receptor family member VI	13725	0.239548902	0.374459298	0.850211728
Aldh1l1	NM_027406	aldehyde dehydrogenase 1 family, member L1	2382	0.286965687	0.02020901	0.381409001
Cth	NM_145953	cystathionase (cystathionine gamma-lyase)	11921	-0.375508112	0.031998775	0.467762624
Ccdc80	NM_026439	coiled-coil domain containing 80	6021	0.415271924	0.000206333	0.017114222
Fmo1	NM_010231	flavin containing monooxygenase 1	7400	0.124589111	0.262224111	0.767885729
Slc30a10	NM_001033286	solute carrier family 30, member 10	5692	-0.037021347	0.703970111	0.960317821
Slc6a11	NM_172890	solute carrier family 6 (neurotransmitter transporter, GABA), member 11	1896	-0.277725236	0.002864096	0.125924539
Fgfr3	NM_008010	fibroblast growth factor receptor 3	4515	-0.043031394	0.678385571	0.953926854
Slc4a4	NM_018760	solute carrier family 4 (anion exchanger), member 4	1918	-0.234656813	0.072056878	0.590834101
Gdpd2	NM_023608	glycerophosphodiester phosphodiesterase domain containing 2	9545	0.058053625	0.622682501	0.944380086
Ppp1r3c	NM_016854	protein phosphatase 1, regulatory (inhibitor) subunit 3C	4766	-0.027068146	0.762456851	0.971876794
Grhl1	NM_145890	grainyhead-like 1 (Drosophila)	9135	-0.10649538	0.420427911	0.875495096
Entpd2	NM_009849	ectonucleoside triphosphate diphosphohydrolase 2	10673	0.239044521	0.126572513	0.672580358
Egfr	NM_207655	epidermal growth factor receptor	6471	0.050150376	0.639931301	0.948149482
Otx1	NM_011023	orthodenticle homolog 1 (Drosophila)	13889	0.346454169	0.127614834	0.672580358
Nwd1	NM_176940	NACHT and WD repeat domain containing 1	4084	-0.045321667	0.657015886	0.951192367
Atp13a4	NM_172613	ATPase type 13A4	10175	-0.105172049	0.464079123	0.896835553
Kcnn3	NM_080466	potassium intermediate/small conductance calcium-activated channel, subfamily N, member 3	9069	-0.043023149	0.755230395	0.970199891
Ptx3	NM_008987	pentraxin related gene	12724	0.695044342	0.002718691	0.121018132
Tnc	NM_011607	tenascin C	1694	0.100745596	0.391534146	0.860305217
Sox9	NM_011448	SRY-box containing gene 9	10650	0.308349186	0.166857534	0.73721666
Abcd2	NM_011994	ATP-binding cassette, sub-family D (ALD), member 2	3906	-0.18869129	0.136426215	0.673019588
Fzd10	NM_175284	frizzled homolog 10 (Drosophila)	13084	-0.523107234	0.021524324	0.393993282
Lrig1	NM_008377	leucine-rich repeats and immunoglobulin-like domains 1	3523	0.227819869	0.013584507	0.317091435
Mlc1	NM_133241	megalencephalic leukoencephalopathy with subcortical cysts 1 homolog (human)	2123	-0.006330452	0.960778921	0.999799332
Chrdl1	NM_031258	chordin-like 1	8257	-0.070152825	0.525274299	0.923729908
Aifm3	NM_175178	apoptosis-inducing factor, mitochondrion-associated 3	8937	-0.212183922	0.113933383	0.672580358
Gli1	NM_010296	GLI-Kruppel family member GLI1	12940	-0.09888453	0.68710067	0.955722478
Gli2	NM_001081125	GLI-Kruppel family member GLI2	13962	-0.005603269	0.983111882	0.999799332
Gli3	NM_008130	GLI-Kruppel family member GLI3	10901	0.018947867	0.910919758	0.999799332
Sox9	NM_011448	SRY-box containing gene 9	10650	0.308349186	0.166857534	0.73721666
Hes5	NM_010419	hairy and enhancer of split 5 (Drosophila)	10404	-0.401134165	0.017992369	0.362070245
Rfx4	NM_027689	regulatory factor X, 4 (influences HLA class II expression)	11462	0.300504924	0.071945367	0.590834101
Pax6	NM_013627	paired box gene 6	9404	0.086841866	0.483653263	0.906491957
Dbx2	NM_207533	developing brain homeobox 2	10267	-0.018155334	0.898150438	0.999799332

Table A6. Analysis of astrocyte enriched transcripts. RNA-sequencing was performed on P10 forebrain tissue from *Fig4*^{+/+} (WT) and *Fig4*^{-/-} littermate pups. *Fig4* dependent changes in gene expression were compared to transcripts enriched in astrocytes, (Zhang et al., 2014). A heat-map with log₂ fold-change in gene expression of *Fig4*^{-/-} versus WT tissue is shown (logFC *Fig4*^{-/-} vs WT). *p* values and false discovery rates (FDR) were calculated. Changes in gene expression with p-values < 0.05 are shown in red (if increased) or in green (if decreased). Genes with an FDR of < 0.1 are highlighted in pink. The "rank" indicates the relative abundance of expression in WT forebrain.

gene	refSeq	protein (microglia enriched)	rank	logFC_Fig4-/-_vs_WT	p Value	FDR_WT_vs_Fig4-/-
Slfn2	NM_011408	schlafen 2	13106	1.903159221	8.01E-12	3.22E-09
Gpr84	NM_030720	G protein-coupled receptor 84	15304	-0.111683313	0.739290897	0.966581673
Bcl2a1d	NM_007536	B-cell leukemia/lymphoma 2 related protein A1d	17498	0.543324209	0.400081076	0.864485179
Tnf	NM_013693	tumor necrosis factor	16551	0.319179671	0.523190757	0.922643052
Ncf1	NM_010876	neutrophil cytosolic factor 1	10756	0.919250386	7.45E-05	0.007013166
Gdf15	NM_011819	growth differentiation factor 15	16220	2.738632209	6.36E-06	0.00078564
Osm	NM_001013365	oncostatin M	17071	1.256960282	0.040831478	0.490718526
Lrrc25	NM_153074	leucine rich repeat containing 25	14698	1.208577161	0.000304198	0.02333707
H2-Oa	NM_008206	histocompatibility 2, O region alpha locus	17377	1.232854928	0.0996086	0.669802147
Itgam	NM_008401	integrin alpha M	9474	0.720705975	0.005899076	0.195574365
Cd83	NM_009856	CD83 antigen	8535	0.218341676	0.113261469	0.672580358
Ccl2	NM_011333	chemokine (C-C motif) ligand 2	15003	3.064304794	7.61E-11	2.52E-08
Ccl3	NM_011337	chemokine (C-C motif) ligand 3	15600	1.651772891	4.64E-06	0.000596444
Ccl4	NM_013652	chemokine (C-C motif) ligand 4	17387	3.708623152	8.73E-07	0.000132664
Ccl9	NM_011338	chemokine (C-C motif) ligand 9	13352	0.818826259	0.001837089	0.089775945
Ccl12	NM_011331	chemokine (C-C motif) ligand 12	13166	2.772996751	2.94E-07	5.36E-05
Clec7a	NM_020008	C-type lectin domain family 7, member a	13165	2.788572504	6.51E-08	1.33E-05
Cxcl16	NM_023158	chemokine (C-X-C motif) ligand 16	13526	0.152027388	0.490504356	0.909868048
Cx3cr1	NM_009987	chemokine (C-X3-C) receptor 1	4851	0.434966557	0.045410364	0.511133778
Tlr2	NM_011905	toll-like receptor 2	13180	0.820162384	0.003644327	0.145328166
Slamf8	NM_029084	SLAM family member 8	16831	0.383869728	0.503370872	0.91565675
Gna15	NM_010304	guanine nucleotide binding protein, alpha 15	13513	0.366829182	0.153798357	0.713147096
Il1b	NM_008361	interleukin 1 beta	16234	0.119668665	0.769172653	0.972931321
Tmem119	NM_146162	transmembrane protein 119	11470	-0.044812572	0.899564142	0.999799332
C1qa	NM_007572	complement component 1, q subcomponent, alpha polypeptide	5720	1.002286052	7.60E-06	0.000934025
C3ar1	NM_009779	complement component 3a receptor 1	11694	1.172153822	8.43E-07	0.000128938
Pla2g15	NM_133792	phospholipase A2, group XV	7604	-0.013202669	0.913125806	0.999799332
Ch25h	NM_009890	cholesterol 25-hydroxylase	15002	0.006669239	0.981667335	0.999799332
Hck	NM_010407	hemopoietic cell kinase	11602	0.641427498	0.000263033	0.021040733
Ptafr	NM_001081211	platelet-activating factor receptor	13823	0.730659649	0.098767503	0.668481931
Irf4	NM_013674	interferon regulatory factor 4	16078	0.153730615	0.735772463	0.966040464
Irf5	NM_012057	interferon regulatory factor 5	12564	0.303653307	0.194309418	0.767885729
Irf8	NM_008320	interferon regulatory factor 8	11725	0.914576623	3.42E-05	0.003482872
Selplg	NM_009151	selectin, platelet (p-selectin) ligand	12352	-0.267174071	0.398021541	0.864013023
Sash3	NM_028773	SAM and SH3 domain containing 3	12867	0.548522431	0.040057321	0.490718526
Pltp	NM_011125	phospholipid transfer protein	8165	0.016204498	0.911664032	0.999799332
Trem2	NM_031254	triggering receptor expressed on myeloid cells 2	10683	1.062407855	1.18E-05	0.001369267
P2ry6	NM_183168	pyrimidinergic receptor P2Y, G-protein coupled, 6	13653	1.013304265	0.000355437	0.026455357
Bcl2a1a	NM_009742	B-cell leukemia/lymphoma 2 related protein A1a	18592	1.631964945	0.105879617	0.672580358
Runx1t1	NM_009822	runt-related transcription factor 1; translocated to, 1 (cyclin D-related)	3780	0.069081658	0.448674753	0.88896528
Ikzf1	NM_009578	IKAROS family zinc finger 1	13002	0.574676634	0.023199364	0.407084551
Cebpa	NM_007678	CCAAT/enhancer binding protein (C/EBP), alpha	13350	0.232280978	0.41778605	0.874302304
Mlxipl	NM_021455	MLX interacting protein-like	13946	-0.017925667	0.942396474	0.999799332
Batf3	NM_030060	basic leucine zipper transcription factor, ATF-like 3	15391	0.918715556	0.009718032	0.260981977
Ctsd	NM_009983	cathepsin D	515	0.670540406	0.000109034	0.009842794
Ctsb	NM_007798	cathepsin B	612	0.358520723	0.004366632	0.161436126
Ctsa	NM_008906	cathepsin A	2824	0.313955004	0.000665291	0.04322082
Ctss	NM_021281	cathepsin S	4684	1.356303399	3.77E-07	6.44E-05
Ctsz	NM_022325	cathepsin Z	5301	0.795422844	1.54E-07	2.88E-05
1810011H11	NM_001163616	RIKEN cDNA 1810011H11 gene	14963	0.781724675	0.007018194	0.217293326

Table A7. Analysis of microglia enriched transcripts. RNA-sequencing was performed on P10 forebrain tissue from $Fig4^{+/+}$ (WT) and $Fig4^{-/-}$ littermate pups. $Fig4$ dependent changes in gene expression were compared to transcripts enriched in microglia, (Zhang et al., 2014). A heat-map with $\log_2$ fold-change in gene expression of $Fig4^{-/-}$ versus WT tissue is shown (logFC $Fig4^{-/-}$ vs WT). p values and false discovery rates (FDR) were calculated. Changes in gene expression with p-values < 0.05 are shown in red (if increased) or in green (if decreased). Genes with an FDR of < 0.1 are highlighted in pink. The "rank" indicates the relative abundance of expression in WT forebrain.

PROBEID	ENTREZID	SYMBOL	GENENAME	logFC	AveExpr	t	P.Value	adj.P.Val
17537962	18823	Plp1	proteolipid protein (myelin) 1	-5.0417111	8.92514292	-50.036489	1.73E-18	3.76E-14
17489341	17136	Mag	myelin-associated glycoprotein	-5.6664318	5.87250556	-23.209945	2.05E-13	2.23E-09
17501061	320981	Enpp6	ectonucleotide pyrophosphatase/phosphodiesterase 6	-3.2524003	6.73095365	-18.295515	7.13E-12	4.83E-08
17352175	17196	Mbp	myelin basic protein	-3.4122406	6.65805496	-18.024325	8.89E-12	4.83E-08
17391332	17153	Mal	myelin and lymphocyte protein, T cell differentiation protein	-2.6405754	5.69736163	-15.128037	1.15E-10	5.02E-07
17542501	19703	Renbp	renin binding protein	1.74253348	4.02436592	14.7903689	1.60E-10	5.80E-07
17535644	140571	Plxnb3	plexin B3	-1.941471	5.88615982	-14.462081	2.21E-10	6.88E-07
17344822	17441	Mog	myelin oligodendrocyte glycoprotein	-2.8313012	5.16817256	-13.575091	5.50E-10	1.33E-06
17513092	338521	Fa2h	fatty acid 2-hydroxylase	-1.8782323	7.71919129	-13.488953	6.02E-10	1.33E-06
17310837	20356	Sema5a	sema domain, seven thrombospondin repeats (type 1 and type 1-like), transmembrane domain (TM) and short cytoplasmic domain, (semaphorin) 5A	-1.802137	6.84367311	-13.472529	6.12E-10	1.33E-06
17523192	17433	Mobp	myelin-associated oligodendrocytic basic protein	-3.582302	6.478955	-13.374927	6.79E-10	1.34E-06
17367055	22352	Vim	vimentin	2.12118477	7.76040348	12.3848775	2.02E-09	3.66E-06
17308956	319903	9630013A20	RIKEN cDNA 9630013A20 gene	-1.6934173	7.08898414	-12.283845	2.27E-09	3.71E-06
17503942	17748	Mt1	metallothionein 1	1.2109918	9.49134086	12.2382145	2.39E-09	3.71E-06
17317056	18606	Enpp2	ectonucleotide pyrophosphatase/phosphodiesterase 2	-1.1869666	9.52955398	-11.989917	3.19E-09	4.62E-06

17351587	17203	Mc5r	melanocorti n 5 receptor	-2.4023037	5.88336793	-11.728534	4.34E-09	5.59E-06
17523199	NA	NA	NA	-2.3578016	5.33331121	-11.722434	4.37E-09	5.59E-06
17548193	22352	Vim	vimentin	2.31843717	6.97231646	11.5698459	5.25E-09	6.34E-06
17256404	12799	Cnp	2',3'-cyclic nucleotide 3' phosphodie sterase	-1.4037081	7.06050265	-11.442354	6.12E-09	7.00E-06
17219546	98365	Slamf9	SLAM family member 9	1.83504139	4.52745308	11.3484489	6.86E-09	7.31E-06
17226916	269116	Nfasc	neurofascin	-1.390822	7.38675976	-11.325612	7.06E-09	7.31E-06
17399802	20198	S100a4	S100 calcium binding protein A4	-1.3344183	6.9832288	-11.22838	7.95E-09	7.86E-06
17434742	108151	Sema3d	sema domain, immunoglo bulin domain (Ig), short basic domain, secreted, (semaphori n) 3D	-1.3171049	6.09156288	-11.007475	1.05E-08	9.89E-06
17548916	11363	Acadl	acyl-Coenzyme A dehydrogen ase, long-chain	1.38311688	6.67563791	10.8342786	1.30E-08	1.14E-05
17520171	12045	Bcl2a1b	B cell leukemia/ly mphoma 2 related protein A1b	1.45201113	5.80111647	10.8307707	1.31E-08	1.14E-05
17506571	57247	Zfp276	zinc finger protein (C2H2 type) 276	-1.3594094	3.81139369	-10.774959	1.40E-08	1.17E-05
17309580	105445	Dock9	dedicator of cytokinesis 9	-1.3381094	7.18812273	-10.685102	1.57E-08	1.23E-05
17401072	70747	Tspan2	tetraspanin 2	-1.3537393	6.92563326	-10.681264	1.58E-08	1.23E-05
17404796	11747	Anxa5	annexin A5	1.37271733	6.6075935	10.6193803	1.71E-08	1.27E-05
17292562	NA	NA	NA	-1.8210443	5.93662655	-10.603925	1.75E-08	1.27E-05
17319045	207393	Elfn2	leucine rich repeat and fibronectin type III, extracellular 2	-1.3687384	6.01190816	-10.334007	2.48E-08	1.74E-05
17332766	224454	Zdhhc14	zinc finger, DHHC domain containing 14	-0.9546147	6.796484	-10.270469	2.70E-08	1.83E-05
17488556	100503790	Gm19897	predicted gene, 19897	-1.1262969	5.06842139	-10.241943	2.80E-08	1.85E-05
17319494	214685	Chadl	chondroadh erin-like	-1.3897269	6.3480223	-10.165725	3.10E-08	1.98E-05
17511878	67801	Pllp	plasma membrane proteolipid	-1.2644077	9.10661943	-10.111782	3.33E-08	2.07E-05

17226473	72160	Tmem163	transmembrane protein 163	-1.1476376	6.93868387	-10.017032	3.78E-08	2.29E-05
17410114	22239	Ugt8a	UDP galactosyltransferase 8A	-1.607799	8.98359445	-9.9762368	4.00E-08	2.35E-05
17362616	225908	Myrf	myelin regulatory factor	-2.1646047	5.80973218	-9.9547594	4.12E-08	2.35E-05
17220370	67330	1700047M11	RIKEN cDNA 1700047M11 gene	-1.9083622	5.93923248	-9.9071233	4.39E-08	2.45E-05
17396652	18417	Cldn11	claudin 11	-1.7389947	7.16844343	-9.7206674	5.66E-08	3.08E-05
17380031	73303	Bcas1os2	breast carcinoma amplified sequence 1, opposite strand 2	-1.6434411	5.81545308	-9.6103905	6.60E-08	3.50E-05
17289717	74559	Elovl7	ELOVL family member 7, elongation of long chain fatty acids (yeast)	-1.4052204	6.2250157	-9.5328209	7.35E-08	3.72E-05
17433888	320587	Tmem88b	transmembrane protein 88B	-1.3278087	4.70659567	-9.5320716	7.36E-08	3.72E-05
17399783	67860	S100a16	S100 calcium binding protein A16	-1.0912163	6.20864775	-9.4721397	8.00E-08	3.95E-05
17342740	106672	AI413582	expressed sequence AI413582	1.24311535	6.266792	9.38689904	9.02E-08	4.36E-05
17353267	574402	Gpr17	G protein-coupled receptor 17	-1.4030092	10.0015419	-9.35101	9.49E-08	4.49E-05
17396971	NA	NA	NA	1.35775141	6.93096933	9.32112298	9.90E-08	4.58E-05
17219248	240913	Adamts4	a disintegrin-like and metallopeptidase (reprolysin type) with thrombospondin type 1 motif, 4	-1.8357544	4.56348575	-9.2937619	1.03E-07	4.66E-05
17529575	12047	Bcl2a1d	B cell leukemia/lymphoma 2 related protein A1d	1.3131567	6.31735487	9.25565397	1.09E-07	4.78E-05

Table A8. Differential gene expression in acutely isolated *Pikfyve*-deficient PDGFRα$^+$ OPCs. Gene transcripts are sorted by *p*-value (smallest to highest), top 50 hits displayed.

PROBEID	ENTREZID	SYMBOL	GENENAME	logFC	AveExpr	t	P.Value	adj.P.Val
17364588	226115	Opalin	oligodendrocytic myelin paranodal and inner loop protein	-5.1030674	3.74970973	-29.060931	6.90E-15	8.84E-11
17391332	17153	Mal	myelin and lymphocyte protein, T cell differentiation protein	-5.3559132	5.69736163	-28.747457	8.13E-15	8.84E-11
17523199	NA	NA	NA	-5.8236224	5.33331121	-27.125992	1.96E-14	1.42E-10
17483891	101476	Plekha1	pleckstrin homology domain containing, family A (phosphoinositide binding specific) member 1	-2.4106892	6.40213794	-25.124908	6.23E-14	3.39E-10
17537962	18823	Plp1	proteolipid protein (myelin) 1	-2.6389655	8.92514292	-24.53717	8.90E-14	3.60E-10
17292569	20354	Sema4d	sema domain, immunoglobulin domain (Ig), transmembrane domain (TM) and short cytoplasmic domain, (semaphorin) 4D	-2.7984746	4.53469522	-24.139481	1.14E-13	3.60E-10
17288616	72948	Tppp	tubulin polymerization promoting protein	-3.6198369	6.15007613	-24.111333	1.16E-13	3.60E-10
17292562	NA	NA	NA	-4.2458297	5.93662655	-23.162775	2.12E-13	5.75E-10
17344822	17441	Mog	myelin oligodendrocyte glycoprotein	-4.9518841	5.16817256	-22.243803	3.89E-13	9.39E-10
17523192	17433	Mobp	myelin-associated oligodendrocytic basic protein	-6.3009144	6.478955	-22.040158	4.46E-13	9.70E-10
17370209	227753	Gsn	gelsolin	-2.9219702	5.67270009	-21.732814	5.50E-13	1.09E-09
17226847	18557	Cdk18	cyclin-dependent kinase 18	-3.4923962	4.08076301	-21.244011	7.73E-13	1.36E-09

17484419	76484	Kndc1	kinase non-catalytic C-lobe domain (KIND) containing 1	-3.9173894	5.01033899	-21.091968	8.61E-13	1.36E-09
17401072	70747	Tspan2	tetraspanin 2	-2.85055	6.92563326	-21.071632	8.73E-13	1.36E-09
17283502	170952	Prima1	proline rich membrane anchor 1	-3.3300615	3.50294812	-20.670963	1.16E-12	1.69E-09
17226916	269116	Nfasc	neurofascin	-2.6399392	7.38675976	-20.1403	1.71E-12	2.24E-09
17433888	320587	Tmem88b	transmembrane protein 88B	-2.9897985	4.70659567	-20.108312	1.75E-12	2.24E-09
17509642	77113	Klhl2	kelch-like 2, Mayven	-2.2366778	6.46711191	-19.952622	1.97E-12	2.38E-09
17212696	56363	Tmeff2	transmembrane protein with EGF-like and two follistatin-like domains 2	-2.2558784	5.26425226	-19.854123	2.12E-12	2.43E-09
17289717	74559	Elovl7	ELOVL family member 7, elongation of long chain fatty acids (yeast)	-3.0907675	6.2250157	-19.643788	2.48E-12	2.70E-09
17308956	319903	9630013A20	RIKEN cDNA 9630013A20 gene	-2.8471515	7.08898414	-19.34919	3.11E-12	3.22E-09
17326428	12892	Cpox	coproporphyrinogen oxidase	-2.5389162	5.55222018	-19.283942	3.27E-12	3.23E-09
17489341	17136	Mag	myelin-associated glycoprotein	-5.0059466	5.87250556	-19.21023	3.46E-12	3.27E-09
17385398	77767	Ermn	ermin, ERM-like protein	-5.9254321	4.75798075	-19.126817	3.69E-12	3.34E-09
17330188	12374	Casr	calcium-sensing receptor	-3.1092522	3.55674908	-18.785258	4.82E-12	4.19E-09
17226473	72160	Tmem163	transmembrane protein 163	-2.2556896	6.93868387	-18.445716	6.32E-12	5.28E-09
17312032	NA	NA	NA	-2.8370621	4.98333357	-18.061115	8.62E-12	6.94E-09
17324616	NA	NA	NA	-3.4549675	2.98221048	-17.924879	9.64E-12	7.49E-09
17542501	19703	Renbp	renin binding protein	2.22242131	4.02436592	17.6728325	1.19E-11	8.91E-09
17259430	208990	Npb	neuropeptide B	-3.3867471	3.44044794	-17.304083	1.62E-11	1.07E-08
17535644	140571	Plxnb3	plexin B3	-2.4742292	5.88615982	-17.267191	1.67E-11	1.07E-08
17231925	17761	Map7	microtubule-associated protein 7	-2.8794605	4.47936701	-17.256543	1.69E-11	1.07E-08

17329759	11815	Apod	apolipoprotein D	-1.9923476	8.39930679	-17.243005	1.71E-11	1.07E-08
17301746	213469	Lgi3	leucine-rich repeat LGI family, member 3	-2.7293032	6.33168678	-17.235789	1.72E-11	1.07E-08
17510772	15245	Hhip	Hedgehog-interacting protein	-2.944317	4.0018016	-17.2357	1.72E-11	1.07E-08
17449989	320292	Rasgef1b	RasGEF domain family, member 1B	-2.3612739	6.07998059	-17.115792	1.90E-11	1.15E-08
17382729	51875	Tmem141	transmembrane protein 141	-2.8089551	6.01939839	-17.011049	2.08E-11	1.22E-08
17267420	77864	Ypel2	yippee-like 2 (Drosophila)	-2.8930007	5.73530915	-16.946472	2.20E-11	1.22E-08
17239023	215748	Cnksr3	Cnksr family member 3	-3.2282044	5.26941469	-16.931392	2.23E-11	1.22E-08
17329074	208158	Map6d1	MAP6 domain containing 1	-2.2547639	5.7553457	-16.924757	2.24E-11	1.22E-08
17530243	22041	Trf	transferrin	-2.6031996	6.69326459	-16.753222	2.61E-11	1.38E-08
17258064	286942	Kif19a	kinesin family member 19A	-2.3091236	4.22364842	-16.619696	2.93E-11	1.50E-08
17390997	70354	Secisbp2l	SECIS binding protein 2-like	-2.3877096	7.17031518	-16.609183	2.96E-11	1.50E-08
17278561	68519	Eml1	echinoderm microtubule associated protein like 1	-2.781284	6.04726053	-16.432898	3.46E-11	1.67E-08
17260644	13195	Ddc	dopa decarboxylase	-2.8712721	3.43795858	-16.417563	3.51E-11	1.67E-08
17500391	68867	Rnf122	ring finger protein 122	-2.695915	8.18130965	-16.409725	3.53E-11	1.67E-08
17276743	211945	Plekhh1	pleckstrin homology domain containing, family H (with MyTH4 domain) member 1	-2.9683195	4.15620385	-16.35546	3.71E-11	1.71E-08
17240880	17155	Man1a	mannosidase 1, alpha	-2.3381414	4.83740059	-16.291074	3.93E-11	1.78E-08
17350824	20496	Slc12a2	solute carrier family 12, member 2	-1.9232603	8.08546146	-16.257888	4.04E-11	1.79E-08

Table A9. Differential gene expression in acutely isolated *Pikfyve*-deficient O4$^+$ OLs.
Gene transcripts are sorted by *p*-value (smallest to highest), top 50 hits displayed.

Id	name	ConceptType	#Genes	Coeff	OddsRatio	P-Value	FDR	Direction
GO:0031982	vesicle	GOCC	239	0.083491501	1.680122916	4.20E-09	6.30E-07	up
GO:0031988	membrane-bounded vesicle	GOCC	226	0.081716437	1.661690791	1.63E-08	8.09E-07	up
GO:0043230	extracellular organelle	GOCC	191	0.087420617	1.721653002	2.70E-08	8.09E-07	up
GO:0065010	extracellular membrane-bounded organelle	GOCC	191	0.087420617	1.721653002	2.70E-08	8.09E-07	up
GO:0070062	extracellular vesicular exosome	GOCC	191	0.087420617	1.721653002	2.70E-08	8.09E-07	up
GO:0005737	cytoplasm	GOCC	468	0.061170894	1.462508527	9.91E-08	2.48E-06	up
GO:0031224	intrinsic component of membrane	GOCC	325	-0.059326905	0.691637389	3.10E-07	6.64E-06	down
GO:0043209	myelin sheath	GOCC	14	-0.299860919	0.155125922	1.79E-06	2.98E-05	down
GO:0044421	extracellular region part	GOCC	253	0.063823426	1.486816985	1.76E-06	2.98E-05	up
GO:0043226	organelle	GOCC	560	0.054920132	1.406785191	2.32E-06	3.48E-05	up
GO:0016021	integral component of membrane	GOCC	314	-0.054478717	0.712793248	2.65E-06	3.62E-05	down
GO:0000323	lytic vacuole	GOCC	49	0.191021136	3.277632949	3.59E-06	3.85E-05	up
GO:0005622	intracellular	GOCC	576	0.054683681	1.404719508	3.11E-06	3.85E-05	up
GO:0005764	lysosome	GOCC	49	0.191021136	3.277632949	3.59E-06	3.85E-05	up
GO:0005773	vacuole	GOCC	51	0.172451423	2.920392447	5.99E-06	5.40E-05	up
GO:0044444	cytoplasmic part	GOCC	331	0.054594742	1.403943312	6.06E-06	5.40E-05	up
GO:0044446	intracellular organelle part	GOCC	200	0.066453508	1.511318589	6.12E-06	5.40E-05	up
GO:0044424	intracellular part	GOCC	559	0.05118682	1.37452199	1.00E-05	8.36E-05	up
GO:0005576	extracellular region	GOCC	280	0.053911944	1.397998547	2.09E-05	1.56E-04	up
GO:0043227	membrane-bounded organelle	GOCC	521	0.048626984	1.352828585	2.01E-05	1.56E-04	up
GO:0005739	mitochondrion	GOCC	82	0.101839468	1.88304921	2.43E-05	1.66E-04	up
GO:0044422	organelle part	GOCC	208	0.060435129	1.455836492	2.33E-05	1.66E-04	up
GO:0044425	membrane part	GOCC	370	-0.04704118	0.746512813	3.35E-05	2.18E-04	down
GO:0033267	axon part	GOCC	17	-0.133610957	0.43590117	2.03E-04	0.001269075	down
GO:0045202	synapse	GOCC	47	-0.077512299	0.617727064	6.13E-04	0.003675904	down
GO:0044463	cell projection part	GOCC	44	-0.07853692	0.613806111	7.42E-04	0.004166014	down
GO:0097458	neuron part	GOCC	89	-0.058258082	0.696246754	7.50E-04	0.004166014	down
GO:0005829	cytosol	GOCC	84	0.068749101	1.533033909	0.001555832	0.008334815	up
GO:0098552	side of membrane	GOCC	34	0.115529326	2.050265885	0.002793766	0.014450516	up
GO:0043229	intracellular organelle	GOCC	471	0.033311465	1.23000434	0.002926439	0.014632197	up
GO:0043005	neuron projection	GOCC	71	-0.055377824	0.708821551	0.003560889	0.017230107	down
GO:0009897	external side of plasma membrane	GOCC	33	0.111892985	2.004452684	0.003899268	0.018277817	up
GO:0005887	integral component of plasma membrane	GOCC	71	-0.053631559	0.716555825	0.00478842	0.0205218	down
GO:0009986	cell surface	GOCC	86	0.059192498	1.444637145	0.004761058	0.0205218	up
GO:0031975	envelope	GOCC	34	0.105691895	1.928675905	0.004783204	0.0205218	up
GO:0043231	intracellular membrane-bounded organelle	GOCC	428	0.031476472	1.216057338	0.004997913	0.020824639	up
GO:0031967	organelle envelope	GOCC	33	0.105505441	1.92644236	0.005487057	0.022244825	up
GO:0031226	intrinsic component of plasma membrane	GOCC	76	-0.049673265	0.734401151	0.007254097	0.027952444	down
GO:0043228	non-membrane-bounded organelle	GOCC	152	0.041832342	1.296893271	0.007453985	0.027952444	up
GO:0043232	intracellular non-membrane-bounded organelle	GOCC	152	0.041832342	1.296893271	0.007453985	0.027952444	up
GO:0036477	somatodendritic compartment	GOCC	56	-0.05566829	0.707543191	0.008185224	0.029868807	down
GO:0044464	cell part	GOCC	702	0.035905124	1.249990901	0.008363266	0.029868807	up
GO:0005623	cell	GOCC	704	0.035773796	1.248971139	0.008888596	0.031006731	up
GO:0043233	organelle lumen	GOCC	59	0.065615721	1.503470329	0.010011463	0.033371545	up
GO:0070013	intracellular organelle lumen	GOCC	59	0.065615721	1.503470329	0.010011463	0.033371545	up
GO:0044429	mitochondrial part	GOCC	29	0.10257002	1.891617864	0.010586695	0.034521831	up
GO:0031974	membrane-enclosed lumen	GOCC	62	0.062461347	1.474284504	0.011361116	0.036258882	up
GO:0031410	cytoplasmic vesicle	GOCC	57	0.064622827	1.494221813	0.012381913	0.038693479	up
GO:0005768	endosome	GOCC	42	0.074122271	1.585089487	0.015908871	0.048700624	up
GO:0005615	extracellular space	GOCC	100	0.045193826	1.324270735	0.016922689	0.049772616	up
GO:0030424	axon	GOCC	37	-0.060385234	0.687103347	0.016867719	0.049772616	down

Table A10. The LR path analysis of GO network in acutely isolated control and *Pikfyve*-deficient PDGFRα OPCs. Only differentially expressed genes were used in the analysis.

Id	name	ConceptType	#Genes	Coeff	OddsRatio	P-Value	FDR	Direction
GO:0005694	chromosome	GOCC	124	0.093697638	1.790140486	3.42E-10	8.13E-08	up
GO:0044427	chromosomal part	GOCC	109	0.097362679	1.83138204	1.62E-09	1.93E-07	up
GO:0032993	protein-DNA complex	GOCC	66	0.146711586	2.488686377	7.34E-09	5.83E-07	up
GO:0000775	chromosome, centromeric region	GOCC	48	0.202267827	3.514914754	1.46E-08	8.71E-07	up
GO:0005634	nucleus	GOCC	697	0.031589684	1.21691322	3.28E-08	1.56E-06	up
GO:0000776	kinetochore	GOCC	35	0.247946714	4.668751334	6.01E-08	2.39E-06	up
GO:0032991	macromolecular complex	GOCC	551	0.03011429	1.205806345	9.93E-07	3.38E-05	up
GO:0043209	myelin sheath	GOCC	29	-0.106581746	0.515631052	3.43E-06	1.02E-04	down
GO:0005819	spindle	GOCC	50	0.107813883	1.954278416	1.33E-05	3.05E-04	up
GO:0005876	spindle microtubule	GOCC	15	0.316347879	7.141894583	1.30E-05	3.05E-04	up
GO:0043234	protein complex	GOCC	500	0.027536387	1.186642454	1.41E-05	3.05E-04	up
GO:0012505	endomembrane system	GOCC	412	-0.02525971	0.854721839	7.64E-05	0.001515245	down
GO:0000779	condensed chromosome, centromeric region	GOCC	18	0.234632831	4.298005554	1.18E-04	0.002158689	up
GO:0000777	condensed chromosome kinetochore	GOCC	15	0.253996148	4.847613488	2.06E-04	0.003122677	up
GO:0000793	condensed chromosome	GOCC	34	0.113942995	2.030152799	2.10E-04	0.003122677	up
GO:0044425	membrane part	GOCC	764	-0.020030752	0.882953032	1.87E-04	0.003122677	down
GO:0000228	nuclear chromosome	GOCC	48	0.082641795	1.671274269	2.74E-04	0.003833348	up
GO:0016021	integral component of membrane	GOCC	614	-0.020331007	0.881307004	3.07E-04	0.004060466	down
GO:0005783	endoplasmic reticulum	GOCC	170	-0.032695341	0.816124199	3.54E-04	0.004436412	down
GO:0044428	nuclear part	GOCC	191	0.033923317	1.234690237	4.85E-04	0.005775604	up
GO:0031224	intrinsic component of membrane	GOCC	635	-0.01938195	0.88652033	5.19E-04	0.005877704	down
GO:0005615	extracellular space	GOCC	180	0.0337966	1.233718309	7.18E-04	0.007546451	up
GO:0009897	external side of plasma membrane	GOCC	50	0.071962722	1.563958507	7.29E-04	0.007546451	up
GO:0098588	bounding membrane of organelle	GOCC	133	-0.033664041	0.811225818	9.92E-04	0.00983678	down
GO:0031090	organelle membrane	GOCC	177	-0.028494422	0.837711369	0.001555581	0.014809136	down
GO:0098552	side of membrane	GOCC	60	0.057482112	1.429362866	0.001776953	0.016265957	up
GO:0000785	chromatin	GOCC	48	0.065406881	1.501520304	0.002006868	0.017690174	up
GO:0044454	nuclear chromosome part	GOCC	38	0.075700378	1.60071144	0.002246109	0.019091927	up
GO:0000323	lytic vacuole	GOCC	56	0.056754133	1.42291089	0.002782314	0.021360989	up
GO:0005764	lysosome	GOCC	56	0.056754133	1.42291089	0.002782314	0.021360989	up
GO:0031226	intrinsic component of plasma membrane	GOCC	126	0.0355587	1.247302704	0.002768937	0.021360989	up
GO:0009986	cell surface	GOCC	130	0.033839315	1.234045848	0.003666214	0.027267465	up
GO:0000139	Golgi membrane	GOCC	23	-0.068022583	0.655253107	0.004585311	0.03306982	down
GO:0005887	integral component of plasma membrane	GOCC	115	0.034963497	1.242697514	0.004782936	0.033480551	up
GO:0005768	endosome	GOCC	93	-0.032492531	0.817153477	0.007147547	0.048603322	down
GO:0005794	Golgi apparatus	GOCC	161	-0.024899825	0.856635602	0.008179641	0.054076515	down
GO:0000922	spindle pole	GOCC	20	0.098970155	1.849768928	0.008422932	0.054179941	up
GO:1902495	transmembrane transporter complex	GOCC	46	0.053565039	1.394987878	0.009521641	0.058106427	up
GO:1990351	transporter complex	GOCC	46	0.053565039	1.394987878	0.009521641	0.058106427	up
GO:0000794	condensed nuclear chromosome	GOCC	15	0.123252151	2.151066612	0.010151217	0.059986385	up
GO:0044304	main axon	GOCC	22	-0.062576341	0.677810562	0.010333789	0.059986385	down
GO:0031012	extracellular matrix	GOCC	76	0.03860713	1.27115786	0.011723064	0.064885794	up
GO:0044815	DNA packaging complex	GOCC	14	0.12736776	2.206793844	0.011578401	0.064885794	up
GO:0043233	organelle lumen	GOCC	151	0.026610982	1.179837629	0.012265292	0.066344077	up
GO:0044446	intracellular organelle part	GOCC	575	0.01467588	1.095493384	0.012910247	0.068280863	up
GO:0005773	vacuole	GOCC	60	0.04316621	1.307688505	0.013425948	0.06946469	up
GO:0070013	intracellular organelle lumen	GOCC	150	0.026081336	1.175960524	0.01426525	0.072236799	up
GO:0031974	membrane-enclosed lumen	GOCC	156	0.025067475	1.168574389	0.016147445	0.080064416	up
GO:0031981	nuclear lumen	GOCC	140	0.026253331	1.177218163	0.016996071	0.082552343	down
GO:0055037	recycling endosome	GOCC	16	-0.068110764	0.654894119	0.01764391	0.083985013	down
GO:0034702	ion channel complex	GOCC	44	0.048817475	1.354431045	0.018653246	0.08704848	up
GO:0005576	extracellular region	GOCC	586	0.013655819	1.088570716	0.019749724	0.09039297	up
GO:0044459	plasma membrane part	GOCC	309	0.017104209	1.112150975	0.022942609	0.103025301	up
GO:0044431	Golgi apparatus part	GOCC	45	-0.038011106	0.789603684	0.025999401	0.114589954	down
GO:0043228	non-membrane-bounded organelle	GOCC	493	0.013413778	1.086934529	0.030789064	0.130853522	up
GO:0043232	intracellular non-membrane-bounded organelle	GOCC	493	0.013413778	1.086934529	0.030789064	0.130853522	up
GO:0005578	proteinaceous extracellular matrix	GOCC	59	0.037083659	1.259179609	0.031548453	0.13172863	up
GO:0044421	extracellular region part	GOCC	543	0.012788487	1.08271896	0.033040249	0.135578953	up
GO:0044444	cytoplasmic part	GOCC	761	-0.011269896	0.932358405	0.035618121	0.143679877	down
GO:0044422	organelle part	GOCC	598	0.012164618	1.078529277	0.036244224	0.143768753	up
GO:0030424	axon	GOCC	95	-0.02443925	0.859091055	0.042028798	0.163742998	down
GO:0033267	axon part	GOCC	51	-0.032637965	0.816415255	0.042655739	0.163742998	down
GO:0005657	replication fork	GOCC	14	0.084592329	1.69165641	0.045182324	0.17068878	up
GO:0072562	blood microparticle	GOCC	22	0.059895662	1.450963855	0.049597678	0.184441363	up

Table A11. The LR path analysis of GO network in acutely isolated control and *Pikfyve*-deficient O4[+] OLs. Only differentially expressed genes were used in the analysis.

A

Genotype	Wet Weight (mg)	Dry Weight (mg)	Water Content (%)	Ganglioside Sialic Acid	
				Content (ug/whole brain)	Concentration (ug/100mg dry weight)
Fig4+/+	378.4 ± 6.5	59.4 ± 1.8	84.32 ± 0.21	212.6 ± 6.3	358 ± 5.0
Fig4-/-	355.8 ± 18.6	54.4 ± 3.1	84.73 ± 0.16	217.2 ± 13.0	400 ± 14.1

B

Genotype	GM 1	GD 3	GD1a	LD1	GD1b	GT1b	GQ1b
Fig4+/+	4.7 ± 0.1	1.0 ± 0.5	36.1 ± 0.5	4.5 ± 0.2	7.9 ± 0.1	33.9 ± 0.5	12.0 ± 0.3
Fig4-/-	5.4 ± 0.6	2.2 ± 0.2	35.4 ± 0.7	4.6 ± 0.1	8.0 ± 0.3	33.5 ± 1.1	10.9 ± 0.9

Table A12. Loss of *Fig4* does not alter total content of brain gangliosides or relative abundance of individual ganglioside species. (**A**) Total content of brain gangliosides (µg/whole brain) and ganglioside concentration (µg/100 mg dry weight) in P10 *Fig4*^{+/+} and *Fig4*^{-/-} littermate mice is indistinguishable. (**B**) Individual ganglioside species were analyzed qualitatively and quantitatively by high-performance thin-layer chromatograph, including GM1, GD3, GD1a, LD1, GD1b, GT1b, and GQ1b. No significant differences were observed between P10 *Fig4*^{+/+} and *Fig4*^{-/-} littermate brains.

A14. References

Ando S, Chang NC, Yu RK (1978) High-performance thin-layer chromatography and densitometric determination of brain ganglioside compositions of several species. Anal Biochem 89:437-450.

Armati PJ, Mathey EK (2010) The biology of oligodendrocytes. Cambridge ; New York: Cambridge University Press.

Arroyo EJ, Scherer SS (2000) On the molecular architecture of myelinated fibers. Histochemistry and cell biology 113:1-18.

Arthur JR, Heinecke KA, Seyfried TN (2011) Filipin recognizes both GM1 and cholesterol in GM1 gangliosidosis mouse brain. J Lipid Res 52:1345-1351.

Atanasoski S, Scherer SS, Sirkowski E, Leone D, Garratt AN, Birchmeier C, Suter U (2006) ErbB2 signaling in Schwann cells is mostly dispensable for maintenance of myelinated peripheral nerves and proliferation of adult Schwann cells after injury. J Neurosci 26:2124-2131.

Auer PL, Doerge RW (2010) Statistical design and analysis of RNA sequencing data. Genetics 185:405-416.

Baek RC, Martin DR, Cox NR, Seyfried TN (2009) Comparative analysis of brain lipids in mice, cats, and humans with Sandhoff disease. Lipids 44:197-205.

Bakhti M, Winter C, Simons M (2011) Inhibition of myelin membrane sheath formation by oligodendrocyte-derived exosome-like vesicles. J Biol Chem 286:787-796.

Baldwin KT, Giger RJ (2015) Insights into the physiological role of CNS regeneration inhibitors. Front Mol Neurosci 8:23.

Baraban M, Mensch S, Lyons DA (2015) Adaptive myelination from fish to man. Brain Res.

Barkovich AJ (2000) Concepts of myelin and myelination in neuroradiology. AJNR Am J Neuroradiol 21:1099-1109.

Barres BA, Raff MC (1993) Proliferation of oligodendrocyte precursor cells depends on electrical activity in axons. Nature 361:258-260.

Barres BA, Schmid R, Sendnter M, Raff MC (1993) Multiple extracellular signals are required for long-term oligodendrocyte survival. Development 118:283-295.

Baulac S, Lenk GM, Dufresnois B, Ouled Amar Bencheikh B, Couarch P, Renard J, Larson PA, Ferguson CJ, Noe E, Poirier K, Hubans C, Ferreira S, Guerrini R, Ouazzani R, El Hachimi KH, Meisler MH, Leguern E (2014) Role of the phosphoinositide phosphatase FIG4 gene in familial epilepsy with polymicrogyria. Neurology 82:1068-1075.

Baumann N, Pham-Dinh D (2001) Biology of oligodendrocyte and myelin in the mammalian central nervous system. Physiological reviews 81:871-927.

Behnia R, Munro S (2005) Organelle identity and the signposts for membrane traffic. Nature 438:597-604.

Bei F, Lee HH, Liu X, Gunner G, Jin H, Ma L, Wang C, Hou L, Hensch TK, Frank E, Sanes JR, Chen C, Fagiolini M, He Z (2016) Restoration of Visual Function by Enhancing Conduction in Regenerated Axons. Cell 164:219-232.

Bengtsson SL, Nagy Z, Skare S, Forsman L, Forssberg H, Ullen F (2005) Extensive piano practicing has regionally specific effects on white matter development. Nat Neurosci 8:1148-1150.

Bercury KK, Dai J, Sachs HH, Ahrendsen JT, Wood TL, Macklin WB (2014) Conditional ablation of raptor or rictor has differential impact on oligodendrocyte differentiation and CNS myelination. J Neurosci 34:4466-4480.

Bercury KK, Macklin WB (2015) Dynamics and mechanisms of CNS myelination. Developmental cell 32:447-458.

Bergles DE, Richardson WD (2015) Oligodendrocyte Development and Plasticity. Cold Spring Harb Perspect Biol 8.

Bergles DE, Roberts JD, Somogyi P, Jahr CE (2000) Glutamatergic synapses on oligodendrocyte precursor cells in the hippocampus. Nature 405:187-191.

Bharadwaj R, Cunningham KM, Zhang K, Lloyd TE (2016) FIG4 regulates lysosome membrane homeostasis independent of phosphatase function. Hum Mol Genet 25:681-692.

Blott EJ, Griffiths GM (2002) Secretory lysosomes. Nature reviews Molecular cell biology 3:122-131.

Botelho RJ, Efe JA, Teis D, Emr SD (2008) Assembly of a Fab1 phosphoinositide kinase signaling complex requires the Fig4 phosphoinositide phosphatase. Molecular biology of the cell 19:4273-4286.

Bridges D, Ma JT, Park S, Inoki K, Weisman LS, Saltiel AR (2012) Phosphatidylinositol 3,5-bisphosphate plays a role in the activation and subcellular localization of mechanistic target of rapamycin 1. Molecular biology of the cell 23:2955-2962.

Brill MH, Waxman SG, Moore JW, Joyner RW (1977) Conduction velocity and spike configuration in myelinated fibres: computed dependence on internode distance. J Neurol Neurosurg Psychiatry 40:769-774.

Bucci C, Thomsen P, Nicoziani P, McCarthy J, van Deurs B (2000) Rab7: a key to lysosome biogenesis. Molecular biology of the cell 11:467-480.

Bujalka H, Koenning M, Jackson S, Perreau VM, Pope B, Hay CM, Mitew S, Hill AF, Lu QR, Wegner M, Srinivasan R, Svaren J, Willingham M, Barres BA, Emery B (2013) MYRF is a membrane-associated transcription factor that autoproteolytically cleaves to directly activate myelin genes. PLoS Biol 11:e1001625.

Butt AM, Pugh M, Hubbard P, James G (2004) Functions of optic nerve glia: axoglial signalling in physiology and pathology. Eye (Lond) 18:1110-1121.

Cai X, Xu Y, Cheung AK, Tomlinson RC, Alcazar-Roman A, Murphy L, Billich A, Zhang B, Feng Y, Klumpp M, Rondeau JM, Fazal AN, Wilson CJ, Myer V, Joberty G, Bouwmeester T, Labow MA, Finan PM, Porter JA, Ploegh HL, Baird D, De Camilli P, Tallarico JA, Huang Q (2013) PIKfyve, a class III PI kinase, is the target of the small molecular IL-12/IL-23 inhibitor apilimod and a player in Toll-like receptor signaling. Chemistry & biology 20:912-921.

Campeau PM, Lenk GM, Lu JT, Bae Y, Burrage L, Turnpenny P, Roman Corona-Rivera J, Morandi L, Mora M, Reutter H, Vulto-van Silfhout AT, Faivre L, Haan E, Gibbs RA, Meisler MH, Lee BH (2013) Yunis-Varon syndrome is caused by mutations in FIG4, encoding a phosphoinositide phosphatase. American journal of human genetics 92:781-791.

Carbajal KS, Mironova Y, Ulrich-Lewis JT, Kulkarni D, Grifka-Walk HM, Huber AK, Shrager P, Giger RJ, Segal BM (2015) Th Cell Diversity in Experimental Autoimmune Encephalomyelitis and Multiple Sclerosis. Journal of immunology 195:2552-2559.

Chen C, Westenbroek RE, Xu X, Edwards CA, Sorenson DR, Chen Y, McEwen DP, O'Malley HA, Bharucha V, Meadows LS, Knudsen GA, Vilaythong A, Noebels JL, Saunders TL, Scheuer T, Shrager P, Catterall WA, Isom LL (2004) Mice lacking sodium channel beta1 subunits display defects in neuronal excitability, sodium channel expression, and nodal architecture. J Neurosci 24:4030-4042.

Chen XS, Zhang YH, Cai QY, Yao ZX (2012) ID2: A negative transcription factor regulating oligodendroglia differentiation. Journal of neuroscience research 90:925-932.

Chivet M, Hemming F, Pernet-Gallay K, Fraboulet S, Sadoul R (2012) Emerging role of neuronal exosomes in the central nervous system. Frontiers in physiology 3:145.

Chow CY, Zhang Y, Dowling JJ, Jin N, Adamska M, Shiga K, Szigeti K, Shy ME, Li J, Zhang X, Lupski JR, Weisman LS, Meisler MH (2007) Mutation of FIG4 causes neurodegeneration in the pale tremor mouse and patients with CMT4J. Nature 448:68-72.

Christian KM, Song H, Ming GL (2014) Functions and dysfunctions of adult hippocampal neurogenesis. Annual review of neuroscience 37:243-262.

Coetzee T, Fujita N, Dupree J, Shi R, Blight A, Suzuki K, Suzuki K, Popko B (1996) Myelination in the absence of galactocerebroside and sulfatide: normal structure with abnormal function and regional instability. Cell 86:209-219.

Colman DR, Kreibich G, Frey AB, Sabatini DD (1982) Synthesis and incorporation of myelin polypeptides into CNS myelin. The Journal of cell biology 95:598-608.

Coman I, Barbin G, Charles P, Zalc B, Lubetzki C (2005) Axonal signals in central nervous system myelination, demyelination and remyelination. Journal of the neurological sciences 233:67-71.

Crawford AH, Tripathi RB, Foerster S, McKenzie I, Kougioumtzidou E, Grist M, Richardson WD, Franklin RJ (2016a) Pre-Existing Mature Oligodendrocytes Do Not Contribute to Remyelination following Toxin-Induced Spinal Cord Demyelination. Am J Pathol 186:511-516.

Crawford Abbe H, Tripathi Richa B, Richardson William D, Franklin Robin JM (2016b) Developmental Origin of Oligodendrocyte Lineage Cells Determines Response to Demyelination and Susceptibility to Age-Associated Functional Decline. Cell Reports 15:761-773.

Czopka T, Ffrench-Constant C, Lyons DA (2013) Individual oligodendrocytes have only a few hours in which to generate new myelin sheaths in vivo. Developmental cell 25:599-609.

D'Urso D, Ehrhardt P, Muller HW (1999) Peripheral myelin protein 22 and protein zero: a novel association in peripheral nervous system myelin. J Neurosci 19:3396-3403.

Danglot L, Galli T (2007) What is the function of neuronal AP-3? Biology of the cell / under the auspices of the European Cell Biology Organization 99:349-361.

De Biase LM, Bergles DE (2011) Same players, different game: AMPA receptor regulation in oligodendrocyte progenitors. Nat Neurosci 14:1358-1360.

De Biase LM, Kang SH, Baxi EG, Fukaya M, Pucak ML, Mishina M, Calabresi PA, Bergles DE (2011) NMDA receptor signaling in oligodendrocyte progenitors is not required for oligodendrogenesis and myelination. J Neurosci 31:12650-12662.

de Hoz L, Simons M (2015) The emerging functions of oligodendrocytes in regulating neuronal network behaviour. BioEssays : news and reviews in molecular, cellular and developmental biology 37:60-69.

Delarasse C, Daubas P, Mars LT, Vizler C, Litzenburger T, Iglesias A, Bauer J, Della Gaspera B, Schubart A, Decker L, Dimitri D, Roussel G, Dierich A, Amor S, Dautigny A, Liblau R, Pham-Dinh D (2003) Myelin/oligodendrocyte glycoprotein-deficient (MOG-deficient) mice reveal lack of immune tolerance to MOG in wild-type mice. J Clin Invest 112:544-553.

Dessaud E, Yang LL, Hill K, Cox B, Ulloa F, Ribeiro A, Mynett A, Novitch BG, Briscoe J (2007) Interpretation of the sonic hedgehog morphogen gradient by a temporal adaptation mechanism. Nature 450:717-720.

Dobin A, Davis CA, Schlesinger F, Drenkow J, Zaleski C, Jha S, Batut P, Chaisson M, Gingeras TR (2013) STAR: ultrafast universal RNA-seq aligner. Bioinformatics 29:15-21.

Dong XP, Shen D, Wang X, Dawson T, Li X, Zhang Q, Cheng X, Zhang Y, Weisman LS, Delling M, Xu H (2010) PI(3,5)P(2) controls membrane trafficking by direct activation of mucolipin Ca(2+) release channels in the endolysosome. Nat Commun 1:38.

Dove SK, Cooke FT, Douglas MR, Sayers LG, Parker PJ, Michell RH (1997) Osmotic stress activates phosphatidylinositol-3,5-bisphosphate synthesis. Nature 390:187-192.

Duan Y, Wang SH, Song J, Mironova Y, Ming GL, Kolodkin AL, Giger RJ (2014) Semaphorin 5A inhibits synaptogenesis in early postnatal- and adult-born hippocampal dentate granule cells. eLife 3.

Dubois-Dalcq M, Behar T, Hudson L, Lazzarini RA (1986) Emergence of three myelin proteins in oligodendrocytes cultured without neurons. The Journal of cell biology 102:384-392.

Dugas JC, Emery B (2013) Purification and culture of oligodendrocyte lineage cells. Cold Spring Harbor protocols 2013:810-814.

Dupree JL, Coetzee T, Suzuki K, Popko B (1998) Myelin abnormalities in mice deficient in galactocerebroside and sulfatide. J Neurocytol 27:649-659.

Durand B, Raff M (2000) A cell-intrinsic timer that operates during oligodendrocyte development. BioEssays : news and reviews in molecular, cellular and developmental biology 22:64-71.

Dyck PJ, Lambert EH (1968) Lower motor and primary sensory neuron diseases with peroneal muscular atrophy. I. Neurologic, genetic, and electrophysiologic findings in hereditary polyneuropathies. Arch Neurol 18:603-618.

Egami Y, Taguchi T, Maekawa M, Arai H, Araki N (2014) Small GTPases and phosphoinositides in the regulatory mechanisms of macropinosome formation and maturation. Frontiers in physiology 5:374.

Emery B, Agalliu D, Cahoy JD, Watkins TA, Dugas JC, Mulinyawe SB, Ibrahim A, Ligon KL, Rowitch DH, Barres BA (2009) Myelin gene regulatory factor is a critical transcriptional regulator required for CNS myelination. Cell 138:172-185.

Emery B, Dugas JC (2013) Purification of oligodendrocyte lineage cells from mouse cortices by immunopanning. Cold Spring Harbor protocols 2013:854-868.

Emery B, Lu QR (2015) Transcriptional and Epigenetic Regulation of Oligodendrocyte Development and Myelination in the Central Nervous System. Cold Spring Harb Perspect Biol 7:a020461.

Etxeberria A, Mangin JM, Aguirre A, Gallo V (2010) Adult-born SVZ progenitors receive transient synapses during remyelination in corpus callosum. Nat Neurosci 13:287-289.

Fancy SP, Baranzini SE, Zhao C, Yuk DI, Irvine KA, Kaing S, Sanai N, Franklin RJ, Rowitch DH (2009) Dysregulation of the Wnt pathway inhibits timely myelination and remyelination in the mammalian CNS. Genes Dev 23:1571-1585.

Faust PL, Kaye EM, Powers JM (2010) Myelin lesions associated with lysosomal and peroxisomal disorders. Expert review of neurotherapeutics 10:1449-1466.

Feldmann A, Amphornrat J, Schonherr M, Winterstein C, Mobius W, Ruhwedel T, Danglot L, Nave KA, Galli T, Bruns D, Trotter J, Kramer-Albers EM (2011) Transport of the major

myelin proteolipid protein is directed by VAMP3 and VAMP7. The Journal of neuroscience : the official journal of the Society for Neuroscience 31:5659-5672.

Ferguson CJ, Lenk GM, Jones JM, Grant AE, Winters JJ, Dowling JJ, Giger RJ, Meisler MH (2012a) Neuronal expression of Fig4 is both necessary and sufficient to prevent spongiform neurodegeneration. Hum Mol Genet 21:3525-3534.

Ferguson CJ, Lenk GM, Jones JM, Grant AE, Winters JJ, Dowling JJ, Giger RJ, Meisler MH (2012b) Neuronal expression of Fig4 is necessary and sufficient to prevent spongiform neurodegeneration. Hum Mol Genet.

Ferguson CJ, Lenk GM, Meisler MH (2009) Defective autophagy in neurons and astrocytes from mice deficient in PI(3,5)P2. Hum Mol Genet 18:4868-4878.

Ferguson CJ, Lenk GM, Meisler MH (2010) PtdIns(3,5)P2 and autophagy in mouse models of neurodegeneration. Autophagy 6:170-171.

Fields RD (2008) White matter in learning, cognition and psychiatric disorders. Trends Neurosci 31:361-370.

Fields RD (2015) A new mechanism of nervous system plasticity: activity-dependent myelination. Nat Rev Neurosci 16:756-767.

Folkerth RD (1999) Abnormalities of developing white matter in lysosomal storage diseases. J Neuropathol Exp Neurol 58:887-902.

Follett PL, Rosenberg PA, Volpe JJ, Jensen FE (2000) NBQX attenuates excitotoxic injury in developing white matter. J Neurosci 20:9235-9241.

Forss-Petter S, Danielson PE, Catsicas S, Battenberg E, Price J, Nerenberg M, Sutcliffe JG (1990) Transgenic mice expressing beta-galactosidase in mature neurons under neuron-specific enolase promoter control. Neuron 5:187-197.

Franklin RJ, Ffrench-Constant C (2008) Remyelination in the CNS: from biology to therapy. Nat Rev Neurosci 9:839-855.

Fruhbeis C, Frohlich D, Kramer-Albers EM (2012) Emerging roles of exosomes in neuron-glia communication. Frontiers in physiology 3:119.

Fruhbeis C, Frohlich D, Kuo WP, Amphornrat J, Thilemann S, Saab AS, Kirchhoff F, Mobius W, Goebbels S, Nave KA, Schneider A, Simons M, Klugmann M, Trotter J, Kramer-Albers EM (2013) Neurotransmitter-triggered transfer of exosomes mediates oligodendrocyte-neuron communication. PLoS Biol 11:e1001604.

Gardner A, Jukkola P, Gu C (2012) Myelination of rodent hippocampal neurons in culture. Nat Protoc 7:1774-1782.

Gautier HO, Evans KA, Volbracht K, James R, Sitnikov S, Lundgaard I, James F, Lao-Peregrin C, Reynolds R, Franklin RJ, Karadottir RT (2015) Neuronal activity regulates remyelination via glutamate signalling to oligodendrocyte progenitors. Nat Commun 6:8518.

Gibson EM, Purger D, Mount CW, Goldstein AK, Lin GL, Wood LS, Inema I, Miller SE, Bieri G, Zuchero JB, Barres BA, Woo PJ, Vogel H, Monje M (2014) Neuronal activity promotes oligodendrogenesis and adaptive myelination in the mammalian brain. Science 344:1252304.

Giese KP, Martini R, Lemke G, Soriano P, Schachner M (1992) Mouse P0 gene disruption leads to hypomyelination, abnormal expression of recognition molecules, and degeneration of myelin and axons. Cell 71:565-576.

Gillooly DJ, Morrow IC, Lindsay M, Gould R, Bryant NJ, Gaullier JM, Parton RG, Stenmark H (2000) Localization of phosphatidylinositol 3-phosphate in yeast and mammalian cells. EMBO J 19:4577-4588.

Gillooly DJ, Simonsen A, Stenmark H (2001) Cellular functions of phosphatidylinositol 3-phosphate and FYVE domain proteins. Biochem J 355:249-258.

Girao H, Geli MI, Idrissi FZ (2008) Actin in the endocytic pathway: from yeast to mammals. FEBS Lett 582:2112-2119.

Goebbels S, Bormuth I, Bode U, Hermanson O, Schwab MH, Nave KA (2006) Genetic targeting of principal neurons in neocortex and hippocampus of NEX-Cre mice. Genesis 44:611-621.

Golan N, Adamsky K, Kartvelishvily E, Brockschnieder D, Mobius W, Spiegel I, Roth AD, Thomson CE, Rechavi G, Peles E (2008) Identification of Tmem10/Opalin as an oligodendrocyte enriched gene using expression profiling combined with genetic cell ablation. Glia 56:1176-1186.

Goldman SA (2016) Stem and Progenitor Cell-Based Therapy of the Central Nervous System: Hopes, Hype, and Wishful Thinking. Cell Stem Cell 18:174-188.

Gomez-Sanchez JA, Carty L, Iruarrizaga-Lejarreta M, Palomo-Irigoyen M, Varela-Rey M, Griffith M, Hantke J, Macias-Camara N, Azkargorta M, Aurrekoetxea I, De Juan VG, Jefferies HB, Aspichueta P, Elortza F, Aransay AM, Martinez-Chantar ML, Baas F, Mato JM, Mirsky R, Woodhoo A, Jessen KR (2015) Schwann cell autophagy, myelinophagy, initiates myelin clearance from injured nerves. The Journal of cell biology 210:153-168.

Gregson NA, Hall SM (1973) A quantitative analysis of the effects of the intraneural injection of lysophosphatidyl choline. Journal of cell science 13:257-277.

Grishchuk Y, Sri S, Rudinskiy N, Ma W, Stember KG, Cottle MW, Sapp E, Difiglia M, Muzikansky A, Betensky RA, Wong AM, Bacskai BJ, Hyman BT, Kelleher RJ, 3rd, Cooper JD, Slaugenhaupt SA (2014) Behavioral deficits, early gliosis, dysmyelination and synaptic dysfunction in a mouse model of mucolipidosis IV. Acta neuropathologica communications 2:133.

Guo J, Ma YH, Yan Q, Wang L, Zeng YS, Wu JL, Li J (2012) Fig4 expression in the rodent nervous system and its potential role in preventing abnormal lysosomal accumulation. J Neuropathol Exp Neurol 71:28-39.

Hall S (2005) The response to injury in the peripheral nervous system. J Bone Joint Surg Br 87:1309-1319.

Harlow DE, Saul KE, Komuro H, Macklin WB (2015) Myelin Proteolipid Protein Complexes with alphav Integrin and AMPA Receptors In Vivo and Regulates AMPA-Dependent Oligodendrocyte Progenitor Cell Migration through the Modulation of Cell-Surface GluR2 Expression. J Neurosci 35:12018-12032.

Hartline DK, Colman DR (2007) Rapid conduction and the evolution of giant axons and myelinated fibers. Curr Biol 17:R29-35.

Hauser EC, Kasperzyk JL, d'Azzo A, Seyfried TN (2004) Inheritance of lysosomal acid beta-galactosidase activity and gangliosides in crosses of DBA/2J and knockout mice. Biochem Genet 42:241-257.

Hauser SL, Chan JR, Oksenberg JR (2013) Multiple sclerosis: Prospects and promise. Ann Neurol 74:317-327.

Hayashi S, McMahon AP (2002) Efficient recombination in diverse tissues by a tamoxifen-inducible form of Cre: a tool for temporally regulated gene activation/inactivation in the mouse. Dev Biol 244:305-318.

Heffer-Lauc M, Lauc G, Nimrichter L, Fromholt SE, Schnaar RL (2005) Membrane redistribution of gangliosides and glycosylphosphatidylinositol-anchored proteins in brain tissue sections under conditions of lipid raft isolation. Biochimica et biophysica acta 1686:200-208.

Hertz DL, Owzar K, Lessans S, Wing C, Jiang C, Kelly WK, Patel JN, Halabi S, Furukawa Y, Wheeler HE, Sibley A, Lassiter C, Weisman LS, Watson D, Krens SD, Mulkey F, Renn CL, Small EJ, Febbo PG, Shterev I, Kroetz D, Friedman PN, Mahoney JF, Carducci MA, Kelley MJ, Nakamura Y, Kubo M, Dorsey SG, Dolan ME, Morris MJ, Ratain MJ, McLeod HL (2016) Pharmacogenetic Discovery in CALGB (Alliance) 90401 and Mechanistic Validation of a VAC14 Polymorphism That Increases Risk of Docetaxel-Induced Neuropathy. Clin Cancer Res.

Hildebrand C (1971) Ultrastructural and light-microscopic studies of the nodal region in large myelinated fibres of the adult feline spinal cord white matter. Acta Physiol Scand Suppl 364:43-79.

Hill RA, Grutzendler J (2014) In vivo imaging of oligodendrocytes with sulforhodamine 101. Nat Methods 11:1081-1082.

Hill RA, Medved J, Patel KD, Nishiyama A (2014a) Organotypic slice cultures to study oligodendrocyte dynamics and myelination. J Vis Exp e51835.

Hill RA, Patel KD, Goncalves CM, Grutzendler J, Nishiyama A (2014b) Modulation of oligodendrocyte generation during a critical temporal window after NG2 cell division. Nat Neurosci 17:1518-1527.

Hill RA, Patel KD, Medved J, Reiss AM, Nishiyama A (2013) NG2 cells in white matter but not gray matter proliferate in response to PDGF. J Neurosci 33:14558-14566.

Hofmann I, Munro S (2006) An N-terminally acetylated Arf-like GTPase is localised to lysosomes and affects their motility. Journal of cell science 119:1494-1503.

Holtz AM, Griffiths SC, Davis SJ, Bishop B, Siebold C, Allen BL (2015) Secreted HHIP1 interacts with heparan sulfate and regulates Hedgehog ligand localization and function. The Journal of cell biology 209:739-757.

Hong NH, Qi A, Weaver AM (2015) PI(3,5)P2 controls endosomal branched actin dynamics by regulating cortactin-actin interactions. The Journal of cell biology 210:753-769.

Hornig J, Frob F, Vogl MR, Hermans-Borgmeyer I, Tamm ER, Wegner M (2013) The transcription factors Sox10 and Myrf define an essential regulatory network module in differentiating oligodendrocytes. PLoS genetics 9:e1003907.

Hughes EG, Appel B (2016) The cell biology of CNS myelination. Current opinion in neurobiology 39:93-100.

Hughes EG, Kang SH, Fukaya M, Bergles DE (2013) Oligodendrocyte progenitors balance growth with self-repulsion to achieve homeostasis in the adult brain. Nat Neurosci 16:668-676.

Huotari J, Helenius A (2011) Endosome maturation. EMBO J 30:3481-3500.

Hutagalung AH, Novick PJ (2011) Role of Rab GTPases in membrane traffic and cell physiology. Physiological reviews 91:119-149.

Ikonomov OC, Sbrissa D, Delvecchio K, Xie Y, Jin JP, Rappolee D, Shisheva A (2011) The phosphoinositide kinase PIKfyve is vital in early embryonic development:

preimplantation lethality of PIKfyve-/- embryos but normality of PIKfyve+/- mice. J Biol Chem 286:13404-13413.

Ikonomov OC, Sbrissa D, Fligger J, Delvecchio K, Shisheva A (2010) ArPIKfyve regulates Sac3 protein abundance and turnover: disruption of the mechanism by Sac3I41T mutation causing Charcot-Marie-Tooth 4J disorder. J Biol Chem 285:26760-26764.

Ikonomov OC, Sbrissa D, Shisheva A (2009) YM201636, an inhibitor of retroviral budding and PIKfyve-catalyzed PtdIns(3,5)P2 synthesis, halts glucose entry by insulin in adipocytes. Biochem Biophys Res Commun 382:566-570.

Inoue K (2005) PLP1-related inherited dysmyelinating disorders: Pelizaeus-Merzbacher disease and spastic paraplegia type 2. Neurogenetics 6:1-16.

Ishibashi T, Dakin KA, Stevens B, Lee PR, Kozlov SV, Stewart CL, Fields RD (2006) Astrocytes promote myelination in response to electrical impulses. Neuron 49:823-832.

Jahn R, Scheller RH (2006) SNAREs--engines for membrane fusion. Nature reviews Molecular cell biology 7:631-643.

Jean S, Cox S, Nassari S, Kiger AA (2015) Starvation-induced MTMR13 and RAB21 activity regulates VAMP8 to promote autophagosome-lysosome fusion. EMBO reports 16:297-311.

Jean S, Kiger AA (2012) Coordination between RAB GTPase and phosphoinositide regulation and functions. Nature reviews Molecular cell biology 13:463-470.

Jefferies HB, Cooke FT, Jat P, Boucheron C, Koizumi T, Hayakawa M, Kaizawa H, Ohishi T, Workman P, Waterfield MD, Parker PJ (2008) A selective PIKfyve inhibitor blocks PtdIns(3,5)P(2) production and disrupts endomembrane transport and retroviral budding. EMBO reports 9:164-170.

Jin N, Chow CY, Liu L, Zolov SN, Bronson R, Davisson M, Petersen JL, Zhang Y, Park S, Duex JE, Goldowitz D, Meisler MH, Weisman LS (2008) VAC14 nucleates a protein complex essential for the acute interconversion of PI3P and PI(3,5)P(2) in yeast and mouse. EMBO J 27:3221-3234.

Jin N, Lang MJ, Weisman LS (2016) Phosphatidylinositol 3,5-bisphosphate: regulation of cellular events in space and time. Biochem Soc Trans 44:177-184.

Jin N, Mao K, Jin Y, Tevzadze G, Kauffman EJ, Park S, Bridges D, Loewith R, Saltiel AR, Klionsky DJ, Weisman LS (2014) Roles for PI(3,5)P2 in nutrient sensing through TORC1. Molecular biology of the cell 25:1171-1185.

Kang SH, Fukaya M, Yang JK, Rothstein JD, Bergles DE (2010) NG2+ CNS glial progenitors remain committed to the oligodendrocyte lineage in postnatal life and following neurodegeneration. Neuron 68:668-681.

Kantheti P, Qiao X, Diaz ME, Peden AA, Meyer GE, Carskadon SL, Kapfhamer D, Sufalko D, Robinson MS, Noebels JL, Burmeister M (1998) Mutation in AP-3 delta in the mocha mouse links endosomal transport to storage deficiency in platelets, melanosomes, and synaptic vesicles. Neuron 21:111-122.

Karadottir R, Cavelier P, Bergersen LH, Attwell D (2005) NMDA receptors are expressed in oligodendrocytes and activated in ischaemia. Nature 438:1162-1166.

Karim SA, Barrie JA, McCulloch MC, Montague P, Edgar JM, Kirkham D, Anderson TJ, Nave KA, Griffiths IR, McLaughlin M (2007) PLP overexpression perturbs myelin protein composition and myelination in a mouse model of Pelizaeus-Merzbacher disease. Glia 55:341-351.

Kent HM, Evans PR, Schafer IB, Gray SR, Sanderson CM, Luzio JP, Peden AA, Owen DJ (2012) Structural basis of the intracellular sorting of the SNARE VAMP7 by the AP3 adaptor complex. Developmental cell 22:979-988.

Kessaris N, Fogarty M, Iannarelli P, Grist M, Wegner M, Richardson WD (2006) Competing waves of oligodendrocytes in the forebrain and postnatal elimination of an embryonic lineage. Nat Neurosci 9:173-179.

Khwaja O, Volpe JJ (2008) Pathogenesis of cerebral white matter injury of prematurity. Arch Dis Child Fetal Neonatal Ed 93:F153-161.

Kim E, Jung H (2015) Local protein synthesis in neuronal axons: why and how we study. BMB Rep 48:139-146.

Kim JH, Karnovsky A, Mahavisno V, Weymouth T, Pande M, Dolinoy DC, Rozek LS, Sartor MA (2012) LRpath analysis reveals common pathways dysregulated via DNA methylation across cancer types. BMC Genomics 13:526.

Klugmann M, Schwab MH, Puhlhofer A, Schneider A, Zimmermann F, Griffiths IR, Nave KA (1997) Assembly of CNS myelin in the absence of proteolipid protein. Neuron 18:59-70.

Koenning M, Jackson S, Hay CM, Faux C, Kilpatrick TJ, Willingham M, Emery B (2012) Myelin gene regulatory factor is required for maintenance of myelin and mature oligodendrocyte identity in the adult CNS. J Neurosci 32:12528-12542.

Kramer-Albers EM, Bretz N, Tenzer S, Winterstein C, Mobius W, Berger H, Nave KA, Schild H, Trotter J (2007) Oligodendrocytes secrete exosomes containing major myelin and stress-protective proteins: Trophic support for axons? Proteomics Clin Appl 1:1446-1461.

Kramer-Albers EM, White R (2011) From axon-glial signalling to myelination: the integrating role of oligodendroglial Fyn kinase. Cell Mol Life Sci 68:2003-2012.

Kwiecien JM, O'Connor LT, Goetz BD, Delaney KH, Fletch AL, Duncan ID (1998) Morphological and morphometric studies of the dysmyelinating mutant, the Long Evans shaker rat. J Neurocytol 27:581-591.

Kyotani A, Azuma Y, Yamamoto I, Yoshida H, Mizuta I, Mizuno T, Nakagawa M, Tokuda T, Yamaguchi M (2016) Knockdown of the Drosophila FIG4 induces deficient locomotive behavior, shortening of motor neuron, axonal targeting aberration, reduction of life span and defects in eye development. Exp Neurol 277:86-95.

Lachenal G, Pernet-Gallay K, Chivet M, Hemming FJ, Belly A, Bodon G, Blot B, Haase G, Goldberg Y, Sadoul R (2011) Release of exosomes from differentiated neurons and its regulation by synaptic glutamatergic activity. Mol Cell Neurosci 46:409-418.

Langseth AJ, Munji RN, Choe Y, Huynh T, Pozniak CD, Pleasure SJ (2010) Wnts influence the timing and efficiency of oligodendrocyte precursor cell generation in the telencephalon. J Neurosci 30:13367-13372.

Lappe-Siefke C, Goebbels S, Gravel M, Nicksch E, Lee J, Braun PE, Griffiths IR, Nave KA (2003) Disruption of Cnp1 uncouples oligodendroglial functions in axonal support and myelination. Nat Genet 33:366-374.

Lauc G, Heffer-Lauc M (2006) Shedding and uptake of gangliosides and glycosylphosphatidylinositol-anchored proteins. Biochimica et biophysica acta 1760:584-602.

Law CW, Chen Y, Shi W, Smyth GK (2014) voom: Precision weights unlock linear model analysis tools for RNA-seq read counts. Genome biology 15:R29.

Le Douarin NM, Smith J (1988) Development of the peripheral nervous system from the neural crest. Annu Rev Cell Biol 4:375-404.

Lebel C, Gee M, Camicioli R, Wieler M, Martin W, Beaulieu C (2012) Diffusion tensor imaging of white matter tract evolution over the lifespan. Neuroimage 60:340-352.

Lee B, Park JY, Jung WH, Kim HS, Oh JS, Choi CH, Jang JH, Kang DH, Kwon JS (2010) White matter neuroplastic changes in long-term trained players of the game of "Baduk" (GO): a voxel-based diffusion-tensor imaging study. Neuroimage 52:9-19.

Lee C, Patil S, Sartor MA (2016) RNA-Enrich: a cut-off free functional enrichment testing method for RNA-seq with improved detection power. Bioinformatics 32:1100-1102.

Lee H, Raiker SJ, Venkatesh K, Geary R, Robak LA, Zhang Y, Yeh HH, Shrager P, Giger RJ (2008) Synaptic function for the Nogo-66 receptor NgR1: regulation of dendritic spine morphology and activity-dependent synaptic strength. J Neurosci 28:2753-2765.

Lee S, Chong SY, Tuck SJ, Corey JM, Chan JR (2013) A rapid and reproducible assay for modeling myelination by oligodendrocytes using engineered nanofibers. Nat Protoc 8:771-782.

Lee Y, Morrison BM, Li Y, Lengacher S, Farah MH, Hoffman PN, Liu Y, Tsingalia A, Jin L, Zhang PW, Pellerin L, Magistretti PJ, Rothstein JD (2012) Oligodendroglia metabolically support axons and contribute to neurodegeneration. Nature 487:443-448.

Lenk GM, Ferguson CJ, Chow CY, Jin N, Jones JM, Grant AE, Zolov SN, Winters JJ, Giger RJ, Dowling JJ, Weisman LS, Meisler MH (2011) Pathogenic mechanism of the FIG4 mutation responsible for Charcot-Marie-Tooth disease CMT4J. PLoS genetics 7:e1002104.

Lenk GM, Frei CM, Miller AC, Wallen RC, Mironova YA, Giger RJ, Meisler MH (2016a) Rescue of neurodegeneration in the Fig4 null mouse by a catalytically inactive FIG4 transgene. Hum Mol Genet 25:340-347.

Lenk GM, Meisler MH (2014) Mouse models of PI(3,5)P2 deficiency with impaired lysosome function. Methods in enzymology 534:245-260.

Lenk GM, Szymanska K, Debska-Vielhaber G, Rydzanicz M, Walczak A, Bekiesinska-Figatowska M, Vielhaber S, Hallmann K, Stawinski P, Buehring S, Hsu DA, Kunz WS, Meisler MH, Ploski R (2016b) Biallelic Mutations of VAC14 in Pediatric-Onset Neurological Disease. American journal of human genetics 99:188-194.

Li C, Tropak MB, Gerlai R, Clapoff S, Abramow-Newerly W, Trapp B, Peterson A, Roder J (1994) Myelination in the absence of myelin-associated glycoprotein. Nature 369:747-750.

Li JY, Popovic N, Brundin P (2005) The use of the R6 transgenic mouse models of Huntington's disease in attempts to develop novel therapeutic strategies. NeuroRx 2:447-464.

Li X, Wang X, Zhang X, Zhao M, Tsang WL, Zhang Y, Yau RG, Weisman LS, Xu H (2013) Genetically encoded fluorescent probe to visualize intracellular phosphatidylinositol 3,5-bisphosphate localization and dynamics. Proc Natl Acad Sci U S A 110:21165-21170.

Liang CC, Tanabe LM, Jou S, Chi F, Dauer WT (2014) TorsinA hypofunction causes abnormal twisting movements and sensorimotor circuit neurodegeneration. J Clin Invest 124:3080-3092.

Lin CH, Tallaksen-Greene S, Chien WM, Cearley JA, Jackson WS, Crouse AB, Ren S, Li XJ, Albin RL, Detloff PJ (2001) Neurological abnormalities in a knock-in mouse model of Huntington's disease. Hum Mol Genet 10:137-144.

Lin SC, Huck JH, Roberts JD, Macklin WB, Somogyi P, Bergles DE (2005) Climbing fiber innervation of NG2-expressing glia in the mammalian cerebellum. Neuron 46:773-785.

Liu J, Casaccia P (2010) Epigenetic regulation of oligodendrocyte identity. Trends in neurosciences 33:193-201.

Lodish HF (2008) Molecular cell biology. New York: W.H. Freeman.

Lopez ME, Klein AD, Dimbil UJ, Scott MP (2011) Anatomically defined neuron-based rescue of neurodegenerative Niemann-Pick type C disorder. J Neurosci 31:4367-4378.

Lopez-Verrilli MA, Picou F, Court FA (2013) Schwann cell-derived exosomes enhance axonal regeneration in the peripheral nervous system. Glia 61:1795-1806.

Lundgaard I, Luzhynskaya A, Stockley JH, Wang Z, Evans KA, Swire M, Volbracht K, Gautier HO, Franklin RJ, Charles F-C, Attwell D, Karadottir RT (2013) Neuregulin and BDNF induce a switch to NMDA receptor-dependent myelination by oligodendrocytes. PLoS Biol 11:e1001743.

Maier O, Hoekstra D, Baron W (2008) Polarity development in oligodendrocytes: sorting and trafficking of myelin components. Journal of molecular neuroscience : MN 35:35-53.

Makinodan M, Rosen KM, Ito S, Corfas G (2012) A critical period for social experience-dependent oligodendrocyte maturation and myelination. Science 337:1357-1360.

Man HY, Lin JW, Ju WH, Ahmadian G, Liu L, Becker LE, Sheng M, Wang YT (2000) Regulation of AMPA receptor-mediated synaptic transmission by clathrin-dependent receptor internalization. Neuron 25:649-662.

Marinelli C, Bertalot T, Zusso M, Skaper SD, Giusti P (2016) Systematic Review of Pharmacological Properties of the Oligodendrocyte Lineage. Frontiers in cellular neuroscience 10:27.

Martinez-Arca S, Rudge R, Vacca M, Raposo G, Camonis J, Proux-Gillardeaux V, Daviet L, Formstecher E, Hamburger A, Filippini F, D'Esposito M, Galli T (2003) A dual mechanism controlling the localization and function of exocytic v-SNAREs. Proceedings of the National Academy of Sciences of the United States of America 100:9011-9016.

Martini R (1999) P0-deficient knockout mice as tools to understand pathomechanisms in Charcot-Marie-Tooth 1B and P0-related Dejerine-Sottas syndrome. Ann N Y Acad Sci 883:273-280.

Martini-Stoica H, Xu Y, Ballabio A, Zheng H (2016) The Autophagy-Lysosomal Pathway in Neurodegeneration: A TFEB Perspective. Trends Neurosci 39:221-234.

Masaki T (2012) Polarization and myelination in myelinating glia. ISRN neurology 2012:769412.

Mayinger P (2012) Phosphoinositides and vesicular membrane traffic. Biochimica et biophysica acta 1821:1104-1113.

Mc AJ, Milburn NS, Chapman GB (1958) The fine structure of Schwann cells, nodes of Ranvier and Schmidt-Lanterman incisures in the central nervous system of the crab, Cancer irroratus. J Ultrastruct Res 2:171-176.

McCartney AJ, Zhang Y, Weisman LS (2014a) Phosphatidylinositol 3,5-bisphosphate: low abundance, high significance. BioEssays : news and reviews in molecular, cellular and developmental biology 36:52-64.

McCartney AJ, Zolov SN, Kauffman EJ, Zhang Y, Strunk BS, Weisman LS, Sutton MA (2014b) Activity-dependent PI(3,5)P2 synthesis controls AMPA receptor trafficking during synaptic depression. Proc Natl Acad Sci U S A 111:E4896-4905.

McGoldrick P, Joyce PI, Fisher EM, Greensmith L (2013) Rodent models of amyotrophic lateral sclerosis. Biochimica et biophysica acta 1832:1421-1436.

McKenzie IA, Ohayon D, Li H, de Faria JP, Emery B, Tohyama K, Richardson WD (2014) Motor skill learning requires active central myelination. Science 346:318-322.

Medina DL, Fraldi A, Bouche V, Annunziata F, Mansueto G, Spampanato C, Puri C, Pignata A, Martina JA, Sardiello M, Palmieri M, Polishchuk R, Puertollano R, Ballabio A (2011) Transcriptional activation of lysosomal exocytosis promotes cellular clearance. Developmental cell 21:421-430.

Mei F, Fancy SP, Shen YA, Niu J, Zhao C, Presley B, Miao E, Lee S, Mayoral SR, Redmond SA, Etxeberria A, Xiao L, Franklin RJ, Green A, Hauser SL, Chan JR (2014) Micropillar arrays as a high-throughput screening platform for therapeutics in multiple sclerosis. Nat Med 20:954-960.

Menezes MP, Waddell L, Lenk GM, Kaur S, MacArthur DG, Meisler MH, Clarke NF (2014) Whole exome sequencing identifies three recessive FIG4 mutations in an apparently dominant pedigree with Charcot-Marie-Tooth disease. Neuromuscul Disord 24:666-670.

Menn B, Garcia-Verdugo JM, Yaschine C, Gonzalez-Perez O, Rowitch D, Alvarez-Buylla A (2006) Origin of oligodendrocytes in the subventricular zone of the adult brain. J Neurosci 26:7907-7918.

Mensch S, Baraban M, Almeida R, Czopka T, Ausborn J, El Manira A, Lyons DA (2015) Synaptic vesicle release regulates myelin sheath number of individual oligodendrocytes in vivo. Nat Neurosci 18:628-630.

Mi S, Miller RH, Lee X, Scott ML, Shulag-Morskaya S, Shao Z, Chang J, Thill G, Levesque M, Zhang M, Hession C, Sah D, Trapp B, He Z, Jung V, McCoy JM, Pepinsky RB (2005) LINGO-1 negatively regulates myelination by oligodendrocytes. Nat Neurosci 8:745-751.

Mirantes C, Eritja N, Dosil MA, Santacana M, Pallares J, Gatius S, Bergada L, Maiques O, Matias-Guiu X, Dolcet X (2013) An inducible knockout mouse to model the cell-autonomous role of PTEN in initiating endometrial, prostate and thyroid neoplasias. Dis Model Mech 6:710-720.

Mironova YA, Giger RJ (2013) Where no synapses go: gatekeepers of circuit remodeling and synaptic strength. Trends Neurosci 36:363-373.

Mironova YA, Lenk GM, Lin JP, Lee SJ, Twiss JL, Vaccari I, Bolino A, Havton LA, Min SH, Abrams CS, Shrager P, Meisler MH, Giger RJ (2016) PI(3,5)P biosynthesis regulates oligodendrocyte differentiation by intrinsic and extrinsic mechanisms. eLife 5.

Mizuguchi R, Sugimori M, Takebayashi H, Kosako H, Nagao M, Yoshida S, Nabeshima Y, Shimamura K, Nakafuku M (2001) Combinatorial roles of olig2 and neurogenin2 in the coordinated induction of pan-neuronal and subtype-specific properties of motoneurons. Neuron 31:757-771.

Muller C, Bauer NM, Schafer I, White R (2013) Making myelin basic protein -from mRNA transport to localized translation. Frontiers in cellular neuroscience 7:169.

Najm FJ, Madhavan M, Zaremba A, Shick E, Karl RT, Factor DC, Miller TE, Nevin ZS, Kantor C, Sargent A, Quick KL, Schlatzer DM, Tang H, Papoian R, Brimacombe KR, Shen M, Boxer MB, Jadhav A, Robinson AP, Podojil JR, Miller SD, Miller RH, Tesar PJ (2015) Drug-based modulation of endogenous stem cells promotes functional remyelination in vivo. Nature 522:216-220.

Nave KA (2010) Myelination and support of axonal integrity by glia. Nature 468:244-252.

Nave KA, Ehrenreich H (2014) Myelination and oligodendrocyte functions in psychiatric diseases. JAMA Psychiatry 71:582-584.

Nave KA, Trapp BD (2008) Axon-glial signaling and the glial support of axon function. Annual review of neuroscience 31:535-561.

Nawaz S, Sanchez P, Schmitt S, Snaidero N, Mitkovski M, Velte C, Bruckner BR, Alexopoulos I, Czopka T, Jung SY, Rhee JS, Janshoff A, Witke W, Schaap IA, Lyons DA, Simons M (2015) Actin filament turnover drives leading edge growth during myelin sheath formation in the central nervous system. Developmental cell 34:139-151.

Nicholson G, Lenk GM, Reddel SW, Grant AE, Towne CF, Ferguson CJ, Simpson E, Scheuerle A, Yasick M, Hoffman S, Blouin R, Brandt C, Coppola G, Biesecker LG, Batish SD, Meisler MH (2011) Distinctive genetic and clinical features of CMT4J: a severe neuropathy caused by mutations in the PI(3,5)P(2) phosphatase FIG4. Brain : a journal of neurology 134:1959-1971.

O'Brien JS, Sampson EL (1965) Lipid composition of the normal human brain: gray matter, white matter, and myelin. J Lipid Res 6:537-544.

Oberheim NA, Takano T, Han X, He W, Lin JH, Wang F, Xu Q, Wyatt JD, Pilcher W, Ojemann JG, Ransom BR, Goldman SA, Nedergaard M (2009) Uniquely hominid features of adult human astrocytes. J Neurosci 29:3276-3287.

Ohno M, Hiraoka Y, Matsuoka T, Tomimoto H, Takao K, Miyakawa T, Oshima N, Kiyonari H, Kimura T, Kita T, Nishi E (2009) Nardilysin regulates axonal maturation and myelination in the central and peripheral nervous system. Nat Neurosci 12:1506-1513.

Orthmann-Murphy JL, Freidin M, Fischer E, Scherer SS, Abrams CK (2007) Two distinct heterotypic channels mediate gap junction coupling between astrocyte and oligodendrocyte connexins. J Neurosci 27:13949-13957.

Osorio MJ, Goldman SA (2016) Glial progenitor cell-based treatment of the childhood leukodystrophies. Exp Neurol.

Pagany M, Jagodic M, Schubart A, Pham-Dinh D, Bachelin C, Baron van Evercooren A, Lachapelle F, Olsson T, Linington C (2003) Myelin oligodendrocyte glycoprotein is expressed in the peripheral nervous system of rodents and primates. Neurosci Lett 350:165-168.

Pan B, Fromholt SE, Hess EJ, Crawford TO, Griffin JW, Sheikh KA, Schnaar RL (2005) Myelin-associated glycoprotein and complementary axonal ligands, gangliosides, mediate axon stability in the CNS and PNS: neuropathology and behavioral deficits in single- and double-null mice. Exp Neurol 195:208-217.

Pappas SS, Darr K, Holley SM, Cepeda C, Mabrouk OS, Wong JM, LeWitt TM, Paudel R, Houlden H, Kennedy RT, Levine MS, Dauer WT (2015) Forebrain deletion of the dystonia protein torsinA causes dystonic-like movements and loss of striatal cholinergic neurons. eLife 4:e08352.

Pappas SS, Leventhal DK, Albin RL, Dauer WT (2014) Mouse models of neurodevelopmental disease of the basal ganglia and associated circuits. Curr Top Dev Biol 109:97-169.

Park HC, Appel B (2003) Delta-Notch signaling regulates oligodendrocyte specification. Development 130:3747-3755.

Perez-Cerda F, Sanchez-Gomez MV, Matute C (2015) Pio del Rio Hortega and the discovery of the oligodendrocytes. Front Neuroanat 9:92.

Perlman SJ, Mar S (2012) Leukodystrophies. Advances in experimental medicine and biology 724:154-171.

Pfeiffer SE, Warrington AE, Bansal R (1993) The oligodendrocyte and its many cellular processes. Trends Cell Biol 3:191-197.

Poliak S, Peles E (2003) The local differentiation of myelinated axons at nodes of Ranvier. Nat Rev Neurosci 4:968-980.

Polito VA, Li H, Martini-Stoica H, Wang B, Yang L, Xu Y, Swartzlander DB, Palmieri M, di Ronza A, Lee VM, Sardiello M, Ballabio A, Zheng H (2014) Selective clearance of aberrant tau proteins and rescue of neurotoxicity by transcription factor EB. EMBO Mol Med 6:1142-1160.

Prolo LM, Vogel H, Reimer RJ (2009) The lysosomal sialic acid transporter sialin is required for normal CNS myelination. J Neurosci 29:15355-15365.

Pusic AD, Kraig RP (2014) Youth and environmental enrichment generate serum exosomes containing miR-219 that promote CNS myelination. Glia 62:284-299.

Raiker SJ, Lee H, Baldwin KT, Duan Y, Shrager P, Giger RJ (2010) Oligodendrocyte-myelin glycoprotein and Nogo negatively regulate activity-dependent synaptic plasticity. J Neurosci 30:12432-12445.

Raine CS (1984) On the association between perinodal astrocytic processes and the node of Ranvier in the C.N.S. J Neurocytol 13:21-27.

Rasband MN, Tayler J, Kaga Y, Yang Y, Lappe-Siefke C, Nave KA, Bansal R (2005) CNP is required for maintenance of axon-glia interactions at nodes of Ranvier in the CNS. Glia 50:86-90.

Reifler A, Lenk GM, Li X, Groom L, Brooks SV, Wilson D, Bowerson M, Dirksen RT, Meisler MH, Dowling JJ (2013) Murine Fig4 is dispensable for muscle development but required for muscle function. Skelet Muscle 3:21.

Reindl M, Di Pauli F, Rostasy K, Berger T (2013) The spectrum of MOG autoantibody-associated demyelinating diseases. Nat Rev Neurol 9:455-461.

Rempe D, Vangeison G, Hamilton J, Li Y, Jepson M, Federoff HJ (2006) Synapsin I Cre transgene expression in male mice produces germline recombination in progeny. Genesis 44:44-49.

Renna M, Jimenez-Sanchez M, Sarkar S, Rubinsztein DC (2010) Chemical inducers of autophagy that enhance the clearance of mutant proteins in neurodegenerative diseases. J Biol Chem 285:11061-11067.

Roach A, Boylan K, Horvath S, Prusiner SB, Hood LE (1983) Characterization of cloned cDNA representing rat myelin basic protein: absence of expression in brain of shiverer mutant mice. Cell 34:799-806.

Roach A, Takahashi N, Pravtcheva D, Ruddle F, Hood L (1985) Chromosomal mapping of mouse myelin basic protein gene and structure and transcription of the partially deleted gene in shiverer mutant mice. Cell 42:149-155.

Robinson MD, McCarthy DJ, Smyth GK (2010) edgeR: a Bioconductor package for differential expression analysis of digital gene expression data. Bioinformatics 26:139-140.

Rowitch DH, Kriegstein AR (2010) Developmental genetics of vertebrate glial-cell specification. Nature 468:214-222.

Saab AS, Tzvetanova ID, Nave KA (2013) The role of myelin and oligodendrocytes in axonal energy metabolism. Current opinion in neurobiology 23:1065-1072.

Saher G, Brugger B, Lappe-Siefke C, Mobius W, Tozawa R, Wehr MC, Wieland F, Ishibashi S, Nave KA (2005) High cholesterol level is essential for myelin membrane growth. Nat Neurosci 8:468-475.

Saher G, Rudolphi F, Corthals K, Ruhwedel T, Schmidt KF, Lowel S, Dibaj P, Barrette B, Mobius W, Nave KA (2012) Therapy of Pelizaeus-Merzbacher disease in mice by feeding a cholesterol-enriched diet. Nat Med 18:1130-1135.

Salzer JL (2003) Polarized domains of myelinated axons. Neuron 40:297-318.

Sardiello M, Palmieri M, di Ronza A, Medina DL, Valenza M, Gennarino VA, Di Malta C, Donaudy F, Embrione V, Polishchuk RS, Banfi S, Parenti G, Cattaneo E, Ballabio A (2009) A gene network regulating lysosomal biogenesis and function. Science 325:473-477.

Savas JN, Toyama BH, Xu T, Yates JR, 3rd, Hetzer MW (2012) Extremely long-lived nuclear pore proteins in the rat brain. Science 335:942.

Schain AJ, Hill RA, Grutzendler J (2014) Label-free in vivo imaging of myelinated axons in health and disease with spectral confocal reflectance microscopy. Nat Med 20:443-449.

Schardt A, Brinkmann BG, Mitkovski M, Sereda MW, Werner HB, Nave KA (2009) The SNARE protein SNAP-29 interacts with the GTPase Rab3A: Implications for membrane trafficking in myelinating glia. Journal of neuroscience research 87:3465-3479.

Scholz J, Klein MC, Behrens TE, Johansen-Berg H (2009) Training induces changes in white-matter architecture. Nat Neurosci 12:1370-1371.

Schuller U, Heine VM, Mao J, Kho AT, Dillon AK, Han YG, Huillard E, Sun T, Ligon AH, Qian Y, Ma Q, Alvarez-Buylla A, McMahon AP, Rowitch DH, Ligon KL (2008) Acquisition of granule neuron precursor identity is a critical determinant of progenitor cell competence to form Shh-induced medulloblastoma. Cancer cell 14:123-134.

Schulze U, Vollenbroker B, Braun DA, Van Le T, Granado D, Kremerskothen J, Franzel B, Klosowski R, Barth J, Fufezan C, Wolters DA, Pavenstadt H, Weide T (2014) The Vac14-interaction network is linked to regulators of the endolysosomal and autophagic pathway. Molecular & cellular proteomics : MCP 13:1397-1411.

Schweitzer JK, Krivda JP, D'Souza-Schorey C (2009) Neurodegeneration in Niemann-Pick Type C disease and Huntington's disease: impact of defects in membrane trafficking. Curr Drug Targets 10:653-665.

Settembre C, Di Malta C, Polito VA, Garcia Arencibia M, Vetrini F, Erdin S, Erdin SU, Huynh T, Medina D, Colella P, Sardiello M, Rubinsztein DC, Ballabio A (2011) TFEB links autophagy to lysosomal biogenesis. Science 332:1429-1433.

Settembre C, Zoncu R, Medina DL, Vetrini F, Erdin S, Erdin S, Huynh T, Ferron M, Karsenty G, Vellard MC, Facchinetti V, Sabatini DM, Ballabio A (2012) A lysosome-to-nucleus signalling mechanism senses and regulates the lysosome via mTOR and TFEB. EMBO J 31:1095-1108.

Sharma K, Schmitt S, Bergner CG, Tyanova S, Kannaiyan N, Manrique-Hoyos N, Kongi K, Cantuti L, Hanisch UK, Philips MA, Rossner MJ, Mann M, Simons M (2015) Cell type- and brain region-resolved mouse brain proteome. Nat Neurosci 18:1819-1831.

Shen D, Wang X, Li X, Zhang X, Yao Z, Dibble S, Dong XP, Yu T, Lieberman AP, Showalter HD, Xu H (2012) Lipid storage disorders block lysosomal trafficking by inhibiting a TRP channel and lysosomal calcium release. Nat Commun 3:731.

Simons M, Kramer EM, Macchi P, Rathke-Hartlieb S, Trotter J, Nave KA, Schulz JB (2002) Overexpression of the myelin proteolipid protein leads to accumulation of cholesterol and proteolipid protein in endosomes/lysosomes: implications for Pelizaeus-Merzbacher disease. The Journal of cell biology 157:327-336.

Simons M, Kramer EM, Thiele C, Stoffel W, Trotter J (2000) Assembly of myelin by association of proteolipid protein with cholesterol- and galactosylceramide-rich membrane domains. The Journal of cell biology 151:143-154.

Simons M, Lyons DA (2013) Axonal selection and myelin sheath generation in the central nervous system. Current opinion in cell biology 25:512-519.

Simons M, Trajkovic K (2006) Neuron-glia communication in the control of oligodendrocyte function and myelin biogenesis. Journal of cell science 119:4381-4389.

Snaidero N, Mobius W, Czopka T, Hekking LH, Mathisen C, Verkleij D, Goebbels S, Edgar J, Merkler D, Lyons DA, Nave KA, Simons M (2014) Myelin membrane wrapping of CNS axons by PI(3,4,5)P3-dependent polarized growth at the inner tongue. Cell 156:277-290.

Soriano P (1999) Generalized lacZ expression with the ROSA26 Cre reporter strain. Nat Genet 21:70-71.

Spampanato C, Feeney E, Li L, Cardone M, Lim JA, Annunziata F, Zare H, Polishchuk R, Puertollano R, Parenti G, Ballabio A, Raben N (2013) Transcription factor EB (TFEB) is a new therapeutic target for Pompe disease. EMBO Mol Med 5:691-706.

Stassart RM, Fledrich R, Velanac V, Brinkmann BG, Schwab MH, Meijer D, Sereda MW, Nave KA (2013) A role for Schwann cell-derived neuregulin-1 in remyelination. Nat Neurosci 16:48-54.

Stenmark H (2009) Rab GTPases as coordinators of vesicle traffic. Nature reviews Molecular cell biology 10:513-525.

Stritt C, Stern S, Harting K, Manke T, Sinske D, Schwarz H, Vingron M, Nordheim A, Knoll B (2009) Paracrine control of oligodendrocyte differentiation by SRF-directed neuronal gene expression. Nat Neurosci 12:418-427.

Sturrock RR (1980) Myelination of the mouse corpus callosum. Neuropathol Appl Neurobiol 6:415-420.

Sudhof TC, Rothman JE (2009) Membrane fusion: grappling with SNARE and SM proteins. Science 323:474-477.

Takatori S, Fujimoto T (2016) A novel imaging method revealed phosphatidylinositol 3,5-bisphosphate-rich domains in the endosome/lysosome membrane. Communicative & Integrative Biology 9:e1145319.

Takei N, Inamura N, Kawamura M, Namba H, Hara K, Yonezawa K, Nawa H (2004) Brain-derived neurotrophic factor induces mammalian target of rapamycin-dependent local activation of translation machinery and protein synthesis in neuronal dendrites. J Neurosci 24:9760-9769.

Tomassy GS, Berger DR, Chen HH, Kasthuri N, Hayworth KJ, Vercelli A, Seung HS, Lichtman JW, Arlotta P (2014) Distinct profiles of myelin distribution along single axons of pyramidal neurons in the neocortex. Science 344:319-324.

Toth AB, Terauchi A, Zhang LY, Johnson-Venkatesh EM, Larsen DJ, Sutton MA, Umemori H (2013) Synapse maturation by activity-dependent ectodomain shedding of SIRPalpha. Nat Neurosci 16:1417-1425.

Trajkovic K, Dhaunchak AS, Goncalves JT, Wenzel D, Schneider A, Bunt G, Nave KA, Simons M (2006) Neuron to glia signaling triggers myelin membrane exocytosis from endosomal storage sites. The Journal of cell biology 172:937-948.

Tress O, Maglione M, May D, Pivneva T, Richter N, Seyfarth J, Binder S, Zlomuzica A, Seifert G, Theis M, Dere E, Kettenmann H, Willecke K (2012) Panglial gap junctional

communication is essential for maintenance of myelin in the CNS. J Neurosci 32:7499-7518.

Tripathi RB, Clarke LE, Burzomato V, Kessaris N, Anderson PN, Attwell D, Richardson WD (2011) Dorsally and ventrally derived oligodendrocytes have similar electrical properties but myelinate preferred tracts. J Neurosci 31:6809-6819.

Tsai HH, Niu J, Munji R, Davalos D, Chang J, Zhang H, Tien AC, Kuo CJ, Chan JR, Daneman R, Fancy SP (2016) Oligodendrocyte precursors migrate along vasculature in the developing nervous system. Science 351:379-384.

Tyler WA, Gangoli N, Gokina P, Kim HA, Covey M, Levison SW, Wood TL (2009) Activation of the mammalian target of rapamycin (mTOR) is essential for oligodendrocyte differentiation. J Neurosci 29:6367-6378.

Vaccari I, Carbone A, Previtali SC, Mironova YA, Alberizzi V, Noseda R, Rivellini C, Bianchi F, Del Carro U, D'Antonio M, Lenk GM, Wrabetz L, Giger RJ, Meisler MH, Bolino A (2015) Loss of Fig4 in both Schwann cells and motor neurons contributes to CMT4J neuropathy. Hum Mol Genet 24:383-396.

Virchow R (1854) Ueber das ausgebreitete Vorkommen einer dem Nervenmark analogen Substanz in den thierischen Geweben. Archiv für pathologische Anatomie und Physiologie und für klinische Medicin 6:562-572.

von Budingen HC, Mei F, Greenfield A, Jahn S, Shen YA, Reid HH, McKemy DD, Chan JR (2015) The myelin oligodendrocyte glycoprotein directly binds nerve growth factor to modulate central axon circuitry. The Journal of cell biology 210:891-898.

Wake H, Lee PR, Fields RD (2011) Control of local protein synthesis and initial events in myelination by action potentials. Science 333:1647-1651.

Wake H, Ortiz FC, Woo DH, Lee PR, Angulo MC, Fields RD (2015) Nonsynaptic junctions on myelinating glia promote preferential myelination of electrically active axons. Nat Commun 6:7844.

Wang S, Bates J, Li X, Schanz S, Chandler-Militello D, Levine C, Maherali N, Studer L, Hochedlinger K, Windrem M, Goldman SA (2013) Human iPSC-derived oligodendrocyte progenitor cells can myelinate and rescue a mouse model of congenital hypomyelination. Cell Stem Cell 12:252-264.

Wang S, Sdrulla AD, diSibio G, Bush G, Nofziger D, Hicks C, Weinmaster G, Barres BA (1998) Notch receptor activation inhibits oligodendrocyte differentiation. Neuron 21:63-75.

Wang W, Zhang X, Gao Q, Xu H (2014) TRPML1: an ion channel in the lysosome. Handb Exp Pharmacol 222:631-645.

Wang X, Zhang X, Dong XP, Samie M, Li X, Cheng X, Goschka A, Shen D, Zhou Y, Harlow J, Zhu MX, Clapham DE, Ren D, Xu H (2012) TPC proteins are phosphoinositide-activated sodium-selective ion channels in endosomes and lysosomes. Cell 151:372-383.

Weisheit CE, Dauer WT (2015) A novel conditional knock-in approach defines molecular and circuit effects of the DYT1 dystonia mutation. Hum Mol Genet 24:6459-6472.

White R, Kramer-Albers EM (2014) Axon-glia interaction and membrane traffic in myelin formation. Frontiers in cellular neuroscience 7:284.

Winters JJ, Ferguson CJ, Lenk GM, Giger-Mateeva VI, Shrager P, Meisler MH, Giger RJ (2011) Congenital CNS hypomyelination in the Fig4 null mouse is rescued by neuronal expression of the PI(3,5)P(2) phosphatase Fig4. J Neurosci 31:17736-17751.

Winterstein C, Trotter J, Kramer-Albers EM (2008) Distinct endocytic recycling of myelin proteins promotes oligodendroglial membrane remodeling. Journal of cell science 121:834-842.

Woodhoo A, Sommer L (2008) Development of the Schwann cell lineage: from the neural crest to the myelinated nerve. Glia 56:1481-1490.

Yaghootfam A, Gieselmann V, Eckhardt M (2005) Delay of myelin formation in arylsulphatase A-deficient mice. Eur J Neurosci 21:711-720.

Yang N, Zuchero JB, Ahlenius H, Marro S, Ng YH, Vierbuchen T, Hawkins JS, Geissler R, Barres BA, Wernig M (2013) Generation of oligodendroglial cells by direct lineage conversion. Nat Biotechnol 31:434-439.

Yao D, McGonigal R, Barrie JA, Cappell J, Cunningham ME, Meehan GR, Fewou SN, Edgar JM, Rowan E, Ohmi Y, Furukawa K, Furukawa K, Brophy PJ, Willison HJ (2014) Neuronal expression of GalNAc transferase is sufficient to prevent the age-related neurodegenerative phenotype of complex ganglioside-deficient mice. J Neurosci 34:880-891.

Ye F, Chen Y, Hoang T, Montgomery RL, Zhao XH, Bu H, Hu T, Taketo MM, van Es JH, Clevers H, Hsieh J, Bassel-Duby R, Olson EN, Lu QR (2009) HDAC1 and HDAC2 regulate oligodendrocyte differentiation by disrupting the beta-catenin-TCF interaction. Nat Neurosci 12:829-838.

Yeung MS, Zdunek S, Bergmann O, Bernard S, Salehpour M, Alkass K, Perl S, Tisdale J, Possnert G, Brundin L, Druid H, Frisen J (2014) Dynamics of oligodendrocyte generation and myelination in the human brain. Cell 159:766-774.

Yin X, Kiryu-Seo S, Kidd GJ, Feltri ML, Wrabetz L, Trapp BD (2015) Proteolipid protein cannot replace P0 protein as the major structural protein of peripheral nervous system myelin. Glia 63:66-77.

Yool DA, Edgar JM, Montague P, Malcolm S (2000) The proteolipid protein gene and myelin disorders in man and animal models. Hum Mol Genet 9:987-992.

Young KM, Psachoulia K, Tripathi RB, Dunn SJ, Cossell L, Attwell D, Tohyama K, Richardson WD (2013) Oligodendrocyte dynamics in the healthy adult CNS: evidence for myelin remodeling. Neuron 77:873-885.

Yu T, Lieberman AP (2013) Npc1 acting in neurons and glia is essential for the formation and maintenance of CNS myelin. PLoS genetics 9:e1003462.

Zhang J, Liu Q (2015) Cholesterol metabolism and homeostasis in the brain. Protein Cell 6:254-264.

Zhang L, He X, Liu L, Jiang M, Zhao C, Wang H, He D, Zheng T, Zhou X, Hassan A, Ma Z, Xin M, Sun Z, Lazar MA, Goldman SA, Olson EN, Lu QR (2016) Hdac3 Interaction with p300 Histone Acetyltransferase Regulates the Oligodendrocyte and Astrocyte Lineage Fate Switch. Developmental cell 36:316-330.

Zhang X, Chow CY, Sahenk Z, Shy ME, Meisler MH, Li J (2008) Mutation of FIG4 causes a rapidly progressive, asymmetric neuronal degeneration. Brain : a journal of neurology 131:1990-2001.

Zhang Y, Chen K, Sloan SA, Bennett ML, Scholze AR, O'Keeffe S, Phatnani HP, Guarnieri P, Caneda C, Ruderisch N, Deng S, Liddelow SA, Zhang C, Daneman R, Maniatis T, Barres BA, Wu JQ (2014) An RNA-sequencing transcriptome and splicing database of glia, neurons, and vascular cells of the cerebral cortex. J Neurosci 34:11929-11947.

Zhang Y, McCartney AJ, Zolov SN, Ferguson CJ, Meisler MH, Sutton MA, Weisman LS (2012) Modulation of synaptic function by VAC14, a protein that regulates the phosphoinositides PI(3,5)P(2) and PI(5)P. EMBO J 31:3442-3456.

Zhang Y, Zolov SN, Chow CY, Slutsky SG, Richardson SC, Piper RC, Yang B, Nau JJ, Westrick RJ, Morrison SJ, Meisler MH, Weisman LS (2007) Loss of Vac14, a regulator of the signaling lipid phosphatidylinositol 3,5-bisphosphate, results in neurodegeneration in mice. Proc Natl Acad Sci U S A 104:17518-17523.

Zielasek J, Martini R, Toyka KV (1996) Functional abnormalities in P0-deficient mice resemble human hereditary neuropathies linked to P0 gene mutations. Muscle Nerve 19:946-952.

Ziskin JL, Nishiyama A, Rubio M, Fukaya M, Bergles DE (2007) Vesicular release of glutamate from unmyelinated axons in white matter. Nat Neurosci 10:321-330.

Zolov SN, Bridges D, Zhang Y, Lee WW, Riehle E, Verma R, Lenk GM, Converso-Baran K, Weide T, Albin RL, Saltiel AR, Meisler MH, Russell MW, Weisman LS (2012) In vivo, Pikfyve generates PI(3,5)P2, which serves as both a signaling lipid and the major precursor for PI5P. Proc Natl Acad Sci U S A 109:17472-17477.

Zonouzi M, Scafidi J, Li P, McEllin B, Edwards J, Dupree JL, Harvey L, Sun D, Hubner CA, Cull-Candy SG, Farrant M, Gallo V (2015) GABAergic regulation of cerebellar NG2 cell development is altered in perinatal white matter injury. Nat Neurosci 18:674-682.

Zou J, Hu B, Arpag S, Yan Q, Hamilton A, Zeng YS, Vanoye CG, Li J (2015) Reactivation of Lysosomal Ca2+ Efflux Rescues Abnormal Lysosomal Storage in FIG4-Deficient Cells. J Neurosci 35:6801-6812.

Zou Y, Jiang W, Wang J, Li Z, Zhang J, Bu J, Zou J, Zhou L, Yu S, Cui Y, Yang W, Luo L, Lu QR, Liu Y, Chen M, Worley PF, Xiao B (2014) Oligodendrocyte precursor cell-intrinsic effect of Rheb1 controls differentiation and mediates mTORC1-dependent myelination in brain. J Neurosci 34:15764-15778.

Zuchero JB, Barres BA (2013) Intrinsic and extrinsic control of oligodendrocyte development. Current opinion in neurobiology 23:914-920.

Zuchero JB, Fu MM, Sloan SA, Ibrahim A, Olson A, Zaremba A, Dugas JC, Wienbar S, Caprariello AV, Kantor C, Leonoudakis D, Lariosa-Willingham K, Kronenberg G, Gertz K, Soderling SH, Miller RH, Barres BA (2015) CNS myelin wrapping is driven by actin disassembly. Developmental cell 34:152-167.